

DISTRIBUTION STATEMENT A:  
Approved for Public Release -  
Distribution Unlimited

# ICMAC

## International Conference for Manufacturing of Advanced Composites

27 - 28 September 2001  
Belfast Waterfront Conference Centre  
Belfast, Northern Ireland

Organised by



IOM Communications

Sponsored by



Conference Preview

AD NUMBER	DATE	DTIC ACCESSION
1. REPORT IDENTIFYING INFORMATION		R/
A. ORIGINATING AGENCY Univ. of Ulster, Northern Ireland		1.
B. REPORT TITLE AND/OR NUMBER Impact Internat. Conf. for manufacturers of advanced composites		2.
C. MONITOR REPORT NUMBER N68171-01-M-6334		3.
D. PREPARED UNDER CONTRACT NUMBER R+D 9117-MS-02		4.
2. DISTRIBUTION STATEMENT		5.
APPROVED FOR PUBLIC DISTRIBUTION		1
DISTRIBUTION UNLIMITED		2
PROCEEDINGS		1

20020215 129

CTIONS ARE OBSOLETE

RFD 9117-MS-02  
N68171-01-M-6334  
UNIVERSITY OF ULSTER  
Co. ANTRIM N.I.



IOM Communications



THE INSTITUTE OF  
MATERIALS

**ICMAC**  
**International Conference for Manufacturing**  
**of Advanced Composites**

27-28 September 2001  
Belfast Waterfront Conference Centre  
Belfast, Northern Ireland

ISBN 1-186125-153-X

Published By

IOM Communications Ltd  
1 Carlton House Terrace  
London, SW1Y 5DB  
United Kingdom

Tel: +44 (0) 20 7451 7300

Fax: +44 (0) 20 7839 2289

*IOM Communications Ltd is a wholly owned subsidiary of The Institute of Materials.  
Registered Charity number: 1059475*

20020215 129

#### **ORGANISING COMMITTEE**

R McIlhagger (Chairman)	University of Ulster at Jordanstown
G Bishop	NetComposites
G Cather	Bombardier Aerospace - Short Brothers plc
N Fawcett	Ford Motor Company
Q Fontana	BAE Systems, Advanced Technology Centres, Sowerby
AG Gibson	University of Newcastle
M Lawton	Chelton Radomes Ltd
F Matthews	Imperial College of Science, Technology & Medicine
RF McCarthy	Dowty Aerospace Propellers
CD Rudd	University of Nottingham
J Summerscales	University of Plymouth

#### **INTERNATIONAL ADVISORY COMMITTEE**

J Anders Holmberg	Swedish Institute of Composites, Sweden
J Brandt	Daimler Benz AG, Germany
C Johnson	Ford Motor Company, USA
PJ Mallon	University of Limerick, Ireland
R Paton	CRC-ACS, Australia
JA Manson	Swiss Federal Institute of Technology, Switzerland
M Neitzel	Universitat Kaiserlautern, Germany
R Parnas	NIST, USA
CMÓ Brádaigh	University of Galway, Ireland
S Ramakrishna	National University of Singapore
N Svensson	Xdin AB, Sweden
F Trochu	Ecole Polytechnique de Montreal, Canada

#### **ACKNOWLEDGEMENTS**

The Conference Organisers wish to thank the following organisations for the sponsorship which they have given to the ICMAC Conference.

Bombardier Aerospace – Short Brothers plc  
Clarehill Plastics Ltd  
The European Research Office  
The Industrial Research and Technology Unit (IRTU)  
Nottingham University Composites Club  
The Old Bushmills Distillery Co Ltd  
The University of Ulster Engineering Composites Research Centre  
The Institute of Materials

## CONTENTS

### SESSION 1: PROCESSING TECHNOLOGY

- Keynote: Materials, the Tip of the Iceberg**  
C Johnson (Ford Motor Company, USA) 3
- Continuous monitoring of three-dimensional resin flow through a fibre preform**  
T Stöven, F Weyrauh, P Mitschang, M Nietzel (Institute für Verbundwerkstoffe GmbH, Germany) 6
- Manufacture of thick composite primary structures using resin transfer infusion**  
G Wright (Bombardier Aerospace Shorts, Northern Ireland) 15
- Recent advances in glass fiber preforming: Implementation of the Ford programmable preform process**  
JE deVries, NG Chavka, JS Dahl (Ford Motor Company, USA) 22

### SESSION 2: TEXTILE TECHNOLOGY & MODELLING

- Geometrical modelling based process control of a triaxial braiding machine equipped with a flexible madrel system**  
P Potluri, A Rawal, M Rivaldi and I Porat (UMIST, UK) 25
- WiseTex - virtual textile software**  
SV Lomov, I Verpoest (Katholieke Universiteit Leuven, Belgium) 36
- Design methodology for 3D woven fabric architectures**  
JA Soden, BJ Hill (University of Ulster, Northern Ireland) 44
- Geometric modelling of orthogonal 3-D woven textiles**  
D Brown, Z J Wu (University of Ulster, Northern Ireland) 52
- Modelling of draping and deformation for textile composites**  
AC Long, MJ Clifford, P Harrison, CD Rudd (University of Nottingham, UK) 66

### SESSION 3: PROCESSING & MODELLING

- Keynote: UK Polymer Composites Sector: Competitive Analysis and Foresight Study**  
GD Sims (NPL Materials Centre, UK) G Bishop (NetComposites, UK) 79
- Numerical simulation of void formation in LCM**  
J Bréard, A Saouab, G Bouquet (Université du Havre, France) 80
- Permeability prediction for industrial textile**  
F Robitaille, AC Long, CD Rudd, BJ Souter (University of Nottingham, UK) 91
- Shear flow characterisation of GMT, and use of the Brinkman equation in modelling the interaction of the flowing materials with the mould surface**  
G Kotsikos, A G Gibson (University of Newcastle upon Tyne, UK) 100

---

#### **SESSION 4: PROCESS MONITORING & CONTROL**

**Impedance cure and flow monitoring in the processing of advanced composites**  
A Skordos, IK Partridge (Cranfield University, UK) 103

**Controlling complex cure cycles via real-time dielectric measurements**  
MC Kazilas (Cranfield University, UK) GM Maistros (INASCO UK Ltd, UK) IK Partridge  
(Cranfield University, UK) 113

**Implementation of a dielectric on-line process monitoring system**  
W Wenger (Bombardier Aerospace Shorts, Northern Ireland) 121

#### **SESSION 5: MATERIAL CHARACTERISATION & COMPOSITE PERFORMANCE**

**Evaluation of a carbon thermoplastic to titanium bonded joint**  
GF Leon, M Trezza, J Hall (General Dynamics Electric Boat Company, USA)  
K Corona-Bittick (Production Products, USA) 131

**Quantifying the error in fibre orientation measurement and its application to evaluating numerical simulations**  
CN Eberhardt, AR Clarke (University of Leeds, UK) 141

**Effect of sizing on the flow of resin within a glass fibre composite**  
J Quinn, AT McIlhagger, R McIlhagger, P Rogers (University of Ulster, Northern Ireland) 151

**The influence of post-cure time and temperature on the mechanical and dielectric properties of glass fibre epoxy composite**  
AT McIlhagger, J Quinn, D Brown, R McIlhagger, PPJ Rogers (University of Ulster, Northern Ireland) 159

#### **SESSION 6: PROCESSING OF THERMOPLASTIC COMPOSITES**

**Manufacturing and anisothermal squeeze flow of glass fabric/glass mat reinforced polypropylene hybrid composites**  
KW Houston, PJ Mallon (University of Limerick, Ireland) 169

**Development of thin-walled fibre-reinforced structures**  
G Gately (National University of Ireland, Ireland) A B. Coffey (Athlone Institute of Technology, Ireland) CM O'Bradaigh (National University of Ireland, Ireland) A Brazier (Athlone Institute of Technology, Ireland) 170

**Vacuum bag moulding of large parts in commingled glass/PET and glass PETG composites**  
N Dodds, AG Gibson (University of Newcastle upon Tyne, UK) 171

**Induction-based processing of thermoplastic carbon fiber laminates**  
B Fink, NB Shevchenko (U.S. Army Research Laboratory, USA) H-J Kim, S Yarlagadda, JJ Tierney (University of Newark, USA) 181

## SESSION 7: INDUSTRIAL APPLICATIONS & CASE STUDIES

<b>Keynote: Aerospace Composites Commercial Potential a Real Option</b> G Cather, S Wilson (Bombardier Aerospace - Short Brothers plc, Northern Ireland)	195
<b>Manufacture and future development of advanced composite engine nacelle acoustic liner components</b> R Parkes (Bombardier Aerospace - Short Brothers plc, Northern Ireland)	215
<b>RTM - A cost effective composite manufacturing process for control surfaces</b> M Braniff (Bombardier Aerospace - Shorts, N Ireland)	225
<b>Effect of the processing parameters on crash energy absorbing composite structures made by RTM</b> TA Turner, NA Warrior, F Robitaille, CD Rudd, EJ Cooper (University of Nottingham, UK)	238
<b>Vacuum injection moulding for large structural applications</b> WD Brouwer, ECFC van Herpt, M Labordus (Centre of Lightweight Structures TUD-TNO, The Netherlands)	248
<b>POSTERS</b>	
<b>Automated preform manufacture: robotic handling, in-situ measurement of preform properties and lay-up simulation</b> P Potluri (UMIST, UK)	259
<b>Bias extension measurements on dry and preimpregnated non-crimp fabric carbon fibre reinforcement</b> K Potter (University of Bristol, UK)	268
<b>Application of fibre metal laminates on a future regional jet aircraft</b> K Poston (Bombardier Aerospace - Short Brothers plc, Northern Ireland)	278
<b>Investigation into the effects of dry media paint removal on composite aircraft structures</b> F Andrews (Bombardier Aerospace - Short Brothers plc, Northern Ireland)	279
<b>Towards the design of sandwich panel composites with enhanced thermal and mechanical properties by virtue of possessing an auxetic core</b> JPM Whitty, B. Kandola, P Myler, A Alderson (Bolton Institute, UK)	280
<b>The application of a general fibre architecture model for composite mechanical property prediction</b> J Crookston, BJ Souter, AC Long, IA Jones (University of Nottingham, UK)	290
<b>Ultrasonic cure monitoring of RTM6 Epoxy Resin</b> J McHugh, J Döring, W Stark (Federal Institute for Materials Research and Testing, Germany), IK Partridge (Cranfield University, UK)	299
<b>Hybrid processing of composite/metal laminates for automotive body structures</b> BM Weager, CD Rudd (University of Nottingham, UK) CF Johnson (Ford Motor Company, USA)	300
<b>A modified system for design and analysis of 3D woven preforms</b> J Quinn, R McIlhagger, A McIlhagger, P Rogers (University of Ulster, Northern Ireland)	306

---

<b>The automatic generation of a solid model of a plain weave structure</b> D Brown, M Morgan (University of Ulster, Northern Ireland)	313
<b>Maintaining the stability of a three-dimensional woven preform by incorporating a thermoplastic yarn within the weave structure</b> PPJ Rogers, AT McIlhagger, J Quinn, R McIlhagger (University of Ulster, Northern Ireland)	322
<b>Roll-formed composite blade stiffeners</b> JA Lee (Airbus, UK)	329
<b>Assessing quality in composites manufacture</b> GD Sims, W Broughton, D Mulligan, S Gnaniyah (NPL Materials Centre, UK)	336
<b>Effect of lay-up and fiber angle on drilling behaviour of GFRP laminates</b> J Ramkumar, SK Malhotra, R Krishnamurthy (Indian Institute of Technology, Madras, India)	345
<b>Multi-scale modelling of resin transfer moulding</b> SC McCallum, PD Lee, CJ Lawrence, T Selerland, PDM Spelt, FL Matthews (Imperial College of Science Technology and Medicine, UK)	346

## Foreword

It gives me great pleasure to welcome you to the International Conference for Manufacturing of Advanced Composites (ICMAC) and I am delighted that the Organising Committee selected Belfast as the venue for this event.

This conference is the successor to the previously successful International Conferences on Automated Composites (ICAC) series. Due to the response from the Bristol conference in 1999 it was felt that this new name more readily reflected the theme of the conference.

Reduction in manufacturing costs remains the main driver towards expansion of the use of composites in many engineering and other applications. In addition limited performance data, including the interactions between material selection, processing parameters and performance characteristics, has inhibited growth in the sector. All of these factors make the design and manufacture of composite components to meet stringent design criteria a very complex process. It is these ingredients which provide the central theme for the ICMAC conference which will highlight the latest developments and new directions for composites' design and manufacture from textile technology to new and improved processing methods and routes for novel uses.

ICMAC is a very focused conference which will address many of the above issues and will benefit the composites' industry by promoting a greater acceptance of composite materials in an ever-widening range of applications.

The authors of papers and presenters of poster sessions have come from all around the world retaining the international flavour of this event. The Conference has been divided up into seven plenary sessions, with parallel poster reviews. It is confidently expected that industrialists and researchers will benefit equally from attendance at the Conference to learn of the latest developments in the manufacture of advanced composites, to have an opportunity to discuss current research in a focused forum and build up collaborative partnerships with experts in the field. I hope that you avail yourself of this unique opportunity.

I wish to express my sincere thanks to all the authors for their contributions to the conference, to the keynote speakers for their willingness to participate, to the sponsors for their very considerable support without which the conference would not have taken place, to the Organising Committee for their continuing support, encouragement and guidance and to the staff of the Institute of Materials for their hard work in the overall organisation of the conference.

Finally I wish to express my sincere gratitude to all the conference delegates whose participation in the event makes the whole thing worthwhile. I hope that you have found the conference both informative and rewarding and that your visit to Belfast has been an enjoyable and memorable occasion.

Many thanks to all for your support.

Professor Robert McIlhagger  
Chairman  
Organising Committee

**SESSION 1:**  
**PROCESSING TECHNOLOGY**

ICMAC - International Conference for Manufacturing of Advanced Composites

**Materials, the tip of the iceberg**

Presented by

Dr. Carl F. Johnson

Ford Motor Company Research Laboratory

Dearborn, Michigan, USA

Materials researchers and vehicle development engineers have been working for over two decades to achieve substantial use of lightweight materials in automobiles. Aluminium, polymer composites, and magnesium have been investigated for many uses in vehicle exterior and structural applications. Some investigations have been at the component substitution level while others have involved the build of entire vehicles, however in most cases the substitutions have been maintained briefly to solve temporary weight issues or rejected before initial implementation. The regulatory drivers for the use of light weight materials are well understood, fuel consumption standards and mandatory emissions levels require improvements in powertrain efficiency and lighter weight vehicles. Technology drivers less well understood are those of the consumer, reliability, cost, quality and the desire for new technology and those of manufacturing that include design, investment, and process productivity. Materials of construction are really only the tip of the iceberg; design, assembly, and manufacturing must all be addressed simultaneously with the material to achieve a design that meets both the consumer and regulatory needs. It is now essential for the research community to develop more complete technology bundles with elements that address the entire design, manufacture, and assembly of a vehicle or subsystem including the regulatory performance of the system and the consumer impact of the new developments. Due to the higher cost of new light weight technology and the manufacturing and performance uncertainty normally associated with its introduction, the current implementation path in the automobile industry is through lower volume luxury brands. Only when the factors beyond materials selection are fully addressed and an affordable implementation plan has been developed can a new material be introduced on a broad scale to high volume vehicles. In this keynote presentation, the factors beyond material selection will be identified and examined and some of the possible implementation strategies will be proposed.

C.F. Johnson  
August 10, 2001

**CONTINUOUS MONITORING OF THREE-DIMENSIONAL RESIN FLOW  
THROUGH A FIBRE PREFORM**

Stöven, T. \*; Weyrauch, F.; Mitschang, P.; Neitzel, M.

*Institut für Verbundwerkstoffe GmbH, Erwin-Schrödinger-Str. Geb. 58, D-67663 Kaiserslautern, Germany*

**ABSTRACT**

A basic requirement for an accurate numerical simulation of the resin transfer mould filling process is a set of reliable coefficients describing the permeability of the considered fibre preform. The values of the permeability coefficients are usually obtained from the measurement of flow front movement through a fibre preform. While measuring the in-plane flow to characterise the in-plane permeability is rather simple, ascertaining flow in thickness direction emerges to be difficult. Existing techniques require extensive preparation efforts like the integration of numbers of sensors into the fibre preform, which allow a discontinuous measurement, only. The objective of this work is to overcome these difficulties with the development of a testing equipment, which enables continuous and high resolution monitoring of the transverse resin flow through a fibre preform. Knowledge of an accurate transverse permeability coefficient is important for the numerical simulation of the filling of thick sectioned parts or vacuum assisted infiltration processes like resin film infusion (RFI) or SCRIMP®. The developed testing equipment is based on a mould with tool mounted ultrasonic transducers which work in through transmission mode. First experiments were carried out to correlate the flow front position with time of flight and signal attenuation. Therefore, the fibre preform is infiltrated in layers of determined thickness. Based on the experience obtained from the preliminary testing a special testing equipment for measuring transverse flow front propagation during point injection of a thick sectioned fibre preform was developed. A selected multidirectional non-crimp fabric was characterised by two- and three-dimensional flow experiments. For determination of the transverse permeability the simulation software LCMFlot from L3P INC emulated the three-dimensional filling experiment.

*Keywords:* Liquid-Composite-Moulding (LCM), process monitoring, transverse permeability, ultrasound transmission

**INTRODUCTION**

Resin Transfer Moulding (LCM) has become an economic technique for the manufacture of advanced composite lightweight structures in many cases. Meanwhile the acronym LCM represents more than a dozen of varying process types (1), which all have the principle in common that a liquid monomer is firstly injected into a cavity filled with a reinforcing fibre preform and secondly forms the part by chemically reacting to a solid polymer network. A distinctive feature of the LCM process variations is their applicability to the fabrication of a

\* Corresponding author: Timo Stöven, Institut für Verbundwerkstoffe GmbH, Erwin-Schrödinger-Str. Geb. 58, D-67663 Kaiserslautern, Germany, Phone: +49 (0) 631 2017 438, E-mail: stoeven@ivw.uni-kl.de

variety of different part sizes and shapes. Especially the manufacture of large, complex shaped and thick-sectioned composites by LCM received considerable attention in recent years. Within this development numerical process simulation becomes an important engineering tool for mould design and process control. Thereby the research focuses on simulation of the resin flow through fibre reinforcement. With the software commercially available the mould-filling pattern can be emulated depending on the locations and number of inlet and outlet gates, resin rheology, injection rate and pressure, thermal effects and the physics of liquid flow through the fibre preform. The standard flow modelling bases on a proportional relationship between the flow rate and the applied pressure gradient, which is known as Darcy's law. The describing proportional factor is called the permeability. Its value depends on the considered flow direction because of a non-isotropic structural arrangement of the fibre reinforcement.

While the determination of the permeability of the in-plane directions is intensively investigated by one dimensional and radial flow measurements, Weitzenböck, Trochu, Mogavero (2-4), the research in ascertaining the transverse permeability is still in the beginning due to a lack of efficient techniques available for measuring flow in thickness direction. First known work in this field was done by Stedile (5) who calculated the transverse permeability from the pressure drop of a liquid when flowing through a preform. This technique picked up again by Parnas (6) and Han (7) is restricted to the determination of the transverse permeability of a saturated fibre preform only. Lekakou (8) and Pillai (9) had shown that the permeability of a wetted fabric differs from a dry one significantly. Ballata (10) applied a modified SMART-weave set-up, Walsh (11), in an orthogonal arrangement for 3-dimensional measurement of flow front movement. Lim (12) and Weitzenböck (13) worked with arrays of point sensors, embedded into a laminate stack. Similar to the SMART-weave the embedded sensors allow an incremental determination of the flow front movement only. With the aim to reduce the preparation effort Kissinger (14) injects a fast curing resin through a central injection port into the dry fibres and measures the length of the main axes of the infiltrated and cured ellipsoidal volume.

## APPROACH

The aim of this work is the development of a test equipment based on ultrasonic transmission, which should overcome the drawbacks of existing techniques for measuring the thickness flow as mentioned above. The principal function is shown in Figure 1. An acoustic pulse is sent out, moving perpendicular through the layers of a fibre preform and is received by an ultrasound transducer on the opposite site. Infiltrating the fibre preform with a liquid in thickness direction, as shown in Figure 1, will result in the formation of two media with two different sound speeds. Consequently measuring the time the acoustic wave takes for propagating from the sound source to a receiver (time-of-flight) can give information about the flow front position.

An alternative way is to obtain the flow front location from the relation between the received and sent out acoustic intensities. The amount of energy loss, called acoustic extinction, depends on the material and its thickness the sound has to move through, so that a correlation between the current location of a moving flow front and the acoustic extinction exists.

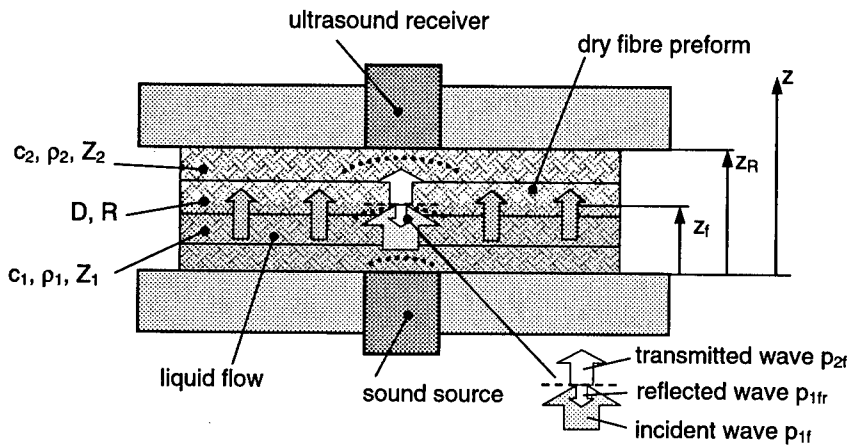


Figure 1: Schematic of measuring the flow front location by ultrasound transmission.

### THEORY

In the following the acoustics of the transverse flow front movement through the fibre preform is modelled as the transmission problem of a longitudinal acoustic wave at the interface of two media (Figure 1).

The time an ultra sound wave takes for propagating the distance  $z_R$  through the media can be formulated with regard to the position of the interface of the two media

$$t_R = \frac{z_f}{c_1} + \frac{z_R - z_f}{c_2} + T_0. \quad (1)$$

Hereby  $T_0$  stands for a test rig dependent time offset. The location of the interface (i.e. the flow front)  $z_f$  can be calculated from

$$z_f = \left( t_R - \frac{z_R}{c_2} - T_0 \right) \frac{c_1 c_2}{c_1 - c_2}. \quad (2)$$

On its way from the sound source to the receiver through a polymer composite the ultrasound wave loses a part of its energy to the environment due to scattering and absorption. It is assumed that the acoustic pressure of a moving ultrasound wave decreases according to an exponential function with increasing distance of the sound source, Schuster (15):

$$p = p_0 \cdot e^{(-\alpha z)}. \quad (3)$$

Thereby  $p_0$  is a referred pressure (e.g. the sound source) and  $\alpha$  represents the acoustic loss coefficient, which takes into account scattering loss,  $\alpha_s$ , and a loss caused by absorption,  $\alpha_a$ . The intensity  $I$  of an acoustic wave is proportional to the square of the acoustic pressure:

$$I = \frac{1}{2} \frac{p^2}{\rho c}, \quad Z = \rho c. \quad (4)$$

$Z$  represents the acoustic resistance defined by the product of the material specific constants  $c$ , the speed of sound, and  $\rho$ , the density.

In case of the perpendicular incidence of an ultrasound wave onto the boundary of two media, like the interface between impregnated and dry fibres, only a part of the waves intensity  $I$  is transmitted, while the other is reflected (Figure 2). A transmission  $D$  and a reflection  $R$  coefficient can be derived from the intensity fractions. The wave resistances of the two medias determine the coefficients in the following way.

$$D = \frac{I_2}{I_1} = \frac{4 \cdot Z_1 Z_2}{(Z_1 + Z_2)^2}, \quad R = \frac{I_{1r}}{I_1} = \left( \frac{Z_2 - Z_1}{Z_2 + Z_1} \right)^2. \quad (5,6)$$

If an acoustic receiver is placed at the location  $z_R$  in the second media it measures an acoustic pressure  $p_R$ , which depends on the transmitted pressure  $p_{2f}$  according to equation (1)

$$p_R = p(z_R) = p_{2f} \cdot e^{-\alpha_2(z_R - z_f)}. \quad (7)$$

Expressing the pressure  $p_{2f}$  by the constants  $p_0$  and  $D$  (eq. 1, 3, 4) equation 8 can be manipulated to the form of equation 1 as

$$p_R = p_0^* \cdot e^{-\alpha^* z_f} \quad (9)$$

with  $p_0^* = p_0 \sqrt{D} \cdot e^{-\alpha_2 z_R}$  and  $-\alpha^* = (\alpha_2 - \alpha_1)$ .

Following equation 9 the position of the interface (e.g. flow front) can be determined by measuring the wave intensities, when the loss coefficients have different values, only.

## EXPERIMENTAL

### TWO DIMENSIONAL APPROACH

In the first stage of this work the applicability of ultrasound transmission for the measurement of thickness flow was evaluated by a special two-dimensional vacuum infusion experiment. Therefore 8 layers of non-crimped stitched fabric were put into bags each and then placed as a stack between two aluminium plates. Each layer had one injection port and one connection to the vacuum pump. The plates support two facing ultrasonic transducers, which are aligned perpendicular to the plate surface (Figure 2).

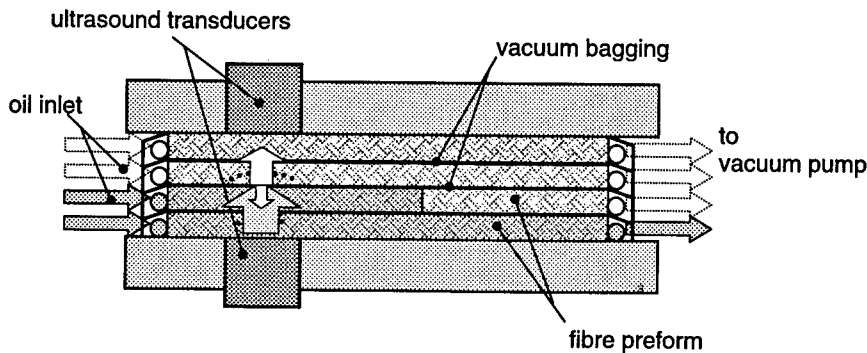


Figure 2: Set-up for investigating how signal strength and time of flight of an ultrasound wave are affected by filling the fibre preform in sections.

The stack of fibres was compressed to a certain thickness. To mimic thickness flow, the layers were infiltrated with salad oil one after the other. After each infiltration step the signal response of the receiving transducer was recorded and compared to the others (Figure 3).

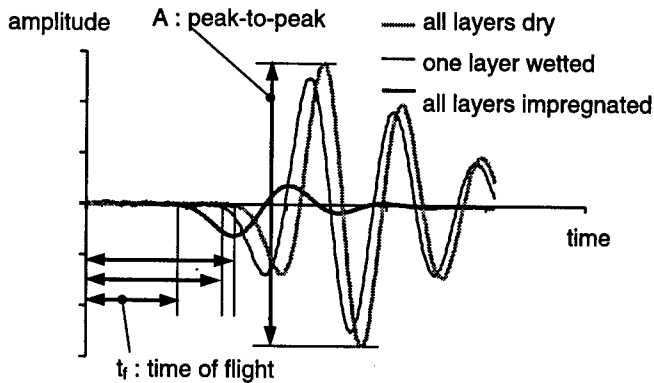


Figure 3: Recorded signal traces triggered on the sent pulse.

Aside from errors caused by the experimental set-up it appears correct that the measured time-of-flight (TOF) drops proportional to the number of infiltrated layers, which corresponds to the theory as shown by the regression function in Figure 4. The exponential correlation of the peak-to-peak values, which are proportional to the acoustic pressure, do not follow the curvature indicated by the measurements, so that the TOF is considered as the more eligible parameter due to the better matching with the theory.

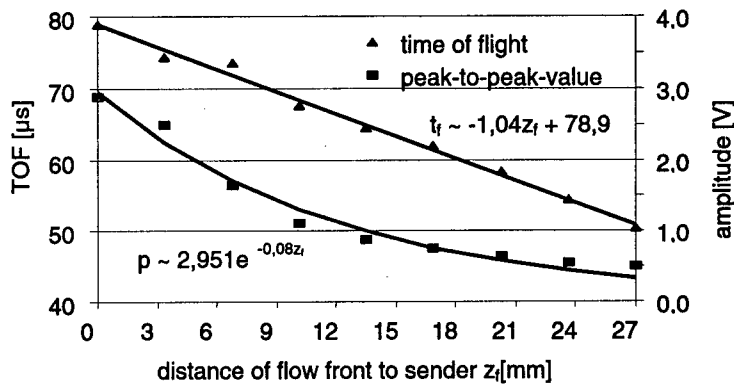


Figure 4: TOF and peak-to-peak value change with the number of impregnated layers. Their regressions are of those types defined in theory.

### THREE DIMENSIONAL FLOW EXPERIMENT

With the experience obtained from the preliminary experiments a testing equipment was designed, which should enable the measurement of thickness flow in a real three-dimensional impregnation scenario of a fibre preform. The ultrasound transducers are placed on the centre-line of the injection port as shown in Figure 5. The zenith of the ellipsoidal flow front moves from one transducer along the centre line to the opposite

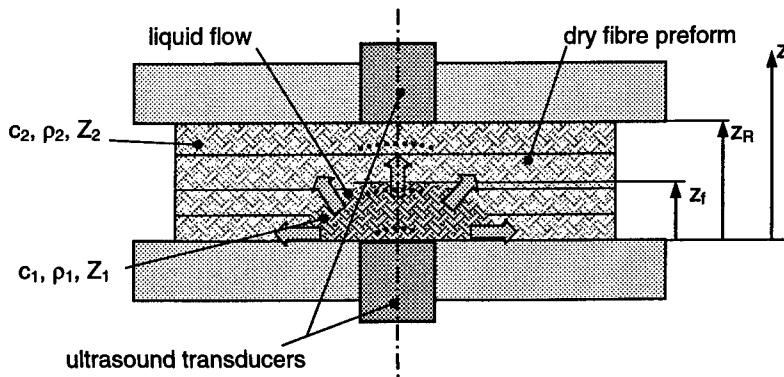


Figure 5: Concept for measuring transverse flow in a three dimensional injection cycle

## RESULTS AND DISCUSSION

### MEASUREMENT OF THREE DIMENSIONAL FLOW

For a first evaluation vacuum assisted infusion was performed with a transparent upper mould half for being able to compare the ultrasound measurements with the observed arrival of the flow front at the upper face of the fibre preform. The change in time-of-flight is shown in Figure 6. The values include an equipment dependent time delay  $T_0$  (e.g. mould walls, injection channels, transducers).

The change of the slope of all three graphs at 4 seconds after the beginning of the injection signifies that the liquid must have reached the fibre preform. In fact it could be demonstrated by covering the injection port with a thin foil that 4 seconds after the beginning of the injection the measured time delay became stationary, indicating that the inner mould liquid supply was filled up to the injection port. With the ongoing infiltration the time-of-flight decreases in a reproducible pattern. Its gradient firstly flattens and then increases again, forming an S-shaped curve. Around 90 seconds after the injection had started the time-of-flight (TOF) becomes almost stationary. This event is indicated by a characteristic dent in the graphs, which, correlates to the time at which the bulk flow visibly touches the upper mould wall. 12 to 16 seconds before the white coloured seams of the non-crimped fabric already started to turn grey, which is seen as the arrival of the flow front driven by capillary pressure (7) that moves ahead to the bulk flow driven by hydrostatic pressure.

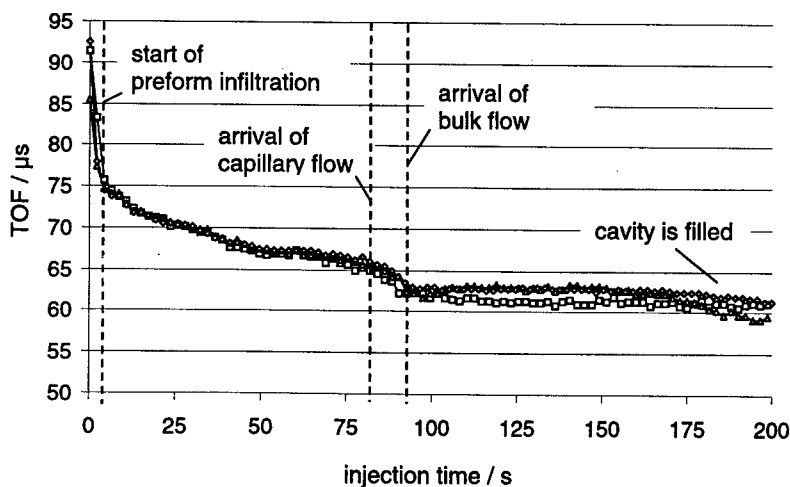


Figure 6: Time at which the first maximum of the received wave is detected

After the zenith of the ellipsoidal flow front had reached the top of the preform a slight decrease of the time of flight down to  $60 \mu\text{s}$  was measured until the cavity was completely filled after 180 to 200 seconds.

PERMEABILITY

Because there is no analytical model available for calculating the transverse permeability from three-dimensional flow it was attempted to determine its value by emulating the performed flow experiment with the flow simulation tool "LCMFlot" from L3P Inc. With the knowledge of the in-plane permeabilities, which were formerly calculated from radial flow measurements, a value of the transverse permeability was determined iteratively. The resulting flow pattern at different time steps is shown in Figure 7.

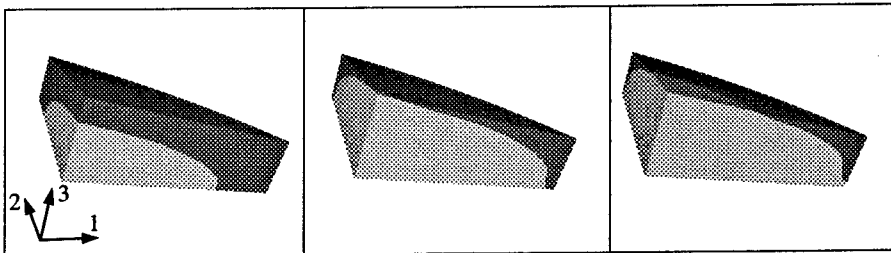


Figure 7: Flow front positions at 30; 92 and 110 seconds. A quarter of the cylindrical model is displayed. Permeabilities:  $K_1 = 2.2 \cdot 10^{-11} \text{ m}^2$ ,  $K_2 = 2.2 \cdot 10^{-11} \text{ m}^2$ ,  $K_3 = 1.6 \cdot 10^{-12} \text{ m}^2$ .

The simulation seems to emulate the real flow pattern realistic. This assumption is endorsed by comparing the calculated and measured values of the injected volume, when the liquid reaches the upper mould face and when the cavity is completely filled (table I). The observed and calculated arrival times of the liquid at the lower circumferential edge of the mould correspond also.

Table I: Significant process stages observed and simulated.

Characteristic process stage	Simulated	Experimental
Volume injected and time when flow reaches upper mould face	31.4 cm <sup>3</sup> / 89.2 s (bulk flow)	23.3 cm <sup>3</sup> / 77 s (capillary flow) 28.6 cm <sup>3</sup> / 93 s (bulk flow)
Arrival of liquid at lower circumferential edge	110 sec	≈120 sec
Volume injected	65.0 cm <sup>3</sup>	63.2 cm <sup>3</sup>

A difference between the calculated and measured values of the injected volume was observed, which alludes to an error in the calculation of the fibre volume fraction. It seems that the actual fibre volume fraction was of a higher value than calculated. The difference between the observed and calculated arrival times of the liquid at the lower circumferential edge endorse this assumption.

Based on the sound speeds of the two media (impregnated or dry fibres), which are derived from the corrected time-of-flight curve at  $z_f = 0$  and  $z_f = z_R$  (equation 1) the flow front position at the z-axis (thickness direction) is estimated and compared to the numerical simulation (Figure 8).

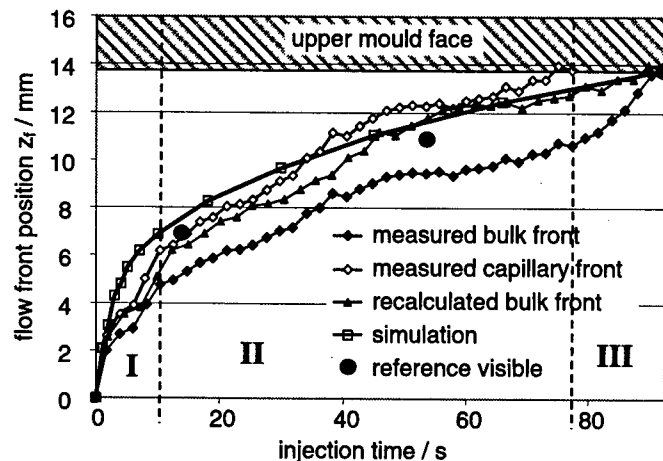


Figure 8: Flow front positions derived from time-of-flight measurements and calculated by numerical flow simulation.

The fact that two flow fronts are observed leads to the question to which one the time-of-flight measurement is associated. In theory (equation 2) the existence of only one bulk flow front is assumed. Following this presumption the time-of-flight measurements are firstly referred to the observed arrival time of the bulk flow at the upper mould face. With equation 1 the corresponding sound speed  $c_1$  can be calculated to  $c_1 \approx 487$  m/s. The sound speed of the dry fibres is  $c_2 \approx 322$  m/s. The resulting curve describing the measured bulk flow front position is displayed in Figure 8. Starting from the origin the bulk flow front seems to propagate slower than the simulated one (region I). A difference of about 2 mm is fully developed at 8 to 10 seconds after the injection had started. At this time the positions derived from the measurements seem to lag behind the simulation constantly until the 77<sup>th</sup> second (region II). During the last 16 seconds the flow in z-direction seems to accelerate so that the lag decreases to zero (region III). The coincidence of the simulation with the measurement at  $z = 13.8$  mm (Figure 8) is compelled by the measurement based iteration of the transverse permeability. It is questionable that the measured curve reflects the real bulk flow front propagation in z-direction, because with increasing distance from the injection port the flow velocity can only decrease due to the continuity law.

Running ahead the bulk flow the capillary flow front emerges as the governing interface for the ultrasound transmission. In Figure 8 the line with the white rhombuses represents the propagation in z-direction of the capillary flow front. A new sound speed  $c_1^* \approx 435$  m/s is calculated from the time-of-flight measured at the observed arrival of the capillary flow at the upper mould face after 77 seconds. The sound speed  $c_1^*$  is herewith assumed as an averaged constant of the two volumes impregnated by capillary flow and bulk flow. The correlation between the position of the bulk flow front and injection time can be derived from the capillary flow front position assuming the existence of a proportional correlation. The scaling factor is defined as the ratio of the arrival times of both flow fronts at a reference point (e.g. the mould face). The measured references at 6.9 and 10.35 mm endorse the applicability of the described approximation.

#### ICMAC - International Conference for Manufacturing of Advanced Composites

It is seen that the discrepancy between the recalculated and simulated flow front positions is caused by the arbitrary structure of the applied multi-axial non-crimped fabric, which cannot be modelled accurately, yet.

#### CONCLUSIONS

The objective of this work is the development and testing of an equipment, which enables continuous and high resolution monitoring of the transverse resin flow front propagation through a fibre preform in a three dimensional impregnation scenario. Another feature of the applied ultrasound transmission principle is a much lower preparation effort as it is required for existing techniques, which are mostly based on embedded sensors. The time an ultrasound wave requires for propagating from the sound source to the receiver is influenced by the position of the flow front of a liquid, which is impregnating a fibre preform. At the current stage of this work a linear model is assumed for calculating bulk and capillary flow front propagation from time-of-flight measurements. The applicability of the model is endorsed by reference measurements. A value of the transverse permeability is obtained from emulating the performed point injection of a thick-sectioned laminate by numerical simulation.

#### ACKNOWLEDGEMENTS

This work is part of the research programme FOR 360/1-1 funded by the Deutsche Forschungsgemeinschaft, DFG.

#### REFERENCES

1. Benjamin W., 'Resin Transfer Moulding, Sampe Monograph No.3', Sampe International Business Office, (Covina), 1999
2. Weitzenböck J.R., Composites: Part A 30 (1999), 781-796
3. Trochu F., 9th International Conference on Composite Material (ICCM/9), Madrid, (12-16 July 1993), III, 481-488
4. Mogavero J., Polymer Composites V18 (1997), 649-655
5. Stedile, 'Felt Permeability Testing Apparatus', US Patent No. 3,577,767, 1971
6. Parnas R.S., Polymer Composites, V16; N6 (1995), 429-445
7. Han K.K., Composites Science and Technology 60 (2000), 2435-2441
8. Lekakou C., Composites: Part A 29 A (1998), 29-37
9. Pillai K.M., Polymer Composites V19, N1 (1998), 71-80
10. Ballata W.O., Reinforced Plastics and Composites V18, N16 (1999), 1450-1463
11. Walsh S.W., 'In-situ Sensor Method and Device', US Patent No. 5,210,499, 1993
12. Lim S.T., Composites Science and Technology 60 (2000), 961-975
13. Weitzenböck J.R., Composites: Part A 29 (1998), 159-169
14. Kissinger C., Advancing with Composites 2000, Milan, (9-11 May 2000) 93-98
15. Krautkrämer J., 'Werkstoffprüfung mit Ultraschall', Springer Verlag (Berlin), 1981

**Manufacture of Thick Composite Primary Structures using Resin Transfer Infusion**

**Dr Graeme Wright (Bombardier Aerospace – Shorts, N Ireland)**

**Introduction**

It is recognised within the aerospace industry that composites offer weight savings, corrosion resistance and resistance to fatigue over equivalent metal designs. This technology has been applied to primary structures within the Bombardier Aerospace – Shorts, most notably the Global Express Horizontal Stabiliser. A major barrier to exploitation of composites has been cost; all recent research activity has focussed on developments offering clear cost benefits.

Bombardier Aerospace – Shorts has developed a technology over the last ten years called Resin Transfer Infusion (RTI). Simplistically RTI is combining aerospace grade resin and a consolidated pre-form within a sealed tool using an autoclave to promote consolidation and resin flow. RTI compliments Resin Transfer Moulding (RTM), and is more applicable to thick structures.

RTI offers ;

- Reductions in lay-up time
- No pre-pregging costs
- No out-life constraints
- Improved dimensional tolerances
- Lower raw material costs
- Ability to co-cure stiffeners.

This paper details the procedure used to manufacture a representative wing skin section. The section selected was the pylon attachment area, which ranged in thickness from 10mm to 30mm, incorporated both chord-wise and span-wise ply drop-offs, and five blade stiffeners.

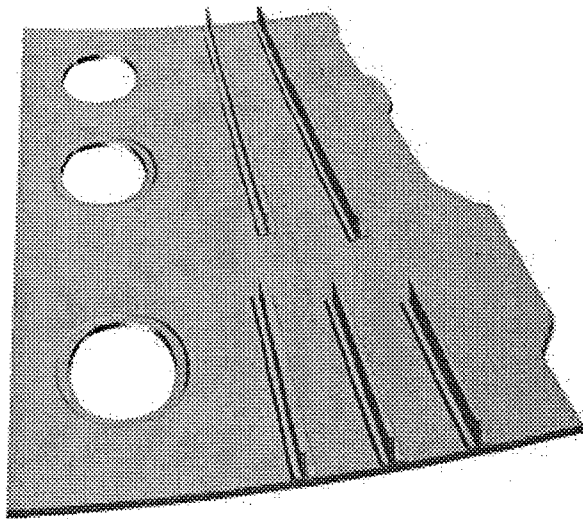


Figure 1 - Schematic of Wing Skin Demonstrator

In the RTM and RTI processes it is necessary to build up the shape of the component using dry fabric, prior to the injection of resin. To minimise cost Non Crimp Fabric carbon fibre plies were utilised, manufactured in Europe. An Engineering Drawing and mylar were generated stipulating the lay-up sequence, fabric type and relative position of each ply. Plies were pre-cut using an ultrasonic knife and supplied in packs to Bombardier Aerospace - Shorts. Lay-up was performed on a flat table in a 'clean air' room facility. To assure ply location a frame was positioned around the periphery of the tool corresponding in size to the oversize mylar. Build up plies were positioned using the mylar and were tacked in place at each corner using a soldering iron.

One of the most time consuming operations during pre-forming is the hot ply debulking operations performed at elevated temperature, under vacuum, every 3 to 4 plies. To reduce cycle time the entire pre-form stack was laid up flat, bagged up using a traditional nylon bag, and compressed at 120°C and 33psi in an autoclave for 60 minutes. The pre-form thickness was approximately 20% above the envisaged cured ply thickness of the wing skin.

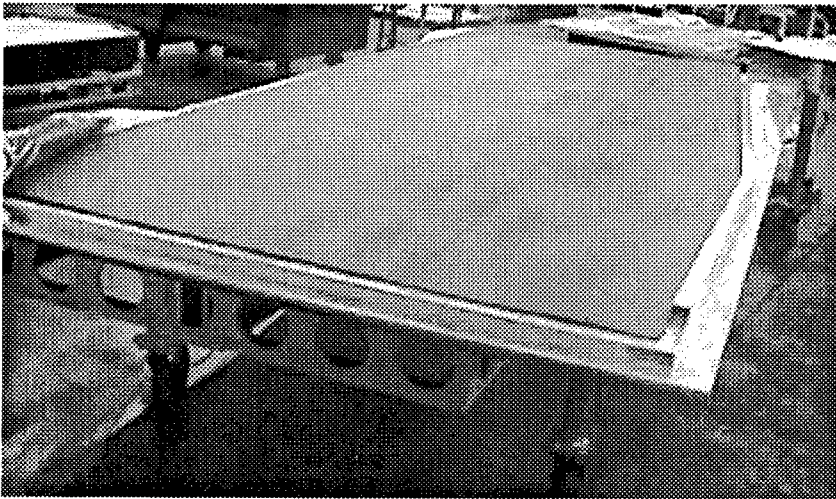


Figure 2 - NCF Plies prior to Pre-forming

Stringer sections were pre-formed on an inexpensive lay-up only tool, and were debulked using a rubber diaphragm tool. Consolidation was performed using a vacuum source. Heat was provided using infrared bulbs. The debulking cycle was as per manufacturers instructions. Once the stringer section was complete, it was cut to length and tapered at the stringer feet using an ultrasonic knife. The stringers were supported by rubber mandrels and attached to the main skin using a dedicated rubber bag. Tooling was designed and manufactured capable of producing the blade stiffened wing skin section.

To minimise mismatch it was considered essential that only materials with compatible coefficients of thermal expansion were considered. Only two materials possess the necessary characteristics, Invar and composite tooling pre-preg. Initial calculations suggested that a complete Invar wing skin tool could weigh in excess of 17 tons, hence Composite tooling was selected. The Outer Mould Line tool was manufactured using a tooling pre-preg with long out-life, good flow characteristics and low, flexible curing parameters. Provision for a silicon O-ring, location dimples, laser targets, access door locations and end of part lines were incorporated in the tool.

The Inner Mould Line tool was manufactured from poly-acrylic rubber and tooling pre-preg providing rigidity where dimensional accuracy is required, and flexibility where extra consolidation is required. Injection and vacuum ports were sited at key locations based on a combination of flow modelling and previous experience.

ICMAC - International Conference for Manufacturing of Advanced Composites

The pre-form was clamped between the IML and OML before being positioned into the autoclave for the injection.

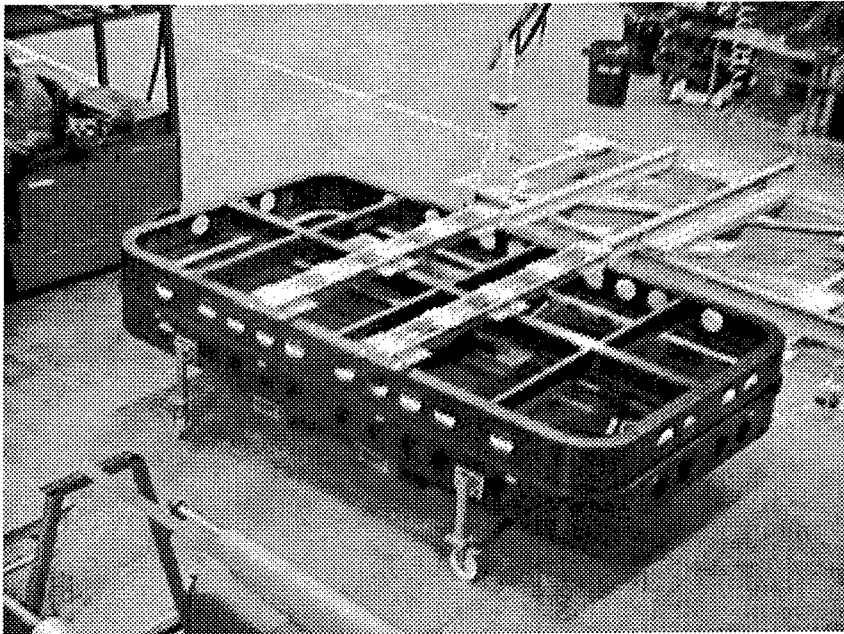


Figure 3 - Tooling Assembly prior to Injection

A large injection vessel was designed and manufactured capable of holding, heating, degassing and injecting up to 100kg of resin. Pipe work from the pressure vessel was routed through the autoclave shell and connected to the Inner Mould Line bag by special fittings. Representatives from the autoclave manufacturer had critiqued the modification. The pipe work was insulated to ensure temperature equilibrium through the system. A series of tests were performed to ensure vacuum integrity of the system. The resin was heated in an oven adjacent to the pressure vessel and poured into the vessel in 5kg increments until 70 kg of resin had been introduced. The temperature of the resin was increased and the resin was degassed.

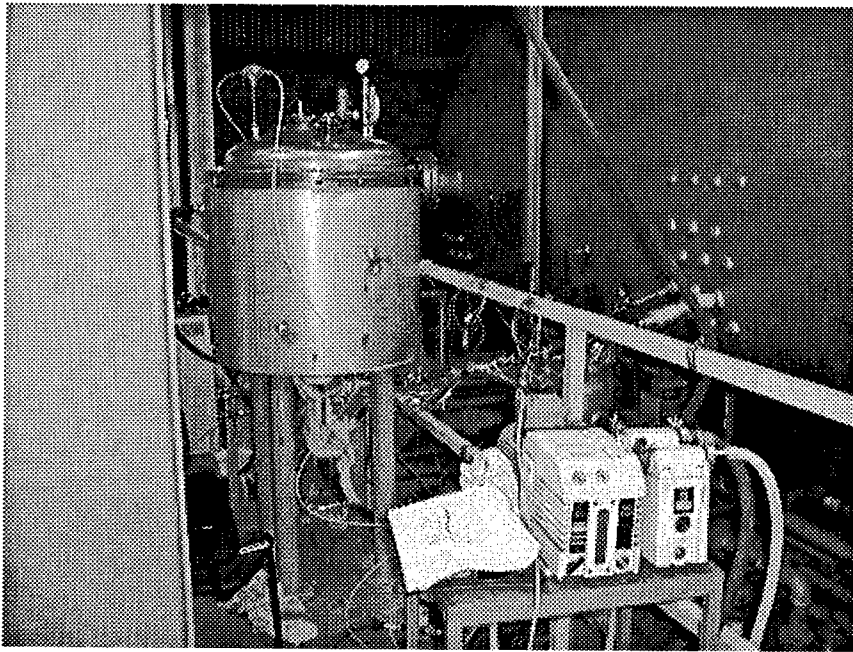


Figure 4 - The injection System

A series of tests were performed to check the vacuum integrity of the system. The autoclave door was shut and the temperature increased to 120°C at 1°C per minute. When the temperature of the NCF stack had achieved equilibrium the valve was opened and the resin was injected through the autoclave wall and into the mould. Once the correct mass of resin was introduced the autoclave pressure was increased to force the resin through the NCF stack. After 30 minutes the autoclave pressure was reduced, and excess resin ejected into a resin dump. The pressure was ramped back up and the mould heated from 120°C to 180°C and held for 120 minutes to fully cross-link the epoxy matrix. The component was cooled down at a controlled rate to 60°C.

After cure the autoclave was opened, the pipe work disconnected, the tool removed and the component demoulded.

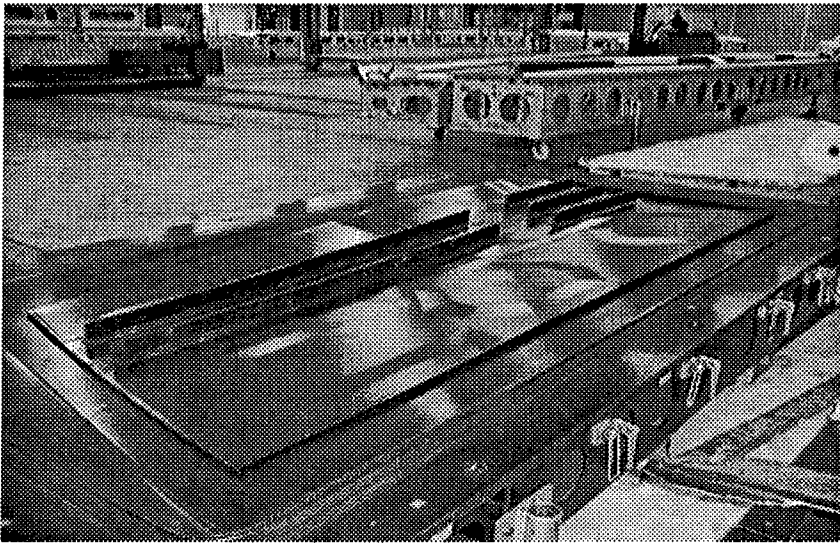


Figure 5 - The Cured Wing Skin Demonstrator

Visual examination showed that the component was well defined, with plies well consolidated and changes in thickness well defined. NDT showed the component to be porosity free. Several off-cuts from the wing skin demonstrator were supplied to the Test Laboratory for micro-examination. Specimens were extracted from the off-cuts, polished using 1200 grade emery and viewed through a metallurgical microscope. Photographs were taken of areas of interest. These confirmed the NDT results that the structure was indeed porosity free.

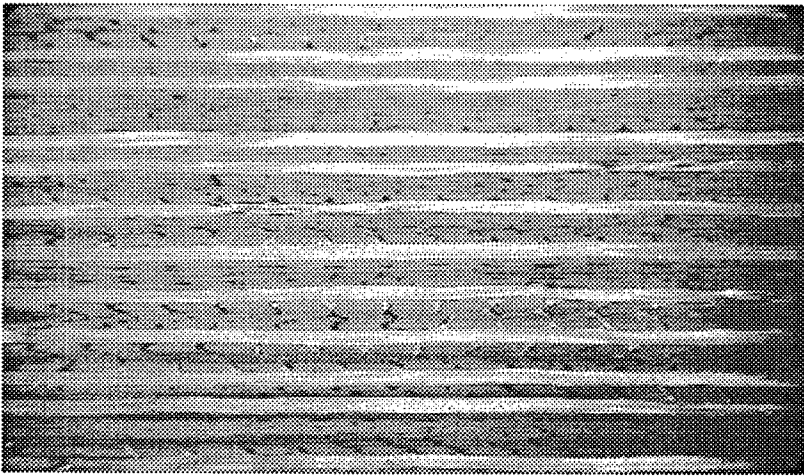


Figure 6 - Typical Micro-section Through Wing Skin Demonstrator

### Conclusions

Manufacture of a thick, complex wing skin demonstrator has shown Resin Transfer Infusion to be a process suitable for aerospace applications. The panel incorporated five co-cured stringers, weighed 159 kg and had an average fibre volume in excess of 55% (by adjusting the process parameters the nominal Vf can be increased to values above that currently for UD prepreg, if required).

By using this technology it is envisaged that significant cost savings can be realised over traditional pre-preg processing, without compromising quality.

**Recent Advances in Glass Fiber Preforming:  
Implementation of the Ford Programmable Preform Process  
(F3P)**

James E. deVries, Norman G. Chavka and Jeffrey S. Dahl  
**Ford Motor Company**

**ABSTRACT**

F3P (Ford Programmable Preforming Process) is a new preforming process that has been developed and implemented to produce high quality glass fiber preforms utilized in semi-structural and Class "A" composite automotive components. The system is a highly automated process that produces low cost, net shape glass preforms, resulting in a scrap rate of less than 3%. This process differs from previous systems by providing offline robotic programming, state-of-the-art chopper gun technology, and other machine and process improvements. A combination of a high output chopper gun (4kg/min) and a fast curing binder affords the production of large component preforms every 4 minutes, making the F3P technology a viable manufacturing option for automotive production volumes. Preforms manufactured by F3P and subsequently molded by Resin Transfer Molding (RTM) have successfully been utilized to supply the composite bodysides and upper cargo deck for production of the Aston Martin Vanquish, released in April of 2001. The F3P preforming process as it relates to the manufacture of these components will be discussed.

**SESSION 2:  
TEXTILE TECHNOLOGY &  
MODELLING**

**GEOMETRICAL MODELLING BASED PROCESS CONTROL OF A TRIAXIAL BRAIDING MACHINE WITH A FLEXIBLE MANDREL SYSTEM.**

**P Potluri, A Rawal, M Rivaldi and I Porat  
Textile Composites Group  
Department of Textiles, UMIST, Manchester UK**

**ABSTRACT**

Braiding is a relatively less explored textile process for producing composite preforms. Biaxial braids can be produced as hoses and subsequently be draped over different three-dimensional surfaces. However, triaxial braids are relatively stable structures and should be produced to the desired shape during the braiding process. This is achieved by over-braiding on mandrels that either form part of the finished composite or removed before the moulding process. Triaxial braided composites have superior mechanical properties due to fibre orientations along three directions.

Geometry of a braided structure depends on the number of yarn carriers, rotational speed of the carriers, take-up speed and the effective perimeter of the cross-section of a mandrel. In the present work, a VRML based geometrical visualisation tool has been developed to simulate a braid structure on any predefined mandrel geometry, and using a predefined yarn cross-section. Braid angles, cover factors and yarn volume fractions can be computed from these simulations. A triaxial braiding machine has been developed with an independent servo control of the carrier movement and the take-up mechanism; geometrical simulation is used as an input to the control system to continuously vary the braid structure along the length of a mandrel.

Flexible tooling is important for rapid product development. A flexible mandrel has been developed that can be mechanically adjusted to change the cross-section and the taper. This system enables rapid development of braided preforms.

**INTRODUCTION**

Braiding is the formation of comparatively narrow rope-like structures by interlacing diagonally three or more strands of yarn. In conventional braiders, yarn carriers rotate along a circular track; with half the carriers rotating in a clock-wise direction while the remaining carriers rotate in counter clockwise direction, similar to a maypole arrangement. As a result, the two sets of yarns *interlace* with each other at a bias angle to the machine axis. Braiding has traditionally been used for producing textile structures such as shoelaces and ropes. However, in recent years, development of fibre-reinforced composites and medical implants has become an interesting application area. By using 3-dimensional mandrels, one can produce 3D textile preforms for applications such as aircraft rotor blades. Braided structures are similar to woven structures in terms of the topology of yarn interlacement. For example,

Diamond, Regular and Hercules braids are similar to Plain, 2/2 Twill and 3/3 Twill weaves respectively. Braided structures have a number of advantages over woven broadcloth:

- Woven fabrics have orthogonal interlacement while the braids can be constructed over a wide range of angles, from  $10^\circ$  to  $85^\circ$ .
- A set of axial yarns can be introduced to the braiding process to produce triaxial braids (fig 1); triaxial braids are more stable and exhibit nearly isotropic properties.

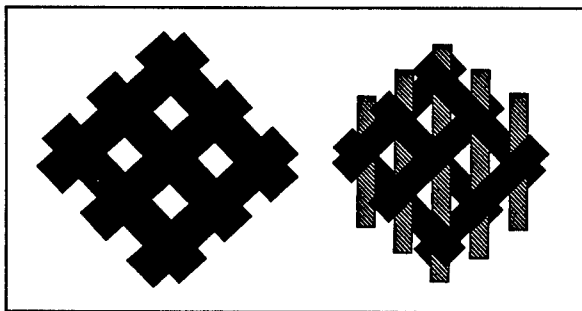


**Figure 1 Biaxial and Triaxial braids (1)**

- Braids can be produced either as seamless tubes or flat fabrics with a continuous selvedge (fig 2). Composites produced with the braided preforms exhibit superior strength and crack resistance in comparison to broadcloth composites.
- Composites with braided holes exhibit about 1.8 times the strength in comparison to cut holes.(fig 3).

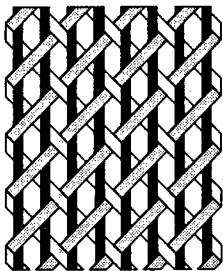
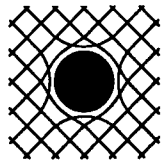
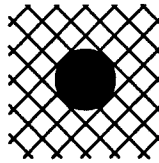


**Fig 2: Triaxial braid with a selvage**



**braided hole  
(without yarn end)**



**cut hole**

**Fig: 3 Braided hole vs cut hole**

- Braids are relatively narrow structures. Recently, employing a large number of yarn carriers and relatively coarse tow has produced several inches wide fabrics. The cost model developed by Mills (2) demonstrated that the level of wastage is proportional to the width of the fabric and hence it is desirable to use narrow fabrics.

Although braiding is an ancient technique, systematic analysis of the braiding process did not start until the 50s. The first reported work on the braid formation was conducted at UMIST by Brunschweiler (3). Douglass (1) published a book on braiding, which is still the only book on this topic. Similar work was reported by Weber (4) and others in Germany during the late 60s. Application of braiding technology to composites was first investigated by the researchers at McDonnell Douglas Aircraft Company in the 70s. Ko (5) researched extensively into braiding for composites.

Tubular and flat braids produced by conventional braider are generally classified as 2D structures, although using complex mandrels can also produce 3D composites. Machines for through-the-thickness 3D braided structures were developed by the Atlantic Research Corporation (6,7). The carriers can be configured in both the Cartesian and circular arrangements, and the through thickness interlacement is achieved by shifting the yarn carriers from one track to other. Similar machines were also developed by Tada (8), Wulfhorst (9) and a number of other research groups in recent years. 3D braiding machines produce superior composites with increased toughness and delamination resistance. However these machines are very expensive and the production rates are not high. In the present work, an attempt has been made to use maypole braiding technology, along with sophisticated controls, to produce complex 2D and 3D parts.

#### **MAYPOLE BRAIDING**

The maypole braider is a relatively simple mechanism to control. It has two sets of yarn carriers rotating on a circular track. One set rotating in the clockwise direction and the other set rotating in the counter clockwise direction, and during this process, they interlace with each other to form a tubular braided structure. The yarn carriers are propelled by horgears

through a slot on the track plate. The braided structures are either produced as sleeves that can be draped over a component, or produced directly over a mandrel. Braiding over a mandrel is a preferred option for composites, which gives a better control over the yarn orientations. A take-up mechanism moves the mandrel at a predetermined speed. Mechanics of braid formation can be described by simple mathematical relations (10,11).

Each yarn forms a helical path around a mandrel. The helix angle ( $\alpha$ ) with respect to the braid axis is the most important parameter in the braiding process. Figure 4 shows the yarn path that depends on the rotational speed of the yarn carriers ( $\omega$ ) and the take-up speed ( $v$ ). The direction vectors are as shown in figure 5. The braid angle ( $\alpha$ ) can be calculated using the relation,

$$\alpha = \tan^{-1}\left(\frac{\omega R}{v}\right) \quad (1)$$

- $\alpha$  = Braiding angle (between threads and vertical direction) (radians)
- $R$  = Radius of cylindrical mandrel (cm)
- $v$  = take-up speed (cm/sec)
- $\omega$  = average angular velocity of bobbins around the machine centre (radians/sec)

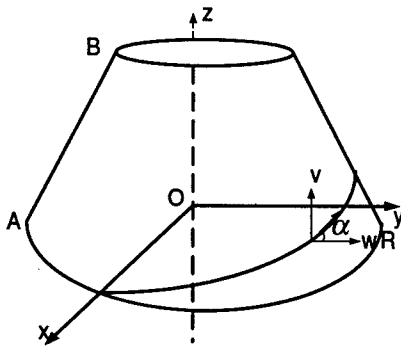


Fig 4: Yarn Path on a mandrel

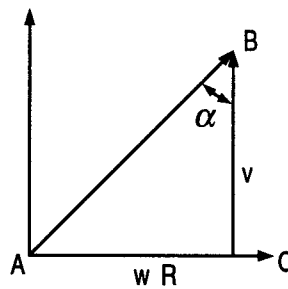
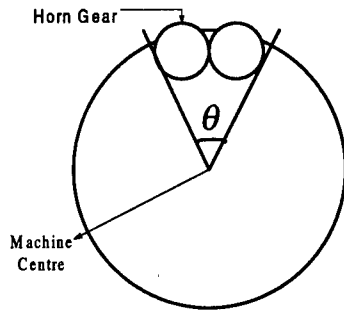


Fig 5: Direction vectors for take-up and carrier rotations

The relation between the horn gear speed and the yarn carrier speed around the machine centre can be established as follows:

- $\omega_h$  = average angular velocity of the horn gears around their own centre (radians/ sec)
- $N_h$  = number of horn gears.
- $t$  = time taken by the horn gear to make one revolution (sec)
- $\theta$  = Angle made by a pair of adjacent horn gears at the machine centre (radians)(fig 6)



**Figure 6: Horn gears on the track**

By the time a horn gear makes one revolution, the yarn carrier rotates by  $\theta$  around the machine centre.

Therefore, the average angular velocity of the bobbins around the machine centre is given by:

$$\omega = \frac{\theta}{t}$$

Time taken by the horn gear to complete one revolution ( $t$ ) =  $\frac{2\pi}{\omega_h}$

$$\theta = \frac{2\pi}{(N_h/2)} = \frac{4\pi}{N_h}$$

Combining the above equations results in:

$$\omega = \frac{2\omega_h}{N_h} \quad (2)$$

Braid angle in terms of horn gear speed;

$$\alpha = \tan^{-1} \left( \frac{2\omega_h R}{N_h v} \right) \quad (3)$$

### GEOMETRICAL MODELLING

Geometry of the braided structure depends on a number of parameters including the carrier speed, take-up speed, mandrel geometry and the yarns cross sections. Geometrical models are useful to visualise the braided structures before manufacturing so that they can be optimised for a desired performance criteria: specified fibre orientation, fibre volume fractions etc. These models can also be used as 'virtual' braids for flow and thermo-mechanical analysis. In the present work, the geometrical models are also used for generating the machine-control instructions.

The geometry of the braid structures was simulated using VRML (Virtual Reality Modelling Language). VRML is a computer language used for describing objects in a scene, using simple text files. VRML codes are not compiled, but are simple ASCII text that can be parsed by a VRML interpreter. These interpreter programs (or parsers) are often called VRML Browser. VRML file names end with the .wrl extensions (sometimes pronounced dot world).

Braided structures have a number of yarns following a helical path in both clockwise and counter clockwise directions. A yarn is created by sweeping a 2D cross-sectional area along a 3D path. The cross-sections can be circular, elliptical, racetrack or lenticular. In the present work, the co-ordinates for the yarn path are calculated using Delphi, based on simple mathematical relations.

For example to generate the yarn around the cylinder of radius ( $r$ ), as shown in the Figure 7, with helix angle ( $\alpha$ ) so the 3-Dimensional coordinates are as follows:

$$\begin{aligned}x &= r \cos \theta \\y &= \pm r \sin \theta \\z &= r\theta \cot \alpha\end{aligned}\tag{4}$$

The value of  $\theta$  ranges from 0 to  $2\pi$  to create one complete helix. In equation (4) the positive value axis shows yarn in clockwise direction, and the negative value shows yarn in counter clockwise direction.



**Fig 7: Yarn path in clockwise and counter clockwise directions**

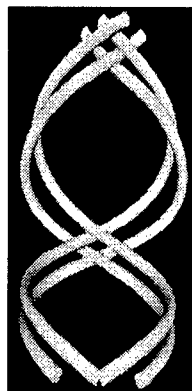


**Fig 8: Yarn path with interlacement**

Figure 8 shows a yarn interlacement model which gives a more realistic simulation.

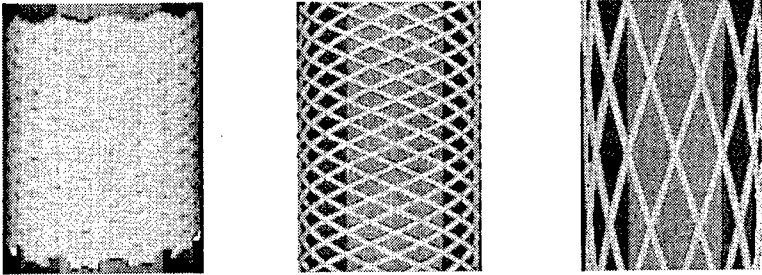


Figure 9: Simulation of braid structures by varying the take-up speed

The effect of changing the take-up speed, and hence the braid angle is shown in figure 9. The maximum braid angle (lock limit) is obtained at a very low take-up speed. As the take-up speed increases, the braid angle decreases, and hence the cover factor.

The cover factor may be defined as the percent of the mandrel surface covered by the yarns. This factor can be related in terms of yarn volume fractions (YVF), which is a commonly used factor in the composites industry.

$$C = \frac{W_y N_c}{2\pi R \cos \alpha} - \left( \frac{W_y N_c}{4\pi R \cos \alpha} \right)^2 \quad (5)$$

where,

C= cover factor

$W_y$ = yarn width

$N_c$ = number of yarn carriers

R = effective mandrel radius

$\alpha$  = braid angle

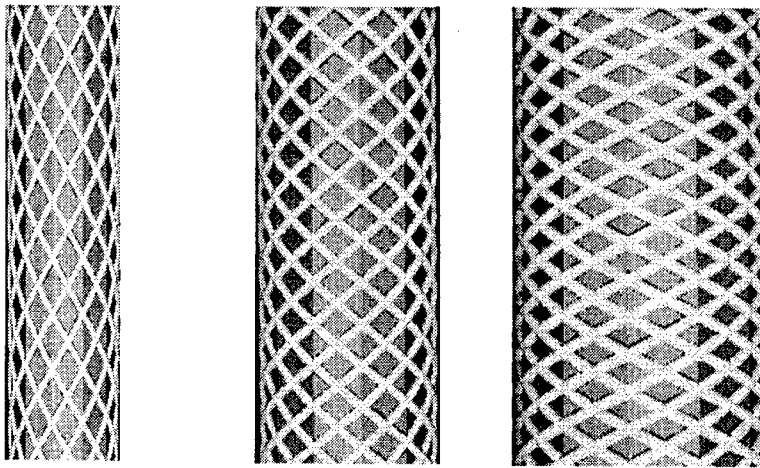
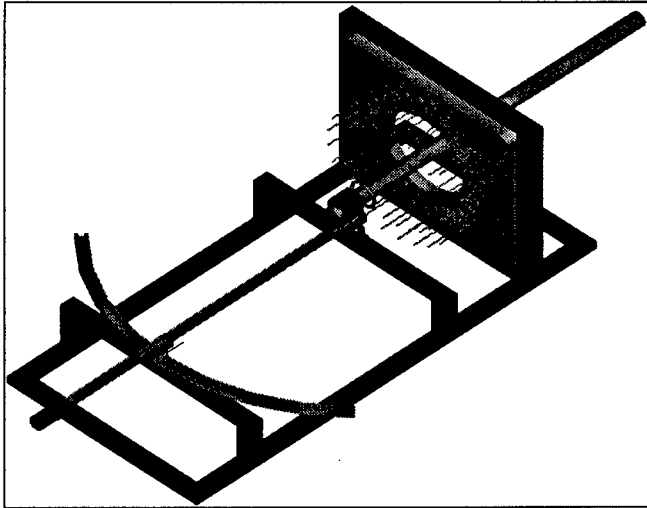


**Fig 10: Simulations with changes in the mandrel diameter**

The braid angle, and hence the cover factor, increases with the increase in mandrel diameter, until the lock limit is reached (fig 10). Of course, there will be an upper limit to the mandrel diameter that can be accommodated in a braiding machine.

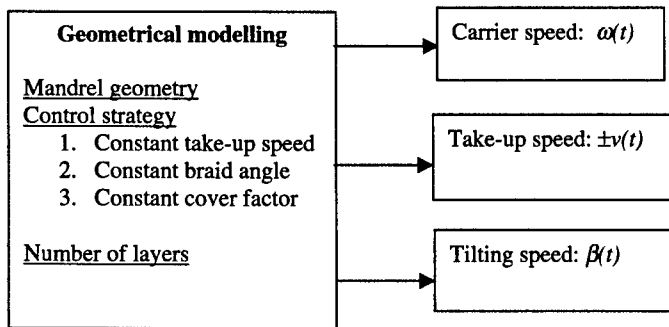
#### **COMPUTER-CONTROLLED BRAIDING MACHINE**

Figure 11 shows the layout of the braiding machine. A conventional maypole braider plate is mounted in a vertical plane. This arrangement is convenient for over-braiding on mandrels. The horn gears are driven by a pair of motors (synchronised) and their speeds can be continuously varied from zero to the maximum machine speed. Mandrel movement is controlled by a ball-screw driven take-up system. A DC servomotor drives the ball-screw; both the speed and the direction can be continuously changed to achieve a desired braid angle. The mandrels are attached to the ball-screw as cantilevers, and hence only lightweight foam materials are suitable. A set of axial (warp) yarns is fed from a creel to create triaxial braid structures, which are superior to traditional biaxial braids.



**Fig: 11 Computer-controlled braiding machine**

Mandrels can be driven both forwards and backwards, at a desired speed, to deposit a number of braid layers. This gives the potential of producing composites with a variable wall thickness. The ball-screw is pivoted with respect to the point of braid formation to accommodate mandrels with 1D bends (the mandrel geometry is resolved into polar coordinates to compute the take-up and tilting speeds). Figure 12 describes the geometrical modelling-based control of the braiding process. At first, a geometrical model is created taking into consideration the mandrel geometry, the number of layers at each position on the mandrel, the braid angle and the cover factors. Instructions for machine control are generated section by section for each mandrel position. The machine can be controlled for maintaining a constant take-up speed, a constant braid angle or a constant cover factor (hence a constant Yarn Volume Factor). In this machine, both the carrier and take-up speeds can be continuously variable thus providing a much better control over the braiding process in comparison to controlling only the take-up speed.



**Fig 12: Machine control based on geometrical modelling**

Biaxial braids can be produced either as a sleeve or on a flexible foam core to be subsequently draped into 3D shapes (12). However, triaxial braids must be produced on mandrels that are of the exact shape. The mandrel may form part of the final component or removed prior to moulding. The concept of adjustable or flexible mandrels is proposed (fig:13) for triaxial braids, where the mandrel does not form part of the final product. The adjustable mandrel consists of a number of plates arranged between two end caps; each plate acts as a braid point. In the present version, the plates can be adjusted to create a range of tapered preforms. Further work is under progress to develop mandrels that can be automatically adjusted to change the circumference at a number of sections.

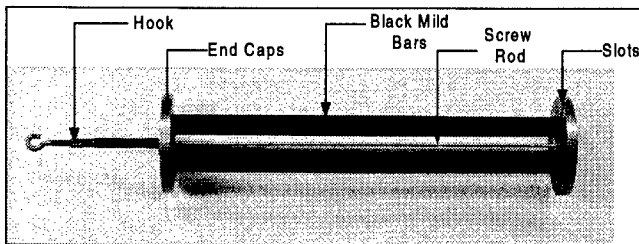


**Fig 13: Concept of an adjustable mandrel**

## CONCLUSIONS

3D braiders are slow-speed and very expensive machines. These machines are suitable for specialised aerospace parts, where cost is not a criterion. Conventional maypole braiders are inexpensive, easily available, flexible and can be run at production speeds. These machines are ideally suited for producing low-cost, high-volume composites. In the present work, a

#### ICMAC - International Conference for Manufacturing of Advanced Composites

computer controlled triaxial braiding machine was developed by adopting a commercial maypole braider. Triaxial braided composites are stronger in comparison to woven or biaxial braids, and exhibit nearly isotropic behaviour. VRML based geometrical simulations were developed for visualising the braided structures. These simulations are also useful in optimising the machine parameters during the braiding process.

#### REFERENCES

1. Douglass W, Braiding and Braiding Machinery, Phillips Tech. Lib, 1964
2. Mills A, Composites: Part A 32(2001) 955
3. Brunschweiler D, Journal of the Textile Institute, 45 (1954), T55.
4. Weber W, Band und Flechtindustrie, 1 (1969), 109
5. Ko F K, in 'Engineering Materials Handbook Volume 1: Composites' ASM International, 1987.
6. Brown R, Through-the-thickness braiding technology, 30<sup>th</sup> National SAMPE Symposium, 1985.
7. Weller R A, A new method of composite reinforcement braiding, 3-D Composite Materials, NASA Conference Publication 2420, November 1985.
8. Tada M, Osada T, Nakai A, Hamada H, Proceedings of 6<sup>th</sup> International SAMPE symposium, Tokyo, 2000.
9. Laourine E, Schneider, Wulfhorst B, Production and analysis of 3D braided textile preforms for composites, Texcomp 5, 18 September 2000, Belgium.
10. Du, G W, Popper P, Journal of the Textile Institute, 85 (1994)316.
11. Zhang Q, Journal of Manufacturing Science and Engineering, 121(1999), 345.
12. Potluri P, Francke M, Day R, Flexural and Torsional Properties of Biaxial and Triaxial Braided Composites for Compliant systems, *European Conference on Composite Materials (ECCM 9)*, Brighton, UK, June 2000

**WISETEX – VIRTUAL TEXTILE SOFTWARE**

**S.V.Lomov<sup>\*†</sup>, I.Verpoest\***

A software package *WiseTex*, a simulation tool for textile structures, is described. The current version of *WiseTex* covers 2D and 3D woven fabrics, 2D braids, 2D braids with inlays and unidirectional multilayered preforms. It features geometrical simulation of a textile, including 3D imaging of the repeat, and simulation of compression of the fabric.

**INTRODUCTION**

Software for simulation of the internal geometry of a fabric is a “must” tool for a designer of industrial or apparel textiles. Whatever is the fabric usage, its structure plays a key role in the performance parameters. One can say that fabric properties are properties of its yarns and fibres, transformed by the structure. The precise knowledge of the internal geometry is of primary importance for such application fields as filters (find the smallest particle stopped by it), composites reinforcements (compute resin flow through the reinforcement and mechanical properties of the composite), paper-making machines clothing (compute air and water permeability through a dryer net), weaving/knitting technology (what is the length of yarns for a given fabric length) etc.

There are some CAD/CAM software tools for textiles available. The disadvantages of them are first, they cover only simple structures and yarn geometry (e.g. circular cross-sections) and that they lack generality, and, second, that they are purely geometry modelling tools, without any reference to mechanical properties of yarns [1-6]. The challenge of the *WiseTex* development is to implement a universal mechanical model of textile structure, which would handle very different and complex topologies of yarn placement and would represent the complex mechanical behaviour of yarns inside the structure.

This development can be summarised as the creation of a **virtual textile**, using knowledge of textile material science gained over the past 60 years. The software uses theories and algorithms, developed since early 90-ies [7-13] and extensively published recently [14-22].

**AIM AND SCOPE**

*WiseTex* serves as:

- Software for modelling of the internal geometry (including 3D imaging) and mechanical behaviour (compressibility in the current version) of textile structures.
- Integrated Textile Preprocessor for hydrodynamical, meso-mechanical and finite elements software packages providing description of the internal geometry and mechanical behaviour of textile structures.

---

\* Department of Metallurgy and Materials Engineering, Katholieke Universiteit Leuven, Belgium

† on leave of absence from St.-Petersburg State University of Technology and Design, Russia

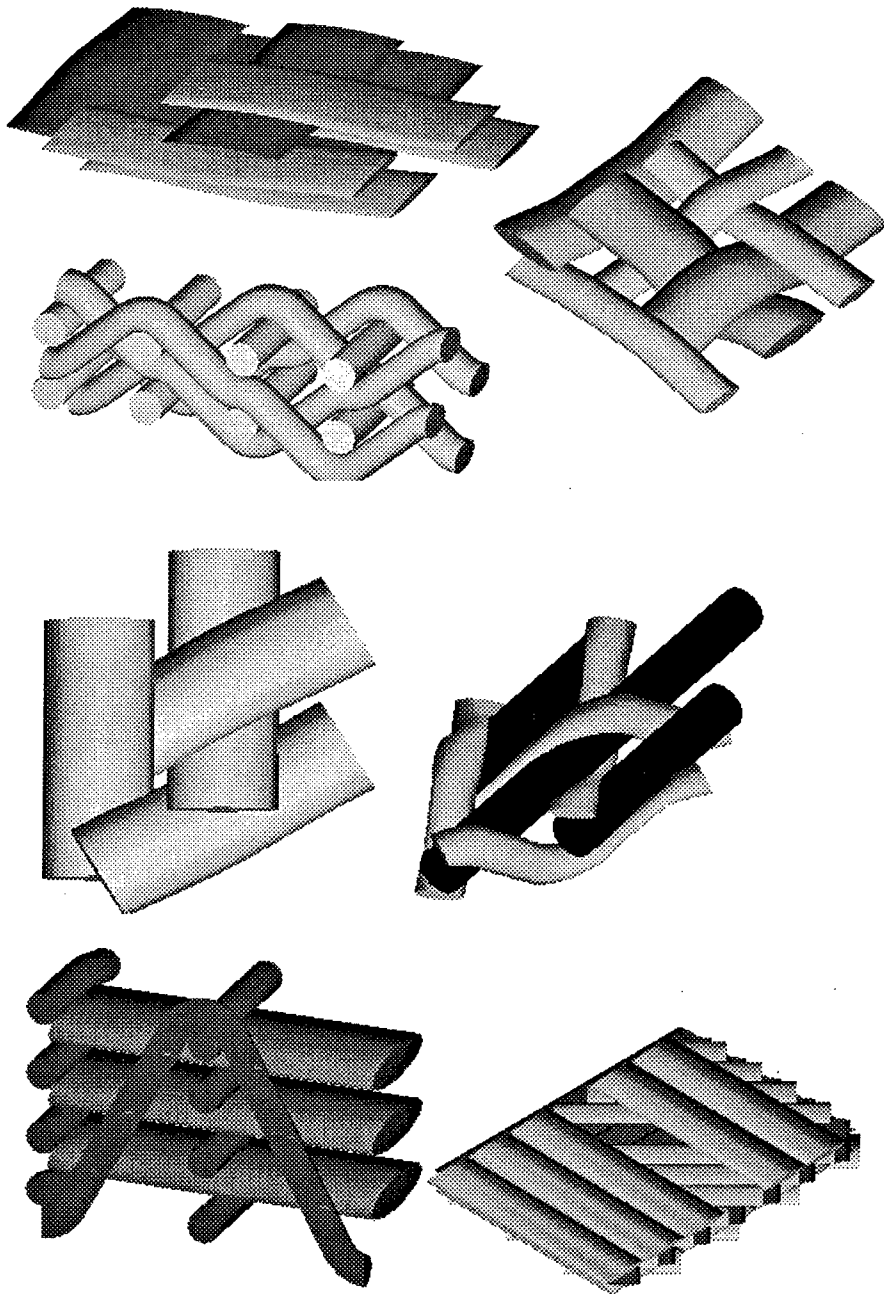


*Fig.1. Examples of structures simulated by WiseTex*

The current version (1.4) covers the following textile structures (Fig.1):

- 2D woven fabrics
- 3D woven fabrics
- 2D braids
- 2D braids with inlays (can also be used to simulate multi-axial woven fabrics)
- multilayered unidirectional (non-crimp) preforms

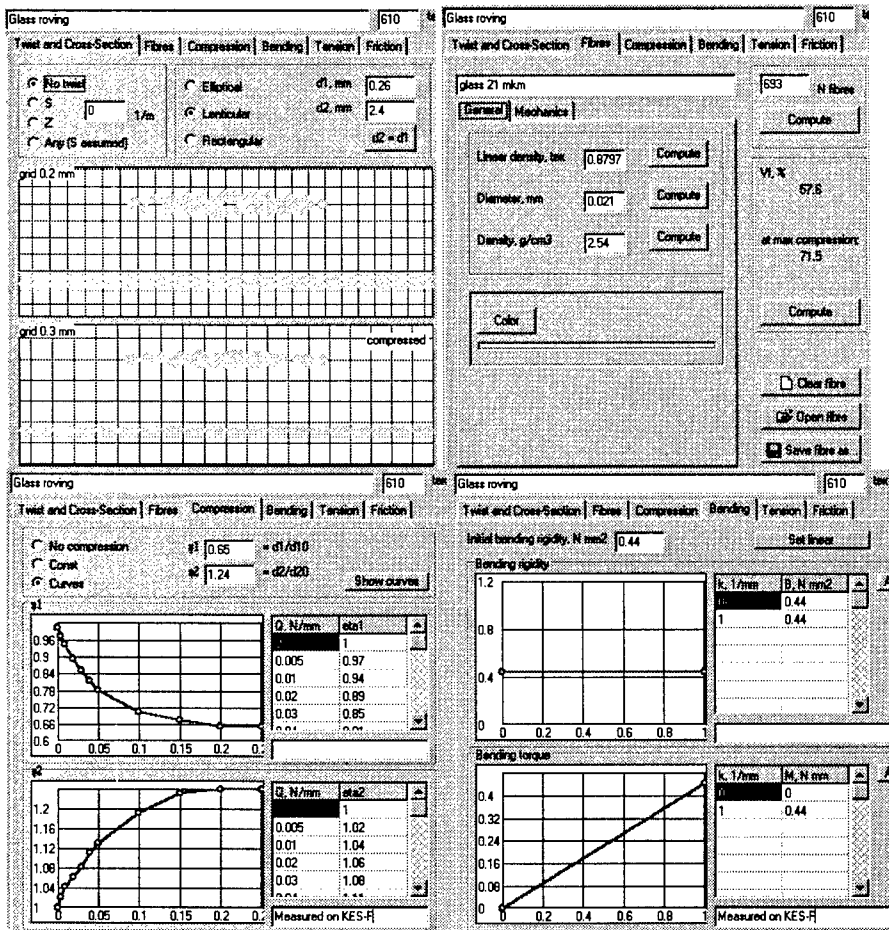


Fig.2. WiseTex input data: yarn properties

## PRINCIPLES OF THE GEOMETRICAL MODELLING OF TEXTILES

Textile materials are characterised by the distinct hierarchy of structure, which should be represented by a model of textile geometry and mechanical behaviour. In spite of a profound

investigation of textile materials and a number of theoretical models existing in the textile literature for different structures, a generic model covering different structures is not available. *WiseTex* takes full advantage of the hierarchical principle of textile modelling, creating a truly integrated modelling and design tool. The simulation algorithm uses extensively the minimum energy principle. It allows handling of complex textile structure, with computer computations times counted in minutes, instead of hours or days needed for FEM implementations of the same non-linear, non-conservative behaviour of yarns in compression and bending.

*WiseTex* considers a single repeat (unit cell) of the fabric. Assume as given (input user data):

- Yarn properties: geometry of the cross-section, compression, bending, frictional and tensile behaviour (Fig.2);
- The topology of the yarn interlacing pattern within the fabric repeat (Fig.3);
- The yarn spacing within the repeat (Fig.4).

The problem is to compute the spatial placement of all yarns in the repeat:

- Determine the spatial placement of all the yarn heart-lines within the repeat;
- Define the yarn cross sectional shape and its dimensions normal to the yarn heart-line for each point along the yarn heart-lines.

This problem is treated in accordance with the hierarchy of a textile structure: considering the sequence of hierarchical levels “fibres – yarns – fabric”, the focus is on the highest level (i.e. the “fabric”). The properties of the elements from the preceding level (“yarns”) together with their interlacing pattern (“topology”) enter the solution via the minimum energy principle.

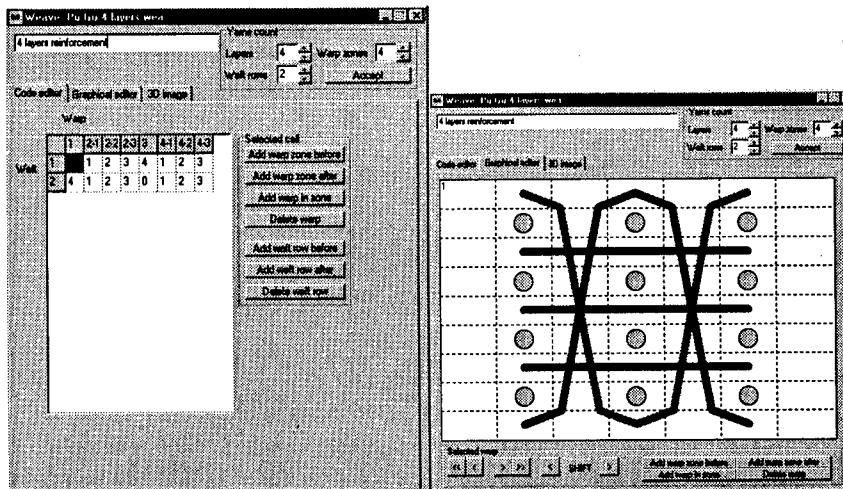


Fig.3. WiseTex input data: code and graphical editors for weave structure

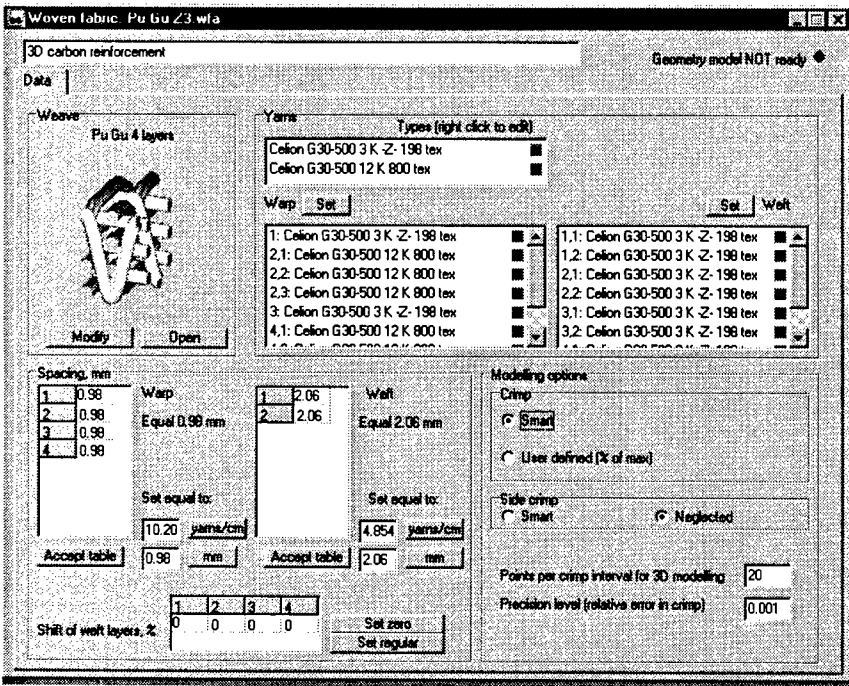


Fig.4. WiseTex input data: full description of woven fabric

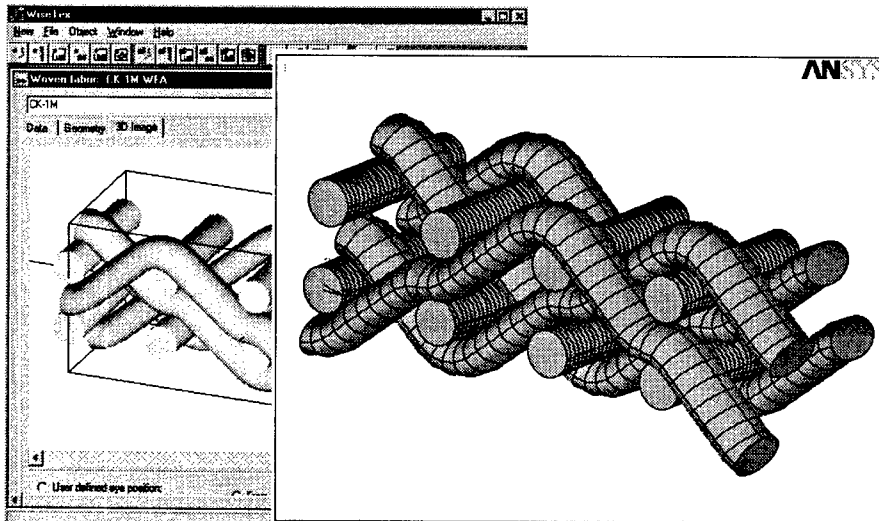


Fig.5. WiseTex as a preprocessor for ANSYS finite element package

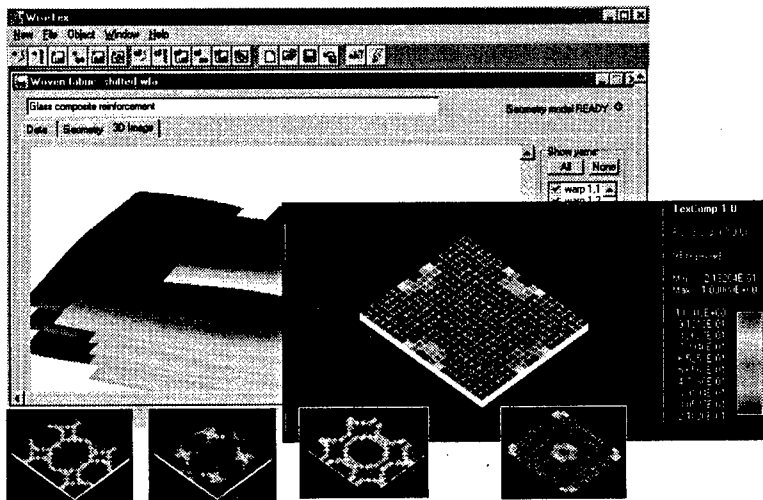


Fig.6. WiseTex as a preprocessor for TexComp – software for micro-mechanical modelling of textile composites

The geometrical models provide the following output:

- Overall geometrical characteristics: unit cell dimensions (including thickness), mass per unit surface area, average porosity/fibrous content and yarn lengths in the unit cell.
- For any point within the unit cell: the fibrous content, the average orientation and an identification of the fibre material in the vicinity of the point.
- Yarn path geometry, position and size of the yarn cross-sections, fibre density and orientation distribution over the yarn cross-section for arbitrary points on any yarn within the fabric repeat.

The description of the internal fabric geometry can be used for various purposes:

- Visualisation: creation of a 3D picture of the unit cell with rotating, zooming and sectioning capabilities;
- Preprocessing for: finite element codes; hydrodynamic permeability models; textile composite micro-mechanics codes etc. (Fig.5 and 6)

### COMPRESSION OF TEXTILE FABRICS

Compression of fabrics is an inevitable part of composite processing; correct predictions of the fibrous content in a composite must take into account the decrease of fabric thickness (and increase of fibre volume fraction) due to compression. Research on compressibility of woven fabrics in composite technological processes is mostly empirical (see [21] for a more detailed discussion of published models). Empirical models, which usually contain two, three or more unknown constants, are useful in the predicting fibre volume fraction in composite forming, providing that these constants are determined for the fabric in question. So far no attempt has been made to connect empirical models of fabric compressibility to the compression resistance of yarns in it and to the fabric internal structure (weave pattern, different crimp of warp and weft etc.).

See [21] for detailed description of the model. Fig. 7 shows an example of comparison of *WiseTex* predictions with experimental data.

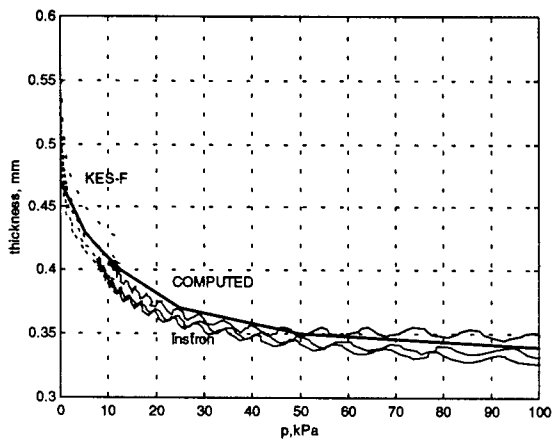


Fig.7. Example of *WiseTex* prediction of compressibility of glass composite woven preform in comparison with experimental data.

## CONCLUSION

The *virtual textile* concept, implemented in the *WiseTex* software provides a tool for design and optimisation of textile structures in the wide range of types of technical textiles and their applications.

## ACKNOWLEDGEMENTS

This work was done in the framework of the project "Development of unified models for the mechanical behaviour of textile composites" (GOA/98/05), funded by the Flemish Government through the Research Council of K.U.Leuven. S.V.Lomov's work on this project was supported by grants for Senior Fellowship by the Research Council of K.U.Leuven (F/98/108, F/99/096). Authors would also like to thank Prof.N.N.Truevtzev (St.-Petersburg State University of Technology and Design) for his constant support of international collaboration in the field of textile mechanics.

## REFERENCES

1. Keefe, M., *Solid modelling applied to fibrous assemblies. Part II. Woven fabrics.* *Journal of the Textile Institute*, 1994. 85(3): p. 350-358
2. Szosland, J., *Identification of structure of inter-thread channels in models of woven fabrics.* *Fibres & Textiles in Eastern Europe*, 1999. 7(2): p. 41-45
3. Kosek, M., *Modeling of textile structures*, in *Spring Conference on Computer Graphics. 2001: Bumerice.* p. [s.p.].

4. Chen, X. and P. Potiyaraj, CAD/CAM for complex woven fabrics. Part I. Backed cloths. *Journal of the Textile Institute*, 1998. **89 part I(3)**: p. 532-545
5. Chen, X. and P. Potiyaraj, CAD/CAM of orthogonal and angle-interlock woven structures for industrial applications. *Textile Research Journal*, 1999. **69(9)**: p. 648-655
6. Chen, X. and P. Potiyaraj, CAD/CAM for complex woven fabrics. Part II. Multi-layer fabrics. *Journal of the Textile Institute*, 1999. **90 part I(1)**: p. 73-90
7. Lomov, S.V. and N.N. Truevtzev, A software package for the prediction of woven fabrics geometrical and mechanical properties. *Fibres & Textiles in Eastern Europe*, 1995. **3(2)**: p. 49-52
8. Lomov, S.V. and A.V. Gusakov, Modellierung von drei-dimensionalen gewebe Strukturen. *Technische Textilien*, 1995. **38**: p. 20-21 (in German ).
9. Lomov, S.V., Computer aided design of multilayered woven structures, part 1. *Technologia Tekstilnoy Promyshlennosty*, 1993(1): p. 40-45 (in Russian ).
10. Lomov, S.V. and A.V. Gusakov, Coding of carcasse-layered weaves. *Technologia Tekstilnoy Promyshlennosty*, 1993(4): p. 40-45 (in Russian ).
11. Lomov, S.V., Computer aided design of multilayered woven structures, parts 2. *Technologia Tekstilnoy Promyshlennosty*, 1993(2): p. 47-50 (in Russian ).
12. Lomov, S.V. and B.M. Primachenko, Mathematical modelling of two-layered woven fabric under tension. *Technologia Tekstilnoy Promyshlennosty*, 1992(1): p. 49-53 (in Russian ).
13. Lomov, S.V., B.M. Primachenko, and N.N. Truevtzev, Two-component multilayered woven fabrics: weaves, properties and computer simulation. *International Journal of Clothing Science & Technology*, 1997. **9**: p. 98-112
14. Gusakov, A.V., S.V. Lomov, and A.N. Mogilny, Mathematical modelling of porosity of plane and 3D woven structures, in *Computer Methods in Composite Materials VI*, S.V. Hoa, W.P. de Wilde, and W.R. Bain, Editors. 1998, Computational Mechanics Publications: Southhampton - Boston. p. 331-340.
15. Lomov, S.V. and A.V. Gusakov, Computation of the porosity of one and multi-layered woven synthetic fabrics. *Chimicheskie Volokna*, 1998(5): p. 52-55 (in Russian ).
16. Lomov, S.V. and A.V. Gusakov, Mathematical modelling of 3D and conventional woven fabrics. *International Journal of Clothing Science & Technology*, 1998. **10(6)**: p. 90-91
17. Lomov, S.V., et al. Textile Geometry Preprocessor for meso-mechanical and permeability modelling of textile composites. in *9th European Conference on Composite Materials*. 2000. Brighton: IOM Communications.
18. Lomov, S.V., et al., Textile composites: modelling strategies, in *TexComp 5: The 5th International Conference on Textile Composites*. 2000, K.U.Leuven: Leuven. p. s.p.
19. Lomov, S.V. and I. Verpoest, Integrated model of textile composite reinforcements, in *Advances in Composites Materials and Structures VII*, W.P. de Wilde, W.R. Blain, and C.A. Brebbia, Editors. 2000, WIT press: Southampton, Boston. p. 367-376.
20. Lomov, S.V., et al., Textile geometry preprocessor for meso-mechanical models of woven composites. *Composites Science and Technology*, 2000. **60**: p. 2083-2095
21. Lomov, S.V. and I. Verpoest, Compression of woven reinforcements: a mathematical model. *Journal of Reinforced Plastics and Composites*, 2000. **19(16)**: p. 1329-1350
22. Lomov, S.V. and G. A.V., Mathematical modelling of the structure of 3D woven fabrics. *Technologia Tekstilnoy Promyshlennosty*, 2000: p. N1,50-53,N3,47-49, N4,7-49 (in Russian ).

**“Design Methodology for 3D Woven Fabric Architectures”**

**J A Soden & B J Hill**

The first step in the development of a fibre reinforced composite structure is the design and manufacture of the textile preform. The preform is comprised of yarns that adopt specific roles and functions within a system of interlacement. It contains a specific layer assemblage with warp and weft sett (yarn spacing), yarn count, interlinking characteristics and a design repeat (unit cell) collectively determining the structural integrity, weight (mass/unit area), shape and drapability. The preform can be manufactured using either a conventional or a non-conventional apparatus.

This paper is firmly rooted in textile design and discusses the range of textile-based factors that must be considered to produce 3D woven preform architectures. It also describes the methodology that was developed to facilitate the creation of a range of conventionally woven preform concepts.

Through a range of fabric architectures, it seeks to highlight the many design problems that must be negotiated or overcome in order to form reinforcements, with desirable attributes, for composite processing. These attributes include tailored fibre proportions and fibre volume off the loom, good fabric integrity, rigidity or conformability to the mould tool, good fibre uniformity and high quality. The structure must also be such that the potential for the formation of resin-rich regions is minimal. Reproducibility, the potential for mass production, cost-effective manufacturing are also factors that have to be considered.

It concludes that three families of fabric architectures emerge with differing properties:

- the integrated type with good drapability and formability to curvatures
- the orthogonal type that exhibit high rigidity and ordered construction
- the near-net shape family that encompasses the more innovative and complex ideas and structures.

### **Introduction**

There are many fibre and fabric configurations that can be used to form fibre reinforcement for a composite material. The data available on the analysis of conventionally woven 3D components is still in its infancy. Therefore until a variety and significant number of architectures have been generated and analysed to provide information for a database, other parameters have to be considered within the design criteria. These are listed below:

- The desired areal density ( $\text{g/m}^2$ ) of the preform, which in turn will determine levels of fibre in the warp and weft axes. A fibre percentage can be estimated for the off-loom reinforcement; i.e. values range from 29% up to 49% (to enable composite  $v_f$ 's to range from 30 – 60% approximately.)
- The loom capacity. The number of shafts on a Dobby loom or the Jacquard harness set-up in terms of warp pattern hooks per cm. The sample looms used had 24 or 48 shafts on the Dobby loom and the Jacquard had a capacity of 24 pattern hooks per cm. This restricts the

#### ICMAC - International Conference for Manufacturing of Advanced Composites

total number of layers possible depending on the warp sett requirement (ends/cm/layer) for an individual preform.

- The tex (g/1000m) of warp yarns and weft yarns. In many cases, the loom set-up is maintained between designs due to the labour intensive and costly process of changing bobbins on the creel and re-threading the loom to specific threading configurations.
- The on-loom configuration of the preform.
- Analysis of composite micro-sections can determine how the different yarn paths within the weave architecture distort during manufacture and processing, providing crucial information for the designer of the preform.

Once these basic parameters are known, a prescribed design method developed through years of practical experiment using Dobby and Jacquard technology can be applied to produce a range of flat or shaped weave architectures. The design method consists of 10 stages and ensures fundamental processes related to weave design are maintained, and that additional processes specifically related and exclusive to 3D reinforced fabrics are included as part of the integral design process (1). This design methodology was adopted and used as the working format for a computer-based CAD system for 3D multilayer and shaped fabrics: the Cross-sectional (XS) Design Program. This program has been used successfully as the main design tool at the University of Ulster for six years.

The program facilitates the flexible construction of 3D flat and shaped weave architectures, the automatic generation of the fabric liftplan, and the option to generate files in compatible formats for transferral into loom production, and engineering modelling and analysis systems. The functions of a multi-disciplinary team also relied on a collaborative system that had a core process common to each section. A cross-sectional schematic of weave architecture [figure 1] is the anchor feature that unites the design, manufacturing and analysis disciplines (2).

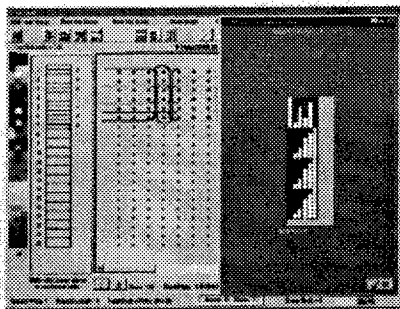


Figure 1: The Cross-sectional Design Program

The following issues need to be considered in the design of a 3D preform:

1. Identifying the total number of warp and weft layers required within the reinforcement and arranging the layer assemblage within the fabric
2. Choosing the warp and weft sett of each layer
3. Choosing the weave construction for each layer
4. Arranging and distributing the through-the-thickness interlinks over the course of the fabric repeat
5. Denting the warp yarns
6. Calculating the unit cell repeat of the fabric architecture
7. Creating the fabric liftplan
8. Weft insertion
9. Applying the pattern to either Dobby or Jacquard weaving processes
10. Transferring the information into the appropriate design system or loom controller for manufacture.

#### Fabric types

From the research undertaken at the University of Ulster, three fabric architecture categories have emerged (1). These are grouped according to the main characteristics of the weave structure. These can all be designed using the cross-sectional design program and manufactured using Jacquard looms.

- Integrated family
- Orthogonal family
- Near-net shaped family.

The angle interlock family would create an additional category but is not included, as it has not been developed to the same extent.

The characteristics of these three main groups have the following general properties: The integrated category uses mainly traditional weave structures, particularly twills, to form a range of fabrics that exhibit good drapability and conformability to curvatures, uniform surfaces and even yarn distribution over the architecture repeat [figure 2]. The fabrics can be designed to exhibit a wide range of yarn proportions in the three perpendicular directions due to the interlacing nature of the numerous traditional weave structures and derivatives available. Through-the-thickness interlinks can penetrate a proportion of, or the total thickness.

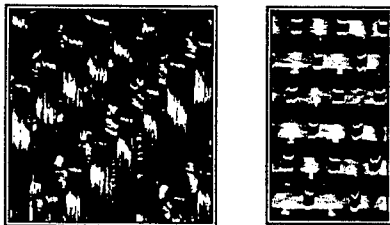


Figure 2: Integrated (left) and orthogonal (right) fabrics

The orthogonal category uses warp binding architectures to produce primarily rigid fabrics with formal and ordered layer arrangements, and organised levels of yarn proportion in the Z-direction. A skeletal system of straight warp stuffers is interspersed at regular intervals with binder yarns penetrating the total fabric thickness [figure 2]. Variations to the structure are achieved by altering the sett of the skeletal stuffer system or by increasing the binder sett and /or yarn count. These structures show very poor drapability characteristics, unless the weft sett is low.

The near-net shape category uses a combination of weave types and yarn paths to form a diverse range of specific woven shapes that will conform to curvatures and unfold after manufacture to form a shaped configuration. These reinforcements have a dual role; firstly, like the integrated category, as reinforcements with good formability characteristics, even surfaces and good distribution of yarn proportions. Secondly, as a shaped preform with the ability to form a shaped configuration free from resin- rich areas; to contain specific sub-areas of a particular dimension that carry out a particular function; and to contain localised or unusual yarn paths for innovative structural concepts [figure 3].

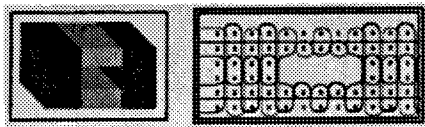


Figure 3: shaped architecture

#### **Constructing a 3D woven fabric and building the fabric architecture**

The main points of the design methodology that are applicable to all fabric categories are discussed below. It highlights the most important factors that need to be addressed before an architecture can be woven.

#### **Identifying the total number of warp and weft layers required within the reinforcement and arranging the layer assemblage within the fabric**

Most 3D architectures are designed to replace 2D laminates by providing a preform with superior delamination and interlaminar shear resistance by incorporating through-the-thickness reinforcement. The overall weight of the textile in the laminated preform is usually known. With this information and with knowledge of the tex of the yarn available for the manufacture of the 3D preform, it is possible to calculate how many warp and weft layers are required. An attempt is made to correspond as closely as possible to the stacking sequence of the laminate, with the exception of yarns in the  $\pm 45^\circ$  direction. The layer assemblage can be symmetrical or asymmetrical about the mid-plane; the set-up between adjacent yarn groups across the fabric width can vary as can the number of warp and weft layers. In most cases, an arrangement with more warp layers than weft layers is common. The warp is regarded as the principle stress direction and weave structures are frequently designed to be warp-faced.

---

#### ICMAC - International Conference for Manufacturing of Advanced Composites

The ability to change the layer assemblage and numbers of layers within a fabric design permits customised architectures such as localised reinforcements, where the fabric contains sections with steps from 4 to 6 to 8 layers, for example. The flexibility of the design method and program to permit changes to sett within designs produces fabrics that contain different sett ratios between layers (2). The on-loom orientation of the preform can also be modified depending on the component dimension.

#### Choosing the warp and weft sett of each layer

Warp sett is frequently decided upon before yarn roles and weave structures are assigned to the layers as the warp direction or X-axis orientation is usually the principle stress direction within a woven reinforcement. Integrated flat structures can be quite simple architectures where sett and yarn roles between layers are similar producing an uncomplicated 3D reinforcement. The total number of warp layers selected for a new design determines the maximum warp end density possible per cm for each layer. For example, if the maximum pattern ends possible is 24 per cm, and a 6 layer fabric is required, then the maximum setting is 4 ends/cm/layer. If a 10 layer fabric is required, then a maximum of only 2.4 ends/cm/layer is possible. The ability of the machine to weave at such densities is also an important consideration in the selection of warp sett/layer. Some weave constructions can be woven more readily than others, depending on the interlacement frequency or the tortuous nature of the yarn paths. Over time, a warp end density of 3 ends/cm/layer has been selected as the default setting using 12k (800 tex) carbon tow yarns. Total warp densities of up to 24 ends/cm have been manufactured with minimal yarn damage. Warp yarn alignment must be carefully considered when such warp sett densities are used.

Weft sett or weft pick density normally constituted the second largest proportion of fibre within the reinforcement. It is usually predetermined from the overall weight of the preform, once the warp sett and yarn count have been established. Once the pick density has been set for the whole preform it is difficult to make sudden alterations to accommodate different layer set-ups. If a fabric changes from 4 to 8 layers, the overall weft pick density/cm increases at that designated point, and manual alterations to the pick meter must be made at that stage. Weft picks are inserted from top to bottom, and ideally, lie in vertical columns directly below each other.

#### Choosing a weave construction for each layer

Each layer is normally assigned a yarn role and an interlacing sequence, which is normally a traditional weave structure. There are 5 yarn roles (1): *Through-The-Thickness Binders or Interlinkers* connect layers together with interlinks or binding links that penetrate the total fabric thickness. *Through-the-thickness interlacers* form through-the-thickness connections to any other layer but penetrate only a proportion of the total fabric thickness. *Inplane Interlacers* do not contribute to the through-thickness fibre proportion. Instead, yarns are assigned a particular weave structure and remain in their plane of origin at all times, interlacing only with their counterpart weft layer. *Warp Stuffers* are straight, uncrimped reinforcement yarns that lie in their plane of origin at all times and do not partake in any interlacement. *Localised or supplementary yarns* are an additional group introduced to the structure in specific localities to add reinforcement and assist with tailoring of fibre proportions and fabric properties in complex woven and near-net shaped preforms.

#### ICMAC - International Conference for Manufacturing of Advanced Composites

Weave structures assigned are frequently chosen according to whether the preform is required to be shape moulded during processing, or used as a flat plaque specimen, as the former necessitates the preform to have reasonable drapability characteristics. A weave construction can be chosen from a traditional structure; can be a derivative from one or more of these structures or can be a custom arrangement using different elements. Particular architectures can be used if a reinforcement requires extra stiffness, and other architectures may be selected because they contain a small repeat size, or can supply high levels of through-the-thickness reinforcement. If more than one weave type is used; each yarn path in each layer must be carefully co-ordinated to avoid tortuous arrangements.

The tapering of the reinforcement across the width or in the thickness direction or the joining of fabrics with different layer configurations can be achieved through the cross-sectional CAD system. We believe it is one of the first systems to offer this facility (2, 3). Joining or tapering fabrics are 'customised' processes specific to certain designs or near-net shaped components. In the future, fully-fashioned (shaped) fabrics may be required for a range of non-aerospace applications. The overall reduction in fibrous waste is an overriding concern to industry as a whole as more stringent (European) guidelines for disposal and recycling are implemented (4).

#### **Arranging and distributing the through-the-thickness interlinks over the course of the fabric repeat**

The weave structure determines the frequency of interlacements and potential opportunities for through-the-thickness interlinks over a given length. Through-the-thickness links can only be formed at the natural interlacing points of the weave pattern. Interlinks normally span one pick column. However, interlinks can span two or more pick columns or have an angled configuration spanning numerous pick columns if the interlacing paths of ground weave permit (e.g. 2/2 twill or angle interlock structures). A stitch formed over one pick allows a particular warp yarn to interconnect the layers a maximum number of times over a given fabric length, providing the maximum level of through-the-thickness reinforcement (5). It is important to place links as uniformly as possible within and between cross-sectional groups to ensure a good balance and distribution throughout the fabric length, width and depth of the fabric, resulting in good structural uniformity and integrity (1). Poor co-ordination of repeats and tortuous yarn paths is often the result of a poorly considered design.

#### **Calculating the unit cell repeat of the fabric architecture**

The unit cell repeat is the fundamental unit of arbitrary size which represents the complete pattern repeat of the weave architecture. It contains all the necessary yarn paths and functions to form a particular fabric architecture. The unit cell or total repeat is multiplied to form the dimensions of the complete preform, or the unit cell itself can form the entire preform dimension (1,2).

It is the key constituent and most important element of the fabric architecture that is required, by designers, manufacturers and composite analysts for the design, production, and analysis of 3D woven fabrics. The cross section design program automatically determines the unit cell repeat from the number of weave architectures within the preform structure.

### Factors that affect fabric integrity

The action of through-the-thickness yarns penetrating the thickness and the effects of weft pick density are the two main factors that affect the integrity of a multilayer preform, regardless of category (1). These effects can be summarised as follows:

#### Through-the-thickness yarns:

- When through-the-thickness yarns penetrate the fabric, the diameter of individual interlinking yarns and the frequency of the interlinking contributes significantly to yarn distortions. These distortions manifest themselves as bending, buckling and compression of yarns from their idealised path at specific localities. It particularly applies to yarns from the inner layers and weft yarns [see orthogonal weave, figure 2 and figure 4 below].
- During through-the-thickness stitch formation, the penetration of through-the-thickness yarn upsets the regular spacing of weft yarn columns as it isolates an individual column of weft yarns around which it links, as shown in [figure 5].



Figure 4: distortion of inner warp yarns

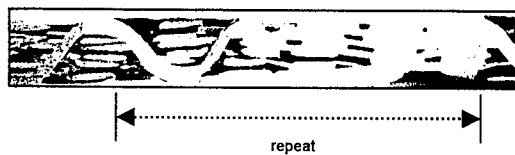


Figure 5: effect of through-the-thickness interlinks on weft pick alignment

#### Weft pick density:

- A low weft pick density value affects the vertical alignment of the sides of the through-the-thickness interlink. Consequently, levels of Z-axis reinforcement are subject to inconsistency.
- Unequal weft pick density between layers causes weft yarn misalignment and subsequent uneven levels of take-up between layers.
- An increase in weft pick density translates to a decrease in the ability of the fabric to conform to 90° curvatures.
- Weft pick density is affected by the thickness of yarns used in both warp and weft orientations, the diameter and frequency of through-the-thickness interlinks over a linear length, and the amount of yarn crimp within the weave structure.

## ICMAC - International Conference for Manufacturing of Advanced Composites

Other less significant factors affecting the preform integrity are:

- The most common and basic of all weave structures; plain weave has inherently high levels of yarn crimp which is undesirable as the wavy action of the yarns can ultimately reduce tensile strength of the yarns.
- Long surface float weaves (for example satin weave) are subject to misalignment during processing.
- Crimping of the warp stuffer yarns is significant due to the penetrating action of the through-the-thickness surface binder.
- The layer assemblage has to take account of the near-net shaping possibilities of fabrics that fold to shape, ensuring that all constituent parts maintain a balanced construction after folding has occurred.
- The use of localised warps and weft layers in sections of the reinforcement frequently results in the formation of floats on the surface of these yarns between sections. These have to be trimmed but present a potential area of weakness on the fabric surface.

### Conclusions

This paper demonstrates that the Cross Section (XS) Design Program is a very successful tool for the design, manufacture and analysis of a wide range of preforms with a variety of weave architectures and complex assemblies. It also indicates the main issues which have to be considered when designing a 3D preform and some of the problems which must be carefully considered to ensure a high quality product is manufactured.

### References

- 1 Soden JA '3D Weave Structures for Engineering Preforms', DPhil Thesis, School of Art and Design, University of Ulster, 2000
- 2 Soden JA, Hill BJ, McIlhagger R, Miller L, 'An Integrated Computer System for The Design and Analysis of 3D Woven Engineering Composites', Proceedings of International Conference on Advanced Composites (ICAC), Hurghada, Egypt, 15-18 December 1998, 227-237
- 3 Hill BJ, Soden JA, McIlhagger R, Miller L, 'A Textile Design System for Engineering Preforms', Polymer and Polymer Composites, Vol 8, Part 1, 2000 19-25
- 4 Ellison J, 'The Use of Natural Fibre Composites in the European Automotive Industry', ACTIN conference 'Natural Fibres for the Automotive Industry', UMIST, 28<sup>th</sup> November 2000, no pagination.
- 5 Harper CM, 'The Production of Preforms for Mass Produced Components', DPhil Thesis, School of Art and Design, University of Ulster, 1994

## Geometric Modelling of Orthogonal 3-D Woven Textiles

D. Brown\* and Z. J. Wu\*\*

\*Engineering Composites Research Centre, University of Ulster at Jordanstown,  
Newtownabbey BT37 0QB, Northern Ireland, UK

\*\*Manchester School of Engineering, University of Manchester, Manchester, M13 9PL, UK

### Abstract

An analytical assessment of the geometric properties of 3-D woven orthogonal fabrics is presented. The predicted proportions of fibre in the three mutually perpendicular directions X, Y and Z indicating warp, weft and through-the-thickness directions, respectively, are determined. The formulae for the calculation of the overall fibre volume fraction and fabric areal density are also given. The method adopted is based on the analysis of a kind of representative unit cell as used in the stiffness modelling of composites. The comparison between experimental results and those predicted by this method demonstrates its applicability in practical textile engineering. It can be applied to the design of complicated hybrid woven structures.

### Introduction

Micromechanical models of textile composite materials - models for evaluating the stiffness matrix for a representative unit cell - rely on the accuracy of the geometrical description of the yarns and their positions within textile structures. Models published so far either require input data from measurements of composite cross-sections under the microscope, or use a simple geometrical representation (Peirce model [1] for example). The former approach requires manufacture before predictions of properties can be made; the latter may neglect some important features of the architecture, particularly for 3-D woven composites due to the complicated geometry. For example, the prediction of the fabric thickness, which is strongly dependent on the fabric architecture and loom control, is not yet solved completely [2].

Researchers at the Engineering Composites Research Centre, University of Ulster, have developed a series of analytical assessments of the properties of 3-D orthogonal woven structures [3-5]. These predict the percentages of fibre in the three mutually perpendicular directions and the thickness of fabrics. This provides an

#### ICMAC - International Conference for Manufacturing of Advanced Composites

opportunity to design fabrics for specific applications. However, particularly in one respect, the existing approach was considered to have limitations. The selection of a fixed dimension cell (e.g., 1m×1m) of the fabric make the application of some analytical parameters and formulae to the prediction of stiffness indirect. The representative unit cell for stiffness prediction depends on the fabric architecture. Generally it does not coincide with the fixed dimension cell.

The aim of the present analysis is to provide an alternative method for the prediction of the geometric properties for orthogonal structures. The unit cell selected for the calculation of the fibre volume fraction and thickness of the fabrics is exactly the RVE used for stiffness prediction as given in a separate publication [6]. The method can be used directly in the analysis of fabrics with hybrid yarn structures.

### Architecture

It is well known that the performance of a fabric composite depends not only on the type of the fibre and matrix and the nature of the fibre-matrix interface, but also on the fabric architecture in the composite. Compared with 2-D laminated composite structures, 3-D woven architecture provides composites with higher delamination resistance, through-thickness fracture toughness and impact damage tolerance. These improvements in properties, together with reduced manufacturing costs, have made 3-D fabric reinforcement more viable alternatives to traditional engineering materials or even 2-D layered structures. However, as indicated in [7], there is still poor understanding of the influence of geometric design and weaving parameters on the performance of the architecture and composite properties for example, stiffness, strength, etc. The correct geometrical description of the yarns and their positions within textile structures are fundamental requirements to give an appropriate prediction of relevant properties.

The methodology of describing the architecture is illustrated for the particular case of orthogonal 3-D woven structures in this paper. These are 3-D interlinked woven textile fabrics, in which the fibre yarns are perpendicular to each other in three mutually directions without interlacing. For this relatively crimp free structure which is bound together by warp weaver (or binder) yarns on the top and bottom surface, linking through the entire thickness of the structure, some relevant parameters and

corresponding nomenclature definitions are given in figures 1 and 2. Warp stuffers and weft fillers alternate in layers through the thickness, with the fillers always having one more layer than that of the stuffers. Hence, if the number of warp stuffer layers in a fabric is  $n$ , there will be  $n+1$  layers of the weft fillers. In general terms the type of structure under consideration is a 3-D interlinked woven fabric with

- $P_s, P_f$  --- Ends /cm and picks /cm per stuffer and filler layer, along weft and warp directions respectively, counting on the top (or bottom) surface of the fabric,  
 $m$  --- Ratio of warp stuffers per layer to the total warp weavers within the cell,  
 $\lambda$  --- The number of fillers that a warp weaver passes around in weft filler layer before reversing its direction,

The architecture of the fabric can be described based on these parameters and total stuffer layers  $n$ . Figure 1 is a typical fabric, in which  $m=2, n=5$  and  $\lambda=2$ . For the cases of  $\lambda=1, 3$ , the side views of the corresponding fabrics are shown in figure 2.

### Cross Sections of Yarns

Although the architecture of a fabric has been specified in above section, it is not enough to describe the exact geometric properties of the fabric, for example, the thickness of the fabric. The geometric descriptions of the constituent yarns themselves and their cross sections are necessary. To do this, it will be assumed that

$T_s, T_f, T_w$  --- Yarn Count of warp stuffer, weft filler and warp weaver yarns (Tex = g/km),

$\rho_s, \rho_f, \rho_w$  --- Density of warp stuff, weft filler and warp weaver yarn material ( $\text{g/cm}^3$ ),

$\beta_s, \beta_f, \beta_w$  --- Fibre packing factor of stuffer, filler and weaver yarn cross section,

then the cross-sectional areas of stuffer, filler and weaver's yarns are respectively

$$A_s = \frac{T_s \times 10^{-5}}{\beta_s \rho_s}, \quad A_f = \frac{T_f \times 10^{-5}}{\beta_f \rho_f}, \quad A_w = \frac{T_w \times 10^{-5}}{\beta_w \rho_w}, \quad (1)$$

in which the fibre packing factor  $\beta_i$  ( $i=s, f, w$ ) depends on the layout of fibres within a yarn (Fig.3)

for a rectangular fibre array  $\beta_i \leq \frac{\pi}{4} \approx 0.7854$  , (2)

for a hexagonal fibre array 
$$\beta_i \leq \frac{\pi}{2\sqrt{3}} \approx 0.9069 \quad (3)$$

During the weaving process, the cross-sectional shapes taken up by the yarns depend on the warp and weft tensions, the beat-up and the take-up on the loom. After weaving, all yarns will not keep their virgin off-the-loom state. The deformed yarn cross-sections are assumed to be either elliptical or rectangular. Each of these shapes can be found in 3-D woven fabrics with different weave designs, different fibre yarns and different volume fractions under various loom controls [8]. For these two cross sections, a set of uniform formulae can be introduced to describe the geometric relation of the cross-sectional area with its height and width as shown by

$$2\eta \cdot a_s h_s = A_s, \quad 2\eta \cdot a_f h_f = A_f, \quad 2\eta \cdot a_w h_w = A_w \quad (4)$$

Where  $\eta$  is equal to  $\pi/4$  and 1, respectively, for elliptical and rectangular cross section of yarns.  $2a_s$ ,  $2a_f$ ,  $2a_w$  and  $h_s$ ,  $h_f$ ,  $h_w$  are the widths and heights of the corresponding yarns. The volume fraction and thickness of the fabric can therefore be predicted. For example, the whole thickness of the fabric should be

$$H = nh_s + (n+1)h_f + 2h_w \quad (5)$$

assuming zero yarn crimp.

### Volume Fraction

In order to determine the fibre volume fraction and proportion of each constituent yarn in a fabric, it is a common procedure to choose an appropriate representative unit cell [3-6]. Here, selecting a representative unit cell with  $P_f$  fillers in the X-direction (warp),  $m+1$  ends which include  $m$  stuffers within a single stuffer layer and 1 warp weaver yarn in the Y-direction (weft) and whole thickness of the composite in the Z-direction, hence the length, width and thickness of the unit are 1,  $(m+1)/P_s$  and  $nh_s+(n+1)h_f+2h_w$  cm, respectively.

The total length of the warp weaver in the unit cell is

$$1 + \frac{P_f}{\lambda} [nh_s + (n+1)h_f] \quad (6)$$

It occupies a volume of

$$V_w = A_w + \frac{P_f}{\lambda} [nh_s + (n+1)h_f] \cdot A_w \quad (7)$$

while the total volume of fillers within the cell is

$$V_f = (n+1) \cdot P_f \cdot \frac{m+1}{P_s} \cdot A_f \quad (8)$$

Similarly, the total volume of stuffers within the representative cell is given by

$$V_s = m \cdot n \cdot A_s \quad (9)$$

Obviously, the proportions of weavers, stuffers and fillers in all fibres of the fabric are respectively

$$V_{wp} = \frac{V_w}{V_w + V_s + V_f} \times 100\% \quad (10)$$

$$V_{sp} = \frac{V_s}{V_w + V_s + V_f} \times 100\% \quad (11)$$

$$V_{fp} = \frac{V_f}{V_w + V_s + V_f} \times 100\% \quad (12)$$

In some previous references [3-5], the percentage of yarns in X (warp), Y (weft) and Z (through-the-thickness) directions were considered. According to the definition of Z% , i.e., through-the-thickness proportion of warp weaver yarns, the contribution of the warp weaver to that proportion is only from the second term of right hand side of Eq.(7) and

$$Z\% = \frac{\frac{P_f}{\lambda} [nh_s + (n+1)h_f] \cdot A_w}{V_w + V_f + V_s} = \frac{\frac{P_f}{\lambda} [nh_s + (n+1)h_f] \cdot A_w}{\left\{1 + \frac{P_f}{\lambda} [nh_s + (n+1)h_f]\right\} A_w + (n+1)(m+1) \frac{P_f}{P_s} A_f + m \cdot n A_s} \times 100\% \quad (13)$$

To determine the percentage of yarns in X direction, the volume of the straight section of the interlinking warp weaver yarn as determined in the first part of right hand side of Eq.(7), is added to the volume of stuffer yarn as determined by Eq.(9). This gives

$$X\% = \frac{A_w + m n A_s}{V_w + V_f + V_s} = \frac{A_w + m n A_s}{\left\{1 + \frac{P_f}{\lambda} [nh_s + (n+1)h_f]\right\} A_w + (n+1)(m+1) \frac{P_f}{P_s} A_f + m \cdot n A_s} \times 100\% \quad (14)$$

As to the percentage of yarns in Y direction, it is exactly the value of  $V_{fp}$  in Eq.(12)

$$Y\% = \frac{(n+1)(m+1) \frac{P_f}{P_s} A_y}{V_w + V_f + V_s} = \frac{(n+1)(m+1) \frac{P_f}{P_s} A_y}{\left[1 + \frac{P_f}{\lambda} [nh_x + (n+1)h_y]\right] A_w + (n+1)(m+1) \frac{P_f}{P_s} A_y + m \cdot n A_s} \times 100\% \quad (15)$$

In practical engineering, the total volume fraction of the fibres in textile fabric composites,  $V$ , is a very important parameter to the manufacturer and the users of the composites. Its value can also be calculated based on present unit cell, although the selection of the representative unit cell has no effect on the result of volume fraction, and

$$V = \frac{V_w \beta_w + V_f \beta_f + V_s \beta_s}{1 \cdot \frac{m+1}{P_s} \cdot H} = \frac{\left[1 + \frac{P_f}{\lambda} [nh_x + (n+1)h_y]\right] A_w \beta_w + (n+1)(m+1) \frac{P_f}{P_s} A_y \beta_f + m \cdot n A_s \beta_s}{nh_x + (n+1)h_y + 2h_w} \cdot \frac{P_s}{m+1} \times 100\% \quad (16)$$

Furthermore, the fabric areal density is

$$D = \frac{V_w \beta_w \rho_w + V_f \beta_f \rho_f + V_s \beta_s \rho_s}{1 \cdot \frac{m+1}{P_s}} = \frac{\left[1 + \frac{P_f}{\lambda} [nh_x + (n+1)h_y]\right] \rho_w A_w \beta_w + (n+1)(m+1) \frac{P_f}{P_s} \rho_f A_y \beta_f + m \cdot n \rho_s A_s \beta_s}{m+1} \cdot P_s \quad (17)$$

So far, all expressions about total fibre volume fraction and volume percentage of yarns in different directions are given. The remaining problem is to determine the heights of all yarns, which are still unknown.

### Determination of Height of Yarn

As observed in available 3-D woven fabrics from both our industrial partners and our own laboratory, either adjacent warp yarns (including stuffers and weavers) in the  $X$  direction or the neighbouring fillers in the  $Y$  direction do not have any gaps between them. Generally, if the end density is larger than the pick density, there is a much greater possibility of having no gap between yarns in the weft ( $Y$ ) direction, and vice versa. Without any loss in generality, it is assumed that stuffer and weaver yarns make contact with each other, which leads a geometric relationship in the  $Y$  direction within the representative cell

$$m \cdot 2a_s + 2a_w = \frac{m+1}{P_s} \quad (18)$$

Similarly, if the gap between fillers is  $S$ , and

$$S = 2a_f \xi \quad , \quad (19)$$

where  $\xi$  can be measured directly from the fabric, the geometric relation in  $X$  direction in the cell gives

$$2a_f + S = \frac{1}{P_f} \quad (20)$$

Substituting (19) into (20), then

$$2a_f = \frac{1}{(1+\xi)P_f} \quad (21)$$

In order to facilitate loom set-up, the same yarn is generally used for warp stuffers and weavers. Then the cross section areas of stuffer and weaver yarns are exactly the same, i.e.,  $A_s = A_w$ . Under this circumstance, it is reasonable to assume that  $h_s = h_w$ , then  $a_s = a_w$ .

It is easy to check the relation

$$2a_s = 2a_w = \frac{1}{P_s} \quad (22)$$

from (18). Combining Eqs.(21), (22) with (4), the heights of yarns are given respectively for fillers, stuffers and warp weavers as

$$h_f = \frac{A_f P_f}{\eta_f} (1+\xi) \quad , \quad (23)$$

$$h_s = h_w = \frac{A_s \cdot P_s}{\eta_s} \quad (24)$$

Substituting  $h_f$  and  $h_s$  in (23) and (24) into the relevant expressions in the previous section, the percentages of yarns and the volume fraction of the fibre, etc., can be calculated without any difficulty.

An Excel® spreadsheet incorporating these formulae was created.

## Results

### Example 1

To determine the validity of the present model, the first analysis is performed for a 3-D orthogonal woven geometry with  $m=1.5$ ,  $\lambda=2$ . The number of stuffer layers is  $n=4$ . These parameters determine the architecture of the rectangular hexahedron unit cell in our modelling. The size of the cell depends on the constituent yarns and the material properties which are taken from Cox et al. [2, 9]. All stuffers, fillers and weavers are made of AS4 carbon fibres yarns and the resin is Tactix 138 epoxy.

Based on the specified architecture and the constituent materials, the parameters involved in the modelling calculation are listed in Table 1.

Table 1 Geometric and Material Properties of Yarns

Constituents	Material density ( $\text{g/cm}^3$ )	Yarn Count ( $\text{g/km}$ )	Ends/pick density(/cm)
Stuffer fibre	1.76	1534.0	7.83
Filler fibre	1.76	1534.0	5.10
Weaver fibre	1.76	655.7	

The calculated results for the fractions of all fibres lying in stuffer, filler and weaver directions, total volume fraction, areal density, etc., are given in Table 2. For comparison, the results from Cox and Dadkhah [2] are also provided. The second row in the table is obtained by changing the fibre packing factor (from 0.9 to 0.82) and the filler space parameter (from 0.400 to 0.495). It can be seen that the predicted data from geometric modelling match the measurements very well.

Table 2 Results of Modelling

Models	Volume Fraction of stuffers (%)	Volume Fraction of fillers (%)	Volume Fraction of weavers (%)	Fibre volume fraction (%)	Composite thickness (cm)	Areal density ( $\text{g/cm}^2$ )
Present model $\xi=0.400, \beta_1=0.90$	39.212	53.188	7.600	54.298	0.769	0.735
Present model $\xi=0.495, \beta_1=0.82$	39.042	52.959	7.999	47.789	0.878	0.739
Cox [2]	38.7	52.4	9.0			-
Experimental (Cox)				48.3 $\pm$ 1	0.88	-

**Example 2**

The selected parameters are  $T_s=T_f=T_w=1200\text{Tex}$ ,  $\beta_s=\beta_f=\beta_w=0.7$ ,  $\rho_s=\rho_f=\rho_w=2.54\text{g/cm}^3$  for a glass fibre fabric. Structural parameters are  $n=5$ ,  $m=2$ ,  $\lambda=2$  and  $P_s=3.5/\text{cm}$ ,  $P_f=2.5/\text{cm}$ . Using  $\xi=0.7$ , if  $\pi/4 \leq \eta_i \leq 0.9$  ( $i=s, f, w$ ), i.e., all cross sections of yarns vary between elliptical and approximately rectangular, the volume fraction of the weaver is around 6%. Weave code for this structure was generated at our laboratory. The designs were based on the utilisation of all 24 ends in each dent of the reed in the loom, that is 24 ends /1.875cm (reed pitch=1.875cm). The structure (Fig.1) was successfully woven by our industrial partner, Park Hill Textiles. The results are shown in the following table (Table 3). Fabric thickness measurement correlated well with the predicted value.

Table 3 Result Data for the Orthogonal Glass Fibre Weave Structure

Predicted total fibre volume fraction	Predicted volume fraction of weaver	Predicted thickness (cm)	Measured thickness (cm)
44.57~50.95 %	5.77~6.00 %	0.322~0.369	0.33±0.01

**Conclusion**

An alternative but innovative method to predict the geometric properties is presented. The method proposed takes due account of the direct data link with the downstream process of determining the mechanical properties. Because the representative unit cell selected for the calculation of the fibre volume fraction and thickness of the fabric is exactly the representative volume element used in stiffness prediction [6], the predicted output of geometric parameters can be used in this downstream activity directly. Generally, the methodology used can also be applied to other kinds of designs of 3-D fabrics such as the integrated structures defined in [4].

**Acknowledgements**

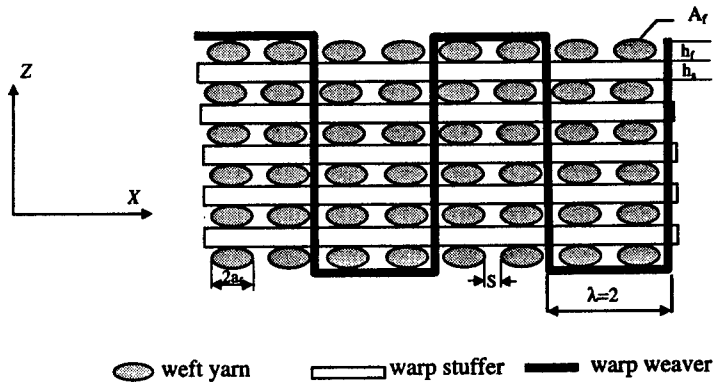
Support for this work within a CRAFT project (BRST CT98 5344) under the EC Brite Euram Industrial and Materials Technologies Programme is gratefully acknowledged. Technical support from the project partners, Park Hill Textiles Ltd, DERA Structural Materials Centre, CTMI, Rex Composites SA and Plastechnol Ltd, is much

**ICMAC - International Conference for Manufacturing of Advanced Composites**

appreciated. Thanks are also due to the staff in the Engineering Composites Research Centre which has received support from the European Regional Development Fund in the form of the Technology Development Programme administered in Northern Ireland by the IRTU.

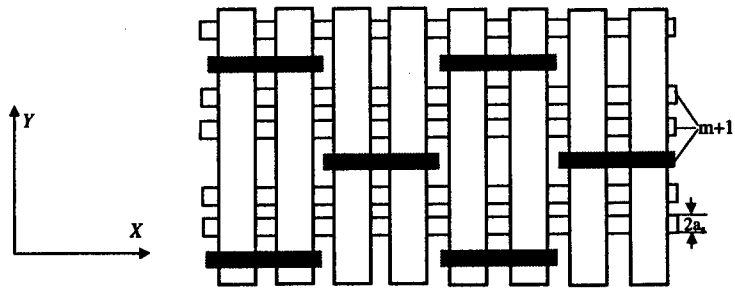
## References

- [1] F. T. Peirce, The geometry of cloth structure. *Journal of the Textile Institute*, **28**(3),1937:T45-T96.
- [2] B. N. Cox & M. S. Dadkhah, The macroscopic elasticity of 3D woven composites. *J. of Compos. Mater.*, **29**(6), 1995: 785-819.
- [3] B. J. Hill and R. McIlhagger, The development and appraisal of 3D interlinked woven structures for textile reinforced composites. *Polymer & Polymer Composites*, **4**(8), 1996: 535-539.
- [4] B. J. Hill and R. McIlhagger, The development and appraisal of 3D fully integrated woven structures for textile reinforced composites. *Polymer & Polymer Composites*, **5**(1), 1997: 49-55.
- [5] B. J. Hill, R. McIlhagger, J. A. Soden, J. R. P. Hanna and E. S. Gillespie, The influence of crimp measurements on the development and appraisal of 3D fully integrated woven structures. *Polymer & Polymer Composites*, **5**(2), 1997: 103-112.
- [6] D. Brown. and Z. J. Wu, Stiffness properties of 3-D orthogonally woven fabric composites, in *Advances in Composite Materials & Structures VII*, eds. W.P. de Wilde, W.R. Blain and C. A. Brebbia, WIT Press, Southampton 2000: 377-386.
- [7] A. P. Mourize, M. K. Bannister, P. J. Falzon and K. H. Leong, Review of applications for advanced three-dimensional fibre textile composites, *Composites Part A* **30**, 1999: 1445-1461.
- [8] S. V. Lomov and I. Verpoest, Compression of woven reinforcements: a mathematical model. Private communication, 2000.
- [9] J. Xu, B. N. Cox, M. A. McGlockton & W. C. Carter. A binary model of textile composites-II: the elastic regime. *Acta Metall. Mater.*, **9**(43), 1995: 3511-3524.



○ weft yarn    — warp stuffer    — warp weaver

Side view



Top view

Fig.1 Geometric design of interlinked orthogonal fabric.

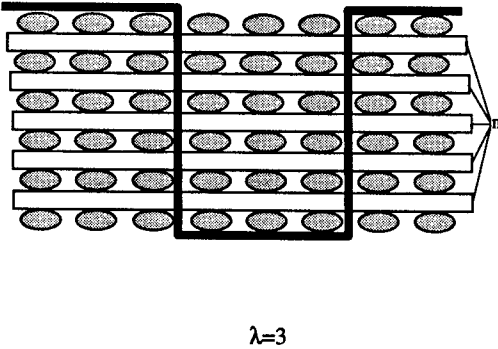
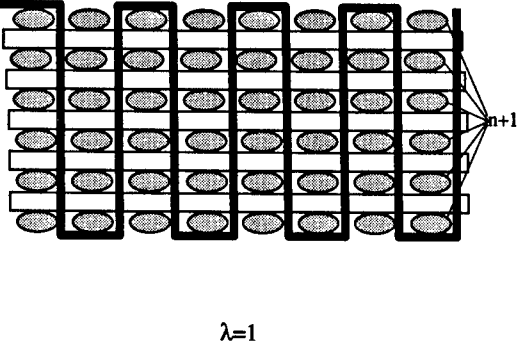
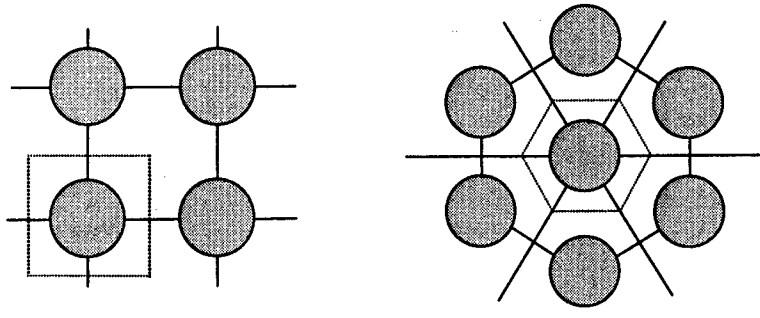


Fig.2 Side view of the architecture of orthogonal 3-D fabric composites.



(a) Rectangular array of fibres

(b) Hexagonal array of fibres

Fig.3 Fibre array in yarns

## MODELLING OF DRAPING AND DEFORMATION FOR TEXTILE COMPOSITES

*A. C. Long, M. J. Clifford, P. Harrison, C. D. Rudd*  
*School of Mechanical, Materials, Manufacturing Engineering and Management*  
*University of Nottingham, University Park, Nottingham NG7 2RD, UK*

### ABSTRACT

Forming of textile composite materials to three dimensional geometries involves a number of deformation mechanisms within the textile structure. Of these intra-ply (in-plane) shear is generally accepted as the dominant mechanism. In this paper results from picture frame shear experiments are described to characterise a number of materials including woven and non-crimp dry fabrics, thermoset prepregs and thermoplastic composites. The latter materials were characterised as a function of rate to illustrate the effects of matrix rheology. Results from these tests were used within an iterative draping algorithm in which fabric shear energy is minimised. A number of forming experiments were conducted to validate the model, illustrating that it was able to determine the effect of textile structure on the formed fibre pattern.

### INTRODUCTION

Textile composites, consisting of a textile reinforcement within a thermoplastic or thermoset polymer matrix, can be processed via a number of techniques. Components can be produced directly by forming of thermoset or thermoplastic prepregs. Alternatively liquid composite moulding (LCM) processes such as resin transfer moulding can be used, in which a dry reinforcement is impregnated with a thermosetting resin, which then cures to form a rigid composite. In these processes the reinforcement is usually formed to the component shape in a separate operation to produce a textile preform.

Whatever the material and process of choice, a forming operation is required to convert the two-dimensional layers or plies into the required three-dimensional geometry. For fabrics based on orthogonal yarns (or tows), a number of deformation mechanisms may occur during this operation (as described for example by Potter (1)). Within individual layers intra-ply (in-plane) shear, corresponding to rotation of tows about their crossovers, is considered to be the dominant deformation mechanism as very high strains can be achieved in the bias direction (ie.  $45^\circ$  to the fibres) at relatively low applied force. Inter-tow slip can also occur, and may be significant when forming to tight radii where the intra-ply shear angle varies significantly (2). For multi-layer components, inter-ply slip is required to accommodate curved surfaces. Tensile forces along the fibres may lead to fibre straightening for woven fabrics, whilst compressive forces can cause buckling leading to wrinkling of the fabric. Experimental measurements suggest that wrinkling occurs at a limiting degree of intra-ply shear known as the locking angle, typically ranging from  $20^\circ$  to  $65^\circ$  (2-4).

A number of researchers have developed simulations of draping or forming for textile composites. Several of these models have been implemented within commercial software packages. Two approaches have been adopted, based on either a geometric (kinematic) mapping, or a mechanical representation solved using an explicit finite element method. Geometric/kinematic models (5-7) represent the fabric structure as a pin-jointed net, which is mapped on to the surface of the component/forming tool by assuming that tow segments are able to shear at the joints (tow crossovers). A unique draped pattern can be obtained by specifying two intersecting tow paths, referred to as generators, on the surface of the forming tool. The remaining tows are positioned using a geometric mapping. Correct specification of the generators is critical, as these will determine the positions of all remaining fibres. The kinematic approach provides a very fast solution, with run times

typically less than 10 seconds. However this approach is unable to differentiate between materials other than in the specification of the locking angle, which is used to indicate possible areas of wrinkling. Consequently an identical fibre pattern is obtained, regardless of variations in material forming characteristics or processing technique.

The mechanical approach involves simulation of the entire forming process over a number of time steps. At each stage equilibrium equations are solved, usually using an explicit finite element technique. This approach has been applied to both dry fabrics (8,9) and thermoplastic or thermoset prepregs (10,11). Provided that accurate processing property data are specified, it is possible to represent material specific behaviour. In addition, ply/tool and ply/ply friction can be modelled. Ply wrinkling is anticipated by the occurrence of in-plane compressive forces, rather than the specification of a locking angle. However this approach is time consuming, both in terms of CPU time and in the collection of the large set of materials data required.

In this paper the deformation characteristics of dry fabrics, thermoset prepregs and thermoplastic composites will be established. The results will be used within an iterative model for forming/draping of textile composites, which minimises fabric shear energy to account for resistance to intra-ply shear. This will be shown to provide more accurate results than obtained using the kinematic modelling approach, whilst associated CPU times are significantly lower than those required for non-linear finite element analysis. Results from a number of forming experiments will be presented to validate the iterative model.

## **INTRA-PLY SHEAR**

### **Experimental Procedure**

In previous studies, resistance to intra-ply shear has been characterised using two approaches. Uniaxial extension of relatively wide samples in the bias direction is favoured by a number of researchers (1,2), as the testing procedure is relatively simple. However the deformation field within the sample is non-uniform, with maximum shear observed in the central region and a combination of shear and inter-tow slip observed adjacent to the clamped edges. In addition the shear angle cannot be obtained directly from the crosshead displacement, so that the test must be monitored visually to measure deformation. An alternative is the picture-frame shear test (3,4,12), in which the fabric is clamped within a frame hinged at each corner, with the two diagonally opposite corners displaced using a mechanical testing machine. Although this test may be sensitive to small variations in material alignment, it is used in this study as it produces uniform shear deformation (if performed with care). This has been confirmed experimentally by Sharma et al (13) using Surface Displacement Analysis (SDA). The authors showed that uniform shear was induced during a picture frame shear experiment, whilst significant non-uniformity was observed during a bias extension test.

The picture-frame shearing equipment used is illustrated in Fig. 1. The apparatus was operated using a Hounsfield mechanical testing machine, which monitored both load and displacement during the experiment. The results were converted into shear force versus shear angle using simple geometric relationships based on crosshead displacement and original rig dimensions. A pre-tension rig was used to position dry fabrics within the picture-frame (14). This served two purposes, to align the material within the rig and to enhance repeatability. Dry fabrics and thermoset prepregs were tested at room temperature, whilst thermoplastics were tested at elevated temperatures within an environmental chamber.

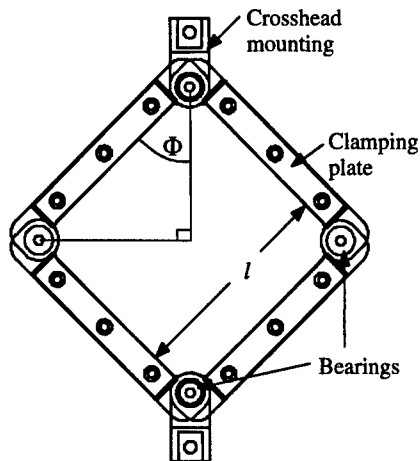


Figure 1. Schematic of the picture-frame shear rig. The distance between the bearings ( $l$ ) was 145 mm, whilst the clamping length was 115 mm.

### Dry Fabrics

Typical shear compliance curves for woven glass fabrics are shown in Fig. 2. This figure compares the behaviour of fabrics with similar surface densities but different fibre architectures. Each test was carried out at 100mm/min (although no significant rate effects were observed for dry fabrics). The plain weave (P800) required the highest force to achieve a particular shear angle, whilst the twill weave (T800) was the most compliant. This is related to the fact that the ratio between tow width and pitch is greatest for this material. However for all fabrics tested two distinct regions may be identified. The initial resistance to shear is relatively low, and is likely to be caused by friction at the tow crossovers. Once adjacent tows come into contact, the resistance increases significantly as the tows are compressed together. This is the region where wrinkling is usually observed. Locking angles of between 55° and 68° were observed for a range of dry fabrics.

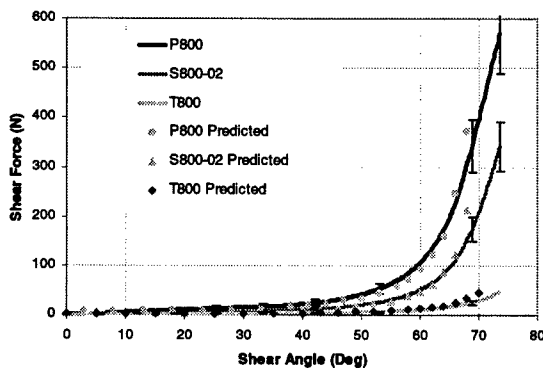
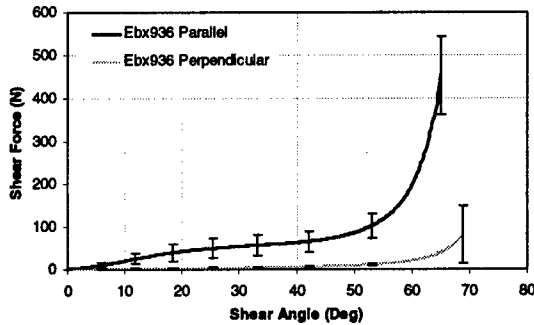


Figure 2. Experimental and predicted shear compliance curves for woven glass fabrics with different architectures: Plain weave (P800), 4-harness satin weave (S800-02), and 2:2 Twill weave (T800). Curves represent mean shear force from a minimum of 6 tests, with error bars showing 90% confidence limit.

Also included in Fig. 2 are predictions obtained using a mechanical model (described in detail elsewhere (14)). This is based on a generalised geometric model for textile reinforcements, which describes yarn paths for both woven and non-crimp fabrics. Deformation of the fibre architecture during in-plane shear is also represented, allowing tow cross-sections to be modified when lateral contact occurs. Tow contact areas are calculated, over which Coulomb friction is assumed to determine the local torque contribution. Contact force is calculated by integrating the tow pressure over the contact area, with a semi-empirical model used to relate pressure to tow volume fraction and fibre modulus. The total torque over the specimen is used to calculate the intra-ply shear force. Comparison of predictions with experimental results illustrates that the model is capable of representing the effects of fibre architecture on compliance.

(a)



(b)

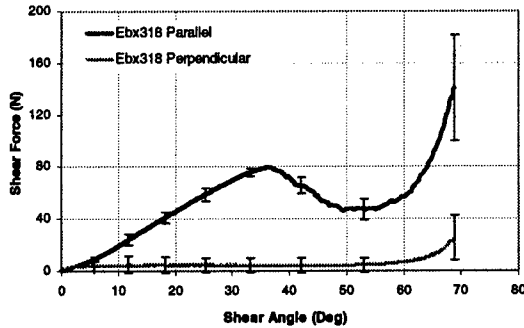
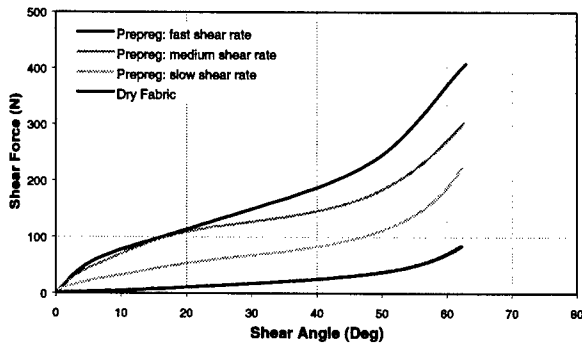


Figure 3. Shear compliance curves for  $\pm 45^\circ$  non-crimp glass fabrics tested parallel and perpendicular to the stitch. (a) Tricot 1&1 warp-knit (Ebx936). (b) Pillar warp-knit (Ebx318). Curves represent mean shear force from a minimum of 6 tests, with error bars showing 90% confidence limit.

Fig. 3 shows typical shear compliance curves obtained for non-crimp fabrics with both a tricot and pillar warp-knitted threads. The tricot warp-knit results in a "zig-zag" stitching thread pattern, whereas the pillar warp-knit is similar to a chain stitch. In both cases it is apparent that the compliance is lower when the fabric is sheared parallel to the stitching direction. Testing in this direction results in a tensile strain within the stitch, which causes an increase in shear force. The effect is more pronounced for the pillar warp-knit, where testing parallel to the stitch results in a linear increase in force until the stitching thread snaps. After this point the force is reduced until inter-tow compaction occurs. The directionality exhibited by non-crimp fabrics during shear can result in non-symmetric fibre patterns during draping, as described later.

**Thermoplastic/Thermoset Prepregs**

Fig. 4 compares shear compliance curves for a 5 harness satin weave carbon/epoxy thermoset prepreg at three shear rates. For these experiments, the crosshead displacement rate was varied during each test to maintain a constant angular shear rate. It is clear that a significant increase in shear force occurs during the start of the test. This is in contrast to the behaviour of dry fabrics, which initially exhibit very little resistance to shearing. However after the first 20° of shear, a steady increase in shear force is observed. The increase is more pronounced above a shear angle of 50° as the fibres become tightly packed. Wrinkling was observed at shear angles of around 60° for all rates. Also included in this figure is the shear compliance curve for the dry fabric used to produce this prepreg. It is clear that the major contribution to shear force is from the viscous matrix.



**Figure 4.** Shear compliance curves for a 5 harness satin weave carbon/epoxy prepreg. Angular shear rates of 0.93, 4.65 and 9.31 deg/s denoted slow, medium and fast respectively.

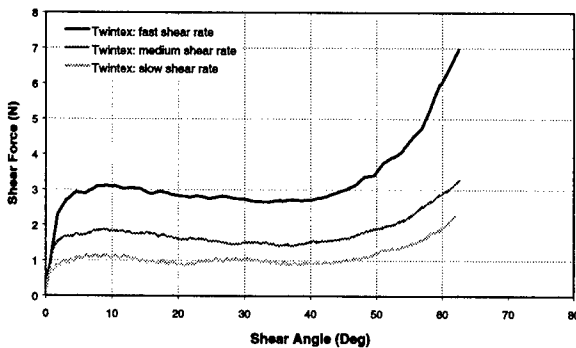


**Figure 5.** Shear compliance curves for 2:2 twill weave glass/PP thermoplastic composite at 180°C. Angular shear rates of 0.93, 4.65 and 9.31 deg/s denoted slow, medium and fast respectively.

Fig. 5 compares shear compliance curves for a glass/polypropylene thermoplastic composite, based on a 2:2 twill weave reinforcement with a fibre volume fraction of 35%. In this case the viscosity of the molten polymer is significantly lower than that of the partially cured epoxy used in Fig. 4, and hence the forces are much lower. Furthermore this material exhibits a relatively constant shear force for the first 40° of shear. The experimental results were obtained at 180°C, although further results have also

## ICMAC - International Conference for Manufacturing of Advanced Composites

been obtained at a range of temperatures (15). An increase in temperature from 190°C to 220°C led typically to a reduction in shear force of 70% to achieve a given shear angle.

Relative motion of reinforcement fibres within prepregs is resisted by a film of matrix, both between individual filaments and between reinforcement tows. Two contributions can be identified, shearing at the crossover point of two perpendicular tows, and relative movement of parallel fibres or tows. An increase in shear force for any given angle was observed with an increase in shear rate, although increasing the rate by a factor of 10 led to only a 3-fold increase in shear force. This would suggest that the matrix undergoes significant shear thinning during testing. Whilst this may seem surprising at the relatively low testing rates involved, the shear strain rates between individual fibres and tows may be high due to the reduction in fibre spacing as the material attains high shear angles. A similar effect was observed for the thermoset prepreg (Fig. 4). These results illustrate the difficulty in modelling forming for prepregs, where the matrix rheology dictates that deformation behaviour will vary with both rate and processing temperature.

### FORMING SIMULATION

Generally the geometric/kinematic approach to drape simulation works well for symmetric shapes draped with balanced materials. However for non-symmetric geometries placement of the two generator fibre paths may be problematic, as it may not be possible to identify two stationary fibre axes. For materials such as non-crimp fabrics, which exhibit a preferential direction for deformation, the fibre pattern may be different to that obtained using a balanced fabric. The use of a mechanical forming simulation may allow consideration of material directionality, although this would be achieved at the expense of increased computation time. The approach presented here is based on the use of a geometric mapping algorithm within an iterative scheme. The energy required to produce each mapping is calculated, with the mapping resulting in the lowest energy assumed to represent the actual behaviour of the fabric. The deformation energy is the sum of several components related to the mechanisms identified in the introduction. At present the model considers only intra-ply shear, as this is thought to be most indicative of the effect of fabric construction on deformation. The fabric shear energy (work done during shearing,  $U_s$ ) can be calculated simply from the area under the torque-shear angle curve:

$$U_s(\theta) = \int_0^{\theta} T(\gamma) d\gamma \quad [1]$$

where  $T(\gamma)$  is the torque required to reach a shear angle  $\gamma$ . This expression can be evaluated either from the intra-ply shear model described above or by fitting an empirical relationship to the measured shear compliance curve. For non-crimp fabrics, two curves may be specified to represent shearing parallel and perpendicular to the stitching thread. The total energy is calculated within the fabric drape simulation by summing the contribution at each node (tow crossover).

A simple way to determine the mapping resulting with the minimum energy is to use an iterative scheme based on the two generator fibre paths. This approach involves finding the two intersecting paths that result in the lowest total energy. A Hooke and Jeeves minimisation method is used, where the generator path is defined one step at a time from a user-defined starting point. Each successive set of nodes is optimised by iterating the generator path angle to achieve the minimum increase in shear energy. For reasons of computational efficiency, this technique is preferred to a global minimisation algorithm in which the entire generator path is modified at each stage of the process. However as nodes in contact with the tool are subject to additional constraints due to friction, the present approach is likely to be reasonably accurate for automated forming operations.

The results of this minimisation algorithm are shown in Fig. 6, which shows predicted fibre patterns for a hemisphere using shear data for a 4 harness satin weave and a  $\pm 45^\circ$  pillar warp-knit (Ebx318,

Fig. 3b). The predictions show a good correlation with the experimental results (Fig. 7). These results are particularly encouraging, as a conventional geometric draping simulation would predict identical fibre patterns for these materials.

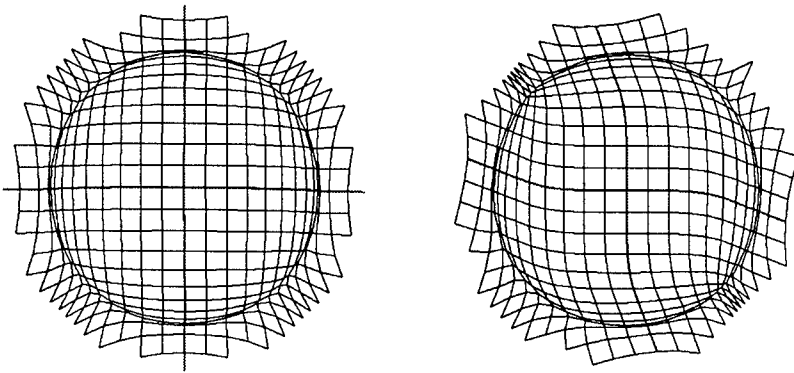


Figure 6. Results from drape simulation over a hemispherical tool using the shear data for S800-002 (left) and EbX318 (right).

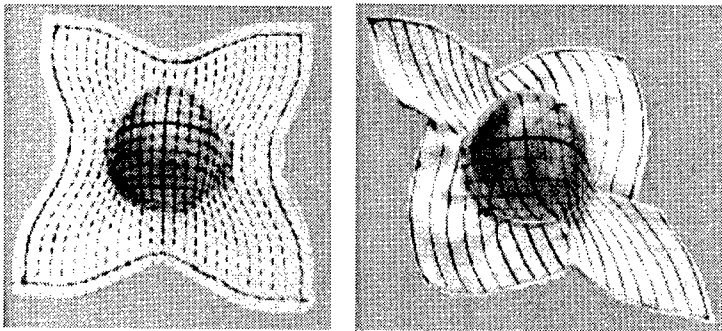


Figure 7. Hemispherical preforms produced using two glass fabrics. Left - 4 harness satin weave (S800-02). Right -  $\pm 45^\circ$  pillar warp-knit (EbX318).

An automotive transmission tunnel was used to evaluate the iterative draping simulation for a component with no axial symmetry. Preforms were produced by hand lay-up over a male former. An arrangement of several discrete forming pads was developed to hold the fabric onto the component surface during lay-up. These assisted in the lay-up process and resulted in improved repeatability during preform manufacture. Fig. 8 compares predicted fibre patterns for this geometry obtained using a variety of techniques. Fig. 8(a) was obtained using the purely kinematic algorithm, where generator paths were defined as geodesics. Fig. 8(b) was generated using the energy minimisation algorithm with shear data for a plain weave material (P800). It is clear that the energy minimisation algorithm has reduced the shear deformation over the surface significantly compared to the kinematic model; if the shear energies for each simulation are analysed a reduction of 35% is recorded. Fig. 8(c) was based on shear data for a  $\pm 45^\circ$  non-crimp carbon fabric, having similar shear compliance data to that for EbX936 (Fig. 3a). In this case fabric deformation was increased in fabric quadrants that were sheared in the preferential direction.

Fig. 3b). The predictions show a good correlation with the experimental results (Fig. 7). These results are particularly encouraging, as a conventional geometric draping simulation would predict identical fibre patterns for these materials.

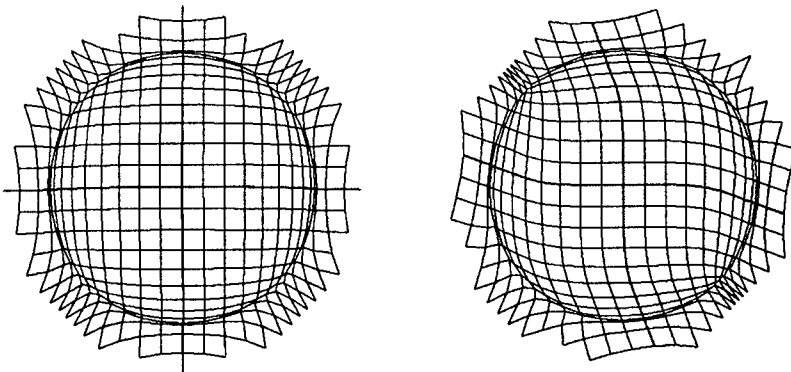


Figure 6. Results from drape simulation over a hemispherical tool using the shear data for S800-002 (left) and Ebx318 (right).

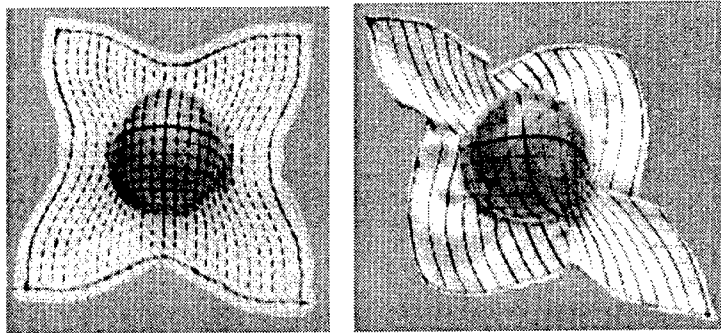
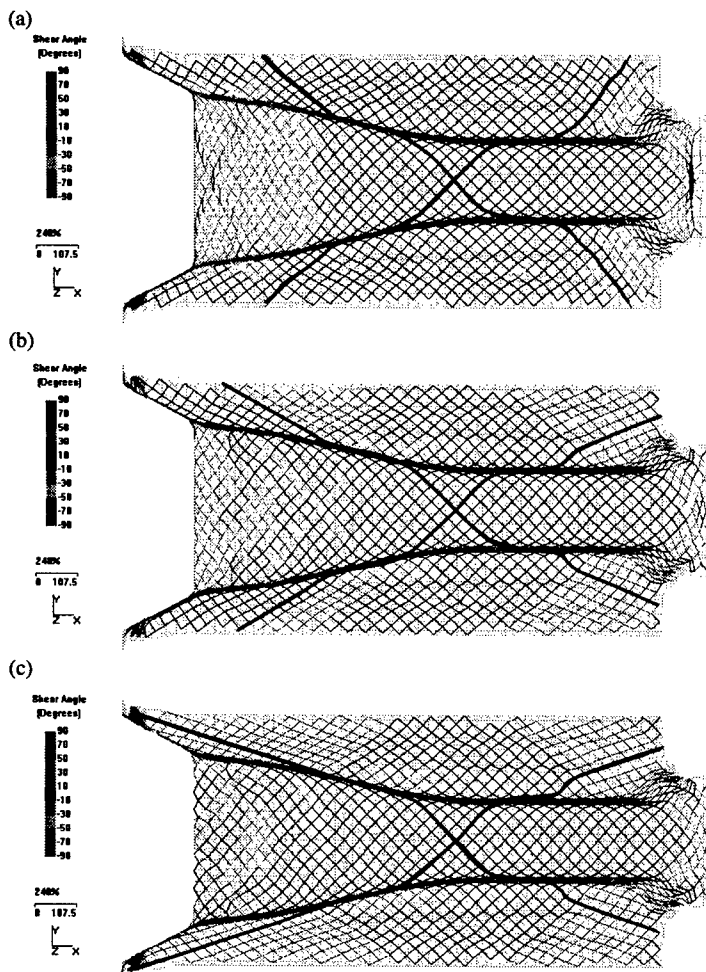


Figure 7. Hemispherical preforms produced using two glass fabrics. Left - 4 harness satin weave (S800-02). Right -  $\pm 45^\circ$  pillar warp-knit (Ebx318).

An automotive transmission tunnel was used to evaluate the iterative draping simulation for a component with no axial symmetry. Preforms were produced by hand lay-up over a male former. An arrangement of several discrete forming pads was developed to hold the fabric onto the component surface during lay-up. These assisted in the lay-up process and resulted in improved repeatability during preform manufacture. Fig. 8 compares predicted fibre patterns for this geometry obtained using a variety of techniques. Fig. 8(a) was obtained using the purely kinematic algorithm, where generator paths were defined as geodesics. Fig. 8(b) was generated using the energy minimisation algorithm with shear data for a plain weave material (P800). It is clear that the energy minimisation algorithm has reduced the shear deformation over the surface significantly compared to the kinematic model; if the shear energies for each simulation are analysed a reduction of 35% is recorded. Fig. 8(c) was based on shear data for a  $\pm 45^\circ$  non-crimp carbon fabric, having similar shear compliance data to that for Ebx936 (Fig. 3a). In this case fabric deformation was increased in fabric quadrants that were sheared in the preferential direction.



**Figure 8.** Deformed fibre pattern for a prototype automotive component using the energy minimisation algorithm. (a) Geodesic generator paths. (b) Shear data for a plain weave. (c) Shear data for a  $\pm 45^\circ$  tricot stitched fabric.

Fig. 9 compares predicted and measured shear angles along the length of the component for the latter material. Fabric layers were marked with an orthogonal grid, and shear angles were determined by measuring the relative position of grid points using digital vernier callipers. The results agree over the majority of the length, although the model over-estimates the shear deformation at the rear of the tunnel. For experimentally produced preforms, wrinkles were present in this location. Darts (triangular cuts) were used to alleviate wrinkling, reducing the overall shear deformation in the region. These discontinuities were not represented in the drape analysis.

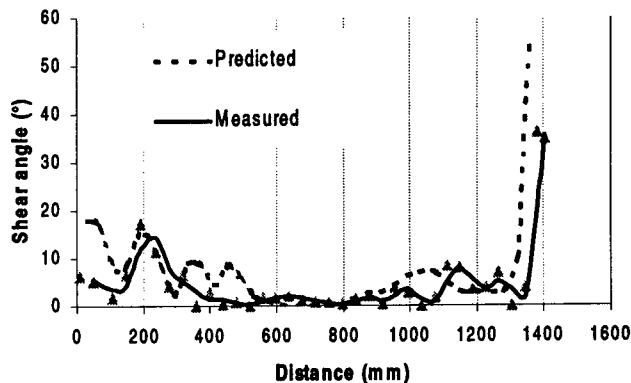


Figure 9. Comparison of predicted and measured shear angles along the length of the transmission tunnel, measured on the centre line from left to right with reference to Fig. 8(c).

## DISCUSSION

This paper has analysed the deformation mechanisms exhibited during forming of textile composites. It is generally accepted that the most important mechanism is intra-ply (in-plane) shear. This can be characterised using a picture-frame shear test, which allows fabric/ply locking angles (maximum shear angle) to be observed, and material compliance to be measured in terms of shear force versus shear angle. For dry fabrics typically two regions are observed in this curve, corresponding to inter-tow shear, resulting in very low forces, followed by lateral tow compaction, resulting in a sharp increase in force as the locking angle is approached. A similar relationship is exhibited by thermoplastic and thermoset prepregs, although here the force is dominated by a polymer film between fibres. Generally the behaviour of dry fabrics was found to be independent of forming rate, whereas prepregs exhibited rate dependency due to the viscosity of the polymer film. Furthermore significant shear thinning was observed for both the thermoplastic and thermoset composites tested. This may make modelling problematic for these materials, as the shear rate will vary spatially over a complex component. For thermoplastic materials, which are usually processed by non-isothermal compression moulding, the temperature dependency of shear compliance may necessitate the use of a sequential forming simulation with a coupled heat transfer model.

The above measurements were performed principally to provide materials data for draping/forming simulations. A novel draping simulation has been developed, in which the traditional geometric mapping is used within an iterative scheme. This is used to minimise fabric shear energy, which can be obtained experimentally or using intra-ply shear models. This approach provides more accurate results than commercially available draping simulations, particularly for non-symmetric components or materials with a preferential direction of shear (such as non-crimp fabrics). More accurate still is the use of an explicit, non-linear finite element analysis code. The author would suggest that a geometric/iterative draping simulation should be used for initial component design and materials selection, followed by a full mechanical analysis to optimise the manufacturing process.

## ACKNOWLEDGEMENTS

The authors would like to acknowledge the work of a number of research assistants and students, in particular Francois Robitaille, Ben Souter, Craig Wilks and Jakapan Thaworn. The following organisations are also thanked for their continued support: The Engineering & Physical Sciences Research Council, Ford Motor Company, ESI Group, BAE Systems, BP Amoco, Brookhouse

---

ICMAC - International Conference for Manufacturing of Advanced Composites

Patterns, DERA, Dowty Aerospace Propellers, Flemings Industrial Fabrics, Hexcel Composites, MSC Software, Rolls Royce, Vetrotex International, University of Cambridge, University of Leeds.

**REFERENCES**

1. Potter K.D. "The influence of accurate stretch data for reinforcements on the production of complex structural mouldings", *Composites*, July 1979, pp. 161-167.
2. Wang J., Page J.R., Paton R. "Experimental investigation of the draping properties of reinforcement fabrics", *Composites Science & Technology*, v 58, 1998, pp. 229-237.
3. Breuer U., Neitzel M., Ketzner V., Reinicke R. "Deep drawing of fabric-reinforced thermoplastics: Wrinkle formation and their reduction", *Polymer Composites*, v 17, 1996, pp. 643-647.
4. Prodromou A.G., Chen J. "On the relationship between shear angle and wrinkling of textile composite preforms", *Composites Part A*, v 28, 1997, 491-503.
5. Van West B.P., Pipes R.B., Keefe M. "A simulation of the draping of bidirectional fabrics over arbitrary surfaces", *J Text Inst*, v 81, 1990, 448-460.
6. Bergsma O.K. "Computer simulation of 3D forming processes of fabric reinforced plastics", *Proc 9<sup>th</sup> Int Conf on Composite Materials*, Madrid, July 1993, IV: 560-567.
7. Long A.C., Rudd C.D. "A simulation of reinforcement manufacture during the production of preforms for liquid moulding processes", *IMEchE J Engineering Manufacture*, v 208, 1994, pp. 269-278.
8. Boisse P., Borr M., Buet K., Cherouat A. "Finite element simulations of textile composite forming including the biaxial fabric behaviour", *Composites Part B*, v 28, 1997, pp. 453-464.
9. Dong L., Lekakou C., Bader M.G. "Solid-mechanics finite element simulations of the draping of fabrics: a sensitivity analysis", *Composites Part A*, v 31, 2000, pp. 639-652.
10. O Brádaigh C.M., Pipes R.B. "Finite element analysis of composite sheet-forming process", *Composites Manufacturing*, v 2, 1991, pp. 161-170.
11. de Luca P., Lefébure P., Pickett A.K. "Numerical and experimental investigation of some press forming parameters of two fibre reinforced thermoplastics: APC2-AS4 and PEI-CETEX", *Composites Part A*, v 29, 1998, 101-110.
12. Canavan R.A., McGuinness G.B., O'Braidaigh C.M. "Experimental intraply shear testing of glass-fabric reinforced thermoplastic melts", *Proc 4<sup>th</sup> Int Conf on Automated Composites*, Nottingham, Sept 1995, pp. 127-138.
13. Sharma S.B., Sutcliffe M.P.F., Clifford M.J., Long A.C. "Experimental investigation of tow deformation during draping of woven fabrics", *Proc 4<sup>th</sup> Int European Scientific Association for Material Forming Conf*, Liège, Belgium, April 2001, pp. 107-110.
14. Souter B.J. "Effects of fibre architecture on formability of textile preforms", PhD Thesis, University of Nottingham, 2001.
15. Wilks C.E., Rudd C.D., Long A.C., Johnson, C.F. "Rate dependency during processing of glass/thermoplastic composites", *Proc 12<sup>th</sup> Int Conf on Composite Materials*, Paris, July 1999.

**SESSION 3:  
PROCESSING & MODELLING**

ICMAC - International Conference for Manufacturing of Advanced Composites

## **UK POLYMER COMPOSITES SECTOR - COMPETITIVE ANALYSIS AND FORESIGHT STUDY**

**Graham D Sims (NPL Materials Centre)  
Gordon Bishop (NetComposites)**

It is recognised that the composites industry is extremely scattered, as composed of a wide range of materials suppliers (eg fibre and resin manufacturers, compound suppliers), fabricators, major OEMs and end users. Companies vary from having a total dependence on composites to companies where it forms a small part of their operations. A range of technology levels are also present in the industry from hand lay-up GRP to autoclaved cured aerospace companies. Hence, the polymer composites sector could be easily and variably effected by different external pressures, such as, changing environmental regulations, shortage of skilled engineers, lower cost competition.

NPL, in conjunction with NetComposites, have undertaken on behalf of the DTI Chemicals Directorate (Innovation and Skills Partnership) a competitive analysis and foresight study of the UK polymer composites sector. The study was developed in conjunction with the Institute of Materials (IoM), Composites Division Board following its response to the identification by the Foresight Materials Panel of "composites" as one of the specific sectors to be reviewed (as noted in the Foresight Materials Panel recent publication "Materials: Shaping our Society" - page 29]). The study aims to establish both the current competitive position and the longer-term "Foresight" requirements of the UK composites industry. Establishing the current competitiveness position of the industry is an essential pre-cursor to any Foresight study.

The study has reviewed the current position of the industry (eg turnover, markets) and the future trends and needs. These conclusions were discussed at a workshop held at the Institute of Materials prior to developing and prioritising recommendations for the future research, business approaches, market targets etc. needed for maintaining and improving the competitiveness of the composites industry. The work identifies the major opportunities and threats to the industry, and the appropriate responses needed.

The review was undertaken through approaching different constituencies, such as, trade associations, research organizations, SMEs, major suppliers and major end users supported by a more widely distributed survey. The British Plastics Federation - Composites Group and the Composites Processors Association have supported the study through their membership and by serving on the steering group. Other groups such as the Network Group on Composites in Construction and the Nottingham University Composites Club have publicised the survey to their membership.

A public version of the report is expected to be available during September, 2001. Further information and a web version will be available from NPL and NetComposites web sites [[www.npl.co.uk/cog/](http://www.npl.co.uk/cog/) and [www.netcomposites.com](http://www.netcomposites.com)].

## NUMERICAL SIMULATION OF VOID FORMATION IN LCM

Joël Bréard, Abdelghani Saouab and Guy Bouquet

*Laboratoire de Mécanique du Havre, Université du Havre  
25, rue Philippe Lebon – BP 540  
76058 Le Havre cedex, France  
joel.breard@univ-lehavre.fr*

**SUMMARY:** The existence of void type defects in composite laminates manufactured using LCM process alters the mechanical characteristics of the final product. The knowledge of the mechanism leading to the formation, evolution and removal of such defects is thus a challenging issue. So, the object of this paper is to present a procedure to simulate mould filling for fiber reinforced parts and to incorporate void formation. A flow and transport model was developed for simulating transient resin flow in unsaturated porous media containing air and resin. The model is composed of a unique combination of robust and accurated numerical algorithms for solving transport equation.

In the resin flow, we define the saturation. This value is equal to one when resin is present (saturated medium) and to zero when it is not (dry medium). Note that the saturation coefficient varies continuously between zero and one (unsaturated medium). The saturation ratio is a macroscopic entity yet it is clearly the consequence of microscopic phenomena and especially of air entrapment within tows, hence the presence of micropores. The homogenized approach presented here is general, without decoupling the micro-macro effects. The source term explains the increase of the mold inlet pressure which occurs after mold filling. So we obtain a modeling of the source term that depends of Capillary Number and is related to the micro-macro scale effects with the dual-porosity.

In the last step, the optimization of process was developed. The objective functions include cycle time, void content, injection pressure and preform assembly. The diverse combination of these factors and priorities give an optimization methodology. The unsaturated flow and transport model was applied to a variety of rigorous problems and was found to produce accurate, mass conserving solutions when compared to analytical solutions in transport and experimental results in void contents.

**KEYWORDS:** Porous Media, Void Formation, Permeability, Dual Porosity, Saturated-Unsaturated, Macro-micro, Optimization, Transport Modelling

### INTRODUCTION

The main objective of this study is to review the main parameters that describe the physical phenomena encountered in *Liquid Composite Molding* (LCM) when a fibrous preform is injected by a fluid resin. In fact, in order to draw a clear picture of all the connected physical phenomena occurring during resin impregnation, the porous medium must be considered as deformable. Such a study is crucial to develop a better understanding of air entrapment mechanisms, especially because air content is a key parameter that governs the quality of composite parts.

In this work, we study the spatial pressure distribution in a rectangular mold for saturated and unsaturated flows. The quadratic pressure distribution observed for unsaturated flows can be explained by introducing the notion of saturation degree in the equations governing the flow. A systematic interpretation of all the related physical phenomena is given, based on the double scale porosity of fibrous porous media. The concept of permeability is also revisited in order to take into account the notion of saturation, the goal being here to provide more accurate input data for numerical simulations, and ultimately predictive models to control the quality of injected parts in terms of air content.

Introducing the notion of saturation allows to describe in more details the progressive impregnation of a fibrous preform by a fluid resin. In fact, permeability still plays a central role, but expressed as a function of saturation, it will vary between two extreme values used already by several investigators : the unsaturated and saturated permeabilities. In other words, except at very low injection velocity for which capillary effects may come into play, there is more resistance to the flow in a dry preform than when the fabric or mat is already wetted. Usually in numerical simulations, only a single parameter is used, either the saturated or the unsaturated permeability. The difference between these two values may distort significantly the analysis of the resin flow during mold filling. By considering permeability as a function of saturation, the value of this key parameter can be adjusted automatically in the neighborhood of the flow front (*unsaturated permeability*) and in the saturated domain (*saturated permeability*).

In the literature, conflicting results on permeability and thermal conductivity measurements have been given in (Spaid *et al.*) [1] and (Bréard) [2] among others. In fact, not only these methods are not systematically reproducible, but some questions remain open regarding the difference between saturated and unsaturated. These considerations have motivated new studies on the micro-macroscopic interactions occurring in flows through fibrous preforms. The explanations provided in these articles mention the non linearity of Darcy's law when the fluid velocity is high or capillary effects when the velocity is low. Notwithstanding the interest of these discussions, they are based mainly on qualitative assessments and do not bring any new information that can be used in numerical simulations to improve the understanding of the resin flow behavior. In fact, the observed experimental discrepancies can be explained easily if two phenomena are taken into account simultaneously: (1) the saturation of the porous medium, and (2) the deformations of the fiber bed under the effect of resin pressure.

Firstly, some generalities on flows through deformable porous media will be recalled. In fact, it is important to study separately each phase of the porous medium. In the literature, some flow behaviors have been related to non-linear effects not accounted for by Darcy's law. In fact, these abnormalities can be explained by considering the deformability and saturation of the porous medium. In particular, the mass conservation equation needs to include a two phase formulation (for the reinforcement and for the fluid), which explains the quadratic spatial pressure distribution observed experimentally for unsaturated flows. Finally, our work discusses the results in terms of the double scale porosity structure of fibrous reinforcements and provides a general framework for a further study of saturated and unsaturated flows, including the macro/micro phenomena that govern air bubble formation.

### SPATIAL PRESSURE DISTRIBUTION IN SATURATED/UNSATURATED POROUS MEDIA

First of all, we assume that the permeability tensor  $K_{ij}$  and the strain tensor of the skeleton  $\varepsilon_{ij}$  both depend on the saturation parameter  $S$ . We can integrate the transient effect  $\alpha$ , in Darcy's law. Therefore Darcy's equation and the continuity equation are modified as follows:

$$\begin{cases} q_i + \alpha_i \partial_i q_i = -\frac{K_{ij}(S)}{\mu} \nabla p \\ \nabla \cdot q_i = -\partial_i \varepsilon_{kk}(S) \end{cases} \quad (1)$$

For unsaturated flows, the porosity variation associated to fiber rearrangement within the fabric may be neglected compared to variations in the saturation degree, and it is the same condition for the transient effect.

Experiments were carried out in a rectangular mold used to measure permeability with a preform of length 0.3 m. Pressure transducers were placed along the elongated direction of the mold. In this case, Darcy's law models a purely resistive phenomenon in which  $K$  is the hydraulic conductivity. Some measurements were performed for unsaturated flows, i.e., before the mold is completely filled. The experimental pressure distribution plotted in Fig. 1 is no longer linear, but parabolic in the local unsaturated zone at the beginning of mold filling.

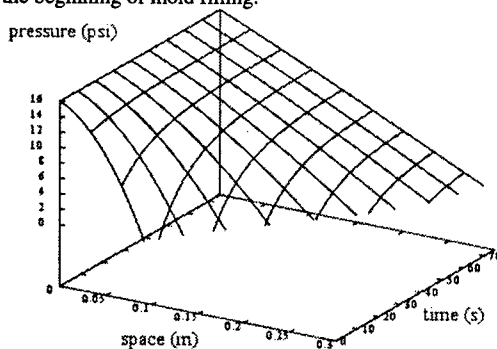


Fig. 1: The spatial pressure distribution in unsaturated porous medium

However, as the flow front moves towards the extremity of the mold, the pressure distribution takes progressively a linear shape.

This behavior can be easily explained by introducing a saturation parameter  $S$ ,  $0 \leq S \leq 1$ .

Using Darcy's equation, the continuity equation for the unsaturated problem in one dimension writes as follows:

$$\nabla \left( \frac{k_{rel}(S) K_{geo}}{\mu} \nabla p \right) = \phi \partial_i S \quad (2)$$

Permeability in Darcy's law should, in terms of modeling, be considered as the product of the geometrical permeability  $K_{geo}$  which is, in fact, an intrinsic characteristic of the fibrous structure and a relative permeability  $k_{rel}(S)$ . The integration of this equation for a unidirectional flow yields at any given time a quadratic expression of the spatial pressure distribution during mold filling.

As confirmed by the experimental results of Fig. 1, a parabolic pressure distribution is obtained for a one-dimensional flow. So in general, the spatial pressure distribution can be defined with the profile of the pressure at the saturated front position and we give a new description of the pressure value with three time zones: I) wet preform, II) intermediate zone, III) dry preform.

We need to develop two flow conditions: i) pressure constant condition and ii) flow rate constant condition. The front position are describe in case i) by  $W_f = m \cdot f(t)$  and in case ii) by  $W_f = m_s \cdot f(t)$ , where the coefficient  $m$  and  $m_s$  define unsaturated and saturated flow respectively. We precise that in all case  $m_s > m$ . It is why, we have double front position during the filling. This result show the presence of a zone where air bubbles develop. In the final discussion of this paper, we caracterize a saturation scalar value to define the rate of air bubble.

Note that micro-scale effects took into account the radial flows through fiber tows. However, the homogenized approach presented here is more general, without decoupling the micro-macro effects. This can be explained in the qualitative variations in time of the injection pressure. The flow rate behaviour at injection is identified with the same evolution. The presence of this source term in the flow equation explains the increase of the mold inlet pressure which occurs after mold filling. Actually, we develop some works about the modeling of the source term that depends of Capillary

Number  $Ca = \frac{q\mu}{\gamma_v \cos\theta}$  where  $\gamma_v$  is the surface tension of the liquid, and  $\theta$  is the advancing contact

angle of the liquid-fiber system.  $Ca$  is related to the micro-macro scale effects and defines the balance of the viscous and capillary forces. And in the case where the preform is very large in length, we have a new basic theory. In fact, for pressure constant condition and for a long injection time, a capillary effect develops. In the same way, for flow rate condition and for a long injection time, an inertial effects develops and non-linearity appears. So in these cases, we can not use the Darcy law.

## MECHANISMS OF FLUID IMPREGNATION THROUGH A DRY FIBROUS REINFORCEMENT

### Permeability ratio between unsaturated and saturated flow

The dependence of permeability on the saturation degree has often been discussed in soil mechanics by (Bear) [4], and also for LCM processes by (Spaid *et al.*) [1] for example. In (Bréard) [3], the permeability measured for one-dimensional flows in unsaturated preforms was found to differ from the values obtained for saturated preforms by a ratio that ranges from 0.4 for unidirectional reinforcements to 0.8 for fiber mats. In Fig. 2, the portion of data to the right of the vertical dotted line indicates the behavior after the injection condition is finished. Then, we obtain a relaxation of physical value due to the relaxation of flow rate condition. The observed ratio depends on the geometrical structure of the reinforcement, which can have a single scale of pores (random mat) or a double scale of pores (woven fabric). This double scale corresponds to flows between the fiber tows and inside the tows respectively. Hence  $K$ , that is usually assimilated to a constant parameter called *permeability*, should rather be considered in unsaturated flows as a variable hydraulic conductivity term depending on the saturation degree. (Patel *et al.*) [5] give more details about fiber wetting and void formation during mold filling.

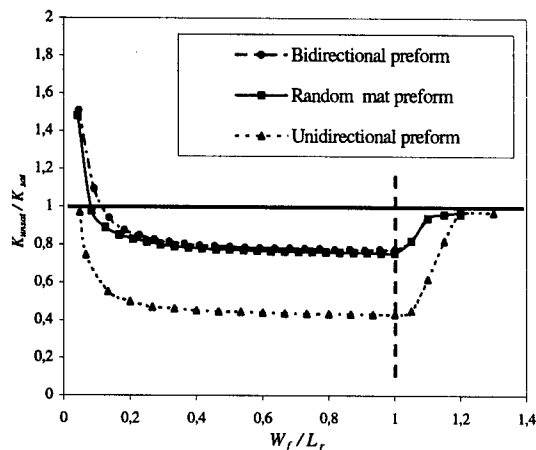


Fig. 2: Study of the unsaturated/saturated ratio for different fibrous structures

The convex shape of the pressure distribution that was observed experimentally in Fig. 1 for unsaturated flows also explains qualitatively the fact that  $K_{sat} > K_{unsat}$  (Fig. 2). As a matter of fact, since the permeability is smaller at the flow front than in the saturated domain, the local pressure gradient will be higher.

The permeability previously measured for the permanent flow (*saturated permeability*  $K_{sat}$ ) was higher than the permeability for the transient flow (*unsaturated permeability*  $K_{unsat}$ ). This result is illustrated in Fig. 2, which plots the evolution of the ratio  $R_s = \frac{K_{unsat}}{K_{sat}}$  in function of the ratio  $\frac{W_f}{L_r}$  of the flow

front position ( $W_f$ ) versus a reference length ( $L_r$ ). This ratio becomes stable more rapidly in some cases, such as for isotropic mats for instance. According to (Patel *et al.*) [6], a wide variety of behaviors may occur between those two observations which depend on the nature of the reinforcement studied. Note that this difference is greater in the case of a unidirectional reinforcement (UD).

Permeability is an intrinsic property of the reinforcement; it should not change with the fluid. If we use different resins, the difference in front evolution is only connected with capillary effects introduced which can be accounted for in the saturation parameter and it has often been discussed by (Binetruy *et al.*) [7], (Kang *et al.*) [8] and (Lundström *et al.*) [9]. The difference between the two flow regimes can be explained by the two scales of flow resistance. The first level of resistance is encountered when the fluid flows initially around the fiber tows (inter-tow flow). Then, when the fluid begins to impregnate the tows (intra-tow flow), the resistance to the flow diminishes (Fig. 3).

In the case of a mat preform, there is a little intermediate zone, i.e., few tow effects are present because of the much smaller average size of the fibers and because they bound on a thermoplastic film. In addition to these micro and macro scales of resistance, deformation of the mold and preferential flows along the mold edges must also be taken into account in numerical simulations.

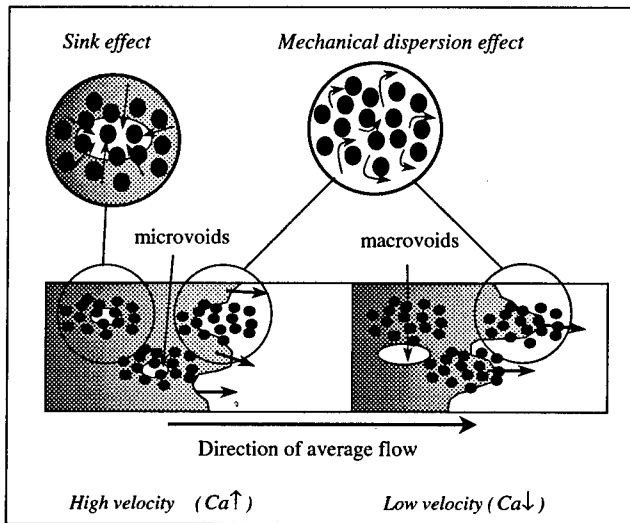


Fig. 3: Mechanisms of void formation in unsaturated porous medium

### Intrinsic and relative permeabilities

The relative permeability  $k_{rel}(S)$  depends on the saturation degree  $R_s \leq k_{rel}(S) \leq 1$ :

$$K(S) = k_{rel}(S)K_{geo} \quad (3)$$

The notion of saturation degree is of primal interest in modeling, since it can provide a good prediction of local defaults. The less saturated is the preform, the more defaults are likely to happen.

We define a new profile in Fig. 4 for the relative permeability by the power law :

$$k_{rel}(S) = [(1 - R_s^*)S + R_s^*]^\beta \quad (4)$$

where  $\beta$  is a constant factor and  $R_s^* = R_s^\beta$ .

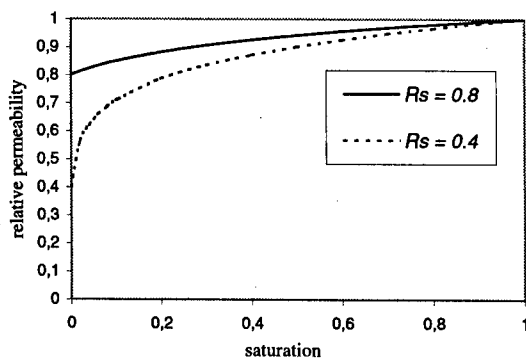


Fig. 4: Profile of relative permeability

**TRANSPORT MODEL FOR VOID FORMATION**

**Experimental measurement**

The objective of this study is the saturation measurement during liquid injection on fibrous medium. The reinforcement (double porosity) and the dual flow (capillary effect on intra tow and viscous flow on inter tow) develop the air bubble entrapment. The saturation of liquid phase permit us to quantify the bubble rate with creating and spreading phenomena.

Our study is an experimental device to permit us the snap detection of bubbles by a dynamical measurement of saturation during injection (Labat *et al.*) [10]. Our technic use to the electrical conductivity of liquid. This method is commonly develop in soil mechanics.

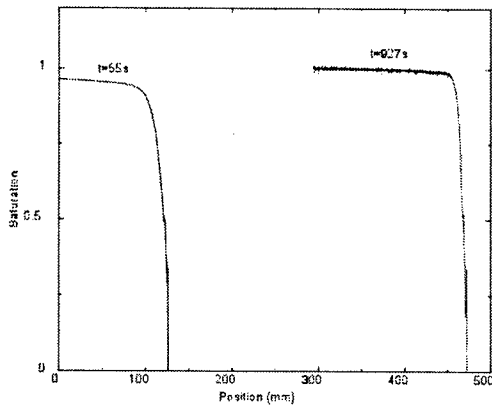


Fig. 5 Temporal and spatial evolution examples of saturation diagram

The saturation curves are obtained with sensor to permit us the flow analysis of create and removal bubbles phenomena in Fig. 5. The viewpoint of this experimental study is to quantify a constitutive law for process optimization with a minimizing bubble test. In Fig. 6, three domains are observed for the void distribution. The first one corresponds to part with high macro voids. The second domain corresponds to high injection pressure and the micro voids increases in the parts. Between these two ranges, we can observe a domain that we call "processability window" corresponds to the injection conditions leading to parts without void.

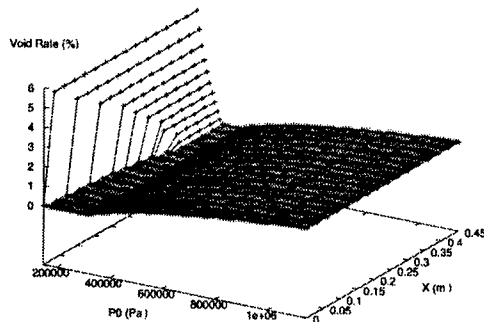


Fig 6. Void fraction as a function of positions and injection pressures

**The phenomenon of dispersion**

A term appear in the general macroscopic balance equation for the saturation phase, represents the dispersive flux of the component (per unit area of fluid). It is a macroscopic flux relative to the uniform (average) flow but also normal to it. The region occupied by the fluid will continue to grow, both longitudinally in the direction of the uniform flow, and transversally normal to it. The spreading phenomenon described above is called hydrodynamic dispersion as developed by (Quintard *et al.*) [11]. It is a nonsteady, irreversible, process in which the mass of the saturation continuously spreads out. The two basic factors that produce mechanical dispersion are, therefore, flow and the presence of a pore system through which flow takes place.

So, the following equation governs the transport model for saturation :

$$\partial_t S + \frac{q_i}{\phi} \nabla S = D_{ij} \nabla^2 S - Q_s \tag{5}$$

The velocity is defined by the experimental pressure field  $p(x,t) = \frac{\tilde{a}(t)}{2} x^2 - \frac{P_0}{L} x + P_0$  where  $\tilde{a}(t) = ae^{bt}$ , and the data parameters in table 1.

$P_0$ (psi)	$L$ (m)	$\mu$ (Pa.s)	$\phi$	$K_{geo}$ (m <sup>2</sup> )	$R_s$	$a$ (psi)	$b$ (s <sup>-1</sup> )
16	0,3	0,11	0,6	$3.10^{-10}$	0,8	-1326	$-6,83.10^{-2}$

Table 1 : Parameter for numerical transport model

In Fig. 7, we present the numerical solution for the saturation diagram of time.

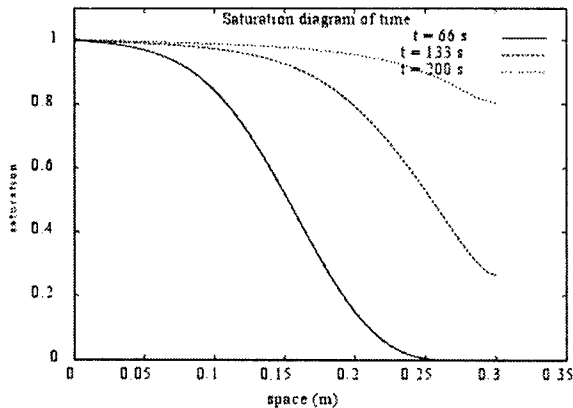


Fig. 7: Numerical saturation diagram of time

Also, such velocity variations alone cannot explain the ever-growing width of the zone occupied by saturation normal to the direction of flow. In order to explain the latter observed spreading, we must refer to an additional phenomenon that takes place in the tow place, sink effects. Several mechanisms account for the sink phenomenon, primarily adsorption. It is a phenomenon of accumulation of the fluid on the tow at a fluid-solid interface and depends of Capillary Number. In Fig. 8, we compare experimental and numerical front position  $W_f(S=0)$  and consider the evolution of the dispersive and sink effects. In this case, we obtain a good agreement with  $D=1,5.10^{-5}m^2.s^{-1}$  and  $Q_s=10^{-3}e^{-0,01s^{-1}}$ .

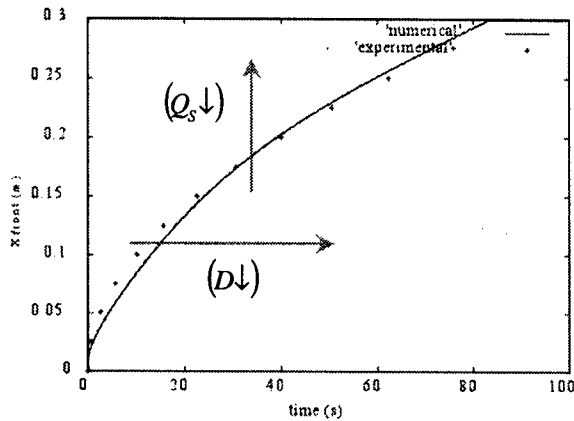


Fig. 8: Experimental and numerical front position

The experimental front position is defined by the measurement and the analytical solution with  $m=3,1.10^{-2}$ .

For another example for numerical study, we give a comparison in Fig. 9 with the experimental test about the saturation curves in Fig. 5. The data parameters are defined in Table 2.

$P_0$ (psi)	$L$ (m)	$\mu$ (Pa.s)	$\phi$	$K_{geo}$ ( $m^2$ )	$R_s$	$a$ (psi)	$b$ ( $s^{-1}$ )
14,5	0,5	0,1	0,4	$3.10^{-10}$	0,4	-500	$-3.10^{-2}$

Table 2 : Parameter for numerical transport model

In this case, we obtain a good agreement with  $D=10^{-7}m^2.s^{-1}$  and  $Q_s=10^{-3}e^{-0.01s^{-1}}$ .

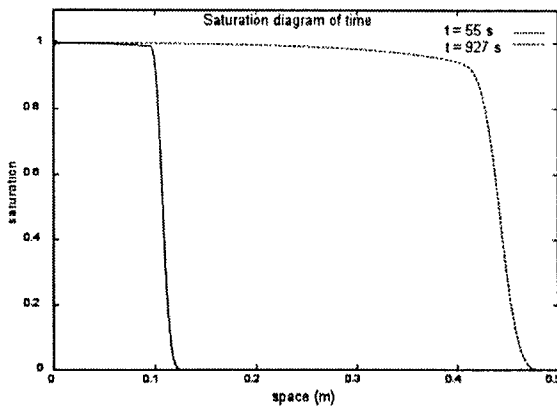


Fig. 9: Numerical comparison with experimental measurement of saturation

### Optimization

We expose the reasons why the optimisation exhibits real interests in treating problems concerning the manufacturing processes and the mechanical uses of polymer matrix composite materials.

## ICMAC - International Conference for Manufacturing of Advanced Composites

Our optimization method is based on a combination between the theories developed by Broyden, Fletcher, Goldfarb, Shano (B.F.G.S.) and the Goldstein's rule. We develop the economical unidirectional research based on the Goldstein's rule, (Bonnans) [12].

In the case of the injection for thin composite plates, we use the analytical expression of the objective function we want to minimize and we calculate its minimal value (Saouab *et al.*) [13]. In order to validate our method, we chose some cases where an analytical solution of the problem is a priori known. The first application concerns the optimization of the mould filling time and the associated resin waste, taking into account the reinforcement and mould relative positions.

### CONCLUSION

This work presents a new approach to characterize the void formation of a porous medium. The conclusions of this investigation were presented for the hydraulic conductivity, but could also be extended to the thermal conductivity. The spatial pressure distribution in unsaturated porous medium was found to be quadratic, and not linear as predicted by Darcy's law in a saturated preform. Not only has this result been verified experimentally, but it can also be derived by solving the flow equation when permeability depends on the degree of saturation. The notion of double scale porous medium was also introduced. This concept is central to provide an understanding of the physical phenomena that occur in *Liquid Composite Molding*. Not only can the hydraulic conductivity or permeability be related to this double scale porosity structure, but it is true also for the thermal conductivity and elastic characteristics. The notions of double scale porous medium and saturation degree will allow ultimately to model with better tools the impregnation of a dry preform by a fluid resin and control the quality of injected parts in terms of air content. Experimental results have allowed to identify a ratio characterizing the difference between saturated and unsaturated permeabilities. As observed in soil mechanics, the transient unsaturated permeability is always lower than the saturated permeability. The next step will be to study a global optimization of void formation in order to clarify this matter and establish a relationship between pressure and the saturation degree of a fiber bed. Finally, the motion of air bubbles in a fibrous reinforcement must also be analyzed in relation with its macro/micro structure, while taking into account its potential deformations.

### REFERENCES

1. Spaid, M. and Phelan, F., "Modeling Void Formation Dynamics in Fibrous Porous Media with the Lattice Boltzmann Method", *Composite Part A*, 1998, Vol. 29
2. Bréard, J., Saouab, A. and Bouquet, G., "Dependence of the Reinforcement Anisotropy on a Three Dimensional Resin Flow Observed by X-Ray Radioscopy", *Journal of Reinforced Plastics and Composites*, 1994, Vol. 18, No. 9
3. Bréard, J., Henzel, Y. and Trochu, F., "A Standard Characterization of Saturated and Unsaturated Flow Behaviors in Porous Media", *Proceedings of ICCM--12*, 5--9 July, 1999, Paris, France
4. Bear, J., "Continuum Approach and Contaminant Transport in Ground Water Flows - Modelling and Applications of Transport Phenomena in Porous Media", *Von Karman Institute for Fluid Dynamics - Lecture Series 1990-01*, 1990
5. Patel, N. and Lee, L.J., "Modeling of Void Formation and Removal in Liquid Composite Molding. Part II: Model Development and Implementation", *Polymer Composites*, 1996, Vol. 17, No. 1

---

ICMAC - International Conference for Manufacturing of Advanced Composites

6. Patel, N. and Lee, L.J., "Effects of Fiber Mat Architecture on Void Formation and Removal in Liquid Composite Molding", *Polymer Composites*, 1995, Vol. 16, No. 5
7. Binetruy, C. and Hilaire, B., "Tow Impregnation Model and Void Formation Mechanisms during RTM", *Journal of Composite Materials*, 1998, Vol. 32, No. 3
8. Moon Koo Kang, Woo Il Lee and H. Thomas Hahn, "Formation of microvoids during resin-transfer molding process", *Composites Science and Technology*, 2000, Vol.60, No. 12
9. Lundström, T.S. and Gebart, B.R. , "Influence from Process Parameters on Void Formation in Resin Transfer Molding", *Polymer Composites*, 1994, Vol. 15, No. 1
10. Labat, L., Grisel, M., Bréard, J. and Bouquet, G., "Original Use of Electrical Conductivity for Voids Detection during Injection of Composite Materials", *Comptes Rendus de l'Académie des Sciences Série IIB - Mécanique*, (accepted March 2001).
11. Quintard, M. and Whitaker, S., "Transport in Chemically and Mechanically Heterogeneous Porous Media", *Advances in Water Resources*, 1998, Vol. 22
12. Bonnans, J.F., Gilbert, J.C., Lemaréchal, C. and Sagastizabal, C., "Optimisation numérique, Aspect théoriques et pratiques", *Collection SMAI, Mathématique & Application N° 27*, 1997, Springer-Verlag
13. Saouab, A., Bréard, J. and Bouquet, G., LCM Process Optimal Control, JNC Cachan – France, pp. 1117-1126 (2000).

## PERMEABILITY PREDICTION FOR INDUSTRIAL TEXTILE PREFORMS

F. Robitaille, A.C. Long and C.D. Rudd

School of Mechanical, Materials, Manufacturing Engineering and Management,  
University of Nottingham, Nottingham NG7 2RD, UK

### ABSTRACT

This paper describes an algorithm for the prediction of directional permeability values for general planar preforms. The porous medium is represented as a series of interconnected channels; the main task is to provide an adequate representation of the channel geometry. The implementation is based on a textile modeller developed by the authors. Flow is assumed to occur mainly in the plane of the textile, corresponding to the case of thin preforms. The algorithm reduces the 3D flow domain to a multi-faceted curved surface. This surface describes the channels and can be associated to the streamlines followed by the fluid in the preform. A tow permeability or local gap height is associated to each point of the surface depending if this point is located inside or outside of a tow. Darcy's law and a compatible equation for viscous flow in a channel are solved using a standard finite difference technique and a value of the directional permeability is obtained. The paper describes the main geometric operations involved in the algorithm.

### INTRODUCTION

A general textile modeller (figure 1) was developed by the authors. This provides generic geometric definitions of many textiles under a unified format (1, 2). The objective was to create textile geometries that can be used in integrated simulations for textile composites. For example, the configuration taken by a dry textile when it is draped and compacted can be evaluated using appropriate methods. If the mesh is extended to the empty zones between the tows the model can be used for the prediction of the mechanical properties of textile composites; such work is currently in progress (3). Here the model is used for the calculation of the permeability of preforms (4-7). Figure 1 shows images and 3D meshes of a) a plain weave and b) a  $\pm 45^\circ$  stitched textile obtained from the TexGen software.

The first phase of the algorithm proceeds as follows. The free volume around the tows is split in basic volumes (figure 2). Basic volumes are continuous volumes with vertical walls, delimited by a single entity (tow or domain boundary) on their lower and higher surfaces (figure 2a). At the same time, pairs of connection surfaces are identified. The two surfaces forming one pair coincide in the flow domain but are associated to neighbouring basic volumes (figure 2b). Bisector planes are then created, each separating a basic volume into two superimposed equal volumes (figure 2c). The bisector planes represent the direction of fluid flow in a basic volume. Finally the bisector planes are connected (figure 2d); the information provided by the connection surfaces is used to do this.

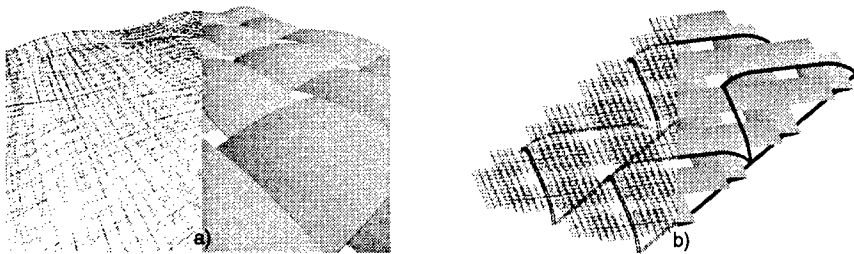


Figure 1. Meshes used by the algorithm

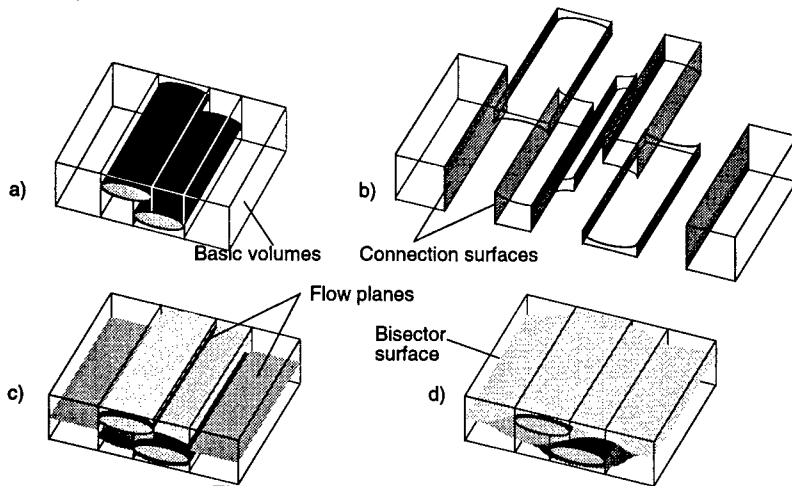


Figure 2. First phase of algorithm

The above steps create a surface corresponding to the streamlines that one would draw to represent the flow field in a fairly open, low  $v_f$ , configuration. However, real preforms always feature contact between the tows. The tows and textile layers are often heavily deformed and their shapes differ greatly from the generic ones shown in figures 1, 2. The algorithm includes a second phase that account for this (figure 3).

The second phase of the algorithm proceeds as follows. Once the basic volumes and the first bisector planes are defined the algorithm identifies zones where the thickness of these basic volumes is zero (figure 3e). The perimeters of these zero-thickness zones are projected along  $z$ . Areas where these projections interfere are identified (figure 3f). The volumes extending continuously between superimposed zero-thickness zones are merged (figure 3g). Bisector planes are created for these merged volumes and connected with those created previously (figure 3h).

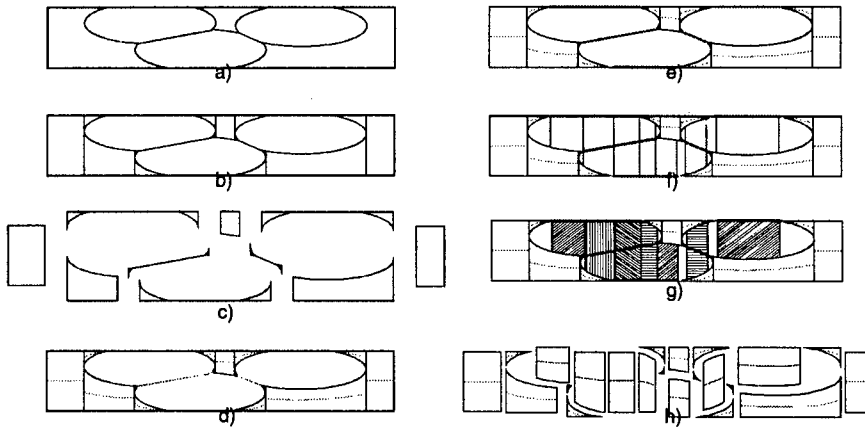


Figure 3. Second phase of algorithm

The second phase of the algorithm identifies volumes in the preform where the fluid cannot flow in an open channel; only under such circumstances will the fluid flow in the less permeable tows. Hence the localisation of high flow rates zones is initially done by the geometric algorithm and completed by the numerical FD solution.

### ALGORITHM

Firstly, the lower and higher tow surfaces and lateral tow edges are defined (figure 4). The tows are given as ensembles of three-node elements forming open-ended envelopes that extend beyond the domain boundaries. The elements in each envelope are separated in two groups: the lower and higher tow surfaces. These surfaces are bound by two lateral tow edges; these are the two continuous series of element edges (lines) that lie furthest from the centreline of the tow. Start and end points are associated with each tow edge. In addition to the edges, co-ordinate data are stored for the left edge start, left edge end, right edge start and right edge end.

The second operation consists of trimming the envelopes to the boundaries of the flow domain. This is straightforward as the elements making the tow surfaces are triangular. The triangular elements that are located inside the domain are not changed, those located entirely out of the domain are removed, and those crossing the boundaries of the domain are split into one or more new triangular elements located in the domain. This last operation involves the creation of new nodes located on the boundary of the flow domain (figure 5).

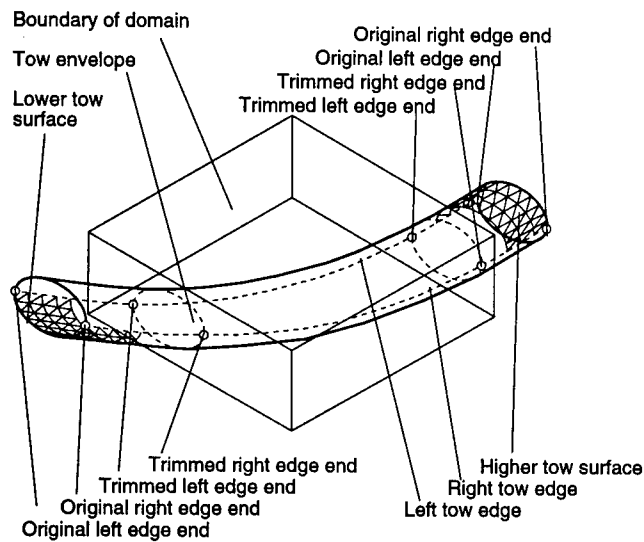


Figure 4. Tow envelopes, lateral tow edges, higher and lower surfaces

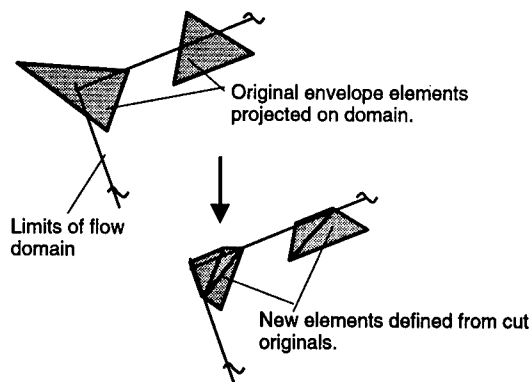


Figure 5. Trimming of envelopes and creation of new elements

The third operation consists of identifying control points for each pair of tows present in the domain. Control points are defined in the  $x, y$  plane as the positions where projections of the 4 lateral tow edges coincide; left and right edges starts and ends and the corners of the domain are also included (figure 6). Most points in the first group correspond to crossovers of two lateral edges but parallel projections of lateral tow edges can't be neglected. The former are termed crossover control points while the latter are collinear control points. This operation is done for each pair of tows.

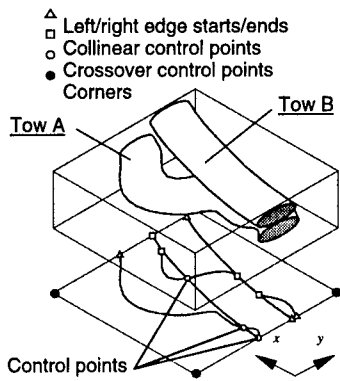


Figure 6. Control points

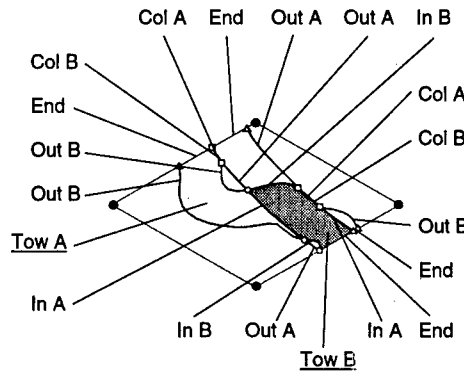


Figure 7. Types of tow edge segments

The fourth operation consists of identifying superimposition surfaces for each pair of tows. Superimposition surfaces are continuous zones of the  $x, y$  plane where the projection of two tows intersect; the number of distinct surfaces that can be defined for two given tows A and B is unlimited. This is done by splitting each lateral tow edge into edge segments, extending between two control points (figure 7). Edge segments from tow A are tagged as being inside or outside of tow B, or collinear to one of its lateral edges; edge segments from tow B are characterised similarly. Superimposition surfaces (shaded in figure 7) are easily identified as their perimeter must be closed and extend along projected edge segments that are inside a tow or collinear with one of its edges ("In" and "Col" in figure 7), or along projected tow ends defined on the boundary ("End" in figure 7). Each surface is stored as the  $x, y$  coordinates of the control points defining its perimeter; the information also identifies the two 3D tow surfaces facing each other over the domain. In figure 7 these are the higher surface of tow A and lower surface of tow B.

The fifth operation consists of identifying void surfaces for each pair of tows. Void surfaces are continuous zones of the  $x, y$  plane where no tow projection is present. Void surfaces (shaded in figure 8) are identified as their perimeters must be closed and extend along projected edge segments that are outside a tow or collinear with one of its edge ("Out" and "Col" in figure 8), or along the domain boundary. The void surfaces are stored as  $x, y$  co-ordinates of the control points defining their perimeter.

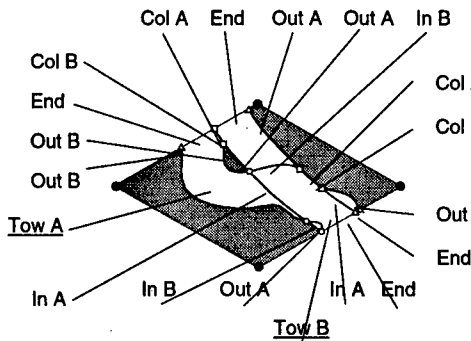


Figure 8. Void surfaces

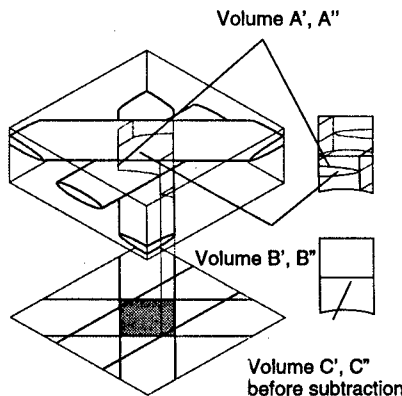


Figure 9. Basic volumes between tows

The sixth operation consists of creating the first basic volumes, namely those defined between the lower surface of a tow and the higher surface of another tow. This operation is straightforward as the 3D surfaces associated with the superimposition surfaces defined above are used. Each couple of 3D surfaces is considered in turn.

Firstly, couples of 3D surfaces  $A'$  and  $A''$  (associated to superimposition surface  $A$ ) between which no other 3D surfaces  $B'$  or  $B''$  (associated to any other superimposition surface  $B$ ) can be found are identified. These surfaces  $A'$  and  $A''$  are identified by verifying that the 3D surfaces  $B'$  and  $B''$  of which the superimposition surface  $B$  intersects the superimposition surface  $A$  (in the  $x, y$  plane) are not defined between  $A'$  and  $A''$ . This is easily done as the identity of the tows associated to each superimposition surface was stored in step 4, and the definitions of the tow surfaces are available from step 1. The volume defined between the 3D surfaces  $A'$  and  $A''$  is a basic volume; when such a volume is created the 3D surfaces are tagged as being part of a volume and the relevant information is stored (figure 9).

Secondly, couples of 3D surfaces  $C'$  and  $C''$  between which the only 3D surfaces that can be found are already part of a volume (such as  $A', A''$ ) are identified using a similar process. In order to create basic volumes (one or more), the superimposition surface  $A$  must be subtracted from the superimposition surface  $C$ . The algorithm also handles cases where two couples of surfaces  $A', A''$  and  $B', B''$ , both forming independent basic volumes, must be subtracted from a volume defined between  $C'$  and  $C''$ ; there is no theoretical limitation to the number of such couples which may have to be subtracted simultaneously from a larger volume enclosing them (figure 9).

One last remark is made regarding the operation detailed in the above paragraph. When a volume such as the one defined between  $C'$  and  $C''$  is created, all the volumes enclosed in it (such as the one defined between  $A'$  and  $A''$ ) are tagged as enclosed volumes. If a third volume  $D', D''$  is defined around  $C, C''$ , then only this one ( $C', C''$ ) must be subtracted from  $D', D''$ . The initial volume  $A', A''$  does not affect the process anymore, and the couple of surfaces  $A'$  and  $A''$  is bypassed altogether.

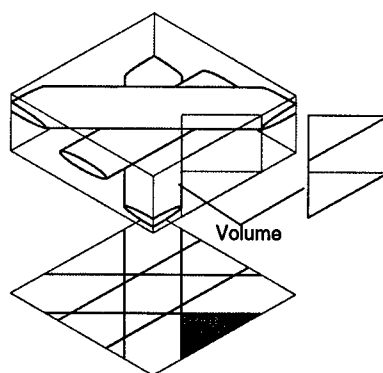
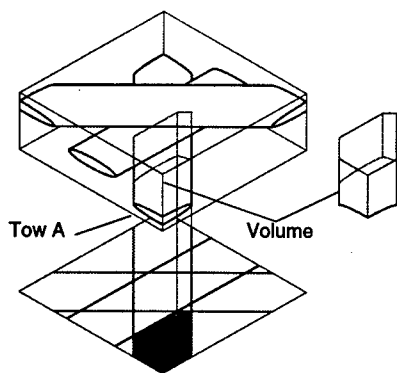


Figure 10. Volume between tow and wall      Figure 11. Volume between two walls

The seventh operation consists of creating the basic volumes defined between a tow and a horizontal domain wall. These volumes appear next to a tow surface that is

nearest of a horizontal wall, and on both sides of a tow when no superimposition occurs. All lower and higher tow surfaces are considered in turn. Superimposition surfaces involving the relevant side of tow A, identified in step 4, are subtracted from the projection of the entire tow A in the  $x, y$  plane. Basic volumes are defined directly between the remaining zones of the lower or higher surface of tow A and the appropriate horizontal wall (figure 10).

The eighth operation is the last one where basic volumes are created. Here volumes involving only the top and bottom horizontal walls of the domain are created; these volumes correspond to holes appearing along the  $z$  axis, throughout the preform. The relevant surfaces are easily created by identifying the intersection of all the void surfaces created in step 5. The basic volumes are defined over these intersections, between the horizontal walls. The volumes are identified and stored (figure 11).

At this stage all basic volumes defined between the tows are available; the ninth operation consists of creating the individual bisector planes for each volume. This is a conceptually simple operation involving a number of practical aspects related to the mesh definition; these will not be discussed here.

The tenth operation consists of identifying the connections to be made between the bisector planes associated to neighbouring volumes. Basic volumes extend between two surfaces (parts of a tow envelopes or of a horizontal domain boundaries) of which the corners are identified when the volumes are created. A volume actually extends between the two tows that are furthest apart among those to which the control points forming the corners of the surfaces are associated. All other contacting tows positioned between these two tows, along  $z$ , interact with the volumes on a line contact. The line contacts are defined on lateral tow edges, with their ends located at the same  $x, y$  co-ordinates where the relevant control points are found. Therefore after formally identifying the lateral surfaces of each volume, contacts can be identified simply by considering the control points defined on the projections of lateral tow edges; neighbouring volumes will share at least a segment on one common tow edge.

At this stage the basic volumes and the connections to be made between them are identified. As mentioned above (figure 3), the eleventh step consists of identifying tow volumes for which bisector planes are to be created and connected to the other bisector planes created at step 9. The creation of these bisector planes involves a number of operations that are somewhat similar those previously described. Consequently this part of the algorithm is described in a more general manner; references can be made to the above paragraphs.

Firstly, zones in the initial basic volumes featuring near-zero thickness are identified. This operation is performed by looking at the normal distance separating partially superimposed elements of the bottom and top surfaces. The distance can be calculated in a number of ways and in each case, different criteria can be applied. One way of assessing the normal distance for an element A consists in identifying the elements B, C and D (some of which may be the same) that intersect the normal to each node of element A, and calculating the average distance between the nodes and the elements. On each surface, zero-thickness zones extend on contiguous elements as long as the above distance criterion is satisfied. There is no theoretical

limitation to the number of zero-thickness zones that can be identified on one bottom or top surface, for one volume. The algorithm performs a number of additional operations such as merging neighbouring zero-thickness zones, in order to simplify further processing. The final zero-thickness zones are stored as  $x, y$  perimeters and associated to the relevant basic volumes.

Once the zero-thickness zones are identified they are investigated in turn for superimposition along  $z$ . This is a more straightforward operation than the one described in steps 3 and 4 as the zero-thickness zones are readily defined as closed perimeters. The objective is to create basic tow volumes that expand in the space occupied by the tows, below or above at least one zero-thickness zone; this operation is represented in figures 3f and 3g. The volumes that are defined immediately above or below one such surface, or continuously between two or more such surfaces, are merged into one basic tow volume. If, for example, one zero-thickness zone A superimposes totally with a zero-thickness zone B and partially with another zero-thickness zone C, then one basic tow volume will be created between zero-thickness zones A and C and another adjacent zero-thickness zone will appear between zero-thickness zones A and B (figure 12). Once the basic tow volumes are available, bisector planes are created as described in an operation similar to step 9. Then the connections to be made between these bisector planes and the ones defined for the basic volumes are identified in an operation similar to step 10.

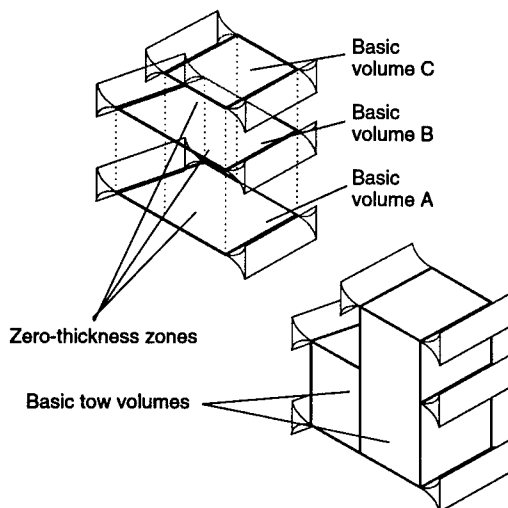


Figure 12. Zero-thickness zones and basic volumes associated to tows

The operations performed after the above 11 steps consist of connecting the bisector planes and meshing. The latter operation is performed using standard finite differences mesh generation on each patch (8). Nodes located at patch connections are created first; then a curvilinear mesh is created for each patch and the individual meshes are connected. At this stage the geometric work is complete; a standard

finite difference method is used to solve the equations for saturated flow over the domain.

## CONCLUSION

This paper presents the geometric operations involved in the automatic processing of a textile preform over a limited flow domain, for the calculation of components of the in-plane permeability tensor. The tow envelopes used as an input can be provided under a large number of configurations; hence the algorithm can process the cases of sheared and compacted, contacting tows indifferently. The current solution involves Darcy's law and analogue expressions for flow between infinite plaques, for a saturated domain; other equations may eventually be implemented in order to simulate unsaturated flow and phenomena such as void entrapment.

## ACKNOWLEDGEMENTS

The continuing support of the Ford Motor Company Limited, Dowty Aerospace Propellers Limited, Rolls Royce Plc, Brookhouse Paxford Limited, Flemings Industrial Fabrics and the Engineering and Physical Sciences Research Council, UK, is gratefully acknowledged.

## REFERENCES

1. Robitaille F, Clayton B R, Long A C, Souter B J and Rudd C D, Proceedings of the Institution of Mechanical Engineers 213, (1999) 69
2. Robitaille F, Clayton B R, Long A C, Souter B J and Rudd C D, Proceedings of the Institution of Mechanical Engineers 214, (2000) 71
3. Crockston J J, Souter B J, Long A C, Jones I A, Proceedings of ICCM-13, (2001)
4. Scheidegger A E, 'The Physics of Flow Through Porous Media', University of Toronto Press (Toronto), 1974
5. Dullien F A L, 'Porous Media: Fluid Transport and Pore Structure', Academic Press (New York), 1979
6. Bear J, 'Dynamics of Fluids in Porous Media', Elsevier (New York), 1974
7. Nield D A and Bejan A, 'Convection in Porous Media', Springer-Verlag (New York), 1992
8. Thompson J F, Warsi Z U A and Mastin C W, 'Numerical Grid Generation', North Holland Ltd (New York), 1985

## **Shear flow characterisation of GMT, and use of the Brinkman equation in modelling the interaction of the flowing material with the mould surface**

G. Kotsikos\* and A.G. Gibson  
Centre for Composite Materials Engineering  
University of Newcastle upon Tyne NE3 1XQ UK

*\*Now at DERA Rosyth*

### **ABSTRACT**

This paper will describe experiments of different types, carried out to characterise the deformation behaviour of molten GMT in simple shear. The results of the work suggest that, in many situations, the material tends to undergo wall slip, rather than uniform shear deformation with a zero velocity boundary condition. This result, which in many ways is not a surprising one, has implications for the way in which the non-isothermal moulding of GMT (and SMC) is modelled. While it is generally accepted that the main flow regime in compression moulding of these materials is biaxial extension, there has been some debate concerning the best way to model the small degree of shear flow that takes place. The Brinkman equation, which can be regarded as a general description of the combined effects of bulk viscous flow and Darcy flow, provides a useful and relatively simple means of describing the flow behaviour of a GMT melt near to a mould wall. The implications of this for modelling of GMT behaviour (and that of other materials in non-isothermal moulding) will be discussed.

**SESSION 4:**  
**PROCESS MONITORING &**  
**CONTROL**

## IMPEDANCE CURE AND FLOW MONITORING IN THE PROCESSING OF ADVANCED COMPOSITES

Alexandros A Skordos\* and Ivana K Partridge\*

### ABSTRACT

The paper presents recent developments in the area of impedance cure and flow monitoring of thermosetting matrix/continuous reinforcement composites. Impedance cure monitoring is a variation of dielectric cure monitoring which follows the progress of the curing reaction and the accompanying structural phenomena by means of the impedance spectrum response of the curing material. Currently, a good correlation between specific features of the imaginary impedance spectrum and the progress of the reaction has been found to hold under isothermal conditions. In this paper the correlation between the impedance and the progress of the reaction is extended to dynamic cure conditions. Impedance flow monitoring of the filling stage of liquid moulding of glass composites, based on lineal sensors, has been developed and reported recently. Here, this technique is extended to the case of conductive reinforcements with the development of a new sensing system. The system performance is tested against visual observation of the flow front position during resin transfer moulding.

### INTRODUCTION

In recent years the need for predictive modelling and for in-situ real time monitoring of composites manufacturing processes has arisen and been met by the development of a family of appropriate techniques. The modelling of the cure stage of composites manufacturing has been investigated extensively [1-6] and cure monitoring methods, such as dielectric [7,8], fibre optic [9,10] and acoustic cure monitoring [11-12], begun to be implemented in an industrial environment. Very recently an interest in flow monitoring techniques based on optical fibre, dc conductivity and dielectric measurements and appropriate for the measurement of filling progress during liquid composite moulding started to be developed [13-16].

Dielectric cure monitoring techniques are based on the dependence of the electric and dielectric measures (complex dielectric constant, conductivity and impedance) on structural properties of the curing system (degree of cure, glass transition temperature and viscosity). The behaviour of a thermoset, when an AC electric field is applied to it, is governed by three phenomena: (i) dipole polarisation, (ii) migrating charges conduction and (iii) electrode polarisation.

A few research groups have chosen to present and process dielectric cure monitoring results in terms of the complex impedance. The essential meaning of the measurement is exactly the same as in the dielectric constants representation, as the phenomena taking place are identical, but in some cases the impedance representation appears to be more natural. In impedance monitoring the electric response of a thermosetting system can be represented by an equivalent circuit, the most widely used circuit is illustrated in Fig. 1 [17-19]. The presence of dipolar relaxation is accounted for by introducing a capacitor  $C_{sd}$  in series with a resistor  $R_{sd}$ , corresponding to the permanent dipoles and connected in parallel with another

\* Advanced Materials Department, Cranfield University, Bedford, MK43 0AL, UK

capacitance  $C_{id}$ , corresponding to the induced dipoles. The migrating charges mechanism is represented by a resistor  $R_I$  connected in parallel with the dipolar relaxation sub-circuit and the electrode polarisation by two capacitors  $C_e$ , one for each electrode, connected in series with the overall circuit. The complex impedance of the circuit is [19]:

$$Z = Z' - jZ'' \quad [1]$$

where

$$Z' = \frac{R_I \left[ \omega^2 C_{sd}^2 R_{sd} (R_{sd} + R_I) + 1 \right]}{\omega^2 (C_{sd} R_I + C_{sd} R_{sd} + C_{id} R_I)^2 + (\omega^2 C_{sd} R_{sd} R_I C_{id} - 1)^2} \quad [2]$$

$$Z'' = \frac{R_I \left[ \omega^3 C_{sd}^2 R_{sd}^2 R_I C_{id} + \omega R_I (C_{id} + C_{sd}) \right]}{\omega^2 (C_{sd} R_I + C_{sd} R_{sd} + C_{id} R_I)^2 + (\omega^2 C_{sd} R_{sd} R_I C_{id} - 1)^2} + \frac{2}{C_e \omega} \quad [3]$$

The impedance spectrum of such a circuit is illustrated in Fig. 2. The response at low frequencies is dominated by the electrode polarisation effect, the conduction mechanism becomes dominant at intermediate frequencies and the dipolar relaxation at high frequencies.

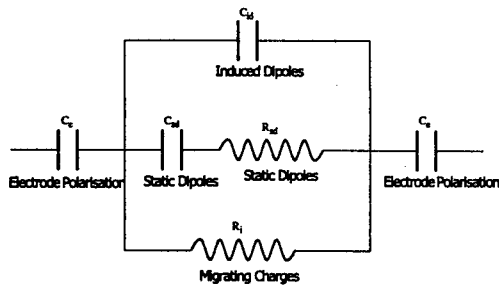


Fig. 1 Equivalent circuit representation of the electrical response of thermosetting materials

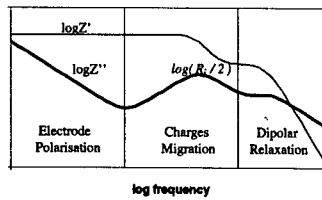


Fig. 2 Impedance spectrum of the electrode polarisation-charge migration-dipolar relaxation circuit

The application of monitoring to industrial situations requires the translation of the impedance results to information related to the chemical or the structural state of the curing material. A correlation between the progress of the reaction and the logarithm of the resistivity as estimated using the peak imaginary impedance value (Fig. 2) has been established. The correlation between normalised resistivity and fractional conversion under isothermal conditions can be expressed as [18, 19]:

$$\alpha = \alpha_{max} \frac{\log \tilde{\rho} - \log \tilde{\rho}_0}{\log \tilde{\rho}_{max} - \log \tilde{\rho}_0} \quad [4]$$

where  $\alpha_{max}$  is the maximum degree of cure at the curing temperature,  $\tilde{\rho}$  the resistivity,  $\tilde{\rho}_0$  the resistivity of the unreacted resin and  $\tilde{\rho}_{max}$  the resistivity of the fully reacted resin.

Empirical evidence suggests that some of the structural phenomena taking place during the cure are manifested in impedance signal. More specifically, vitrification has been found to coincide with a knee in the imaginary impedance versus time curve and a peak in the real impedance versus time curve [19, 20], but the underlying molecular mechanisms causing this correlation have not been elucidated.

Impedance flow monitoring is based on the significant differences between the electric properties of dry and wetted areas of a composite pre-form. A lineal sensor with a semi-cylindrical fringing field placed along the flow path of a non-conductive reinforcement can monitor the progress of filling as it is covered gradually by resin. A sensing setup

implementing this principle has been applied successfully to the filing of glass reinforced preforms [16]. In that case the covered length of the sensor is a linear function of the complex admittance as follows [16]:

$$l_w = \frac{Y_{\text{sensor}} - Y_{\text{dry}}}{Y_{\text{cov}} - Y_{\text{dry}}} l_t \quad [5]$$

where  $Y_{\text{dry}}$  is the admittance of the dry sensor and  $Y_{\text{cov}}$  is the admittance measured when the sensor is fully covered.

In this study results leading to the extension of the applicability of impedance monitoring in composites processing are presented. The impedance cure monitoring response of an epoxy resin is investigated under isothermal and dynamic curing conditions and a methodology correlating impedance signals with fractional conversion under both dynamic and isothermal conditions is established. Impedance flow monitoring is extended to conductive reinforcement with the design implementation and validation of a new sensing setup appropriate for carbon pre-forms.

## EXPERIMENTAL DETAILS

### A. Cure monitoring

An epoxy resin appropriate for resin transfer moulding (Hexcel, RTM6) has been used in this study. Impedance cure monitoring measurements were performed using a Solartron SI 1260 frequency response analyser. The instrument communicated with a computer via an IEEE interface. A purpose built software code has been utilised to drive the frequency response analyser and collect the raw data. Commercial sensors (GIA) comprising an assembly of interdigitated electrodes printed on a polymeric film were used in this study. After soldering on the cables that connect the analyser to the sensor, the sensor was immersed in a glass tube containing liquid resin. Then the glass tube was placed in a hollow copper cylinder surrounded by heating elements, which were controlled by a Eurotherm temperature controller. A control thermocouple was placed in a hole on the wall of the hollow cylinder. A second thermocouple was placed in the glass tube in order to record the actual thermal profile of the resin. Isothermal cure experiments on RTM6 epoxy resin were performed at 130, 140, 150 and 160 °C and dynamic cure experiments were performed at 0.25, 0.5, 0.75, 1, 1.25, 1.5, 1.75 and 2 °C/min. The measurements were performed in the frequency range between 1 Hz and 1 MHz. Twenty-five frequencies were swept on a logarithmic scale.

### B. Flow monitoring

The sensing setup comprises an array of thin insulated wires, that are in contact with the carbon preform and are connected to the impedance analyser. The reinforcement is connected to the analyser and the measurement is performed between the array of wires and the fibres of the pre-form. A schematic of the arrangement of fibre tows and wires is given in Fig. 3. In the case illustrated, the wires are in contact with the RTM glass tool. As the fibre tows conform around the hard wire some pores are formed. With the application of a voltage an electric field is formed between the conductive core of the wire and the fibre. The field occupies the insulating coating of the wire and the pore regions. When the reinforcement is dry the pores are filled with air. As the impregnation process progresses more and more of the pores are filled with the resin. Similarly to the glass reinforcement case, it is expected that the difference in electrical properties of air and of the liquid resin will result in gradual change in the electrical response as the filling progresses.

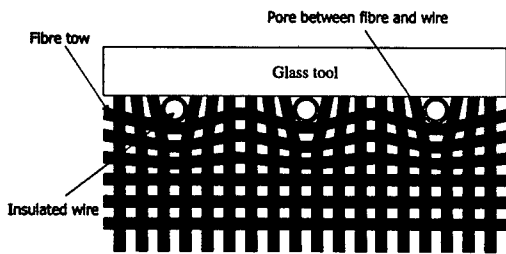


Fig. 3 Sensing configuration for flow monitoring in carbon reinforcements

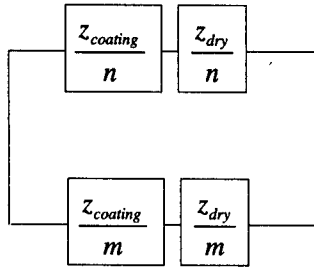


Fig. 4 Equivalent circuit representing the response of the flow sensing setup

The sensing configuration can be considered as the sum of a number of wire and fabric segments with length unity. Assuming that the carbon reinforcement is under uniform potential, all the segments corresponding to one wire are connected in parallel. Each of these segments contains two elements connected in series, one corresponding to the insulating coating and one to the pores. If the unit length is large compared with the size of the pores, the impedance of the element corresponding to pores will be equal to  $z_{dry}$  for all the  $n$  segments in the dry region of the mould, and equal to  $z_{wetted}$  for all the  $m$  segments in the wetted region. This situation can be represented by the circuit of Fig. 4. Consequently, the following equation is expected to hold:

$$Y_{sensor} = m \left( \frac{z_d - z_w}{z_c^2 + z_c z_d + z_c z_w + z_w z_d} \right) + \left( \frac{(m+n)z_c + (m+n)z_w}{z_c^2 + z_c z_d + z_c z_w + z_w z_d} \right) \quad [6]$$

where  $z_c$  denotes the impedance per unit length of the insulating layer of the sensing wire. Similarly to the case of the glass reinforcement, a linear expression of the sensor admittance as a function of the length of the wire in contact with liquid resin (Eq. 5) can be derived.

The sensor performance was validated during the filling and curing of a continuous carbon fibre/RTM6 composite in a partially transparent RTM tool. The carbon non-crimped fabric reinforcement (CTLX, BTI Europe) had a surface density of 816 g/m<sup>2</sup> and comprised three plies with +45/-45/0 orientations. Four layers of this fabric were used, making the total lay-up sequence (+45/-45/0/0/-45/+45)<sub>2S</sub>. The fibre weight fraction in the laminate was 69%. The sensor comprised an array of three insulated (polyurethane coated) copper wires, with a diameter of 0.25 mm, placed in the centre of the mould in contact with the glass top tooling. The distance between the wires was 2 mm. The sensor length was 28 cm and the mould thickness 3.3 mm. The filling was performed at 120°C. Visual determination of the flow front position was recorded against time. After completion of the filling stage the mould temperature was increased to 160°C to cure the composite.

## RESULTS

### A. Cure monitoring

The evolution of real and imaginary impedance spectra during the cure at 150 °C is illustrated in Fig. 5. The results of isothermal experiments at 130,140 and 160 °C show equivalent behaviour. It can be observed that the real impedance spectrum comprises a plateau at low frequencies and a region where the impedance decreases as the frequency increases. The latter region starts as a linear decrease, which becomes less intense towards very high

frequencies, indicating the existence of another plateau at frequencies beyond 1 MHz. The imaginary impedance spectrum comprises three linear regions separated by a minimum and a maximum. At very low frequencies imaginary impedance decreases with frequency, reaches a minimum value and then increases up to a maximum. Further increase of the frequency results in a linear decrease of the imaginary impedance logarithm. Both spectra show a strong dependence upon material state as it changes during the cure. The real impedance plateau value increases as the curing progresses, whereas the frequency where the plateau ends decreases. Both the minimum and maximum of imaginary impedance increase as curing progresses. The whole imaginary impedance spectrum is shifted to lower frequencies as the reaction progresses but, unlike in the case of the real impedance the final linear part remains constant.

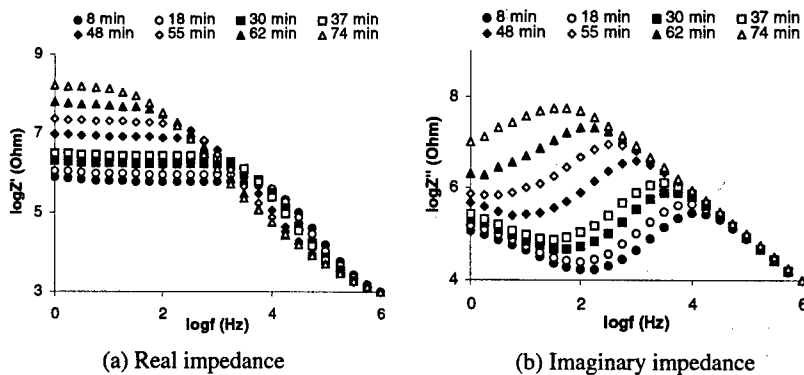


Fig.5 Impedance spectra evolution during isothermal cure at 150 °C

The evolution of the real and imaginary impedance spectra for the experiment at 0.25 °C/min is illustrated in Fig. 6. The behaviour illustrated in Fig. 6 is characteristic of all dynamic cure experiments of RTM6 epoxy resin. The form of both spectra is identical to the isothermal case, i.e. the real impedance spectrum comprises a plateau and a linear decrease region, and the imaginary impedance spectrum comprises a minimum, a maximum and three linear regions. However, the evolution of the spectra is more complicated in the dynamic case due to the combined influences of temperature and of state-of-material changes. In the initial stages of the dynamic cure the real impedance plateau value decreases and the frequency where the plateau ends increases (curves at 50 and 100 °C in Fig. 6a) as a result of the rise in temperature. At higher temperatures (curves at 135, 140 and 150 °C in Fig. 6a) the spectrum shows the behaviour observed in isothermal cure, i. e. the plateau value increases and the plateau end frequency decreases. This can be attributed to the domination of material state connected phenomena to the signal. When temperature increases further the situation reverses (curves at 170, 180, 190 and 210 °C in Fig. 6a) and due to temperature changes domination in the signal, the plateau value decreases and the plateau end frequency increases. Analogous phenomena are observed in the evolution of the imaginary impedance spectrum. At low temperatures the spectrum is shifted to higher frequencies and the maximum and minimum values decrease (curves at 50 and 100 °C in Fig. 6b). At intermediate temperatures (curves at 135, 140 and 150 °C in Fig. 6b) the behaviour observed in isothermal cure is reproduced, i.e. the spectrum is shifted to lower frequencies and the maximum and minimum values increase, implying material state changes domination. Further increase in temperature (curves at 170,

180, 190 and 210 °C in Fig. 6b) leads to temperature changes domination, i.e. the whole spectrum is shifted to higher frequencies and the maximum and minimum values decrease.

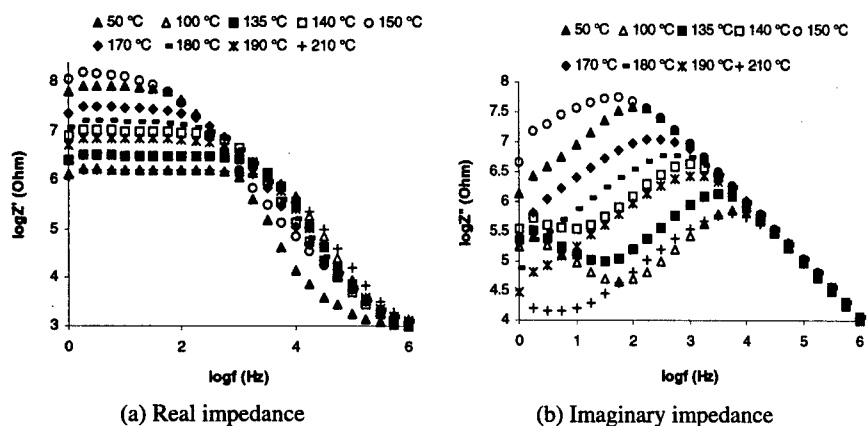


Fig. 6 I impedance spectrum evolution during dynamic cure at 0.25 °C/min

It has been shown that following the changes of the imaginary impedance spectrum maximum can give an accurate estimation of the fractional conversion under isothermal conditions [18, 19]. In Figs. 7 and 8 the evolution of the imaginary impedance maximum together with the degree of cure evolution, as calculated using the kinetic model described elsewhere [21], for the isothermal experiments at 130, 140, 150 and 160 °C and the dynamic experiments at 0.25, 0.5, 0.75 are given. Lines indicating the cure time of maximum reaction rate in each experiment are superimposed on the curves, in order to facilitate the comparison between impedance and progress of reaction data. In Fig. 7 it can be observed that the imaginary impedance maximum imitates the conversion curves very closely. The start, end and maximum rate points are very similar in the two curves. Thus, normalisation of the impedance data can lead to a direct estimation of the reaction progress in isothermal experiments. In contrast, under dynamic conditions, as illustrated in Fig. 8, the combined influence of temperature and reaction complicates the imaginary impedance maximum behaviour. At the beginning of the curing temperature governs the maximum value, which drops as the viscosity of the resin decreases. When reaction becomes fast it starts to dominate the signal and the imaginary impedance maximum increases, as the formation of the network impedes migration of the extrinsic charges. The situation is reversed back to temperature domination towards the end of the reaction. The reaction onset, maximum rate and end points do not coincide with the corresponding points of the impedance versus cure time curves. Consequently following the evolution of maximum impedance cannot provide the means for reaction monitoring under dynamic heating conditions.

Here a different procedure is proposed for the exploitation of impedance data for reaction monitoring. As presented previously the imaginary impedance spectrum has two extremes; a maximum corresponding to charge migration and a minimum at the point where electrode polarisation stops to control the impedance and charge migration becomes the dominant mechanism. Both extremes are shifted during the cure, to lower frequencies as the reaction progresses and to higher frequencies as temperature increases. The minimum of imaginary impedance is shifted outside the experimental spectrum at intermediate to high conversion combined with low and intermediate temperature, thus the available experimental data are limited in isothermal experiments. An observation significant for the monitoring of the

reaction is that the two extremes show similar shifts when temperature changes, whereas the drop of the frequency of the minimum is more sensitive to the reaction progress. This behaviour is manifested clearly in the higher heating rate dynamic curves illustrated in Fig. 9. For example in the 2 °C/min experiment the maximum shifts by 1.7 decades from 18 to 43 min, while the minimum shifts by 1.8 under the influence of the temperature increase, which is not accompanied by progress of the reaction. In contrast between 79 and 93 min, where the progress of reaction dominates the signal, the maximum shifts by 0.6 and the minimum by 1.4. At high heating rates (1.5, 1.75 and 2 °C/min) where both the minimum and maximum remain within the measurement frequency range throughout the cure another observation can be made. The minima of the frequencies of the two extremes appearing towards the end of the reaction occur at different times. This is illustrated by the lines which coincide with the minimum of the lower curves (frequency of minimum) in Fig. 9, whereas they intersect with the upper curves (frequency of maximum) at a time later than their minimum.

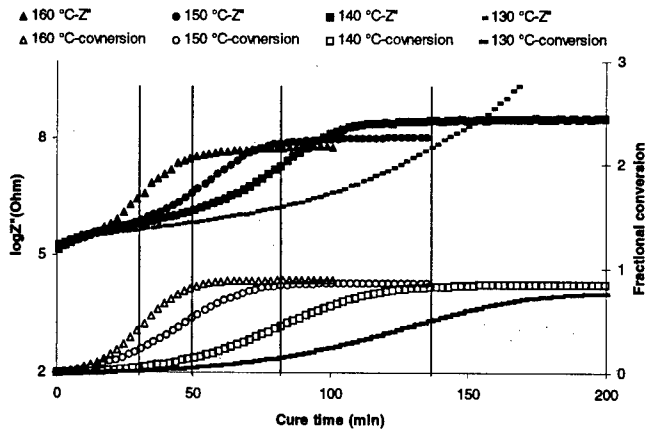


Fig.7 Imaginary impedance maximum and conversion versus time in isothermal cure

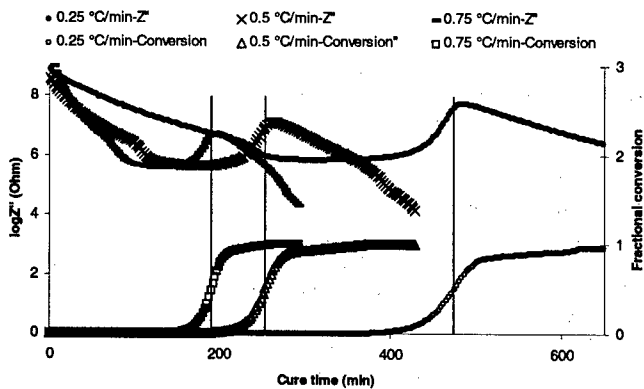


Fig.8 Imaginary impedance maximum and conversion versus time in dynamic cure of at low heating rates

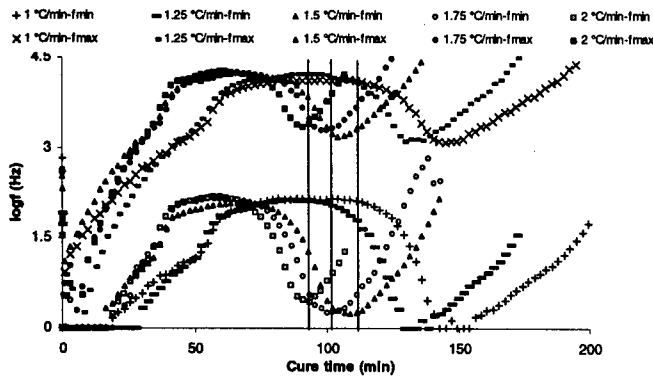


Fig.9 Frequencies of the impedance spectrum maximum and minimum in dynamic cure of RTM6 resin at high heating rates

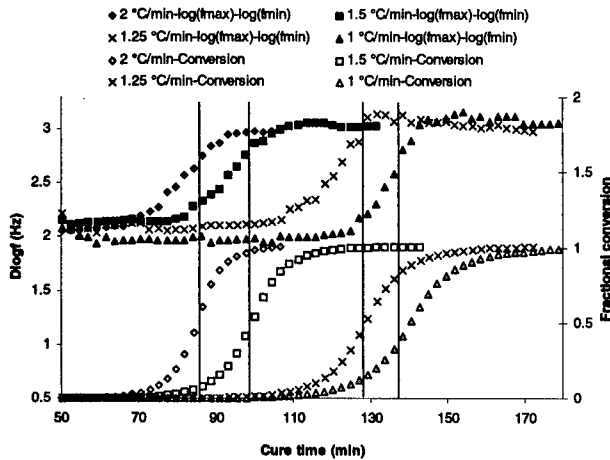


Fig.10 Impedance spectra maximum and minimum frequencies difference and degree of cure versus cure time in dynamic cure of RTM6

The different sensitivities of the extremes shift to the progress of the reaction can be used in order to eliminate the problems arising from the combined influence of temperature and degree of cure on the monitoring signals. In Fig. 10 the difference between the frequency of maximum and the frequency of minimum of the imaginary impedance spectrum is compared with the progress of reaction, for the high heating rate dynamic experiments. The frequency difference undergoes a step change. The times of onset, maximum rate and end of the step coincide with the corresponding times of the kinetics curves. When the material does not react the frequency difference remains constant. Thus, the frequency difference shows a strong dependence on the degree of cure, whereas its sensitivity to temperature variation appears low. In order to quantify the correlation, a third degree polynomial was fitted to the data. The equation of the fit is:

$$\alpha = 0.15D \log f^3 - 0.38D \log f^2 - 0.23D \log f + 0.81 \quad [7]$$

where  $\alpha$  is the fractional conversion and  $D \log f$  is the frequency difference. This relation is purely empirical and limited to the specific resin system sensor combination, but it provides the means for a direct estimation of the degree of cure at any temperature from the instantaneous imaginary impedance spectrum.

**B. Flow monitoring**

Eq. 5 was used to calculate the flow front position from the admittance data. The admittance measured when the sensor is fully covered by resin has been used as  $Y_{cov}$ . The real and imaginary part of the length are illustrated together with the visual flow front position measurement in Fig. 11. The average of the error in flow front location and the is 2 cm at 10 kHz and 0.8 cm at 1MHz. It can be observed that data gathered at 1 MHz are very close to the visual flow front measurement. Data obtained at a lower frequency (10 kHz) present some deviation. The imaginary length shows higher value at the frequency where the error in the flow front location estimation is higher, indicating deviation from linearity as described by Eq. 5. Thus, the imaginary length similarly to the non-conductive reinforcement case [16] offers the means for self estimation of the measurement accuracy. Cure monitoring results obtained using the sensing configuration are illustrated in Fig. 12. There, the evolution of normalised impedance at 10 kHz as calculated is shown. It can be observed that the sensing setup has a response equivalent to that of the microelectrodes. Normalised impedance undergoes a step change during the cure and vitrification is manifested as a knee towards the end of the curing.

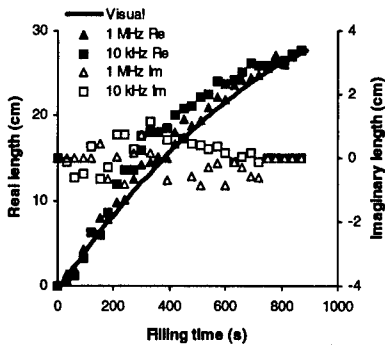


*Fig. 11 Comparison of visual measurement with dielectric flow measurement for filling during resin transfer moulding of an RTM6/carbon composite*

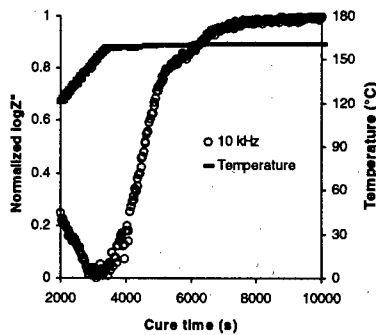


*Fig. 12 Temperature and normalised impedance during cure versus time using the flow monitoring setup in an RTM6/carbon composite moulding*

**CONCLUSIONS**

Results from the application of impedance spectroscopy to the monitoring of isothermal and dynamic cure of RTM6 epoxy resin and the RTM filling of carbon reinforced composites have been presented. The possibility of using impedance spectroscopy for the estimation of the degree of cure in both isothermal and dynamic conditions has been investigated. A purely experimental method based on the different sensitivity of the extremes

of the imaginary impedance spectrum to temperature and conversion has been developed and validated for the specific resin system. A sensing configurations appropriate for flow monitoring during RTM filling of conductive reinforcements was proposed. Equivalent circuit analysis demonstrated the linear dependence of the admittance, measured by the presented sensors, upon the flow front position. Experiments confirmed that the flow front position can be located continuously with a satisfactory accuracy. In addition, the existence of an imaginary component of the measured flow front position can be utilized as self-assessment tool of the measurement performance. The flow sensor also presented the ability to monitor the cure of the resin after the end of the filling stage.

#### REFERENCES

1. Loos AC and Springer GS, Journal of Composite Materials 17 1983 1352.
2. Tzeng JT and Loos AC, Composites Manufacturing 4 1993 157
3. Gao DM, Trochu F and Gauvin R, Materials and Manufacturing Processes 10 1995 57
4. Hojjati M and Hoa SV, Journal of Composite Materials 29 1995 1741
5. Tucker CL III, Polymer Composites 17 1996 60
6. Suratno BS, Ye L and Mai YW, Composites Science and Technology 58 1998; 58 191
7. Kranbuehl DE, Kingsley P, Hart S, Hasko G, Dexter B and Loos AC, Polymer Composites 15 1994 299
8. Maistros GM and I. K. Partridge IK, Composites 19B 1998 245
9. J. Mijovic J and S. Andjelic S, Polymer 36 1995 3783
10. Woederman DL, Spoerre JK, Flynn KM and Parnas RS, Polymer Composites 18 1997 133
11. Whitney TM and Green RE Jr. Ultrasonics 34 1996 347
12. Shepard DD and Smith KR, Journal of Thermal Analysis 49 1997 95
13. Shepard DD, SAMPE Journal 34 1998 31
14. Barooah P, Berker B and Sun JQ, Journal of Materials Processing and Manufacturing Science 6 1998 169
15. Mathur R, Advani SG, Parnas RS and Fink BK, International SAMPE Technical Conference 29 1997 42
16. Skordos AA, Karkanis PI and Partridge IK, Measurement Science and Technology 11 2000 25
17. Bellucci F, Valentino M, Monneta T, Nicodemo L, Kenny J, Nicolais L and Mijovic J, Journal of Polymer Science Part B: Polymer Physics 32 1994 2519
18. Mijovic J and Yee FCW, Macromolecules 24 1994 7287
19. Mijovic J, Andjelic S, Fitz B, Zurawsky W, Mondragon I, Bellucci F and Nicolais L. Journal of Polymer Science Part B: Polymer Physics 34 1996 379
20. Andjelic S, Mijovic J and Bellucci F, Journal of Polymer Science Part B: Polymer Physics 36 1998 641
21. Skordos AA and Partridge IK Polymer Engineering and Science 41 2001 793

## CONTROLLING COMPLEX CURE CYCLES VIA REAL-TIME DIELECTRIC MEASUREMENTS

M C Kazilas\*, G M Maistros\* and I K Partridge\*

### ABSTRACT

The paper considers the potential for real-time control of a complex cure cycle of a modified epoxy resin system commonly utilised in aerospace composite parts. It shows how cure cycle control may become possible through real-time in-situ acquisition of a dielectric signal from the curing resin, analysis of its main components and identification of the significant features. Through additional thermo-analytical modelling of the resin cure, it is then feasible to establish the control parameters and the rules under which the cure cycle can be controlled and optimised.

### BACKGROUND

Dielectric methods for monitoring thermoset cure have advanced during the eighties and are used increasingly to probe the different stages of resin cure in advanced composites processing. Changes in the dielectric behaviour of the resin under cure can give real-time and in-situ information on the advancement of the process parameters. Therefore it is feasible to trace the arrival at a desirable level of degree of cure  $\alpha$  and glass transition temperature  $T_g$ , determining parameters for the composite material performance. The cure monitoring can be applied at different levels: from an academic laboratory tool for the understanding of and optimisation of cure cycles, through to the use in process control using an expert closed loop process control system. Partridge and Maistros [1] have outlined three approaches to the control of the cure of composite materials: (i) temperature-based control, where information from thermocouples is the only monitoring parameter, (ii) sensor-based control, where an active monitoring system is utilized and real time information is recorded through an appropriate sensor and (iii) state-based process control where models relating cure time, temperature, viscosity, ionic conductivity, degree of cure and  $T_g$  are used for determining the optimum cure profile. In the state-based process control, sensors are used in order to ensure that the pre-determined cure profile is actually followed.

### EXPERIMENTAL

The cure cycle employed is given in Table I. The objective of this complicated cycle is to minimise the exotherm during cure of a particularly thick composite part. The complexity is necessitated by the nature of the resin, which contains a mixture of a latent crystalline hardener and an accelerator. Too fast an approach to the final cure temperature is known to result in an uncontrolled exotherm. For this reason the second segment of the normal manufacturing cure cycle covers more than two thirds of the total cure time. This also makes segment 2 the ideal candidate for investigation of the possibility of shortening the total cure cycle with safety. Two shorter durations of the second segment were therefore used in our experiments (Table II) and the effects of these changes on the later stages of cure were explored.

\* Advanced Materials Department, SIMS, Cranfield University, Bedford MK43 0AL

\* INASCO UK Ltd., SIMS Bldg 88, Cranfield University, Bedford MK43 0AL

Table I: Standard Cure cycle	
Segment	Action
1	Heat from ambient to 74 °C at a rate of 1 °C/min
2	Dwell at 74 °C for 9 hours
3	Heat from 74 °C to 82 °C at a rate of 0.5 °C/min
4	Dwell at 82 °C for 30 minutes
5	Heat from 82 °C to 92 °C at a rate of 0.5 °C/min
6	Dwell at 92 °C for 60 minutes
7	Heat from 92 °C to 125 °C at a rate of 1 °C/min
8	Dwell at 125 °C for 60 minutes

Table II: Experiments presented in this study	
	Duration of segment 2
Experiment 1	9 hours
Experiment 2	8 hours
Experiment 3	7 hours

The dielectric measurements were acquired using a Solartron Analytical SI 1260 Frequency Response Analyser and commercially available GIA microsensors. The amplitude of the excitation voltage applied to the sensors was 3V. A sweep of 25 frequencies between 1 Hz and 1 MHz was made. A full description of the experimental aspects of dielectric cure monitoring is given elsewhere [1]. Fig. 1 shows the structure of the dielectric sensor and the experimental cell constructed to achieve good temperature control.

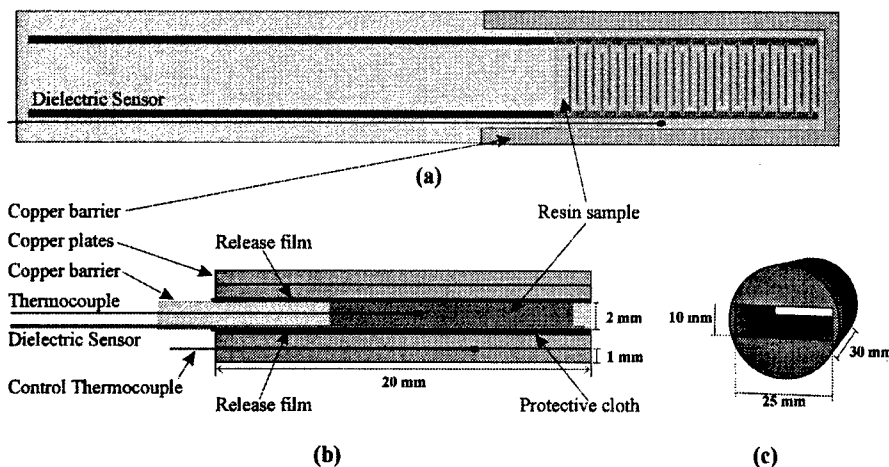


Figure 1: (a) Arrangement of the dielectric sensor and resin, (b) side view of the "sandwich" configuration and (c) the experimental cell

Small copper plates were used as "shelves". A control thermocouple was placed under the sample. A protective cloth was used in order to minimise the interaction between the copper plates and the field produced by the sensor. A release film prevented the resin from adhering

to the cell. The experimental configuration, as shown in Fig 1, was placed in a copper cylindrical cell with a heating element wrapped around it.

## RESULTS

### A. Results from standard cure cycle

Fig. 2 displays the changes in the ionic conductivity  $\sigma$  signal of the curing resin. The complex viscosity  $\eta$  values plotted on the same graph were determined in a separate experiment on a Bohlin 2910 rheometer, making sure that the temperature-time history closely matched that of the dielectric experiments.

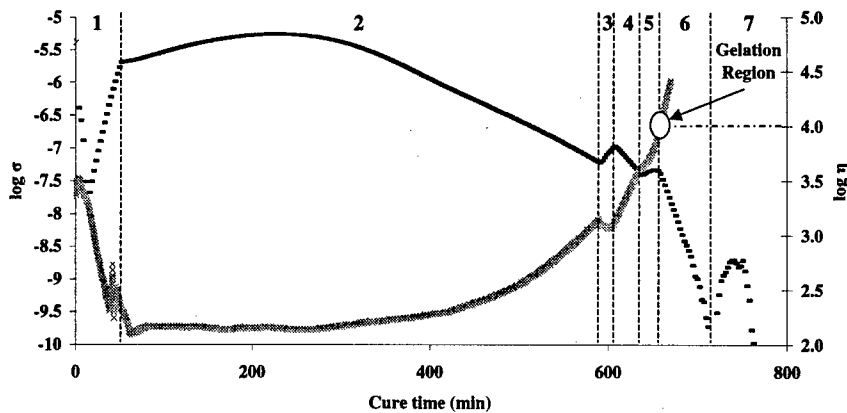


**Figure 2:** Ionic conductivity (black points) and complex viscosity (grey points) plot for the standard cure cycle. Dotted vertical lines define the different segments of the cure profile. Gelation region is indicated.

The viscosity values were recorded up to the measuring limits of the viscometer. In keeping with the previous work in our laboratory [2], an operational definition of gelation is made, as the point where the complex viscosity reaches the value of  $10^4$  Pa.s. In this experiment this point is about 660 min.

The ionic conductivity of the resin is proportional to the concentration of the unbound (free) charged species and to their mobility. For most epoxy and polyester resins, the number of free charged species does not change during cure, neither does their total charge. Therefore, any change in  $\sigma$  during the cure reaction reflects a change in the charge carrier mobility. As resin viscosity  $\eta$  expresses the mobility of the chain segments in the growing network, a very useful relationship exists between viscosity and ionic conductivity. It is proposed that viscosity is inversely proportional to ionic conductivity:

$$\eta = A \cdot \sigma^{-\beta} \quad (\text{Eq.1})$$

where  $A$  and  $\beta$  are resin specific and temperature dependent constants.

This relationship is of great importance in cure monitoring, since it is possible to measure the ionic conductivity in-situ, but not viscosity. Senturia and Sheppard [3] observed that the ionic conductivity does not fall to zero, but remains finite as viscosity tends to infinity after gelation. Therefore, it is expected that Eq. 1 will begin to break down as gelation approaches

and the time during the resin cure when  $d^2(\log \sigma)/dt^2 = 0$  is commonly taken as the first evidence of a gelled system.

Fig. 3 shows how the dielectric permittivity  $\epsilon'$  at different frequencies changes with cure time. The existence of two peaks within segment 2 is clearly apparent. The magnitudes of these peaks decrease as the frequency increases. The second peak "moves" to later times as the measurement frequency decreases.

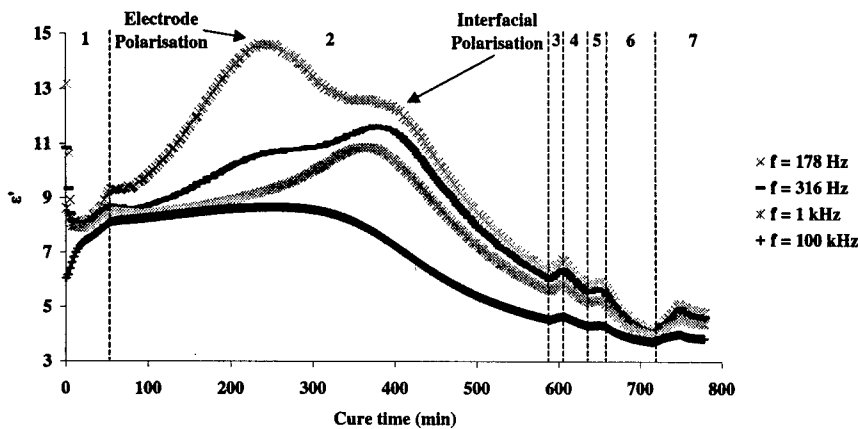


**Figure 3:** Permittivity-cure time graph for different frequencies. The presence of two peaks in segment 2 and the phenomena related to them are shown.

This dielectric parameter is generally associated with polarisation mechanisms, both electrode and interfacial polarisation, the latter being connected with phase separation in thermoset/thermoplastic blends via the Maxwell-Wagner-Sillars relationship [4,5]. The low frequency limit of  $\epsilon'$  is related to both temperature  $T$  and the fractional conversion  $\alpha$  [6].

$$\epsilon_{static} = \frac{D_1}{T} + D_2 + D_3\alpha \quad (\text{Eq.2})$$

where  $D_1$ ,  $D_2$  and  $D_3$  are fitting parameters.

### B. Comparison of alternative cure cycles

The ionic conductivity plots for the three experiments are presented in Fig 4. The different cycle segments overlap and are therefore not identified in the figure. All the curves show a maximum point in segment 2. Two other local maximum points are observed in the 5<sup>th</sup> and the 7<sup>th</sup> segments. In every isothermal segment, a particular final slope in the decreasing ionic conductivity values is attained. Another slope of interest is observed in the last stages of the recorded signal. Additionally, ionic conductivity values increase steadily during the first heating ramp (segment 3). The slopes in the isothermal segments are outlined in Fig. 4 for Experiment 1. They are quantified in Table III.

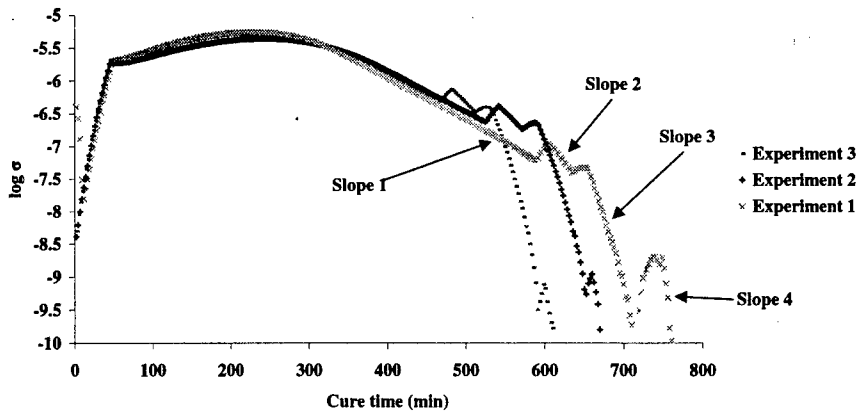


Figure 4: Ionic conductivity-cure time plots for the three different curing profiles. Features for Experiment 1 are outlined as guidance. These features exist in all the curves.

Table III: Features identification of ionic conductivity curves of figure 4

Features	Experiment 1	Experiment 2	Experiment 3
Time of maximum conductivity point (min)	225	242	233
Slope 1 (min <sup>-1</sup> )	- 0.0066	- 0.0063 (+5 %)	- 0.0068 (-3 %)
Slope 2 (min <sup>-1</sup> )	- 0.0140	- 0.0118 (+16 %)	- 0.0103 (+26 %)
Slope 3 (min <sup>-1</sup> )	- 0.0452	- 0.0489 (-8 %)	- 0.0551 (-22 %)
Slope 4 (min <sup>-1</sup> )	- 0.1193	- 0.0950 (+20 %)	- 0.0716 (+40 %)

The percentage difference values (in brackets) are calculated with respect to the corresponding values of the parameter determined in the standard cure cycle (Expt. 1).

**DISCUSSION**

**A. Characterisation of the standard cure cycle**

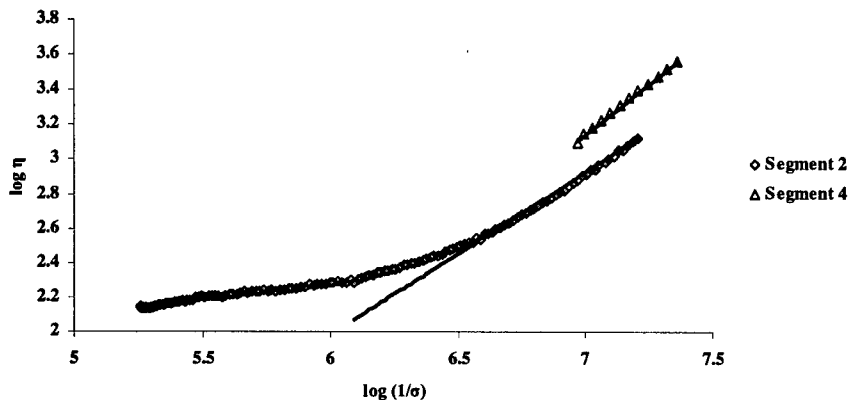
Validity of Eq.1 for this particular resin is assessed by comparing equivalent dielectric and rheology tests in the pre-gelation stages of the standard cure cycle. The equation parameters are summarised in Table IV.

Table IV

Parameters of Eq. 1 determined in the isothermal segments of the standard cure cycle

Segment	Temperature	Pre-exponential parameter A (Pa.s)	Exponent b
2	74 °C	2.10x10 <sup>-4</sup>	0.944
4	82 °C	1.15x10 <sup>-5</sup>	1.151

The fitting to the experimental data is shown in Fig. 5. The validity of Eq. 1 is generally expected to break down near the point where  $T_g$  approaches the instantaneous temperature of cure.



**Figure 5:** Experimental data and modelling curves for Eq 1 validation

From Fig. 5, it is evident that Eq.1 holds for the latter stages of segment 2 and for all the time of segment 4. This behaviour indicates that the  $T_g$  of the system is not sufficiently close to the curing temperature for diffusion effects to slow down the reaction progress. It is noticeable that Eq.1 does not hold for the earlier stages of segment 2. A possible explanation for this is the presence of reaction induced phase separation in this system [7,8].

Permittivity signals are generally suitable for the investigation of interfacial polarisation effects that may be expected to result from such phase separation. At frequencies between 100 Hz and 1 kHz (Fig.3) the permittivity shows a peak at around 350 - 400 min which is likely to be due to the presence of an extra polarisation mechanism (in addition to electrode polarisation) [6].

#### **B. Comparison of alternative cure cycles**

The ionic conductivity plots in Fig. 4 indicate the changes in the mobility of charge carriers in the curing system in response to the temperature changes. The maxima in  $\log \sigma$  in segment 2 are observed close together, as would be expected, since all the curing profiles are identical up to and somewhat beyond that stage. Differences between the cure cycles begin to emerge at the start of segment 3.

##### Segment 3: Heating ramp from 74°C to 82°C at 0.5°C/min

Increased mobility of the charge carriers is reflected in a rapid rise in the conductivity values. The temperature effect dominates the signal.

##### Segment 4: Isothermal dwell at 82°C for 30 mins

The ionic conductivity decreases linearly during this segment (Slope 2), indicating continuing reaction and hence increasing viscosity in the resin. Slope 2 is higher for the shorter cure

cycles (Expts. 2 and 3) - see Table III. This is to be expected as in the shorter cure cycles the conversion reached at the end of segment 2 is lower than in the longer cure cycle and hence the rate of reaction consequent upon the temperature increase will be higher.

Segment 5: Heating ramp from 82°C to 92°C at 0.5°C/min

Unlike in segment 3, in which the conductivity increased linearly throughout the ramp period, in this heating ramp, the ionic conductivity exhibits a local maximum in all the experiments. This indicates that the decrease in the conductivity signal (attributable to the curing reaction) begins to dominate over the simple thermal effect.

Segment 6: Isothermal dwell at 92°C for 60 mins

A sharp decrease in the ionic conductivity is seen (slope 3), leading to final values of ionic conductivity in the order of  $10^{-10}$  S/m for all the curing profiles. This time, the slope is higher for Expt 1 than for Expts. 2 and 3. The higher reaction rates experienced in segment 4 in Expts. 2 and 3 are likely to have progressed the reaction further, closer to the gelation point thus limiting the rate of any subsequent additional reaction.

Segment 7: Heating ramp from 92°C to 125°C at 1°C/min

This segment exhibits another local conductivity 'spike' in the ionic conductivity, indicating the relative level of residual reactivity in the resin. The ionic conductivity then decreases very rapidly as the final crosslinking in the resin rapidly immobilises the charge carriers. (Note the high Slope 4 values in Table III). The height of the conductivity peak thus becomes another potential point of control, as does Slope 4.

### CONTROL POSSIBILITIES IN COMPLEX CURE CYCLES

The resin system and the cure cycle studied here exhibited complex behaviour, as shown by the preceding analysis. This fact makes the control of the cure cycle very challenging. Practical concerns in manufacturing may include overall shortening of the cure cycles, full wetting and compaction of parts, safe and fast processing of thick components, optimisation of laminate structure and/or resin morphology, minimisation of internal stresses. The next step in definition of suitable control parameters is the correlation of the above-mentioned concerns to specific features of the dielectric cure signature and the identification of '*points of control*'. For example, a shorter cure cycle can be achieved by either shortening the dwell time or by ramping at higher rates before the dwells. The end of a dwell can be set when the conductivity signal (dielectric feature) levels off to a constant value, as an indication of reaction cessation at that temperature. Therefore, the slope of the conductivity - cure time curve becomes a '*point of control*'. Further information from the conductivity level can be retrieved, as the final conductivity relates to the end-state mobility of the charges, which depends on the density of crosslinking in the glassy state.

Table V presents a number of available control schemes, alongside the appropriate '*point of control*' and the exploitation limitations of the particular dielectric property involved. The development of such Control systems is still in its early stages. Nevertheless, it can be proposed that Viscosity control can serve to achieve full impregnation of the reinforcement in the part, Phase separation control may help in the achievement of required of microstructures in modified thermosets and the Reaction control assist in achieving safe and short cure cycles for complex structures.

**Table V: Potential control schemes**

<u>Control scheme</u>	<u>Required modelling</u>	<u>Point of control</u>	<u>Limitations</u>
Viscosity control	Conductivity vs. viscosity relationship	(i) $\sigma$ value (ii) slope of $\sigma$ change	Phase separation and melting effects disturb $\sigma$
Phase separation control	MWS interfacial polarisation	$\epsilon'$ at 100 Hz $< f <$ 10 kHz	Thermoplastics show high relaxation time (out of measurable range)
Reaction control	Cure kinetics and dipolar relaxation modelling	(i) $\epsilon_{static}$ at high f (ii) slope $d^2 \log \sigma / dt^2$	Blocking electrode masks dipole effects

**ACKNOWLEDGEMENTS**

The work reported here was made possible by a Project studentship for MCK from EPSRC grant GR/M89454 and with support from the 'CURENET' EPSRC Network project (GR/M00947/01). The authors gratefully acknowledge numerous discussions with Dr A A Skordos.

**REFERENCES**

- [1] I.K.Partridge, G.M.Maistros, Chapter 5.17 in "*Comprehensive Composite Materials*", eds. A.Kelly, C.Zweben, Elsevier Science, 2000
- [2] G.M.Maistros, I.K.Partridge, *Composites Science and Technology*, **53**, 355 (1995)
- [3] S.D.Senturia, N.F.Sheppard, *Advances in Polymer Science*, **80**, 1 (1986)
- [4] K.W.Wagner, in "*Arkiv fur Electrotechnik*", editor H.Schering, Springer - Verlag, Berlin (1914)
- [5] A.Bonnet, J.P.Pascualt, H.Sautereau, J.Rogozinski, D.Kranbuehl, *Macromolecules*, **33**, 3833 (2000)
- [6] G.M.Maistros, C.B.Bucknall, *Polymer Engineering and Science*, **34**(20), 1517 (1994)
- [7] A.Bonnet, J.P.Pascualt, H.Sautereau, Y.Camberlin, *Macromolecules*, **32**, 8524 (1999)
- [8] H.Kim, K.Char, *Industrial and Engineering Chemistry Research*, **39**(4), 955 (2000)

**SYMBOLS**

$\alpha$	= fractional conversion	
$T_g$	= glass transition temperature	K
$\eta$	= complex viscosity	Pa.s
$\sigma$	= ionic conductivity	S/m
A	= pre-exponential parameter	Pa.s
$\beta$	= exponent	
$\epsilon'$	= permittivity	
$\epsilon_{static}$	= static permittivity	
$D_1$	= fitting parameter	K
$D_2$	= fitting parameter	
$D_3$	= fitting parameter	

## IMPLEMENTATION OF A DIELECTRIC ON-LINE PROCESS MONITORING SYSTEM

Wolfgang Wenger\*

### INTRODUCTION

Materials are cured in autoclaves in accordance with specifications, fixing cure parameters such as temperature and time within a rigid tolerance band. Bombardier Aerospace – Shorts manufactures aircraft components under its own as well as under customer specifications, all of which require a validation of the cure performance. Current methods for verifying autoclave cures are based on process control panels being subjected to autoclave cures and subsequent mechanical tests (figure 1). However, there are a number of disadvantages associated with the use of process control panels. These range from potential lay-up discrepancies with respect to fibre orientation, autoclave operator discretion with respect to their location in the autoclave, as well as their small size in comparison to real life components with regards to the temperature profile they experience. Besides those technical issues, lay up and testing of control panels take a significant time and, therefore, a more cost efficient and more representative process control system was proposed: A Dielectric (DEA) Monitoring System.

Among others, the Civil Aviation Authority (CAA) has the task of overlooking a company's adherence to agreed procedures. In order to maintain customer confidence of what was thought to be a major change of the monitoring procedure, the Civil Aviation Authorities (CAA) have been informed in advance about the intentions of getting an alternative cure monitoring system on board. With their principle view of accepting such a move, provided that such a system and the process around it can be proven to substitute the mechanical test procedures traditionally performed, the way was clear for the verification of the concept in a manufacturing environment.

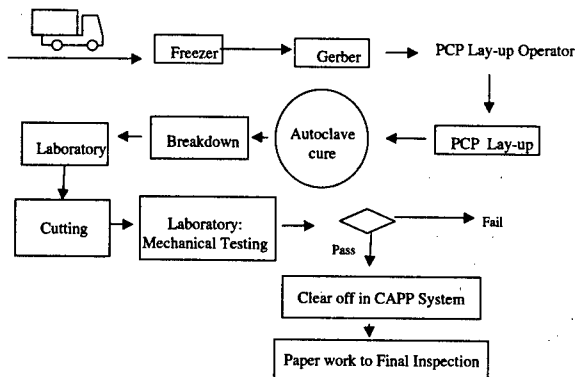


Figure 1: Flow of conventional process control panels through the system

**THE CONCEPT**

The overall flow of the material destined for DEA based process monitoring is described in figure 3 below. The specimen lay-up operator is supplied with the material to be used, which is then laid up onto the sensors provided. These items, now known as coupons, are then supplied to the autoclave operators, who subsequently load them into the platen press beside the autoclave and feed the DEA system with the required data for the current cure run (i.e. cure number, coupon material, etc...).



Figure 2: Concept of DEA cure monitoring

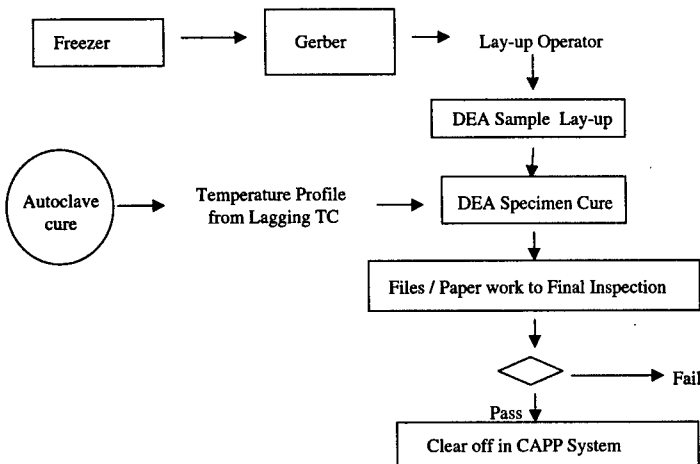


Figure 3: Flow of DEA coupons within the new alternative process monitoring system

All components destined for autoclave cure are loaded into the autoclave and their thermocouples connected as previously undertaken. The platen press of the dielectric monitoring system outside the autoclave is then electrically linked with the autoclave by the flick of a switch. From this moment, the entire bank of thermocouples inside the autoclave is being scanned, and the collected temperature data forwarded to the DEA system. During the heat-up period, a period when thermal profiles of the various components differ due to their position and size, the monitoring system automatically selects the lagging thermocouple, representing the worst case regarding the soak period, and drives the temperature profile of the platen press. In this respect, the sample in the dielectric cure-monitoring system experiences the same condition as the tool with the slowest temperature response. Temperature profile discrepancies from autoclave operator discretion in terms of where to place the process control panel as well as the great difference in size between a control panel

and an actual component is eliminated. The output signal used by the Quality Department is a Log Ion Viscosity curve, characteristic for each resin system monitored.

With the non-existence of process control panels and the elimination of its subsequent mechanical tests as illustrated in figure 3, the process of validating an autoclave cure is greatly simplified and therefore permits an earlier decision. In case of the lagging thermocouple failing, the system automatically switches to the next lagging TC in the autoclave.

### TECHNICAL FEASIBILITY

#### a) Provisions for Generating Reliable Results

In order to generate results, which provide confidence in the system, a coupon lay-up method had to be found which was capable of producing repeatable results for a variety of materials. In order to prevent coupons from being subjected to pressures being too low to provide a sufficient wet-out of the DEA sensor area, it had to be assured, that various coupon lay-ups arrived at the same overall thickness. With the requirement to monitor the progress the cure of carbon prepreg materials, a sufficient buffer distance had to be provided between the sensor surface and the electrically conductive carbon fibres, while at the same time allowing the prepreg resin to penetrate thoroughly into the electric field of the sensor. This was accomplished with the introduction of a dry glass fabric. Carbon fibres in close vicinity to the sensor were found to display artificially low log ion viscosity (LIV) values. This characteristic was reduced by the addition of plies of glass fabric, which, in turn, increased the requirement of providing a sufficient supply of resin from the outer prepreg plies. As the occasional occurrence of voids with an increased sensor to carbon distance made the generated LIV data unreliable, a balance between a low carbon influence and consistent and reliable resin fill within the glass fabric had to be established.

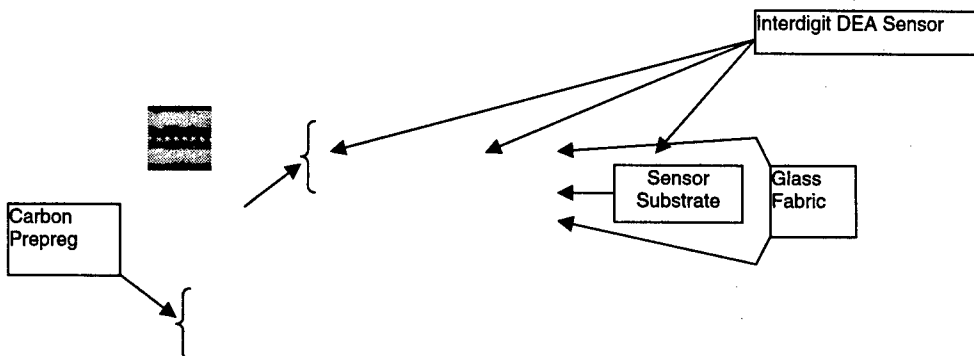


Figure 4: Photomicrograph of a coupon cross-section with its comb sensor sandwiched between adjacent layers of glass fabric and outer layers of carbon prepreg material

Only after having arrived at a satisfactory lay-up method (figure 4), confidence was generated in validating the system.

a) Determination of Baseline Parameters

In order to determine the acceptability of the dielectric system, basic parameters were established, serving as a foundation to correlate DEA data for a particular material with commonly known analysis techniques. The degree of cure obtained via DSC by running simulated temperature profiles at specification limits was felt to be a justified foundation. Hence, any autoclave cure resulting in a degree of cure equivalent or above that obtained by baseline trials were classified as acceptable. Simulated autoclave runs on the DEA system with temperature profiles outside the specified temperature profile provided additional information to the DEA acceptance limits.

b) DEA Results

The End-of-Cure point was defined by the point in time, where the Log Ion Viscosity (LIV) no longer changed during a cure cycle and its derivative reached zero (figure 5: point C). This value then served as a base for DEA cure cycles to be interrupted, i.e. in subsequent cure cycles cooling was initiated at the predetermined end-of-cure point as well as shortly before and after this point. A DSC analysis of the degree of cure on samples having experienced those runs then provided the evidence, that the point C on the LIV trace as shown in figure 5 indeed coincided with a drop in the degree of cure when further reducing the dwell period (figure 6).

In addition, mechanical properties were correlated with characteristic values obtained from DEA runs. Mechanical results being within their specified limits provided a further correlation to the new acceptance data as generated from the LIV traces. The consistency of mechanical results compared to the consistency of the DEA results provided good confidence for the dielectric system to be used as an alternative to the mechanically based process monitoring procedure.



Figure 5: Generic example traces of a carbon prepreg being cured at a 0.5C/min heat-up rate showing log ion viscosity behaviour and its first derivative

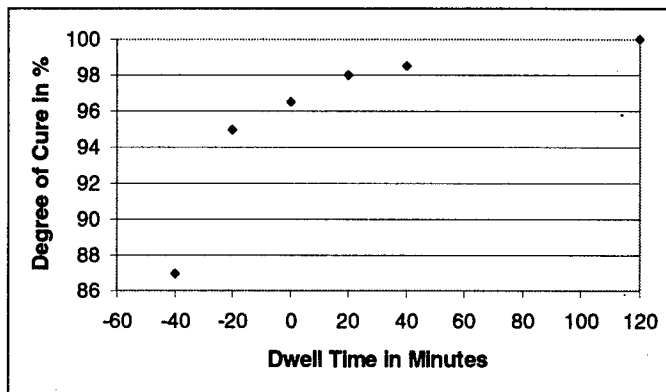


Figure 6: Degree of Cure of a resin system interrupted at various dwell periods (cure conditions as to figure 5)

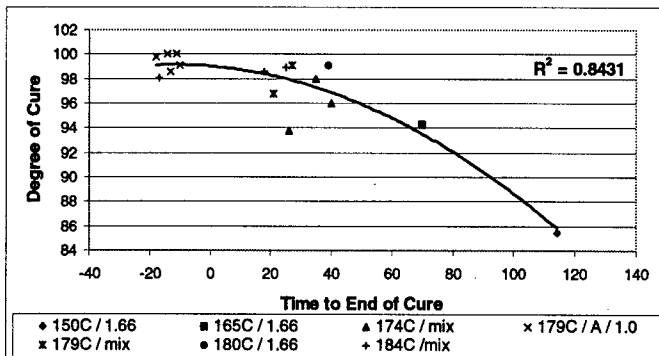


Figure 7: Relationship between Degree of Cure and time required in reaching the End-of-Cure point

Based on the verification tests performed, it became apparent, which characteristic value ranges are of importance when accepting an autoclave cure.

The autoclave process was found to be acceptable using the following criteria:

- The resin viscosity during heat-up must reach a minimum
- The log ion viscosity (after gellation) must reach a material characteristic value
- The first derivative must reach a constant low value.
- The value in c) must be reached within a specified period from the start of the dwell.

The verification of the concept was reported to the Civil Aviation Authority who subsequently gave the go-ahead for the introduction of the proposed cure monitoring system.

## PREPARATION FOR IMPLEMENTATION

Prior to implementing the DEA system, ground work had to be done that justified the implementation also on a commercial bases. Savings in terms of lay-up and testing time were used against capital, running costs and a payback time calculated. Together with the validation report, the quotations of the system and the cost justification was then submitted for approval by head quarters. Only after their approval several weeks later, an order could be placed with the proposed manufacturer, Weniger & Maschinenbau Scholz Gesellschaft für System und Prozesstechnik mbH.

With the implementation of such a cure monitoring system, a number of staff was affected with a change in the procedure. These had to be brought on board in order for them to understand the changes lying ahead, as well as for them to highlight certain issues involved, making a smooth operation of the process possible. As each of the participating parties, based in different departments, were driven by different agendas, they were thus in the position to recognise matters specific to their field. In this way, tasks making up the entire implementation process were grouped and categorised in phases, depending on effort and impact the implementation would make at Bombardier Aerospace – Shorts. Thus, the implementation phases were as follows:

Phase 1: Preparatory work and setting up of the DEA cure monitoring systems

Phase 2: Development of customised software for Operations with network access

Phase 3: Development of customised software for Quality

Phase 1 included essential preparatory work, such as the establishment of acceptance criteria for further materials as stated above. The dielectric cure monitoring process and with it the acceptance criteria were included in the **Process Specification (P. Spec.)**. Based on recommendations from Methods, Standards Department issues such specifications on a company level, containing besides the description of the equipment, material, process and acceptance criteria of each participating material in general.

In order to assure a consistent process, the lay-up of coupons developed by Methods, had to be taken over by Operations, who in turn, had to appoint a suitable operator for this task. In addition, and similarly to all other parts, a work procedure (**Engineering Process Record - EPR**) has been issued by Methods that described verbally step-by-step the progress of the part being manufactured. For the case of the DEA coupons, it states in detail the lay-up of DEA coupons, the way they are to be bagged, handled, cured and routed. As a visualisation aid and part of the above EPR serves the **Illustrated Planning** concept. It remains with the operator and illustrates each ply lay-up as well as the way the component is bagged up. Hence, the DEA lay-up was also included in this concept.

Finally, with the DEA systems installed and linked to each autoclave, implementation phase 1 has been concluded.

#### ICMAC - International Conference for Manufacturing of Advanced Composites

In conjunction with a customisation of the DEA equipment, its integration into the plant environment was task of the following phases 2 and 3. The aims of customisation were as follows:

- Minimising operator workload
- Replacement of autoclave log-book by computerised log entries
- Securing of data
- Convenient access for Quality for data analysis

#### Implementation Phase 2:

It will be unavoidable, that operators experience a minor increase in their workload with the handling of DEA coupons at a busy time of autoclave loading. However, it was attempted to keep the additional workload to a minimum, by relieving administrative responsibilities previously undertaken by operators. Such tasks include the listing of parts to be cured in a log book, as well as noting of times of extraordinary events during cure. Minimising the workload was thought to be possible by means of bar code readers, which allow instant access of part data for entry into the DEA system. Merely vacuum and thermocouple numbers then had to be entered manually. With records generated via the DEA system, it is envisaged that paper records currently used to log components and their performance during cure can then be abandoned. Securing of cure data will be performed through downloading of cure files into the company's network. Finally, from the convenience of their office, Quality personnel will be able to assess the acceptability of each autoclave cure.

Implementation Phase 3 intends to deal with the establishment of a customised analysis of additional qualitative parameters for all cures by the Quality department. Such a software will make it possible to evaluate temperature, vacuum and pressure data for each component on an individual basis.

#### SUMMARY

With the establishment of clear acceptance criteria using DEA, DSC and mechanical data, prove has been provided that the DEA cure monitoring concept is suitable for a manufacturing environment. Also the CAA has been satisfied about its value it will bring as a monitoring process, thus adding to customer satisfaction. A significant amount of provisions have been made, including the set-up of specifications and engineering records, that made the introduction of a basic DEA system possible. A further customisation, to be taken on board in subsequent implementation phases, will be expected to bring a higher degree of efficiency to the operation of the system.

It is to be expected, that after a transition phase of ca 3 months, personnel have become accustomed to proceeding with DEA coupons and thus allow Process Control Panels to be phased out. Thus the introduction of the DEA cure monitoring system is anticipated to lead to significant savings in lay-up and testing. Besides, Quality will be able to get access to the autoclave data in a much more rationalized manner.

**SESSION 5:  
MATERIAL CHARACTERISATION  
& COMPOSITE PERFORMANCE**

**Evaluation of a Carbon Thermoplastic to Titanium Bonded Joint**

George F. Leon  
Michael Trezza  
Jeffrey Hall

General Dynamics Electric Boat Corporation  
75 Eastern Point Road  
Groton, CT 06365, USA

Kelli Corona-Bittick  
Production Products  
706 N. Jefferson Ave.  
St. Louis, MO 63103, USA

**ABSTRACT**

Carbon thermoplastic (AS4/APC-2) to Titanium (6Al-4V) bonded and bonded/bolted joint designs were developed for use in the marine, Composite Storage Module for the Office of Naval Research. Finite element modeling of the design was done using PATRAN and subsequent analyses were performed using ABAQUS finite element code. In order to validate the design and to provide a measure of confidence with the fabrication and assembly of the joint, three, full-scale test specimens were designed, fabricated and tested in a representative tensile load environment. The three joint specimens were fabricated by Production Products and tested at the Naval Surface Warfare Center, Carderock Division. The specimens were 1,69 m ( 66.5 in) in length by 0,254 m ( 10 in) in width by 28,5 mm (1.12 in) in thickness and captured in the 70 mm ( 2.75 in) thick titanium. Two of the specimens were bonded joints and the third was a bonded/bolted joint. The specimens were subjected to three cycles of tensile loading on a 2447 kN ( 550 kip) MTS test machine until failure. One bonded joint specimen failed in the adhesive bondline at 378kN ( 85 kips) and the second bonded joint failed at 600 kN (135 kips). The bonded/bolted joint specimen showed adhesive failure at 489 kN (110 kips) and complete failure in the bolts at 556 kN (125 kips). This paper discusses the theoretical predictions, experimental results and correlation.

**KEYWORDS**

Bonded joint, Bonded/bolted joint, Carbon thermoplastic, Finite element analysis (FEA).

**INTRODUCTION**

The Composite Storage Module (Baker [1]) incorporates a carbon thermoplastic (AS4/APC-2) to titanium (6Al-4V) joint design for access. In order to validate the design and to provide a measure of confidence with the fabrication and assembly of the joint three full-scale joint test specimens were designed, fabricated and tested in a representative tensile load environment. Two of the specimens were bonded joints and the third was a bonded/bolted joint. Since testing of the actual 1,2m ( 48 in) diameter, joint section was not practical, a full scale joint specimen was designed which incorporated the maximum strain and the equivalent strain distribution of the CSM joint. The design specimens were 1,69 m ( 66.5 in) in length by 0,254 m ( 10 in) in width by 29,7 mm ( 1.17 in) in thickness and captured in the 70 mm ( 2.75 in) thick titanium. The three joint specimens were fabricated by Production

Products. The specimens were subjected to three cycles of tensile loading until failure on the 2447kN MTS test machine at Naval Surface Warfare Center.

### TEST SPECIMEN DESIGN AND ANALYSIS

Details of the CSM joint and the finite element analysis using PATRAN [2] and ABAQUS finite element code [3] is discussed in Baker [1]. As a baseline, the finite element model used in Baker [1] was analyzed using the loading for this analysis for comparison of overall joint behavior. Lay-up consisted of 22% 0° plies, 22% ±45° plies, 56% 90° plies, where 0° is along the longitudinal axis. After comparison with the original joint model it was determined that the test fixture model was acting similarly under the same loading condition. The analysis of the test specimen fixture was done for three cases as follows:

1. Test fixture with bolt pre-load to 2/3 yield strength (689MPa) and adhesive
2. Test fixture with adhesive, no bolt
3. Test fixture with a pin and adhesive

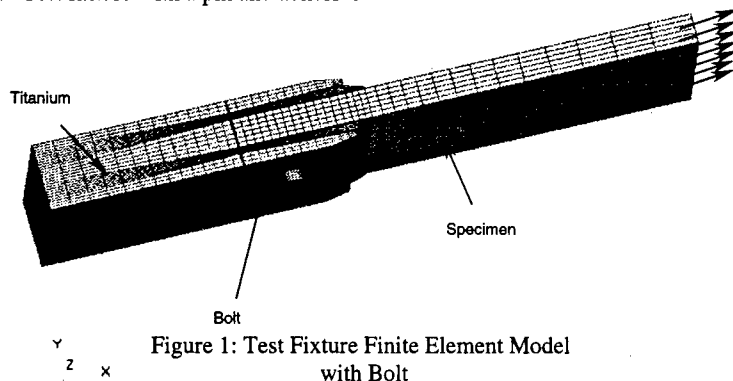


Figure 1: Test Fixture Finite Element Model with Bolt

An additional analysis was done in order to predict failure of the joint specimen and then to compare that prediction to the actual test of the specimen. Figure 1 shows the finite element model of the test fixture. A tensile pressure loading was applied to the specimen, while constraining the model on the back edge. Figure 2 shows the dimensions of the test fixture, finite element model. The case 1 analysis was done in two steps; Step 1 applied the pre-load to the bolt, and step 2 applied the tensile pressure loading. For cases 2 and 3, the analysis was done in only one step with the application of the pressure loading. No pre-loading exists for these cases. For cases 1 and 3, contact was modeled at the bolt/pin interfaces with the fixture (i.e. bolt contact with specimen, pad-up, adhesive, and titanium). For cases 1 and 3, the same finite element model (Figure 1) was used to do the analyses. In case 3, the pre-load on the bolt is removed to represent a pin in the fixture. In case 2, the bolt elements were removed from the model in Figure 1.

All finite element modeling was done using PATRAN [2] and subsequent analyses were performed using the ABAQUS/Standard finite element code [3]. The materials used in the model are shown in Figure 3, with the details of the material properties shown in Table 1. For the model with no bolt, all materials are the same as in the bolt model.

These analyses used 3D solid elements (C3D8) in the mathematical idealization and large deflection theory.

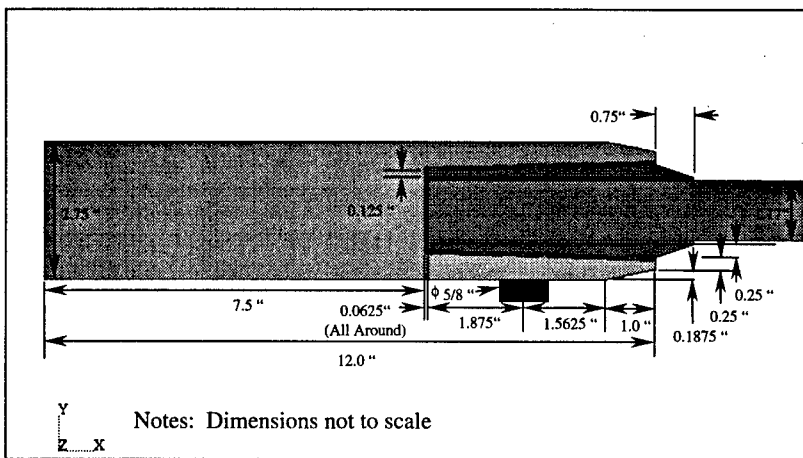


Figure 2: Test Fixture Finite Element Model Dimensions

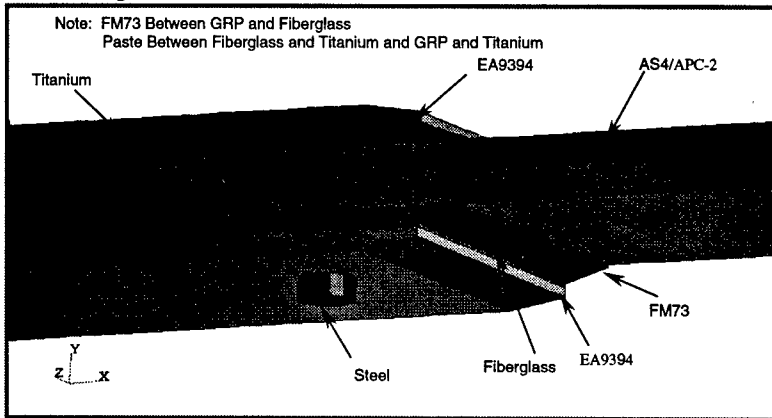


Figure 3: Test Fixture Finite Element Model Materials

Table 2 compares the maximum and nominal axial strain for the three cases analyzed. For the AS4/APC-2 the nominal strain is reported in the middle of the specimen along its length. Contour plots of the axial strain were generated for the AS4/APC-2 composite specimen, the FM73 film adhesive, the EA9394 paste adhesive, the Fiberglass pad-up region, and the titanium. Figure 4 shows the contour plot of the axial strain for the EA9394 paste adhesive. Maximum strain occurs at the back edge of the specimen.

ICMAC - International Conference for Manufacturing of Advanced Composites

Material	$E_1$	$E_2$	$E_3$	$\nu_{12}$	$\nu_{13}$	$\nu_{23}$	$G_{12}$	$G_{13}$	$G_{23}$
Fiberglass	1570000	2850000	2850000	0.17	0.17	0.28	480000	480000	1120000
AS4/APC-2	1840000	9900000	5580000	0.06	0.13	0.21	650000	570000	1520000

ISOTROPIC (ELASTIC)

Material	E	$\nu$
Titanium	16500000	0.33
Steel	30000000	0.30

Coordinate System

- 1 = Radial Direction
- 2 = Hoop Direction
- 3 = Axial Direction

ISOTROPIC (ELASTIC/PLASTIC)

Material	E	$\nu$	$\sigma_{yield}$	$n$
FM73	144160	0.36	7799	0.00
EA9394	615000	0.45	3564	0.00

Table 1. Test Fixture Specimen Material Properties (E, G,  $\sigma$  in psi)

Material	Maximum Strain (in/in)			Nominal Strain (in/in)		
	Case 1	Case 2	Case 3	Case 1	Case 2	Case 3
AS4/APC-2	0.003267	0.002901	0.002959	0.001281	0.001313	0.001267
FM73	0.009391**	0.002332	0.002347	0.005721**	0.001658	0.001623
EA9394	0.015055**	0.00511	0.005221	0.009153**	0.003783	0.003688
FIBERGLASS	0.004724**	0.001155	0.001207*	0.002998**	0.001059	0.001104*

- \* In bolt hole through the thickness
- \*\* In bolt hole (Due to pre-load)

Table 2. Maximum/Nominal Strain Comparison

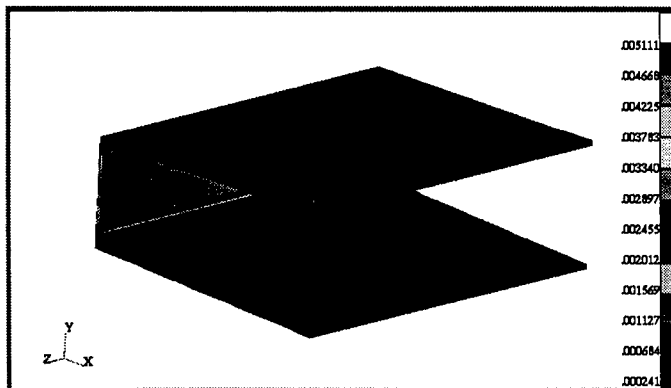


Figure 4: EA9394 Axial Strain (in/in)

Another concern for the test specimen was whether the adhesive used between the AS4/APC-2 and the titanium (FM73), and the adhesive between the fiberglass and titanium (EA9394) would yield. Under this loading condition for the case with no pin, the adhesive materials do not yield. For the case with the pin, the maximum Von Mises stress in the FM73 is 6,310 psi, which has a yield stress of 7,800 psi and the maximum Von Mises stress in the EA9394 is 3,370 psi, which has a yield stress of 3560 psi.

#### FABRICATION AND ASSEMBLY

Production Products, with support from The Boeing Company, manufactured the three thermoplastic joint specimens and bonded them to the titanium sections that were provided by Electric Boat. The lay-up for the panels was based on material thickness of 0.0052 inch for the AS4/APC-2 prepreg supplied by Hexcel Fiberite and required 225 plies for the 1.17 inch nominal thickness. The plies were collated and autoclaved consolidated. (The CSM cylinder will be fiber placed, in-situ consolidated [4], [5]). After autoclave consolidation, the panels were visibly well consolidated. Visual inspection of the panels showed average thickness of 28,5mm (1.12 in) in lieu of the 29,7mm (1.17 in) required. Once the dimensions of the thermoplastic panels and titanium joint pieces were measured, the exact dimensions of the glass/epoxy pad-up was determined. Six layers of FM73 film adhesive were required to achieve the 0,76mm (0.030in) bondline between the pad-up and the thermoplastic panel. The variation in the thermoplastic panel thickness was compensated for in the EA9394 paste adhesive bondline which was nominally 1,59mm (0.0625 in) thick. The glass/epoxy padup was machined from 17 plies of 24 ounce per square yard of woven roving and Shell Epon 862. The glass padup to AS4/PEEK was bonded with film adhesive following surface preparation and bagging. It was cured at 121°F (250°F) for one hour. Following surface preparation of specimen and titanium contact surfaces, the paste adhesive was applied and held in a fixture at 60°C (140°F) for 24 hours until cure. Concurrent AS4/PEEK panels were also fabricated to verify the mechanical properties used in the design [7].

#### FAILURE PREDICTION

For this analysis, a 2D solid model of the joint with no bolt was created. The original 3D solid models were not used for this analysis because of size and analysis time considerations. It was determined from the original analyses that the behavior of the specimen was basically symmetrical through the width and thickness of the model, and therefore a 2D solid model would adequately represent the specimen. The model was corrected for the as-built thickness variation. The loading was applied to this model in 10 increments loading up to twice that of what was used in the above 3D solid models. With the load stepped into 10 increments, a time history could be created of the failure characteristics of the joint specimen. The film adhesive FM73 and the paste adhesive EA9394 were both model with elastic/plastic properties as shown in Table 1 of the previous section. Failure of the specimen would be determined by assessing stresses in the paste adhesive EA9394. This was due to the fact that the yield stress for this material is on the order of ½ that of the film adhesive FM73.

Figure 5 shows a comparison of the 2D solid model and two cases of the 3D solid model. It can be seen that the three models follow very closely, validating the 2D solid model. The primary purpose of this figure is to predict failure of the test specimen. Von Mises stresses were reported to compare to the yield stress of the paste adhesive EA9394. From the figure it can be seen that the paste adhesive has a peak stress at approximately 445kN (100 kips) of

loading. Also observed from this figure is that the pinned 3D model has an increase in stress at approximately 556kN (125 kips) of load. This is due to the pin in the fixture picking up the load as the paste adhesive fails.

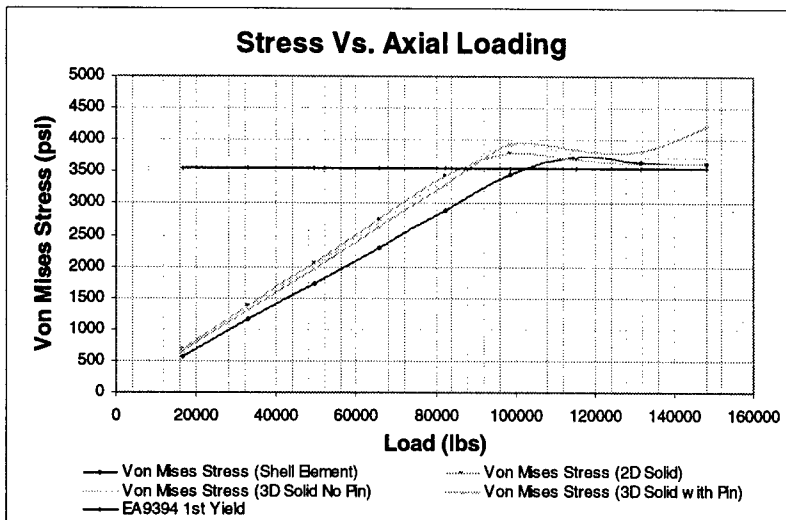


Figure 5: FEA Stress vs. Load From to Predict Failure

## TEST RESULTS

The specimens were tested in the 2446kN (550,000lb) MTS test machine at NSW/CD as shown in Figure 6. Each specimen had 16 strain gages and one acoustic emission transducer attached as depicted in Figure 7. The design failure load of 366kN (82,300lb) was obtained from preliminary finite element analyses of the joint. Each specimen was subjected to three cycles of loading. The first cycle was from 0 to 146kN (32,900lb) to 0, the second cycle was from 0 to 366kN (82,300lb) to 0, and the third cycle was to failure. Figure 6 also shows the loading spectrum.

Strain gage predictions were developed for all 16 gages prior to test. Typical axial strain gage comparisons between predicted and tests are shown in Figure 8 for gages 1 and 10 on the AS4/APC-2 specimen away from the joint (membrane) and Figure 9 for strain gages 3, 4, 5, 12 in the fiberglass pad-up region. Some bending of the joint is observed in Figure 8 for Test 2 with no bolt. More significant bending of the specimen is observed in Figure 9 for the fiberglass pad-up. This is probably due to the asymmetric condition of the as-fabricated specimen dimensions and variations in the paste adhesive bond line and thermoplastic substrate. The figures show both loading and unloading.



LOADING (lbs)		
Cycle 1	Cycle 2	Cycle 3
0	0	0
10000	10000	10000
20000	20000	20000
30000	30000	30000
32900	32900	40000
0	40000	60000
	50000	82300
	60000	90000
	70000	100000
	82300	110000
	60000	120000
	30000	130000
	0	140000
		150000
		160000
		170000
		To Failure

Figure 6. Bonded Joint Specimen in MTS Test Fixture and Loading Cycles

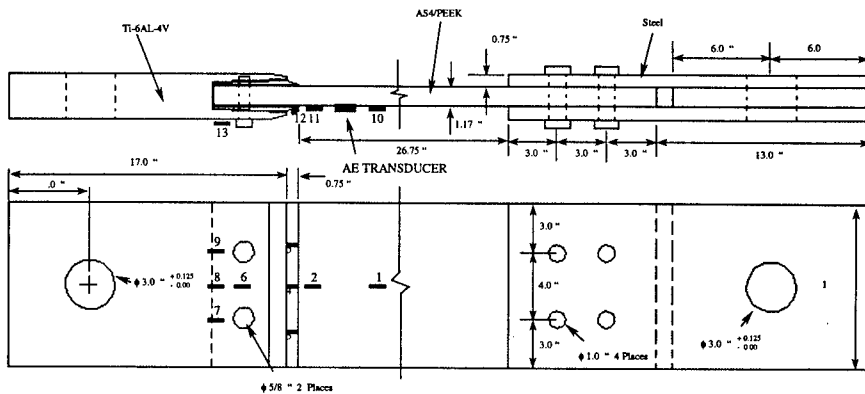


Figure 7. Strain Gage Locations on Test Specimen

Specimen #1, a bonded joint, had a failure at approximately 378 kN (85 kips), whereas specimen #2, also a bonded joint, failed at approximately 600 kN (135 kips). Specimen #3, a bolted/bonded joint, had a partial failure occur at approximately 489kN (110 kips) in the bond of the joint, and complete failure at 556kN (125 kips) with bolt shear.. Figure 10 shows the failed bonded specimen #2, which was used for comparison in the previous section. The failure occurred in the EA9394 paste adhesive on the backside of the AS4/PEEK.

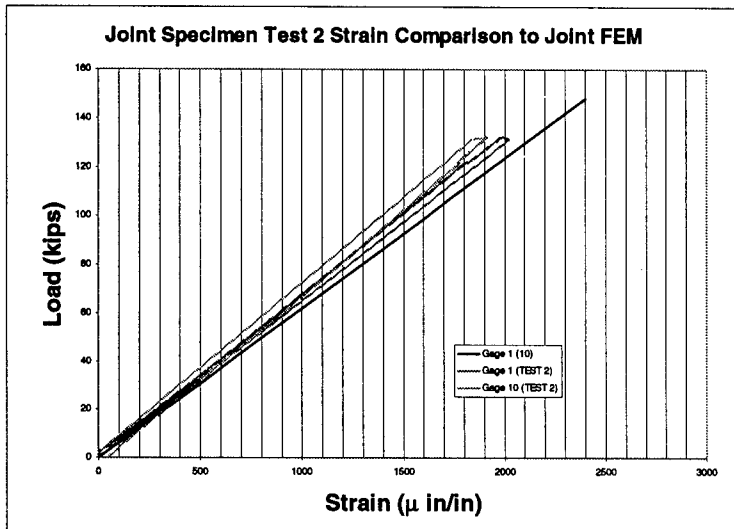


Figure 8. Load versus Strain for Strain Gages #1 and #10

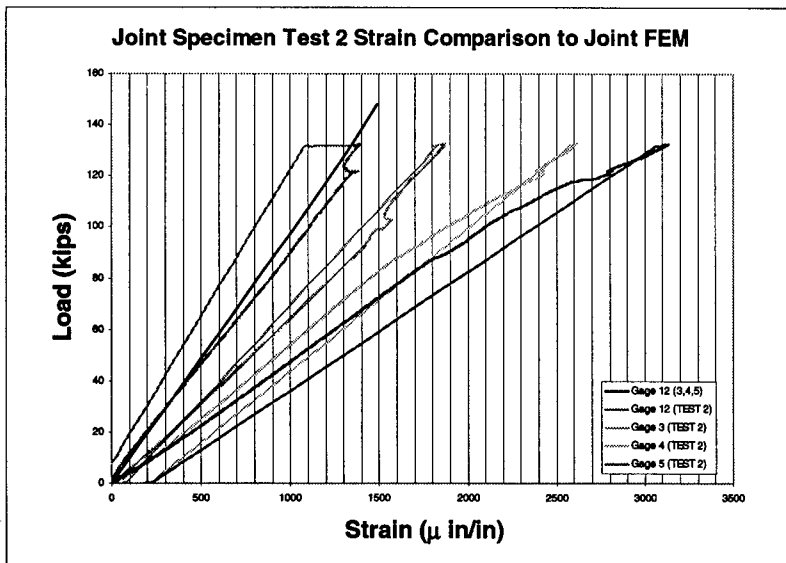


Figure 9. Load versus Strain for Strain Gages #3, #4, #5, #12

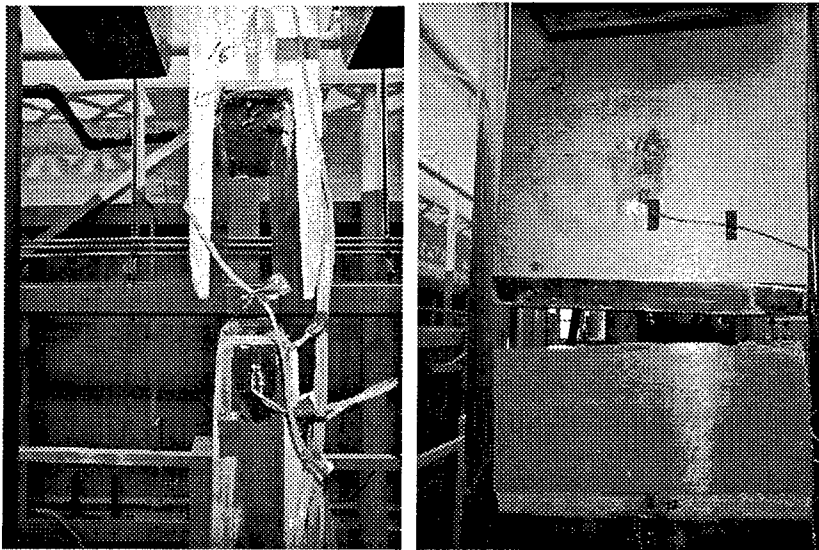


Figure 10. Bonded Joint Specimen #2 Adhesive Failure at 600 kN (135 kips)

Visual inspection of failed specimen #1 showed a large (4 inch diameter) void in the paste adhesive due to trapped air pocket during the assembly of the joint. This defect probably contributed to the premature failure of the joint when compared to the results of specimen #2 and #3. Figure 11 shows the failure of bolted/bonded joint specimen #3. The EA9394 paste adhesive failed again on the back side of the AS4/PEEK and then continued to fail along with bolt failure. The bolt was sheared at failure. A large gap was observed prior to failure.



Figure 11. Bolted/Bonded Joint Specimen #3 Adhesive/Bolt Failure

## SUMMARY

Validation of a carbon thermoplastic to titanium bonded joint design for the Composite Storage Module was performed through destructive testing and comparison to theoretical FEM predictions. Three dimensional and two dimensional solid finite element analyses were developed to perform the large deflection analyses of the components of a carbon thermoplastic, AS4/APC-2, to 6Al-4V, titanium bonded, and bonded/bolted joint using ABAQUS [3]. Three full scale specimens were fabricated by Productions Products. Analytical predictions were compared to with tensile loading results obtained from tests conducted at Naval Surface Warfare Center. Failure load prediction of 445kN (100 kips) for the paste adhesive was in agreement with the average adhesive failure observed of 489kN (110 kips). Although the first adhesive joint failed at 378kN due to large void in the paste adhesive, failure was 1.03 above the design failure load. The insertion of a pin/bolt in the joint provided for additional reserve strength (556kN) after the adhesive failed at 489kN (110kips). However the addition of this "chicken bolt" adds significant cost and difficulty in assembly of the joint and is not required to satisfy the load requirements.

## REFERENCES

1. Baker E, "Design, manufacturing and delivery of a composite storage module for at-sea testing", Touchstone Research Laboratory Report No. NR4018PI, February 2001
2. MSC/PATRAN Version 8.0; The MacNeal Schwendler Corporation.
3. ABAQUS/Standard Version 5.8; Hibbit, Karlson & Sorenson, Inc.
4. Leon G, Hall J, Kelly J, Coffenberry B, "Affordable Thermoplastic processing of marine structures", Proceedings of Flow Processes in Composite Materials '94 Conference, Galway, Ireland, July 1994.
5. Leon G, Hall J, Kelly J, Bubeck K, "Performance Assessment of In-situ consolidated thermoplastic fiber placement", Proceedings of Fourth International Conference on Automated Composites, Nottingham, U.K., Sept. 1995
6. Kelly J, Leon G, Hall J, Woodall C, "Reliable Design and fabrication of composite high performance marine vehicles", Proceedings of the Tenth International Conference on Composite Materials, British Columbia, Canada August 1995.
7. Leon G, Hall J, Kelly J, Bohlmann R, "Design and testing in-situ consolidated thick high performance thermoplastics", 12<sup>th</sup> International Conference on Composite Materials, Paris, July 1999.

## ACKNOWLEDGMENTS

This research work was funded by the Office of Naval Research, under James J. Kelly, Materials Program Manager.

**Quantifying the error in fibre orientation measurement and its application  
to evaluating numerical simulations**

**C.N. Eberhardt\* & A.R. Clarke\***

**ABSTRACT**

Recent developments in numerical simulation of the injection moulding process have made it possible to predict the fibre orientation in finished components with increasingly complex geometry's. In order to evaluate the results of such simulations, vast quantities of accurate fibre orientation data are required. The 2D image analysis method, where the orientations of individual fibres are derived from the shape of their cross-sections, has become a popular method for providing these data. Image processing and automated, large area scanning enables the orientation of many hundreds of fibres to be measured each minute. A new technique for 3D fibre orientation measurement using a confocal microscope has been developed with details published elsewhere. The confocal technique follows individual fibres through successive optical section planes and yields the following advantages:

- i) 3D measurement of fibre orientation enabling the calculation of the entire orientation tensor
- ii) Highly accurate orientation measurement, with sub-degree accuracy possible in some samples.
- iii) Novel 3D characterisations e.g. fibre waviness and ply misalignments.

In this paper, the confocal technique is used to evaluate the errors associated with the 2D image analysis technique. The results show both random and systematic errors in the fibre orientation measurements and their effect on the average orientation tensor is shown. Finally, initial results from our latest research using X-ray microtomography are presented. With this recently developed technique it is possible to non-destructively section materials, as with the confocal microscope but the X-rays give a far superior depth of penetration.

**INTRODUCTION TO FIBRE ORIENTATION RESEARCH**

The techniques for measuring fibre orientation distributions (FODs) have steadily improved over the last thirty years. Many different imaging methods have been used to observe fibre orientations including transmission x-ray micrographs, see Darlington et al (1) and microwave, see Urabe et al (2). However, reflected light microscopy has now become the most widely used technique for imaging fibre reinforced composites. After the sample has been sectioned, polished and etched, the elliptical sections of individual fibres are clearly visible under the microscope. Some of the first FOD measurements were performed by manual measurement of the elliptical parameters by hand, see Fakirov et al (3), although this method is impractical when large quantities of data are required. Bay et al (4) measured the ellipse parameters by the use of a computer and a digitiser tablet, significantly increasing the rate at which fibre parameters could be measured. More recently the increase in affordable computer power has fuelled research into image analysis to automatically extract the orientation data from these images. Image processing problems which have now been largely overcome are the removal of broken fibre fragments and splitting of touching fibre cross-sections which frequently occur in images of high packing fraction specimens, see Toll et al

\* Department of Physics & Astronomy, University of Leeds, Leeds, LS2 9JT.  
<http://mpi.leeds.ac.uk/instrumentation/>

(5). The next section describes the Leeds 2D image analyser system which is capable of measuring the orientations of 1000's of fibres every minute.

### LEEDS 2D IMAGE ANALYSER SYSTEM

The quality of the orientation data from any 2D image analysis system will depend upon the quality of the sample surface preparation. It is necessary to polish the sectioned (and potted) sample with finer and finer sanding disks and to enhance the contrast between fibre and matrix by metallic sputtering, see Mlekusch et al (6). A computer controlled XY translation stage is used to scan large areas of the sectioned sample (mm's x mm's) at high spatial resolution. Pattern matching ensures perfect registration between neighbouring images. The orientation of every fibre that appears within each image is measured using a pixel connectivity algorithm which provides the zeroth, first and second moments of all the objects contained within it, see Davidson et al (7). The semi-major,  $a$  and semi-minor axis,  $b$  lengths, illustrated in figure 1, are computed from the object's moments and a filter is applied to these parameters in order to remove any 'foreign' objects. The out-of-plane angle for each fibre is calculated as follows,

$$\theta = \cos^{-1} (b/a) \quad (1)$$

and the in-plane angle,  $\phi$  is given by the orientation of the fibre major axis with respect to the X-axis. Note that the true orientation of the fibre could be  $(\phi + 180^\circ)$ , but in many cases this ambiguity is not important to the interpretation of the fibre orientation state. The raw orientation data are weighted to take account of the stereological problems associated with inferring 3D features from 2D sections, see Clarke et al (8) for more details.

The quantity of orientation data produced by this system rapidly becomes unmanageable. Hence, a more concise description of the average fibre orientation is desirable which has led many researchers to adopt the orientation tensor description. The orientations of a large number of fibres are combined to give the orientation state at a point in space, i.e. the probability distribution function,  $\psi(\theta, \phi)$ . The orientation tensor is calculated from the moments of the orientation probability distribution function. Because of this function's inherent symmetry all non-even moments are zero, hence the first non-zero orientation tensor is the second-order tensor. The second order tensor is calculated by forming dyadic products of the vector components of individual fibres as follows:

$$a_{i,j} = \frac{1}{n} \left( \sum_{k=1}^n p_i^{(k)} p_j^{(k)} \right) = \begin{pmatrix} a_{11} & a_{12} & a_{13} \\ a_{21} & a_{22} & a_{23} \\ a_{31} & a_{32} & a_{33} \end{pmatrix} \quad i, j = 1, 2, 3 \quad (2)$$

Figure 2 illustrates a number of frequently observed fibre orientation states and their respective second-order orientation tensors.

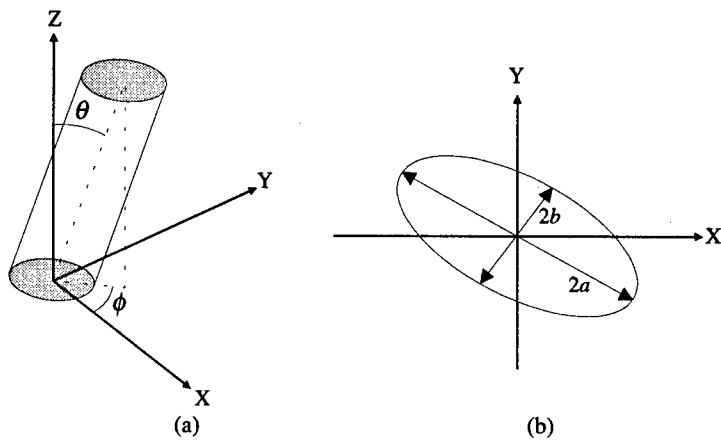


**Figure 1.** Deducing the fibre orientations  $\{\theta, \phi\}$  from the elliptical fibre cross-sections in the XY sectioned plane.

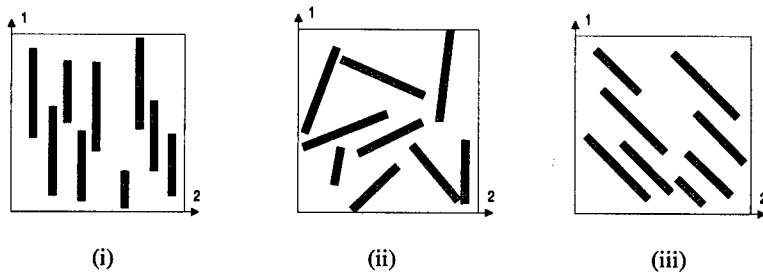


**Figure 2.** Three example orientation distributions, (i) unidirectional,  $\mathbf{a} = \begin{pmatrix} 1 & 0 \\ 0 & 0 \end{pmatrix}$ , (ii) isotropic,  $\mathbf{a} = \begin{pmatrix} 0.5 & 0 \\ 0 & 0.5 \end{pmatrix}$ , (iii) off-axis unidirectional,  $\mathbf{a} = \begin{pmatrix} 0.5 & 0.5 \\ 0.5 & 0.5 \end{pmatrix}$ .

## CONFOCAL MICROSCOPY OF FIBRE-REINFORCED COMPOSITES

With a conventional reflected light microscope it is only possible to image the cross sections of fibres on the samples surface. The recently developed confocal technique uses a pinhole positioned at the back focal plane of the microscope as illustrated in figure 3. This aperture physically blocks all the light reflected from above and below the focal plane resulting in a highly focussed 'spot' image. In confocal laser scanning microscopy (CLSM) a laser provides the sample illumination and scanning optics move the spot in a raster pattern through the objective lens field of view resulting in the formation of a confocal image, see Pawley (9). The CLSM has been used mainly for biological and physiological research and the literature on the Materials Science potential of the CLSM is limited.

With the CLSM it is possible to image in both reflection and fluorescence modes. Images of the sample surface acquired in reflection mode look almost identical to their reflected light microscope counterparts. It has been found that the majority of polymer matrices fluoresce making fluorescence mode imaging the best technique for observing sub-surface features (sub-surface images acquired in reflection mode are complicated by reflections at the fibre-matrix interfaces). In our composites research, the highest sub-micron resolutions are obtained with oil immersion objectives (magnification x60, NA 1.4) which means that the upper limit to the depth of penetration below the surface is the short working distance of the objective (typically 200  $\mu\text{m}$ ). In practice, the penetration depth for glass fibre composites is around 40  $\mu\text{m}$  to 150  $\mu\text{m}$  depending upon the fibre packing fraction and is around 5  $\mu\text{m}$  to 25  $\mu\text{m}$  for carbon fibre composites (depending upon packing fraction), see Clarke et al (10). Figure 4 shows a series of three images acquired using a NORAN Odyssey CLSM where the individual fibres are clearly visible on all three optical section planes.

In order to reconstruct features within a small volume of the sample, a series of optical sections parallel to the sample surface are recorded. The orientation of individual fibres can be calculated from the reflection mode surface image as described in the previous section. An image processing routine has been developed which 'traces' the fibres detected at the sample surface through the sub-surface images (11). By computing the movement in fibre centres between the surface plane and a number of parallel, perfectly registered, optical planes within the sample, each fibre's orientation  $\{\theta, \phi\}$  can be determined with a high level of accuracy. Furthermore, the ambiguity which makes it impossible to distinguish between a fibre with an orientation of  $\phi$  and one with an orientation of  $(\phi + 180^\circ)$  is now removed.

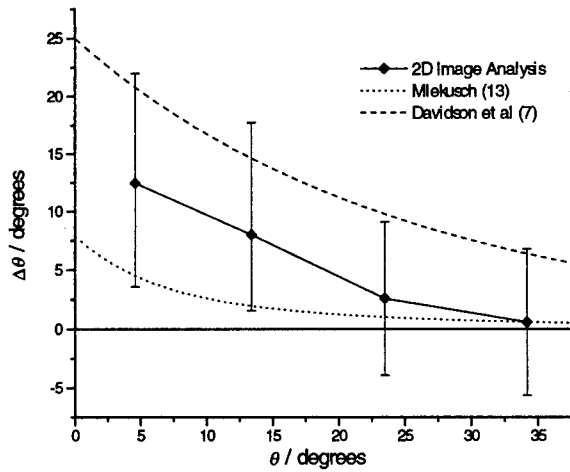


**Figure 5.** Comparison of the experimentally determined error in measuring the out-of-plane angle,  $\theta$  using 2D image analysis. The errors estimated by other researchers are included for comparison.

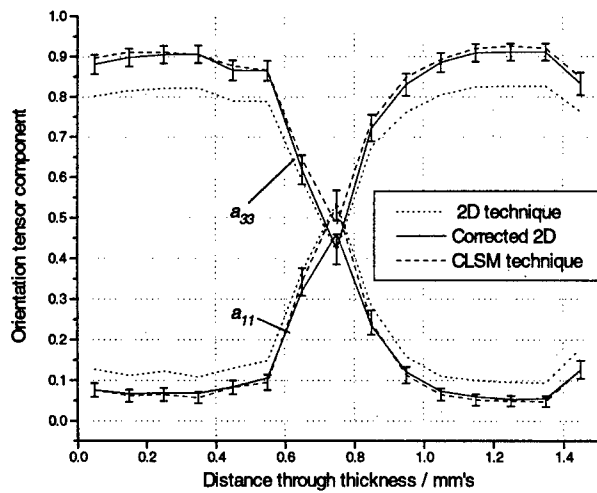


**Figure 6** The variation of fibre orientation tensor across the skin-core-skin region of an injection moulded composite ( $a_{22} \approx 0$ ). The results from the 2D technique are compared to the CLSM technique. The systematic error associated with the 2D technique has been corrected and the error bars denote the derived measurement error.

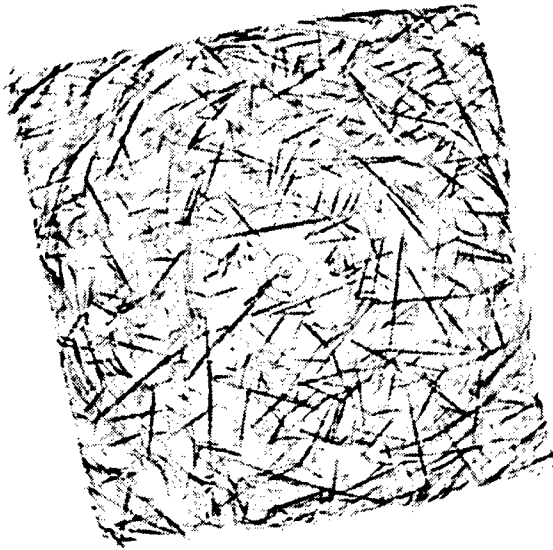


**Figure 7.** A cross section of a glass fibre reinforced polypropylene composite acquired using X-ray microtomography. The sample size is approximately 2mm x 2mm in cross section.

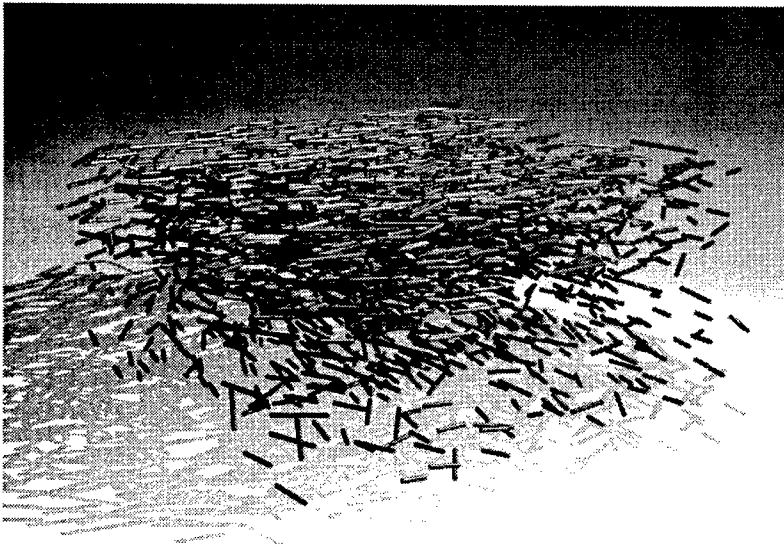


**Figure 8.** A 3D reconstruction taken from a number of serial sections acquired using X-ray microtomography. The reconstructed sample size is approximately 2mm x 2mm x 1.5mm.

$$\theta_c = t \ln \left( \frac{\theta - y}{A} \right) \quad (3)$$

where  $\theta$  is the original measurement,  $\theta_c$  is the corrected measurement and the following values for the constants,  $y = -21$ ,  $A = 36$  and  $t = 73$  were determined from figure 5. The measurement errors by their nature cannot be corrected, hence the random errors associated with individual fibre orientation measurements propagate to give an uncertainty in the derived orientation tensor, for details of the appropriate calculations see Bay et al (4) or Mlekusch (13). Figure 6 shows the effect of measurement errors on the derived orientation tensor. The advantages of correcting the systematic error associated with the 2D analysis technique is visible.

## X-RAY MICROTOMOGRAPHY

Recent advances in laboratory X-ray sources and CCD technologies have made it possible to perform X-ray tomographic imaging with spatial resolutions in the micron range. X-ray microtomographs (XMTs) provide researchers with the ability to reconstruct in 3D large sample volumes. The use of X-rays as opposed to visible light significantly increases the depth penetration through semi-transparent media. Figure 7 shows a single cross section of a short glass fibre reinforced composite acquired using a commercial XMT. The resolution of this imaging technique is high enough for individual fibres to be clearly visible in the cross section. Our group is currently involved in researching methods for extracting fibre orientations from these images and figure 8 shows our initial results of processing 400 serial sections.

## CONCLUSIONS/FUTURE WORK

Despite limited depth of penetration, the CLSM enables highly accurate fibre orientation measurements. As 3D process models are coming on stream, the acquisition of 3D data from complex processed parts will provide confirmation of the validity of the models. The CLSM has enabled the estimation of the errors involved in the more widely used 2D fibre orientation studies. It has been shown that this technique introduces a systematic error in the fibre orientation angle,  $\theta$ , which is due to the non-linear relationship between the ellipse axis lengths from which it is derived. For the first time it has been possible to quantify the error  $\Delta\theta$  and hence it may be corrected in future. With the 2D image analysis technique it is important to filter the data in order to remove the more erroneous measurements, however excessive filtering may lead to a bias. Clearly the key to accurate 2D orientation data is the quality of sample surface preparation before imaging under the microscope.

It looks as though X-ray microtomography will become important for future studies of in-situ fibre orientation and fibre length measurements because of the greater depth of penetration

than the CLSM technique. Our 3D space curve approach, see Clarke & Eberhardt (12), for smoothing out the measurement noise on optical sections should also be valuable in the recreation of fibre waviness and curvature from X-ray sections.

### ACKNOWLEDGEMENTS

We would like to acknowledge many fruitful discussions with Dr Vincent's team at the Ecole des Mines and thank the Anglo-French ALLIANCE programme for funding our collaborative work over the past two years. We would also like to thank Dr. Pyrz at Aalborg University and Dr. Jia at the University of Leeds for access to XMT facilities. We would like to thank EPSRC/MoD for the support on recent research grants (GR/L 96363 and GR/N 18413) and our ex-colleagues Dr N.C. Davidson and Dr G. Archenhold who helped set the scene for these 2D image analyser and CLSM investigations.

### LIST OF SYMBOLS

$\theta$  = out-of-plane angle  
 $\phi$  = in-plane angle  
 $p$  = fibre orientation unit vector  
 $a$  = semi-major ellipse axis length  
 $b$  = semi-minor ellipse axis length  
 $a_{ij}$  = second order orientation tensor  
 $\psi(\theta, \phi)$  = fibre orientation probability distribution function

### REFERENCES

1. M.W. Darlington, P.L. McGinley, G.R. Smith, *J. Mat. Sci.* (1976) 11
2. K. Urabe, S. Yomada, *Adv. Comp. Mat.*, (1991) 1
3. S. Fakirov, C. Fakirova, *Polymer Composites*, (1985) 6
4. R.S. Bay, C.L. Tucker, *Polymer Engineering and Science*, (1992) 32
5. S. Toll, P.O. Andersson, *Composites*, (1991) 22
6. B. Mlekusch, E.A. Lehner, W. Geymayer, *Comp. Sci. Tech.* (1999) 59
7. N.C. Davidson, A.R. Clarke, G. Archenhold, *J. of Microscopy*, (1997) 185
8. A.R. Clarke, G. Archenhold, N.C. Davidson, Chapter 3 from 'Microstructural characterisation of fibre-reinforced composites', Woodhead Publishing Ltd, 1998
9. J. Pawley, 'Handbook of Biological Confocal Microscopy', Plenum Press, 1995
10. A.R. Clarke, N. Davidson, G. Archenhold, *J. of Microscopy* (1993) 171
11. C.N. Eberhardt, A.R. Clarke, *Comp. Sci. Tech.* (2001) **in press**.
12. A. Clarke, C. Eberhardt, *Comp. Sci. Tech.* (1999) 59
13. B. Mlekusch, *Comp. Sci. Tech.* (1999) 59

ICMAC - International Conference for Manufacturing of Advanced Composites

**Effect of Sizing on the flow of resin within a glass fibre composite**

J. Quinn, A.T. McIlhagger\* R. McIlhagger, P.P.J. Rogers.

Engineering Composites Research Centre (ECRE),  
Department of Electrical and Mechanical Engineering,  
University of Ulster at Jordanstown, Shore Road, Newtownabbey,  
Co. Antrim, BT37 0QB, Northern Ireland, UK.

**Abstract**

The aim of this work is to investigate the effects of size/coatings on the processing parameters of a glass fibre composite component. Plaques were manufactured from glass fibre mat with three different finishes applied. The results obtained show the finish to have an effect on the processing of the composite samples. Samples with epoxy based coating are shown to be less compressible and have lower fibre volume fraction in their composite form. Flow results are presented as acquired by SMARTweave™

**Introduction**

Manufacture of high performance composite components can be a costly process involving many man hours and use of high added value materials. Traditionally autoclaves are used because of the high quality and low void content, typically less than 1%. This route of manufacture is highly labour intensive and involves higher costs than liquid composite moulding techniques. Resin transfer moulding (RTM) offers one way to reduce some of the costs involved while still achieving a comparable end result.

RTM is normally a closed mould process involving the injection of resin into a dry preform under pressure. This pressure can range from 1 to 4 bar. The use of low pressure for the moulding of components reduces the need for high cost tooling, with moulds of a lesser structural rigidity sufficing. Within RTM there are a number of factors identified as being crucial to the manufacture of a quality component. These factors include the compaction prior to resin injection, permeability of the preform, flow of resin through the reinforcement, cure parameters and the type of preform used in the process. Flow of the resin within the mould has been highlighted as critically important in the reduction of costs for the overall manufacture of components by RTM [1]

The glass fibre mats used in the manufacture of commercial composites have a "size" coating applied. The coating acts as a barrier, protecting the fibres from damage during handling and also moisture degradation [2]. The finish used by different companies is a mixture of coupling agents, film formers, lubricants and antistatic

\* Corresponding author Tel +44-28-90-366670, E-Mail: [a.mcilhagger@ulst.ac.uk](mailto:a.mcilhagger@ulst.ac.uk) (A.McIlhagger)

agents [3]. The type of fibre finish on a preform will affect the adhesion between the reinforcement and the matrix and hence the properties of the final component [4], added to this the coating will affect the processing parameters during composite manufacture. In cases where the reinforcement is made up from a woven fabric the spaces between the tows of the fabrics provide areas in which the matrix can adhere to the reinforcement. Hence the interaction of size or coupling agent and the resin used is an important factor in the performance of these composites.

Many authors have identified compaction of the preform prior to injection with resin as an important parameter in liquid composite moulding. Compression of fabric preform prior to processing results in changes in fibre fraction, porosity and pore dimensions[5]. These changes in the geometry of the fabric (nesting, tow movement and tow widening) have effects on the processing of the preforms by altering the permeability of the reinforcement to resin flow and the mechanical properties of the final composite.[6] Compression characteristics of fabric structures have been described by Matsudaira and Qin [7]as one of the most important in a fabric's mechanical properties and are closely related to fabric handle. The authors go on to present a model describing the compression of a fabric in three stages and relate the second stage , the overcoming of inter-frictional forces between fibres to decrease the thickness. For a multi-layer reinforcement, nesting has been noted as one of the most important factors in consolidation of the preform[8]. In combining the ideas of nesting and fibre handle it is suggested that the different types of finish have an effect the frictional properties of the fabric. With frictional properties affecting the compression properties of the fabric it will affect the fibre volume fraction prior to resin injection and hence the processing parameters may also be influenced. Added to this the final mechanical properties of the composite component may be altered.

RTM is normally a closed mould process and therefore it is not possible to monitor the state of the mould interior without intruding into the main body of the tool. There are a number of different methods by which this can be achieved. In the past authors have used thermocouples, pressure sensors and thermistors, as well as dielectric instruments, have been used to monitor changes in factors affecting the manufacture of composite components. As previously mentioned all these methods are intrusive and can cause reduction in the mechanical properties of the composite component<sup>9</sup>. SMARTweave™ [10] represents an in-situ method of monitoring the location and state of resin within the reinforcement during liquid composite moulding processes. The system provides valuable information as to the dynamics of the mould filling process, formation of dry spots and the gel and cure time of the resin[11].

SMARTweave™ consists of a sensing grid connected to an electronics package. The grid is made up of a number electrically conductive filaments [12] crossing on non-intersecting planes. The areas in which the lines intersect on a non-planar level create a sensing gap known as a node. The placement of the grids in differing planes allows the medium between them, in this case the resin, to act as a conductor between "crossover" sections of the two sensing lines. In a state of no resin there will be very low conductance and hence no signal will pass from grid to grid. The presence of resin between the sensing filaments allows a signal to pass from one to another and

the controlling software records a reading. The magnitude of the ionic conductance induced by the DC generated voltage depends on a number of factors including the cure state of the resin. The SMARTweave™ software shows the tool as a grid of squares on the computer screen, each square representing a nodal or crossover point. With resin arrival at the nodal points each square changes in colour from black to grey to white as the conductance value increases with the resin passing between the nodal points. As the resin cures the ionic conductance reduces and the signal gradually turns from white to grey and finally black, indicating that there is no measurable value of conductance between the nodal points. The software generates a voltage time plot to enable examination of the cure of resin during the RTM process.

The aim of this work is to examine on the effects three types of fibre finish supplied by CS Interglass have on glass fibre composites manufactured via the RTM process. Results are presented on the influence of the fibre finish on the processability, using SMARTweave™ data generated to characterise the resin movement within an RTM tool. Results are also presented to describe the influence that fibre finish has on the mechanical properties of the glass fibre composite.

**Methodology**

Flat glass fibre plaques were manufacture via the RTM process [13] to dimensions of 280-x-340 mm. The reinforcement used was a plain weave glass, 120 picks/m 120ends/m and 1.63 g/m<sup>2</sup> supplied by CS-Interglass. Each of the plaques was manufactured under identical conditions i.e. same injection pressure and temperature etc. Injection time was recorded in each case .The plaques had three different finishes as outlined in Table 1

Plaque Number	Finish Type
1	(A )No finish, fabric heat cleaned to remove size and other finish agents
2	(B )Saline finish based on epoxy saline.
3	(C) Volan A finish Chromium based

Table I

Selection of the finish types used was based on Matthews et al [14] identifying saline-based finishes as having a large effect on composite properties. Finish No.2 is an epoxy based finish chosen because of the expected similar chemical compatibility properties to the resin system used within the Engineering Composites Research Centre. Finish No3 represents a Volan A finish well known throughout the industry based on chromium chemistry. Finish No. 1 is a heat cleaned fabric to chosen to highlight any advantages or disadvantages the other two finishes will have over a fabric with no finish applied.

**Friction Tests**

Each fabric was tested to obtain both a fabric to fabric, and fabric to steel friction characteristics. This was completed using the sled method described in work completed previously within ECRE [14].

### Compression Tests

The consolidation of the fabric was identified earlier as being an important parameter in composite processing. Compression tests were carried out on layered samples of fabric. The fabric was cut to 100 x 100 mm. Figure 1 shows the plain weave sample, when stacking the sample to make the layered compression specimen great care was taken to ensure alignment of plies. The samples were then compressed under a load of 1 to 10 kN, the speed was kept at a constant 10 mm/min this parameter was set on the computer control unit and is in keeping with work done by other authors<sup>5</sup>. Graphs of thickness against pressure were generated

### Flow data tests

SMARTweave™ data acquisition was used to monitor the arrival of resin at set locations within the mould. 0.12mm shielded copper was used as the sensing and excitation lines. The shielding was removed at the crossover points to allow the flow of current between nodal points. The wire represented an easily attainable resource as well as having no discernible effects on the flow of resin within the mould tool. Video capture of an RTM run was used to investigate any effects the wire sensors would have on the flow of resin. Comparing video files of injection with and without wire showed no detrimental effects on the flow of resin caused by the wires inserted in the reinforcement. Figure No. 2 shows the grid layout used to monitor the flow. The placement of the sensing nodes was based on data generated by video capture methods used previously within ECRE [15].

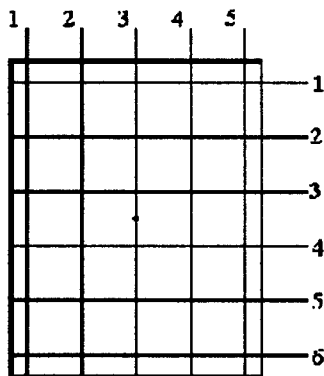


Figure 1 Node locations for 6 row x 5 column grid

### Thermal analysis

Thermal analysis techniques of Differential Scanning Calorimetry (DSC) and Thermogravimetric Analysis (TGA) were used to evaluate the glass transition temperature and fibre volume fraction of each sample plaques. Work by McIlhagger

[16] showed that, although sample size used in the TGA instrument was small, results for fibre volume fraction acquired using this method were representative.

Plaque Number	Finish No.	Coefficient of friction		Injection Time (min)	Average Plaque Thickness (mm)	T <sub>g</sub>	V <sub>f</sub> %
		Fibre to Steel	Fibre to Fibre				
1	A	0.273	0.25	3.8	1.61	102.91	67.8
2	B	0.307	0.32	2.7	1.9	103.45	59.5
3	C	0.301	0.20	3.56	1.61	101.26	65.2

Table II results generated from the various tests completed using the three different fabrics.

Plaque 2 had the fastest injection time and this it is believed was largely due to the reinforcement being thicker than the other two i.e. less compressed. The increased thickness for the same amount of fabric and plaque size indicates that the permeability of the preform was higher in plaque 2 than the other two. Initial tests completed on the fibre friction properties of the samples show that fabric 1 has the highest coefficient of friction when tested against fibre to steel, however fabric 2 is shown to be the highest when the test is fibre to fibre. Fibre friction and fibre interaction/movement is an element in the compaction of the fibres, the results show that the fibre used for fabric number 2 yielded a final composite thicker than fabrics 1 and 3.

Initial compression tests have shown that the fabric used for plaque 2 does not compact as well as the other two for a given of pressure 1 bar, and it is concluded that this is due to the high value of fibre to fibre friction between the layers. The graph Figure. 3 shows that as the pressure increases to 1 bar, the other two fabrics have achieved a higher fibre volume fraction than the fabric with finish B.

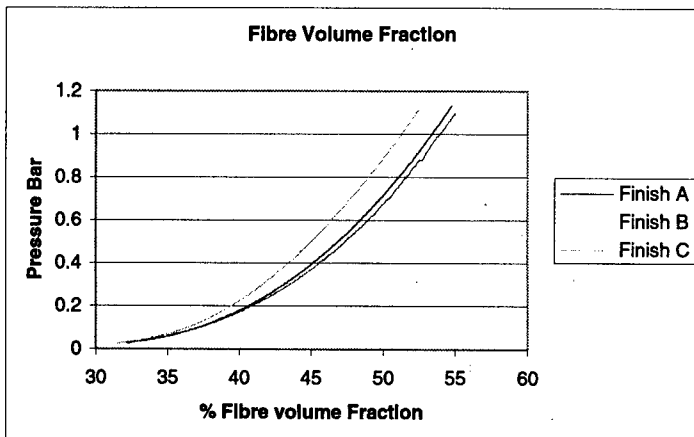


Figure 2 Compaction pressure vs Fibre volume fraction for the three fabrics used

The results indicate that increased fibre to fibre frictional properties caused by the application of a finish have lowered its nesting ability and hence the fibres do not nest as readily.

In order to determine the glass transition temperature ( $T_g$ ) of each of the composite plaques the thermal analysis technique of DSC was used. The results are presents in Table II. These show that the  $T_g$  value for each of the plaques is the same within experimental error indicating the virtually the same cross-link density in each sample. Results were successfully obtained using the SMARTweave™ sensing technology.

The injection time results show that the time to fill for the finish C and finish A samples is very similar however the injection time for the finish B is about 50 seconds shorter. The fabrics are all of the same geometric design i.e. warps and wefts and are of the same materials albeit with different finishes applied. Therefore it is suggested that the reason for the differences in fill time and hence permeability lie with the finish. Previously in this paper it was suggested that the friction properties of the fibres affect the compaction properties and hence the flow of resin within the mould cavity. SMARTweave™ dc sensing equipment was placed in the mould cavity with the reinforcement and the flow of resin was recorded. The times in seconds to reach certain nodes in the mould cavity are shown in Table III.

Node	Finish2	Finish 1	Finish 3
Sensor group 1	Time to reach node (sec)	Time to reach node (sec)	Time to reach node (sec)
1x1	85	80	75
1x5	95	85	80
6x1	85	80	75
6x5	95	85	80
Sensor group 2			
2x2	135	160	155
2x4	145	170	165
4x2	140	160	165
4x4	140	170	165
Sensor group 3			
3x3	160	205	205

Table III Table of times in seconds to reach nodes

The table shows the time in seconds to activate a node. A node was considered to be active when a signal was generated. For this study, times were recorded when the nodal voltage was at it's peak.. The nodes were grouped as shown above, this was to represent different areas of the mould. Sensor group 1 represents a fill in terms of area of approximately 167 cm<sup>2</sup>. The table shows that all plaques took much the same time to reach this point. Sensor group 2 represents the time take for the resin to fill an area of 517 cm<sup>2</sup>. The results show that plaque one with the epoxy finish reaches this point of fill first. Sensor group 3 indicates a region of the mould just prior to resin exit. The results show that the resin reaches this point first in the epoxy finished plaque. The times agree with the video data generated for the placement of the sensors. Sensors forming a perimeter oblong shape register a maximum signal at times to within 10

seconds of each other. Voltage time graphs for the first nodes 1x1 are shown in figure 3, while figure 4 shows the voltage traces at 1x1 and 3x3 for finish B.

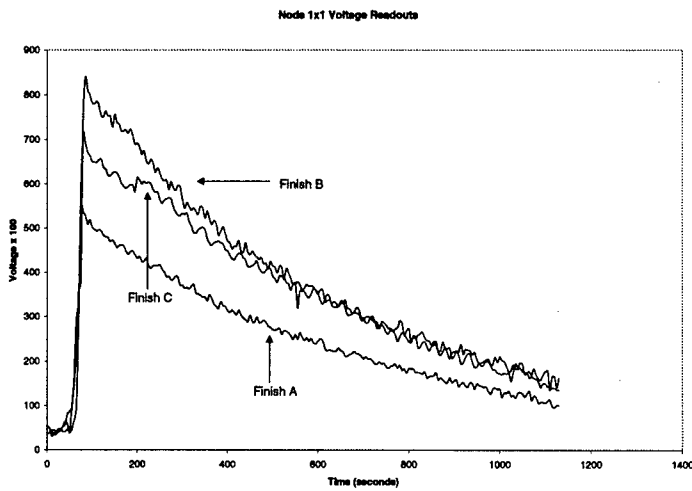


Figure 3 Node 1x1 for each of the plaques

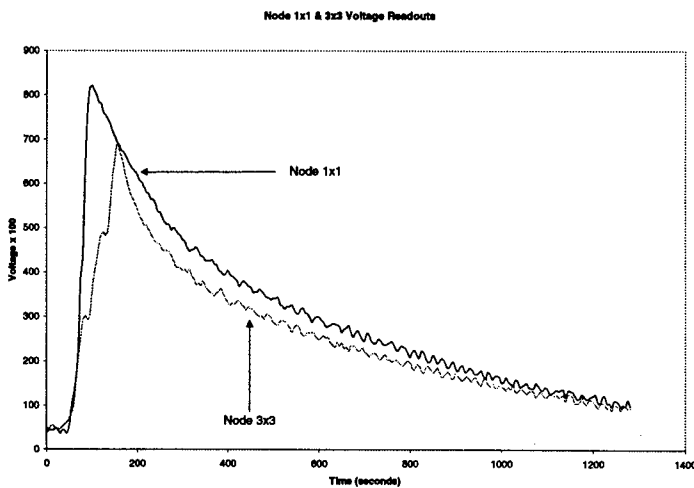


Figure 4 Nodes 1x1 and 3x3 for the plaque made using fabric 2

### Conclusions

Results have been presented on the various tests conducted. The results have shown that the fibre to fibre friction coefficient for Finish B is the highest. Plaques made

using Finish B are the thickest and have the lowest fibre volume fraction. It was suggested that a high coefficient of friction will affect the compaction properties i.e. the higher the coefficient the less the reinforcement will nest. The results support this suggestion. Fibre finish has been shown to have no discernible effect on the  $T_g$ /degree of cross-linking of the composite components. SMARTweave™ results have demonstrated that the resin flow can be mapped. The time to fill the mould as measured using this technique have shown that the flow for reinforcements with finish B are fastest, this is supporting the theory that the sample has compacted less than the other two.. The data generated for flow visualisation largely agrees with video data generated within previously.

#### Acknowledgements

The authors would like thank Roger Price and CS-Interglas for the supply of materials and their continual involvement in this research.

- 
- [1] Carter, E. J.; Fell, A. W.; Griffin, P. R.; Summerscales, J Composites - Part A: Applied Science and Manufacturing, v 27, 4, (1996), p 255-261
  - [2] A Sjogren, R Joffe, L Berglund E Mader Composites Part A 30 (1999) 1009 - 1015
  - [3] Handbook of Composites Knox CE. Fibreglass Reinforcement In Lubin .G editor, . New York: Van Nostrand Reinhold 1982
  - [4] J.L. Thomason, A Noordam and G Walton 15<sup>th</sup> Reinforced Plastics Conference 1986 Nottingham England ( British Plastics Federation London 1986) , pp 131-135
  - [5] R.A.Saunders, C. Lekakou and M.G. Bader Composites Part A 29 A 1998 433-454
  - [6] Lam R.G. and Kardos J.L. Proc Antec '89 American Society for Composites
  - [7] M Matsudaira H. Qin Journal of The Textile Institute No.3 86 1995
  - [8] Baoxing Chen, Tsu-Wei Chou, Composites Science and technology 60 (2000) 2223-2231
  - [9] A.T. McIlhagger PhD Thesis Submitted University of Ulster Jordanstown
  - [10] SMARTweave Patent Walsh S.W .; "In-situ sensor method and device" U.S. Patent No. 5,210,499, May 11 1993
  - [11] SMARTweave Resin Flow Front Analysis System Users Guide Holometrix Micromet Chpt 1 Page 4
  - [12] David D Shepard 43<sup>rd</sup> International SAMPE Symposium, May 31 – June 4 1998
  - [13] ECRE Procedure RTM Manufacture, University of Ulster Shore Road Newtonabbey.
  - [14] Matthews ST, McIlhagger R, Hill. B.J., Shortall C. ECRE in house publication
  - [15] Justin Quinn 3<sup>rd</sup> Annual Sir Bernard Crossland Symposium, Limerick University, 1999
  - [16] A.T. McIlhagger PhD Thesis Submitted University of Ulster Jordanstown

ICMAC - International Conference for Manufacturing of Advanced Composites

**The Influence of Post-cure Temperature and Time on the Thermal and Mechanical Properties of Fibre Reinforced Epoxy Composites.**

A.T. McIlhagger, J. Quinn, R. McIlhagger, D. Brown, P.P.J. Rogers, S.T. Matthews

Engineering Composites Research Centre (ECRE),  
Department of Electrical and Mechanical Engineering,  
University of Ulster at Jordanstown, Shore Road, Newtownabbey,  
Co. Antrim, BT37 0QB, Northern Ireland, UK.

**Abstract**

The aim of this paper is to investigate the effect of the post-cure parameters (i.e. time and temperature) on the thermal and mechanical properties of the composite in order to optimise the conditions for the post-cure operation. Identical composite specimens were post-cured in a temperature controlled oven at different combinations of temperature in the range 120 to 200°C with time and the effect on resin cure was assessed by measuring the glass transition temperature ( $T_g$ ) by Differential Scanning Calorimetry (DSC). A number of combinations of post-cure time and temperature that gave a similar  $T_g$  was used to post-cure composite samples and the mechanical properties of these samples were measured in order to assess the optimum post-cure conditions. The post-cure temperatures of 120°C and 140°C gave the best balance of mechanical properties (flexural and in particular interlaminar shear) but these were accompanied by the longest post-cure times. It is therefore important to consider the required end-use properties of the component and if the post-cure time is a significant factor in the process economics when considering the post-cure temperature.

**Introduction**

Various Resin Transfer Moulding (RTM) processing parameters have been investigated and their effect on the performance of the final composite demonstrated. Young and Tseng (1) studied the pre-heat temperatures and injection pressures during the RTM process and measured the flexural strengths of the finished products in order to assess the influence of these parameters. They discovered that the void content in the composite was dependent upon the pressures used and clearly voids have a detrimental effect on the mechanical performance of composite materials. Stabler et al (2) investigated the formation of voids within composites produced by RTM and found how they can be minimized by altering some of the processing parameters, e.g. lightly waxing and buffing the mould surface and reducing the initial bubble content of the resin. Lundström and Gebart (3) investigated the influence of different process variables on the void content in RTM. It was shown that an efficient way of reducing the void content was to use vacuum assistance during mould filling. The void content could also be decreased by increasing the pressure during cure and by removing the sizing from the fibres before resin impregnation. Increasing the mould temperature was found to increase void content. Haywood and Harris (4) found that the use of vacuum assistance in RTM led to significant improvements in both the mechanical properties and reduces the porosity levels of GRP composites. Variations in resin injection pressure appeared to have no effect on the quality of mouldings. Mould temperature variations, over a modest range of temperatures, did not appear to affect the quality of parts other than by way of resin cure

differences. Haque et al (5) found that the processing parameters of RTM significantly influenced the interlaminar shear and compressive strength (i.e. resin dominant properties) of the materials. This appeared to be due to the presence of voids in the cured resin and improper wetting of the fibre. The tensile and in plane shear strength (i.e. fibre dominant properties) of the composites showed negligible change in magnitude due to the change of RTM process variables. The panel with the best mechanical properties was manufactured with resin that had been degassed and also utilised vacuum assistance.

In composite processing the component may be removed at a time when cure is complete. However the expensive mould and ancillary equipment is being used longer than necessary and this is not practical, nor economic. In an industrial environment the cure cycle can be split into two sections. The first involves the injection and the onset of cross-linking which allows the composite plaque to be removed or demoulded from the tooling. At demoulding the material is viscoelastic and the optimum mechanical properties have not been achieved. The second stage is known as the post-cure stage during which the composite plaque undergoes further heating. Two methods are possible for conducting post-cure operations. The first is to use constant time and various heating rates, this can be used to determine the ramp which results in the highest mechanical properties. This technique is particularly beneficial if processing time is crucial and highly controlled equipment is available. The other method is to maintain a constant temperature and vary the cure time which will result in an optimum cure time at a particular cure temperature. To speed up the process or to ensure more thorough cross-linking a post-curing temperature higher than that of curing may be used. This method is used if equipment heating power is limited. For example, only very slow heating rates may be possible due to the physical size or the rating of the heating element.

Post-curing in a temperature controlled oven allows for resin curing to be conducted off-line, which leads to the possibility of reducing the amount of time that the composite part spends within the production tooling. This reduced tool turnaround time leads to greater productivity. However, before a composite part can be de-moulded it is essential to ensure that the resin is sufficiently cured.

Post-curing is important as it ensures that the resin within the composite has been fully cured and hence optimises the mechanical properties of the composite. Akay et al (6) confirmed that for composite properties to be maximised, it is essential that resin cure be optimised. They also found that traditional static mechanical tests were not sufficiently sensitive to distinguish between cured and significantly undercured composites. Thermal analysis methods indicated more precisely the extent of resin cure and were thus employed as meaningful diagnostic tests in composite production.

## **Experimental Details**

### **Materials**

The reinforcement material used was continuous filament E-glass, 136 tex, supplied by CS-Interglas as a plain weave architecture (71 ends/m in the warp direction and 70 picks/m in the weft direction). Twelve layers of fabric (measuring 355 x 355 mm) were superimposed on each other so that the warp and weft directions of every layer were aligned in the same

respective directions. The matrix was a two-part epoxy system supplied by Ciba Polymers; LY564 resin mixed with HY2954 hardener.

### **Processing**

The resin is mixed and degassed in a vacuum chamber for 1 hour at 30°C to remove moisture and air suspended in the resin. The aluminium tool is held under vacuum at 75°C and the resin injected by a peripheral gating arrangement, into the tool at a supply pressure of 750 mbar absolute. The tool temperature was raised to 100°C at approximately 0.64°C/min and the composite cured for 99 minutes before the composite part was demoulded.

### **Post-curing and Analysis**

Five flat composite plaques were manufactured, each post-cured at specified temperatures between 120°C and 200°C. Each composite plaque was divided into strips and post-cured for varying amounts of time. Five samples (approximately 5–10 mg each) were taken from each strip and the glass transition temperature determined by Differential Scanning Calorimetry (DSC) to produce a relationship between  $T_g$  and post-cure temperature and time.

DSC analysis was conducted using a Du Pont Instruments DSC 10 Differential Scanning Calorimeter (supplied by TA Instruments) at a ramp rate of 10°C per minute and under an inert gas atmosphere (nitrogen).

Post-cure operations were conducted in a large convection oven by switching it on and setting the desired post-cure temperature as the set point temperature. Once the oven temperature had risen to and stabilised at the desired temperature, the relevant samples were placed into the oven on an aluminium tray and the time noted. Each sample was then removed after the required post-cure time and allowed to cool on a wooden table at room temperature.

In the second phase of the work, new plaques were manufactured and post-cured at the different temperatures used in the first phase of the work and the recently established relationship was used to give the corresponding times required at each temperature so that a similar  $T_g$  was achieved in each case. Flexural and interlaminar shear strength (ILSS) test samples were then prepared from each strip and tested so that the influence of post-cure temperature on mechanical properties could be observed.

Mechanical testing was conducted according to the Composite Research Advisory Group (CRAG) standards (7). The test samples were cut to size using a diamond wheel and then ground down to within the relevant tolerances using a specially designed jig and grinding machine.

## Results and Discussion

### Phase 1 – Differential Scanning Calorimetry

The mean  $T_g$  for each of the combinations of post-cure time and temperature included in the testing schedule is shown in Figure 1. 5 samples were taken in each test.

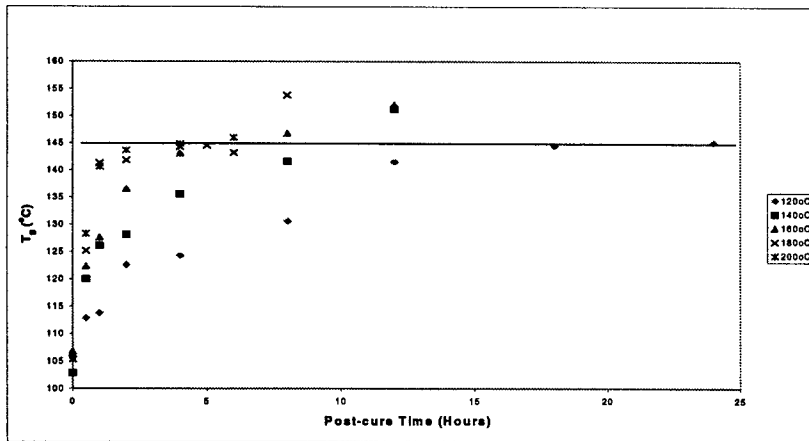


Figure 1: The Relationship between Glass Transition Temperature ( $T_g$ ) and Post-Cure Time and Temperature

From Figure 1 the initial glass transition temperature ( $T_g$ ) of the samples that have been cured at 100°C in the tool for 99 minutes (but have not undergone any post-cure) was approximately 105°C in each case. At all post-cure temperatures from 140°C to 200°C, the  $T_g$  rose dramatically in the first 30 minutes of post-cure to a value of 120-128°C while 30 minutes of post-cure at 120°C resulted in a less significant rise in the  $T_g$  to a value of 112°C. At the two highest post-cure temperatures (i.e. 180°C and 200°C), the next 30 minutes of post-cure also saw another significant increase in  $T_g$  to values of greater than 140°C and then the  $T_g$  levelled out at a value of approximately 145°C as post-cure time increased. There may be secondary degradation reactions of the resin system but further investigation would be required to determine if this was the case and also its effect on the mechanical properties. At the next two lower post cure temperatures (i.e. 140°C and 160°C), the rate of increase of  $T_g$  dropped off after the initial 30 minutes but the  $T_g$  continues to rise and eventually exceeded the plateau level of ~145°C observed at the higher post-cure temperatures. So, although higher post-cure temperatures initially caused a sharper rise in  $T_g$ , it would appear that this use of high temperature affected the resin in such a way that the maximum achievable  $T_g$  is restricted. This may also translate to the mechanical properties being similarly restricted and if this is the case, then it would clearly be inadvisable to post-cure at temperatures of greater than 160°C. At the lowest employed post-cure temperature of 120°C, the  $T_g$  rose steadily over the first

twelve hours before levelling off to a plateau of approximately 145°C which is the same plateau value that was observed when post cure was conducted at 180°C and 200°C.

Upon examination of this graphical relationship, it was decided that for the second phase of the work a  $T_g$  of 145°C by post-curing would be used at each of the five temperatures for varying amounts of time. It was estimated that at this value the composite should possess reasonable mechanical properties. To estimate the required times, a line of best fit was drawn through the points. A horizontal line was then drawn from the y-axis ( $T_g$ ) at 145°C so that it cut through each of the five lines. The time to give an estimate of the required post-cure time at the corresponding temperature was noted. The results are shown in Table 1.

Table I: Post-cure Times Required to Achieve a  $T_g$  of 145°C

Post-cure Temperature	Estimated Time required to give $T_g = 145^\circ\text{C}$
120°C	21 hours 35 minutes
140°C	9 hours 24 minutes
160°C	5 hours 56 minutes
180°C	4 hours 40 minutes
200°C	4 hours 00 minutes

### Phase 2a – Flexural Testing

The new plaques manufactured for the second phase of the work were divided into strips which were post-cured for the five combinations of time and temperature as shown in Table I. Twenty flexural test samples were then prepared from each of these strips and tested. Table II show the mean flexural strengths and flexural moduli respectively for each of the five post-cure conditions. The small figures in parentheses are the standard deviations.

Table II: Flexural Results for Different Post-cure Temperatures with  $T_g$  Nominally at 145°C

Post-cure Temperature (°C)	Flexural Strength $f_F$ (MPa)	Flexural Modulus $E_F$ (GPa)
120	464.4 (25.1)	20.65 (0.97)
140	463.1 (13.8)	21.83 (0.68)
160	431.7 (17.9)	20.70 (0.60)
180	419.5 (16.1)	22.14 (0.98)
200	415.3 (19.9)	22.38 (0.93)

Table II shows that there is no significant difference in the flexural strengths obtained after post-curing at 120°C and at 140°C for 21 hours 35 minutes and 9 hours 24 minutes respectively. However, increasing the post-cure temperature to 160°C and then to 180°C and finally to 200°C causes a drop in flexural strength in each case with the decreases becoming less dramatic at the higher temperatures (6.8%, 9.4% and 10.3% respectively below the value for 140°C). It should also be noted that as the post-cure temperature was increased, the corresponding post-cure times decreased. Hence, there seems to be a clear relationship between flexural strength and post-cure temperature over the temperature range investigated, i.e. as the post-cure temperature was increased above 140°C, the flexural strength decreased. This may be due to higher post-cure temperatures having an adverse affect on the resin as suggested by the first phase of this work.

The relationship between flexural modulus (Table II) and post-cure temperature is not so clear. The two highest results for flexural modulus were achieved by the samples post cured at the two highest temperatures of 180°C and 200°C (for 4 hours 40 minutes and 4 hours even respectively) which were 1.4% and 2.5% higher respectively than the result for post-cure at 140°C. The two lowest results were achieved by the samples post cured at 120°C and 160°C (for 21 hours 35 minutes and 5 hours 56 minutes respectively) which were 5.4% and 5.2% lower respectively than the result for post-cure at 140°C. The first phase of this work indicated that using post-cure temperatures as high as 180°C and 200°C caused an initial dramatic rise in  $T_g$  followed by it levelling off at 145°C. It was clear that the resin had obviously been affected in some way that restricted the maximum achievable  $T_g$ . While increasing the post-cure temperature caused the flexural strength to fall, flexural modulus does not appear to be detrimentally affected by post-cure at these higher temperatures. Indeed, these high post-cure temperature samples gave the highest values of flexural modulus.

#### Phase 2b – Interlaminar Shear Strength (ILSS) Testing

Table III shows the mean ILSS result for each of the five post-cure conditions. Five samples were tested at each of the post-cure conditions. The small figures in parentheses are for the standard deviations.

Table III: ILSS for Different Post-Cure Temperatures with  $T_g$  Nominally at 145°C

Post-cure Temperature (°C)	Interlaminar Shear Strength (MPa)
120	45.85 (1.50)
140	41.91 (1.86)
160	43.08 (1.73)
180	42.09 (2.45)
200	37.79 (2.53)

From Table III it is observed that the highest value of interlaminar shear strength (ILSS) is achieved after post-curing at 120°C for 21 hours 35 minutes. Increasing the post-cure temperature to 140°C, 160°C and 180°C causes a similar decrease in ILSS in each case of 8.6%, 6.0% and 8.2% respectively. Increasing the post-cure temperature up to 200°C causes a dramatic decrease in the ILSS to a value that is 17.6% below the highest value caused by post-curing at 120°C. The relationship between ILSS and post-cure temperature is similar to the relationship for flexural strength in that as the post-cure temperature is increased, the ILSS decreases. Again, this is suspected to be due to the higher post-cure temperatures having an adverse affect on the resin. ILSS was much more significantly affected by altering the post-cure temperature than either of the flexural properties - this is thought to be due to the fact that ILSS is a mainly resin dominant property while flexural properties are mainly fibre dominant.

### **Further Research Areas for Investigation**

Research by McIlhagger (8) has shown this post-cure period in the cure cycle can be continuously monitored, on-line by dielectric analysis (DEA). The identification of several key cure parameters, namely minimum viscosity, gelation, vitrification/completion of cure have also been further demonstrated. The effect of the mechanical properties at the different cure times and temperatures will be investigated and correlated with results from the dielectric technique.

### **Conclusions**

For the glass fibre composites produced by the RTM system high post-cure temperatures (e.g. 180°C and 200°C) caused an initial dramatic increase in  $T_g$  followed by a plateau at approximately 145°C. Lower post-cure temperatures (e.g. 140°C and 160°C) caused a slower initial rise in  $T_g$  but ultimately gave  $T_g$  values of approximately 145°C. Post-cure at 120°C caused a slow steady rise in  $T_g$  for the first 12 hours before a plateau at approximately 145°C is reached. As post-cure temperature was increased, the time required to give a similar  $T_g$  decreased - this effect was most strongly noted at lower temperatures.

Post-curing at 120°C and 140°C gave similar flexural strengths at these temperatures but increases in post-cure temperature between 140°C and 200°C caused a decrease in flexural strength (a constant  $T_g$  may be achieved by decreasing the post-cure time as post-cure temperature is increased).

There is no clear relationship between flexural modulus and post-cure temperature but the highest values were obtained by post-curing at the highest temperatures, i.e. 180°C and 200°C.

The interlaminar shear strength (ILSS) is highest when post-cure is conducted at 120°C and lowest when post-cure was conducted at 200°C with intermediate values of post-cure temperature resulting in similar intermediate values of ILSS.

In summary, it was found that the post-cure temperatures of 120°C and 140°C gave the best balance of mechanical properties (flexural and in particular interlaminar shear) but these were accompanied by the longest post-cure times. It is therefore important to consider the required end-use properties of the component and if the post-cure time is a significant factor in the process economics when considering the post-cure temperature.

### **Acknowledgements**

The authors would like to thank CS-Interglas for supplying the glass fibre. Thanks also to the staff of the Engineering Composites Research Centre. Financial support from the European Regional Development Fund (ERDF) in the form of Technology Development Programme (TDP) funding is also gratefully acknowledged.

### References

1. Young W.B, Tseng C.W, Journal of Reinforced Plastics and Composites **13** (1994) 467-482
2. Stabler W.R, Tatterson G.B, Sadler R.L, El-Shiekh A.H.M, SAMPE Quarterly January (1992) 38-42
3. Lundström T.S, Gebart B.R, Polymer Composites **15, 1** (1994) 25-33
4. Hayward J.S, Harris B, SAMPE Journal, **26, 3** (1990) 39-46
5. Haque A, Mahfuz H, Yu T.X, Jeelani S, 25th International SAMPE Technical Conference (1993) 305-318.
6. Akay M, Cracknell J.G, Farnham H.A, Polymers and Polymer Composites **2, 5** (1994) 317-322.
7. Curtis P.T(editor). "Test Methods for the Measurement of Engineering Properties of Fibre Reinforced Plastics", Royal Aerospace Establishment, Composites Research Advisory Group, Technical Report 88012, 1988.
8. A.T. McIlhagger. Phd Thesis, Submitted, University of Ulster, Jordanstown.

**SESSION 6:  
PROCESSING OF THERMOPLASTIC  
COMPOSITES**

**Manufacturing and Anisothermal Squeeze Flow of Glass fabric/Glass Mat Reinforced Polypropylene Hybrid Composites**

*K.W. Houston*

*P.J. Mallon*

**Composite Research Centre  
Mechanical & Aeronautical Engineering Department,  
University of Limerick, Limerick, Ireland**

**Abstract**

The criteria for selection of an appropriate composite for use in the automotive industry include short processing cycle time, low material cost and superior mechanical properties. GMT has a wide range of application in the automotive industry and is used in components such as bumper beams and door panels where these components are compression moulded using powerful hydraulic presses. However, when GMT is used as the core material and glass fabric reinforced polypropylene is used as the facing material in a hybrid composite, a component is produced which is thinner and lighter than when produced with GMT alone. GMTex™, a hybrid of GMT and commingled glass fabric is used extensively in the automotive industry and is manufactured in a double belt laminator.

However, if unimpregnated glass fabric and glass mat, together with polypropylene film are fed into the double belt laminator, then a consolidated composite with properties equivalent to GMTex™ is produced which eliminates the need for incorporating the more expensive commingled fabric. One of the goals of this project was to research the optimisation of the processing parameters of this composite (pressure, temperature, consolidation, time, etc.) and to document the process behaviour. During manufacture of this hybrid composite, its behaviour in the moulding process has been investigated. The experimental results reported has included the mechanical testing of hybrid composite specimens manufactured using various process parameters. The application of impregnation theory to the manufacture of this hybrid composite is also reported.

## Development of thin-walled fibre-reinforced structures

Participants:

Alan G. Gately<sup>1</sup>  
Austin B. Coffey<sup>2</sup>  
Dr. C. M. O'Bradaigh<sup>1</sup>  
Dr. A. Brazier<sup>2</sup>

<sup>1</sup> - Composite Research Unit, Mechanical Engineering, National University of Ireland, Galway

<sup>2</sup> - Polymer Engineering, Athlone Institute of Technology

Abstract:

There is a need in biomedical engineering for thin-walled, high-performance structures, which could be used as catheters, or as replacement implants in the body. There is a fundamental lack of technology to produce a hollow structure with a wall-thickness less than 0.1 mm. This paper investigates the basic issues associated with thermoplastic filament winding of thin-walled structures, in which an ultra-thin layer (<0.05 mm) reinforcing material is wound onto very small diameter (<0.5 mm) polymer tube. The main advantage of continuous fibre reinforced polymers is that they can be oriented at particular angles in order to optimise their mechanical responses.

The heating, melting and crystallisation of the candidate materials, as well as computational design, mechanical testing and non destructive evaluation, all on smaller size scales than previously attempted, will be examined. Current techniques such as over-braiding of stainless steel and carbon fibre have difficulties producing wall thicknesses below about 0.1 mm with high volume fractions. This new process will involve thermoplastic filament winding of thin layers of aramid and carbon fibre reinforced polymers, such as Polypropylene, Nylon, Polyurethane, Pebax etc. These layers will be wound onto a continuously moving extruded inner polymer core and the wound structure will be over-extruded with a suitable polymer coating. The adhesion at the interfaces of reinforcements, co-extrudates, coatings, etc will be evaluated using various techniques including micro-thermal analysis, microscopy, melt rheometry, and differential thermal analysis.

The objective is to produce high-performance thin-walled polymer structures whose properties are designed, or tailored to the particular application. In this respect, the orientation of the fibre layer is the main variable that can be designed and controlled in the process. Relatively high winding speeds will have to be realised using specially designed winding heads in order to make the process competitive. The integration of the winding heads into an extrusion line results in a continuous production system.

## VACUUM BAG MOULDING OF LARGE THERMOPLASTIC PARTS IN COMINGLED GLASS/PET COPOLYMER

A G Gibson and N Dodds, University of Newcastle upon Tyne, NE1 7RU, UK  
A Sharpe, PERA Technology, Melton Mowbray, LE13 0PB, UK  
H Knudsen, Trevira Neckelmann A/S, Silkeborg, Denmark.

### ABSTRACT

This paper describes the development of a thermoplastic composite system for structural application in the chassis of an electrically propelled bus. The work involved the characterisation and modelling of a vacuum bag moulding process using a woven comingled precursor. The matrix materials were PET and a PET copolymer. The process requires an ambient pressure oven with either composite or metal tooling, and produces excellent laminate with low void content. The temperature profile through the part and the consolidation behaviour were characterised and modelled. The thermal profile could be modelled with adequate accuracy using 'single point' values of thermal properties. Consolidation occurred in two stages: a low temperature debulking near to  $T_g$ , followed by full melt impregnation at a higher temperature. Both processes were modelled separately using a simplified version of the Kamal equation.

### INTRODUCTION

This project, carried out under the Foresight Vehicle Link Scheme, involved the development and characterisation of a vacuum bag process for the manufacture of thermoplastic composite parts on a size and scale suitable for lightweight public transport vehicles. The study centred around the replacement of load-bearing chassis components of an electric bus, Figure 1. One of the challenges was the use of composite tooling, since the high processing temperatures (200-300°C) limited the range of tooling materials that could be used. Metal tooling is viable but, for medium volume production runs of large parts, composite tooling has many attractions, including the ease with which doubly curved shapes can be produced. Improved resin chemistry has resulted in composite tooling with improved thermal capability: the glass/cyanate ester tools from ACG worked well with the PET copolymer for repeated mouldings.

The benefits of this thermoplastic technology<sup>1-5</sup>, include emission-free processing and recyclability of both intermediate scrap and final product. Since both polymers are derivatives of PET, the starting material can, in principle, be derived from the established PET recycle stream. The availability of a lightweight thermoplastic composite will also promote the use of energy efficient transport.

Thermoplastic composites have been investigated for several transport applications, but attention has focused on PP matrices<sup>1</sup>. However, PP is non-polar, with a  $T_g$  of ~0°C, which limits interlaminar properties: a problem for structural applications.

---

## ICMAC - International Conference for Manufacturing of Advanced Composites

PET-based thermoplastic polyesters offer one solution to this problem. Commingled precursor, *Comfil*, was manufactured by Trevira Neckelmann as woven twill fabric. PET homopolymer gives tough laminates with a semi-crystalline matrix<sup>5</sup>, but requires processing at 280°C. Because of the thermal limitations of bagging materials and other system components, a PET copolymer processable at 210-230°C was also employed. This was amorphous ( $T_g = 60^\circ\text{C}$ ) and similar mechanically to thermosetting polyester, but tougher.

The construction of a typical bagged part is shown in Figure 2. One component investigated in the study was a large, highly loaded battery tray. Figure 3 shows the ACG composite tooling for this part, along with a bagged component ready for processing.

After optimising the process the extent of impregnation, as observed by microscopy and measured through void content, was found to be excellent, void contents lower than 1% being typical. Properties of thermoplastic polyester/glass laminates compared very well with their thermosetting counterparts. The manufacture of stiffened parts, using cores and sandwich construction was also investigated, along with methods of providing inserts and attachments.

### PROCESS MODELLING

Before producing tooling for large parts, trials were carried out with a 0.5 m square composite tool, supplied by ACG, capable of operating at up to 300°C. Metal tooling was also investigated. The commingled precursor fabric was placed on the tool and covered by a breather fabric and flexible membrane, as shown in Figure 2, prior to being evacuated and placed in an air-circulating oven. Suitable membrane materials were identified and sourced, and process cycles with different temperature profiles were investigated. Figure 4 shows temperatures recorded in a process cycle.

To model the thermal profile, a finite difference model was implemented, incorporating the key components: membrane, breather, laminate and tooling. To establish thermal constants and external heat transfer coefficients, a large number of instrumented heating and cooling experiments were carried out. Thermal properties were derived by adjusting them to fit the observed response. Surprisingly it was found that most of the cycle could be fitted with reasonable accuracy using single 'average' values of the thermal constants over the temperature range. These are shown in Table 1.

**Table 1** Single point thermal properties for modelling the thermal profile during processing.

	Breather fabric	Laminate
	Airbleed 33N	<i>Comfil</i> twill weave fabric
Thermal diffusivity	$5 \times 10^{-7} \text{ m}^2 \text{ s}^{-1}$	$7.5 \times 10^{-8} \text{ m}^2 \text{ s}^{-1}$
Thermal conductivity	$0.1 \text{ Wm}^{-1} \text{ k}^{-1}$	$0.3 \text{ Wm}^{-1} \text{ k}^{-1}$
Specific heat	$800 \text{ Jkg}^{-1} \text{ k}^{-1}$	$2,200 \text{ Jkg}^{-1} \text{ k}^{-1}$
Density	$250 \text{ kgm}^{-3}$	$1,820 \text{ kgm}^{-3}$

To investigate the consolidation behaviour of the prepreg it had originally been intended to use constant velocity isothermal squeeze flow. However, this technique proved unsuitable

ICMAC - International Conference for Manufacturing of Advanced Composites

because the pressures encountered in vacuum moulding, being just under 1 bar, are much lower than those normally imposed in squeeze flow. After some experimentation with different test methods, including constant pressure squeeze flow, it was decided to measure consolidation *in situ* during the process cycle. This was achieved by using an LVDT transducer, as in Figure 5, to measure the through-thickness contraction that takes place on consolidation. The LVDT itself was located outside the processing oven. This method found to be accurate and reproducible.

By applying the thermal and impregnation models simultaneously, it was possible to simulate the non-isothermal consolidation process quite accurately. Figures 6 and 7 show examples of process cycles in which both temperature and consolidation were measured simultaneously. Figure 6 was a 'typical' cycle. Figure 7 was a 'prolonged' cycle, in which the temperature was raised more slowly by making periodic adjustments to the set temperature. Cycles of different length were used to test the ability of both the thermal and consolidation models to describe events occurring over different timescales.

Figures 6 and 7 show that consolidation takes place in two stages. The first stage occurs near the polymer T<sub>g</sub> and probably involves solid-state stress relaxation along with softening of the polymer fibres, accompanied by local deformation, but no bulk flow. This preliminary debulking accounts for 78% of the total compaction. The second stage, which occurs over a significantly higher temperature range, is in keeping with melt impregnation and wetting. Both compaction stages are thermally initiated.

The processes, referred to as Processes A and B respectively, are sufficiently far apart in temperature to be modelled separately. In considering the type of model to be applied, some consideration was given of previous models for melt impregnation<sup>2-4</sup>. In the most general case it can be expected that the impregnation rate in a thermally activated process is given by

$$\frac{dX}{dt} = F(X)e^{\left(\frac{-B}{T}\right)} \quad [1]$$

The impregnation rate,  $dX/dt$  is influenced by two factors: the temperature (through the Arrhenius term) and the level of impregnation. It was possible to produce a master curve giving the form of  $F(X)$  vs.  $X$  by choosing an appropriate value of the parameter,  $B$ , (related to the activation energy), since

$$F(X) = \frac{dX}{dt} e^{\left(\frac{B}{T}\right)} \quad [2]$$

Good master curves were obtained for both processes (with different values of  $B$ ) and it was found that  $dX/dt$  decreased as  $X$  increased. It was necessary, therefore, to consider laws that reflected this. Taking into account models based on Darcy's Law<sup>2-4</sup> for instance, it might be expected that the compaction rate would be inversely proportional to the degree of impregnation, because of the increasing resistance as impregnation proceeds. However, this

model did not fit the results- it was found that the compaction rate actually declined much more rapidly than the Darcy Law prediction as each of the two phases reached completion. It was therefore decided to look at an empirical model that would simulate this rapid decline. One such empirical law, often used in the modelling of thermoset cure reactions, is the Kamal equation. This law has not, to our knowledge, been used in the modelling of a purely physical process such as impregnation, but there is no reason why this should not be done. A reduced form of the Kamal equation, shown below, contains four constants.

$$\frac{dX}{dt} = Ae^{\left(\frac{-B}{T}\right)} X^n (1 - X)^m \quad [3]$$

An additional constant rate term is often added, since Equation [3] presents modelling difficulties because  $dX/dt = 0$  when  $X = 0$ , but this is not needed here. The  $n = -1$  case corresponds to Darcy's Law. The term in  $(1 - X)$  describes empirically, the final decline in impregnation rate. In the present problem, it is not necessary to consider the  $X$ -dependence of the early part of the impregnation process, so the first term can be taken as unity ( $n = 0$ ). The two impregnation phases can be described well by:

$$\frac{dX_A}{dt} = A_A e^{\left(\frac{-B_A}{T}\right)} (1 - X_A)^{m_A} \quad \text{and} \quad \frac{dX_B}{dt} = A_B e^{\left(\frac{-B_B}{T}\right)} (1 - X_B)^{m_B} \quad [4]$$

In addition to the six constants needed to describe the two rate equations, a seventh is needed to represent the respective size of the contributions from the two processes, so

$$X = fX_A + (1 - f)X_B \quad [5]$$

The continuous lines describing the impregnation level in Figures 6 and 7 were calculated by numerically integrating these equations, using the constants given in Table 2, starting from the point, ( $t = 0, X = 0$ ). There is a minor problem, since  $X_A$  and  $X_B$  appear on the RHS in equations [4]. For data equally-spaced in time, this can be remedied by trial and error, with an initial quadratic estimate of future values of  $X$ , using the finite difference relationship:

$$X_{i+1} = 3X_i - 3X_{i-1} + X_{i-2} \quad [6]$$

**Table 2** Constants used to fit the consolidation behaviour, shown in Figures 6 and 7.

$f = 0.78$	$A_A$ and $A_B$	$B_A$ and $B_B$	$m_A$ and $m_B$
<b>Process A</b>	$10^{27}$	22,500	4
<b>Process B</b>	$3.2 \times 10^{31}$	33,000	2.3

## CONCLUSIONS

This project has demonstrated that it is possible to fabricate large structural components from polyester-based thermoplastic composites using the relatively simple process of vacuum bag moulding. This process carries with it a relatively low capital cost penalty, enabling it to be utilised for short production runs of large components. Applicability of the process extends beyond the lightweight bus sector into general transport, notably rail and small craft.

The ability to simulate the process by a combination of thermal and consolidation models has proved extremely useful in optimising the processing conditions for large parts. *In situ* consolidation measurements were invaluable in process characterisation and monitoring.

## ACKNOWLEDGEMENT

This project formed part of a collaboration between PERA and an industrial consortium, under the Foresight Vehicle LINK and the Structural Materials Programmes. The consortium members were PPG Industries, Trevira Neckelmann A/S, Robert Wright and Son, Advanced Composites Group (ACG) and Hil Technologies.

## REFERENCES

1. A G Gibson, 'Processing and properties of polypropylene composites', *Progress in Rubber and Plastics Technology*, 13, 2, 1997 pp125-137.
2. A G Gibson and J-A E Manson, 'Impregnation technology for thermoplastic matrix composites', *Composites Manufacturing*, 3, 4, 1992.
3. A Miller and A G Gibson, 'Impregnation techniques for thermoplastic matrix composites', *Polymers and Polymer Composites*, 4, 7, 459 1996.
4. A G Gibson, 'Continuous moulding of thermoplastic composites', Chapter 2.29 of *Comprehensive Composite Materials*, eds. A Kelly and C Zweben, Elsevier, London, 2000, pp 979-997.
5. G A Antonsen, 'The Hiform process technology for marine applications', Paper No 10, *Conference on Offshore and marine Composites*, University of Newcastle, 5-6 April, 2000.



Figure 1 Electrically propelled bus, the subject of the case study (Courtesy of Robert Wright and Son, Belfast).

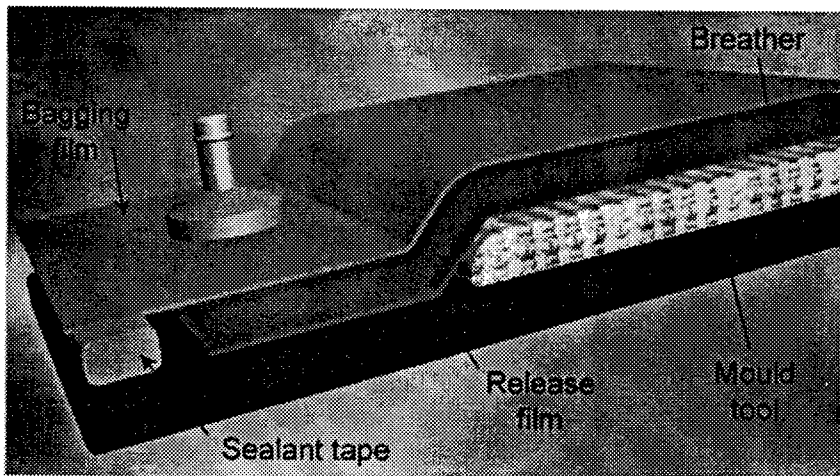
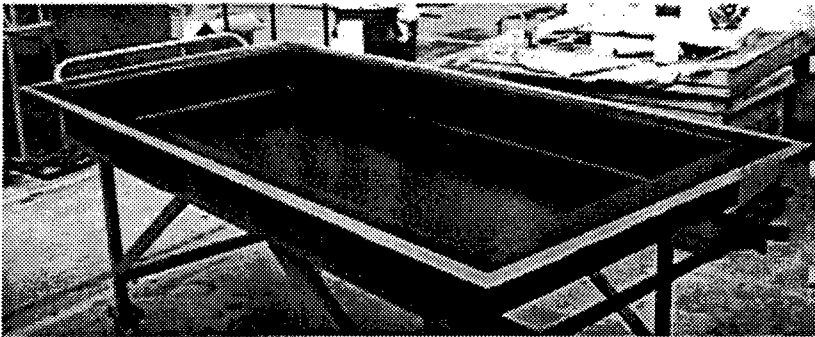


Figure 2 Schematic showing bagging components prior to processing.



**Figure 3** Composite cyanate ester tooling for battery tray, supplied by ACG, and bagged component prior to processing.

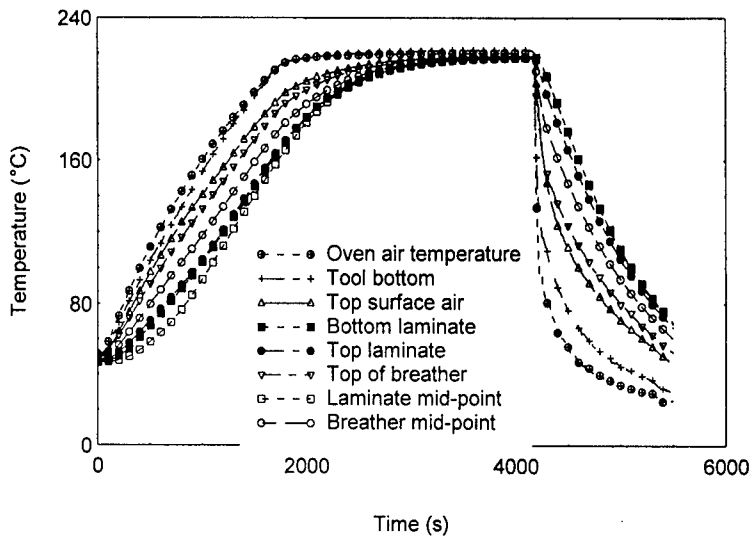


Figure 4 Thermocouple outputs during a *Comfil* processing cycle.

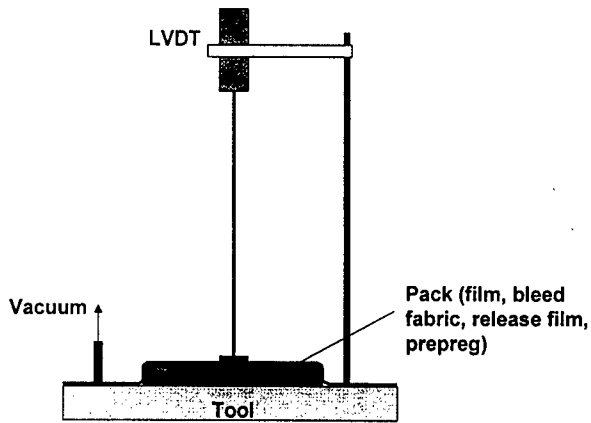


Figure 5 LVDT probe for measuring consolidation during processing.

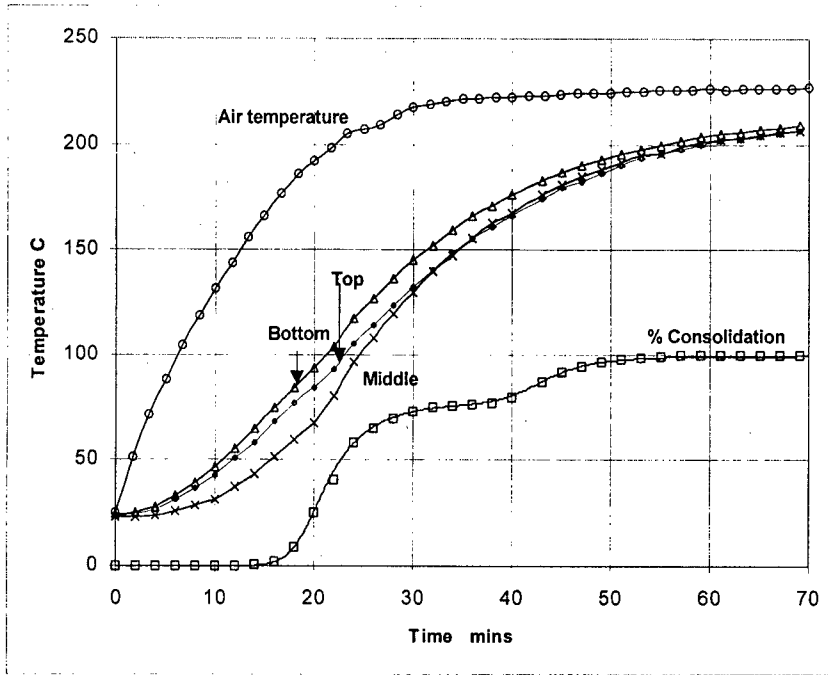
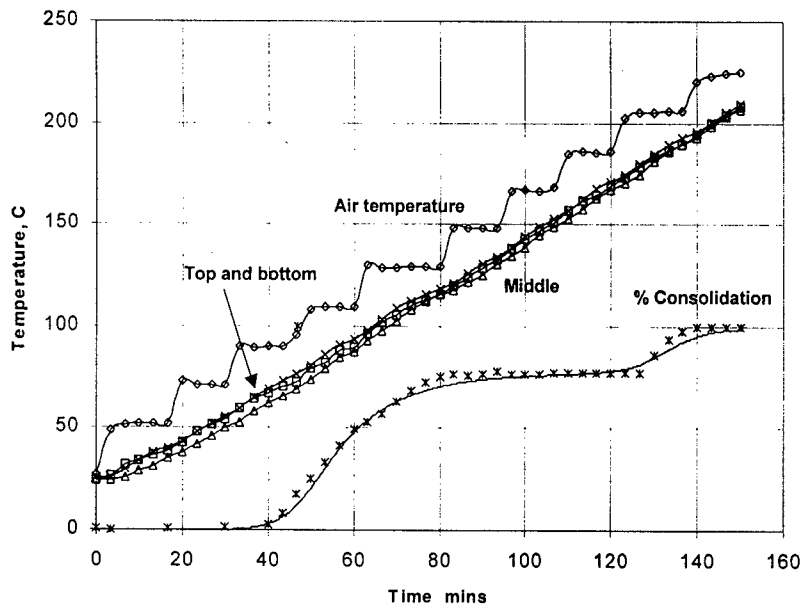


Figure 6 *Comfil* processing cycle, showing temperature in the oven air and in the top, middle and bottom of the moulding pack. Percentage consolidation is also shown: open symbols are experimental data; continuous line is consolidation model, using the parameters in Table 2.



**Figure 7** Comfil processing cycle, with slow heating rate achieved by periodically adjusting the controller set-point. Figure shows the temperature in the oven air and in the top, middle and bottom of the moulding pack. Percentage consolidation is also shown: open symbols are experimental data; continuous line is consolidation model, using the parameters in Table 2.

**INDUCTION-BASED PROCESSING OF THERMOPLASTIC CARBON FIBER LAMINATES – A NUMERICAL STUDY OF HEAT GENERATION OF AS4/PEI PREPREG STACKS**

Hee June Kim\*, Shridhar Yarlagadda\*, John W. Gillespie, Jr.\*\*,  
Nicholas B. Shevchenko† and Bruce K. Fink†

**ABSTRACT**

A numerical model is proposed to predict heat generation patterns during induction processing of carbon fiber reinforced thermoplastics. The model is based on a unified approach that considers three possible heating mechanisms: fiber heating, dielectric loss junction heating, and fiber junction contact heating. A lumped mass approach is used to construct a numerical representation for cross-ply and angle-ply orientations. Heat generation patterns are calculated based on the voltage and current conservation laws. The numerical model is verified with experimental results for induction heating of AS4/polyetherimide (PEI) prepreg stacks under vacuum pressure. Parametric studies are performed to assess relationships between process parameters and heating patterns. The results show that the coil shape, stacking angle between prepreg layers and fiber architecture strongly influence heating patterns.

**INTRODUCTION**

The search for cost-effective manufacturing has led to the study of induction heating for processing of carbon fiber-reinforced thermoplastics. Induction enables rapid volumetric heating of the thermoplastic prepreg stack leading to multi-layer consolidation; resulting in a reduction in cycle times, while maintaining quality, compared to conventional compression molding processes particularly for thick-section composites. Heat generation in conductive fiber reinforced composites, during induction processing, occurs due to induced eddy currents flowing along global conductive loops in the composite, as shown in Figure 1. In each conductive loop, heating occurs wherever there is a voltage drop due to electrical resistance or impedance [1]. The resultant heating is "volumetric" in nature, as it is an internal heat generation mechanism dependent on intrinsic properties of the composite. Initial efforts on the induction heating of composites examined the possibility of induction based fusion bonding using nickel coated graphite prepreg or amorphous film between the composites [2-6]. Border *et al.* obtained good lap shear strength through the volumetric induction heating of carbon fiber reinforced composites, without additional susceptors at the bondline [7].

Miller *et al.* [8-10] examined induction heating of pre-consolidated carbon fiber reinforced thermoplastics for applications such as die-less forming. They also developed theoretical heating models, based on the assumption that good electrical contact is required between crossed plies and Joule heating in the fibers is the primary heat generation mechanism. They focused on the heating behavior of pre-consolidated woven fabric based laminates, for welding and forming applications. An alternative heating mechanism was proposed by Fink *et al.*, [11-14] who observed that in laminates in which the fibers in adjacent plies do not come into direct electrical contact, before or during consolidation, heat generation is caused by dielectric losses in the polymer at the junctions of overlapping fibers from adjacent plies. They developed

\* Center for Composite Materials, University of Delaware, Newark, DE 19716

\*\* Materials Science & Engineering and Civil & Environmental Engineering,  
University of Delaware, Newark, DE 19716

† US Army Research Laboratory, Aberdeen Proving Ground, MD 21005

theoretical models for unconsolidated laminates, based on assumption of dielectric heating dominance and extensively tested AS4 carbon fiber polyetheretherketone-based APC2 consolidated and unconsolidated laminates for varying stacking sequences and coil geometries.

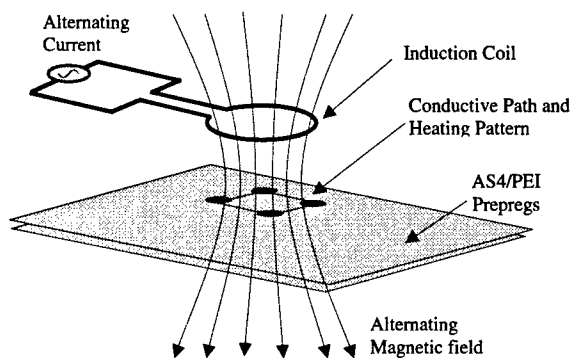


Figure 1. Schematic of the induction heating process.

Recent work on a Rapid Automated Induction Lamination (RAIL) process [15-17] to fabricate high-quality carbon fiber based thermoplastic laminates at high throughputs, has identified a third possible mechanism of heating. The RAIL process uses induction to heat 8-ply prepreg stacks up to process temperature and contact resistance [16, 17] at overlapping fiber junctions between adjacent plies, was found to play a significant role in the heat generation. A unified model was developed [18] that combined all three heating mechanisms and presented a design map that could be used to determine the expected dominant heating mechanism, given the characteristics of the composite and the process parameters. It was shown that prepreg-based systems typically show junction (contact resistance) dominated heating, while woven fabric-based systems can show fiber dominated heating. This study implements the unified model to predict heating response of unconsolidated AS4/PEI prepreg stacks as a function of process parameters and coil and material geometry. A lumped mass-based theoretical model has been developed to predict in-plane heat generation patterns and compared to experimental results. The focus is on two-ply prepreg stacks with varying angles and the ability of the model to correctly predict heating patterns.

## BACKGROUND

If two prepreg plies are oriented with a non-zero stack angle, a global conductive loop is induced in the presence of the alternating magnetic field and the loop is typically [16] a rectangle (cross-ply) or a parallelogram (angle-ply). In the global loop, there are two heating regions: fibers and junctions (where fibers from adjacent plies overlap) as shown in Figure 2. Fibers can generate heat due to their intrinsic resistance and junctions can generate heat due to dielectric hysteresis if the fibers are separated by a small gap of dielectric matrix, or contact resistance heating if the fibers are in direct contact [18]. It has already been shown [18] that the expected dominant heating mechanism for carbon fiber-based prepreg stacks under vacuum pressure, is contact resistance heating. Experiments proving this result have been documented in the literature [16,17], where rectangular or parallelogram-shaped heating patterns with dominant heating at the junctions have been observed. The key parameter is the value of the

contact resistance for the chosen prepreg system (AS4/PEI). In general, contact resistance may depend on pressure between two prepreg plies, temperature and surface quality of prepreg. A procedure to estimate the single fiber contact resistance between carbon fibers at the prepreg interface has been previously documented [18]. Estimates of junction contact resistance at the interface of AS4/PEI prepreg range from  $10^6$  to  $10^7$  ohm, depending on the surface quality of the prepreg. The following section describes the numerical model that is used to predict heat generation patterns in the prepreg stack.

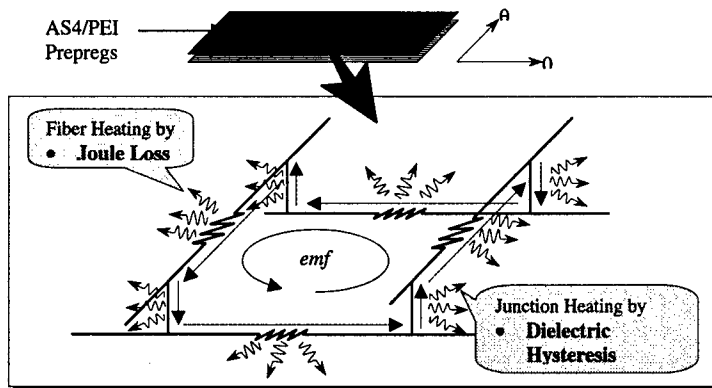


Figure 2. Schematic of fiber heating and junction heating for cross-ply or angle-ply stacking sequence.

**MODEL**

The objective of the numerical model is to predict in-plane heat generation pattern during the induction heating of two unconsolidated AS4/PEI prepregs that have non-zero stack angle, taking into account the three possible heating mechanisms. The fiber volume fraction of AS4/PEI (Cytac Fiberite) was 60% and the electrical resistivity of carbon fiber was  $1530 \mu\Omega\text{-cm}$  at room temperature.

**Numerical Mesh: Lumped System.** For a prepreg with a given fiber volume fraction ( $v_f$ ), the number of fibers in unit length ( $S_f$ ) is given by the following equation.

$$S_f = \frac{2}{d_f} \sqrt{\frac{v_f}{\pi}} \tag{1}$$

There are approximately  $10^5$  fibers/m in an AS4/PEI prepreg sheet, and approximately  $10^{10}$  fiber junctions at the interface of two prepreg plies. It is not possible to develop a numerical model considering each fiber/junction as an entity in the model. Hence, a lumped approach is proposed, as shown in Figure 4. The mesh segments represent lumped fibers and the corners of the mesh represent lumped junctions and higher density meshes are more representative of the system.

**Fiber Resistance and Junction Resistance.** Assuming a regular square meshing scheme for cross-ply and a parallelogram scheme for angle-ply and uniform contact between the two

prepreg plies (same contact resistance over the entire domain), the fiber resistance in the X (or zero direction) is,

$$R_x = \rho_f \frac{dx}{A_f} \left/ \left( dy \cdot t_p \cdot S_f^2 \right) = \frac{\rho_f}{v_f t_p} \left( \frac{dx}{dy} \right). \quad (2-a)$$

The lumped fibers in the zero direction are treated as parallel resistors, and hence the form of the expression above. For a [0/θ] system, the fiber resistance along the θ direction (or s direction) is,

$$R_s = \rho_f \frac{ds}{A_f} \left/ \left( dx \cdot t_p \cdot S_f^2 \right) = \frac{\rho_f}{v_f t_p} \left( \frac{dy}{dx \sin \theta} \right). \quad (2-b)$$

Note that fiber resistance is independent on the mesh size. An interesting feature of Eqn. (2-b) is the low angle case, where the fiber resistance increases exponentially for very small fiber angles. This also results in a highly skewed mesh, which may affect the accuracy of the model at very low angles ( $\sin \theta \sim 0$ ). The lumped junction resistance is,

$$R_j = \frac{\lambda}{dx \cdot dy \cdot S_f^2} = \frac{\pi d_f^2}{4 v_f} \left( \frac{N_x}{l_x} \cdot \frac{N_y}{l_y} \right) \cdot \lambda, \quad (3)$$

where,  $\lambda$  is the junction contact resistance between two single fibers. Note that junction resistance depends on the mesh size and single fiber contact resistance.

**Volume Ratio of Fiber and Junction in the Numerical Mesh.** For the 2-ply system in consideration, assuming a prepreg length of  $l$ , prepreg thickness  $t_p$  ( $\sim 127 \mu\text{m}$  for AS4/PEI) and fiber diameter  $d_f$  ( $8 \mu\text{m}$ ), the fiber to junction volume ratio is,

$$V_f = v_f V_o = l^2 (2 t_p) v_f, \quad (4)$$

$$V_j = (l^2 S_f^2) \left[ 2 \times \left( \frac{\pi d_f^2}{4} \right) d_f \right] = l^2 (2 d_f) v_f, \quad (5)$$

$$\text{and } \frac{V_f}{V_j} = \frac{t_p}{d_f} = 15.9 \text{ (AS4/PEI)}. \quad (6)$$

Equations (4) and (5) assume that the entire thickness of the prepreg is involved in the formation of the global current loop. This may not always be true, as current loops tend to take the shortest path and this will involve the fiber layer closest to the interface and not all the fibers in the prepreg thickness direction. However, heating occurs in the entire thickness of the prepreg and the volume calculation is based on the effective heating volume at the junction and fibers.

**Magnetic Field and Induced Electromotive Force.** The applied magnetic field is calculated from the coil geometry and coil current, using Biot-Savart's law for current carrying conductors, as shown in Eqn. (7). Due to the coil geometry, this is usually a numerical integral resulting in a discretized three-dimensional magnetic field domain. The normal component of the magnetic field in the plane of the 2-ply discretized mesh (Figure 4) is calculated and used to calculate the induced emf in the prepreg system, as shown in Eqn. (8).

$$\vec{B} = \frac{\mu_0 I_c}{4\pi} \int \frac{\vec{r} \times d\vec{s}}{r^3}. \quad (7)$$

$$\text{emf} = \omega A_{\text{loop}} B_z. \quad (8)$$

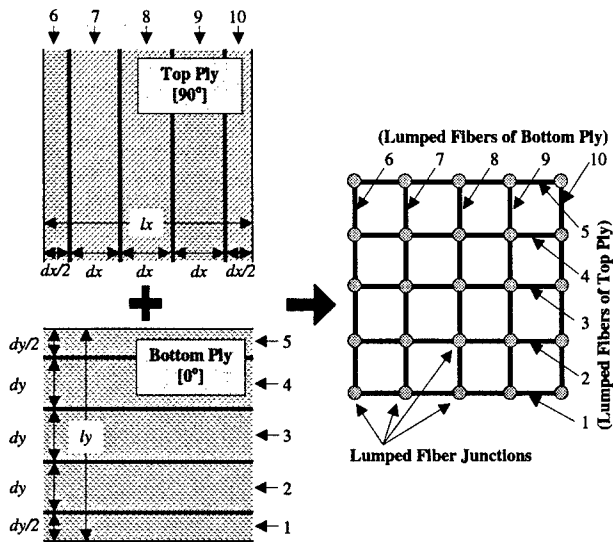


Figure 3. Lumped mesh scheme for fibers and junctions of [0/90°] prepreg plies.

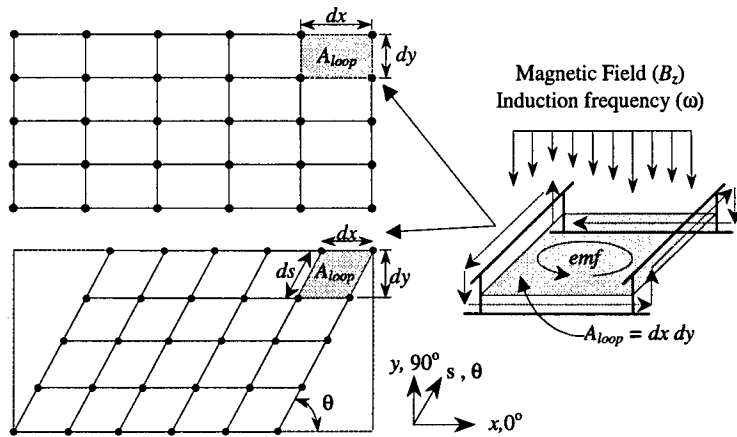


Figure 4. Numerical mesh scheme for cross-ply and angle-ply prepreg stacks.

The lumped mesh system is approximated numerically as a network of resistors with the induced emf calculated from the applied magnetic field. Kirchhoff's voltage and current conservation laws are applied for each conductive loop in the numerical mesh resulting in a linear set of equations in terms of current (or voltage) for each segment and junction in the numerical mesh. A sparse matrix solver is used to calculate the currents in the lumped fiber and junctions, and the heat generated is calculated from the fiber and junction resistances in

Equations (2) and (3). Figure 5 shows the numerical program scheme in the form of a flowchart.

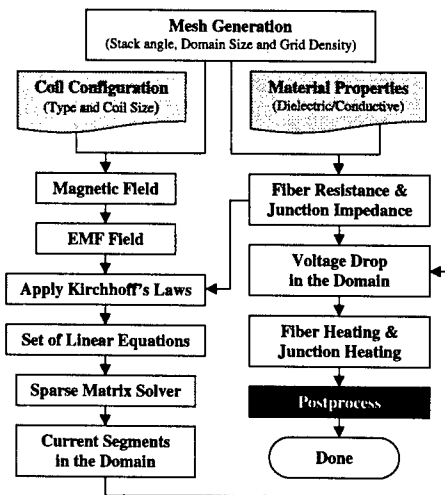


Figure 5. Flow chart of numerical model to predict heat generation.

## RESULTS

Induction heating of the 2-ply prepreg system is characterized by the material properties of fiber and matrix material as well as processing conditions. Parametric studies were performed for the various process variables to determine relationships with heating behavior. Initial studies focused on the numerical convergence and experimental verification of the proposed lumped mesh model. The process parameters for the model are listed in Table 1.

Table 1. Process Parameters and Material Properties

Input Parameter	Value
Coil Frequency ( $f$ )	2.38 MHz
Inner/Outer Diameter of Coil	6.35 cm (2.5 in), 2.54 cm (1.0 in)
Coil Current (A)	1.0
Coil-part Distance	2.54 cm (1.0 in)
Number of Turns ( $N$ )	3
Fiber Diameter of AS-4 ( $d_f$ )	8 $\mu\text{m}$
Fiber Resistivity of AS-4 ( $\rho_f$ )	0.00153 $\Omega\text{-cm}$
Thickness of AS-4/PEI Prepreg ( $t_s$ )	127 $\mu\text{m}$ (5 mil)
Prepreg Size	0.3 m $\times$ 0.3 m
Fiber Volume Fraction of Prepreg ( $v_f$ )	0.6

**Numerical Convergence.** Figure 6 shows the convergence study for two cases: a [0/90] cross-ply system and [0/30] angle-ply system. The parameter studied is the normalized total power, which represents the total heat generated by the 2-ply system, normalized by the total power at the 150 × 150 mesh case. Both cases show converged results for varying junction contact resistance values, for the process parameters shown in Table 1.

**Experimental Verification.** Induction heating tests were performed by heating two-ply prepreg stacks under vacuum pressure. The test setup was identical in configuration to that in Table 1, except for the coil current value. This does not change the heating pattern, but scales the heating rate and heat generation by the appropriate factor. Heating patterns of two cases, [0/90] and [0/45], were compared with model predictions and are shown in Figures 7 and 8, respectively. Excellent agreement is seen in the heating pattern, the location of the “hot spots” and the size of the heating zone.

**Parametric Studies**

**Coil location.** It has been extensively demonstrated in the literature that there are augmented edge heating effects in induction heating of carbon fiber-based systems when the induction coil is close to an edge [7-9, 12, 13]. This behavior is predicted by the present model, as shown in Figure 9. Moving the coil towards the edge results in increased heating at the edge of the prepreg, compared to the interior. The values of heat generation are higher at the edge by a factor of approximately five.

**Stack angle.** There has been little work in the literature on the effect of stacking angle on heating pattern, with the exception of the work of *Fink et al.* [13, 14]. The majority of the work has focused on multi-layered pre-consolidated laminates or woven fabric based laminates. Stack angle is a critical parameter, as current flows along the conductive paths in the prepreg stack and these paths are governed by the fiber direction in each ply.

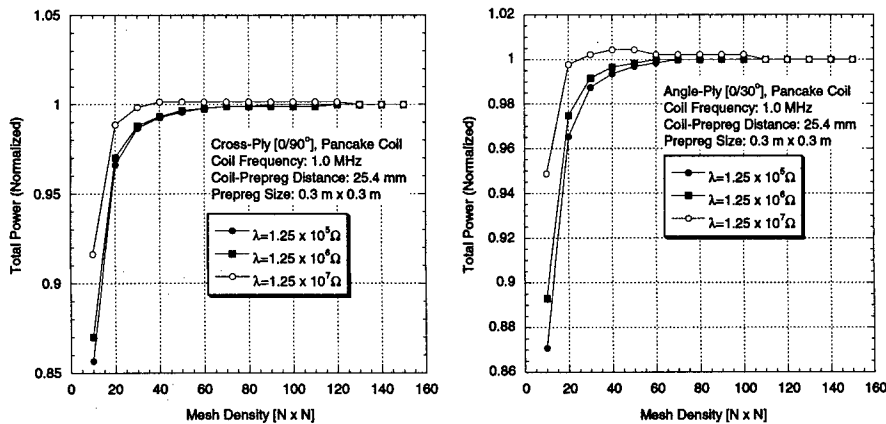


Figure 6. Numerical convergence checks with mesh size.

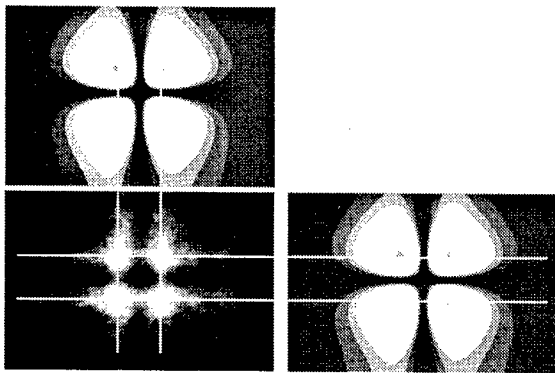


Figure 7. Comparison of model prediction and experimental result for cross-ply [0/90°].



Figure 8. Comparison of model prediction and experimental result for angle-ply [0/45°].

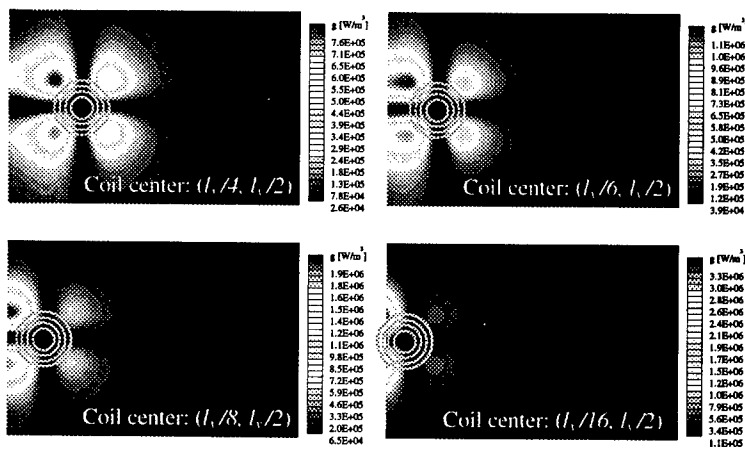


Figure 9. Change of heating pattern with coil location, showing edge heating effects.

Two-ply experiments were conducted with stack angles varying from  $[0/90]$  to  $[0/30]$  and comparisons of experimentally measured patterns and predicted patterns are shown in Figures 10a-d. Overall, the predicted heating patterns are in good agreement. However, at acute angles ( $30^\circ$  or lower), there are two issues: a skewed mesh and edge heating effects. The length of the fiber segment in the  $\theta$  direction is twice the length of the segment in the zero direction and increases further for smaller angles. Edge heating effects are more prominent, as seen in Figure 10a. In general, the expected square/parallelogram global circuit is seen, with dominant heating at the junctions, for all angles. To assess the heating behavior as a function of angle, the total power generated is plotted as a function of angle in Figure 11. The total power generated drops similar to  $(1/\sin\theta)$ , which is expected as the area change from a  $[0/90]$  to  $[0/0]$ , follows a similar trend. The ratio of the maximum heat generated between the junction and the fiber increases with decreasing angle, which may be attributed to the increasing fiber length and hence resistance, resulting in more current flow in the junctions.

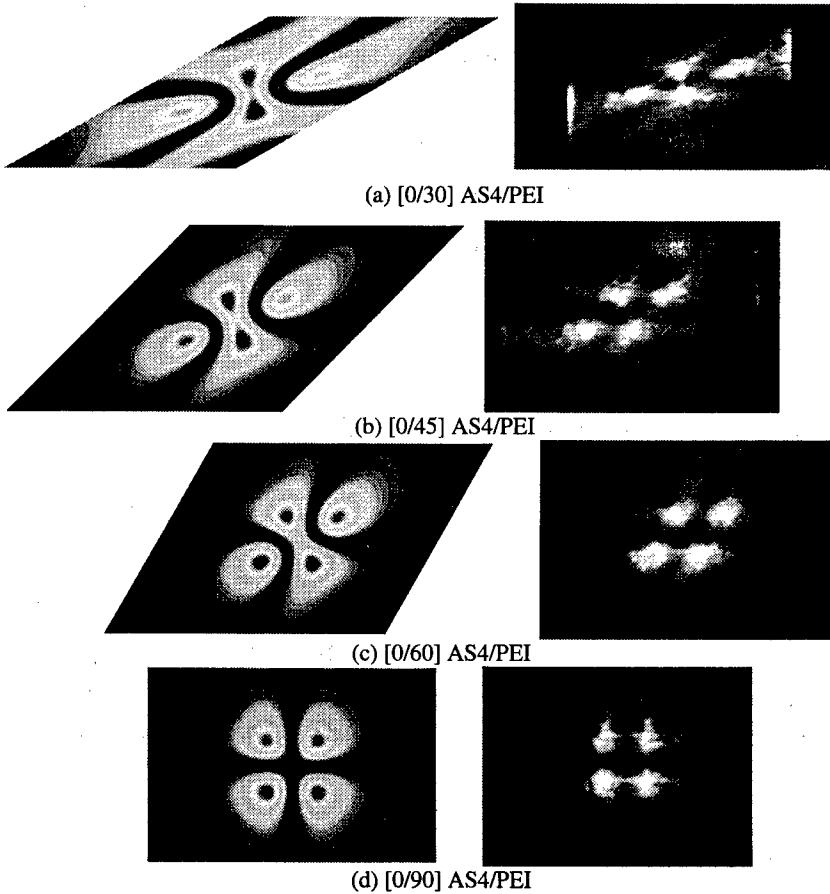


Figure 10. Predicted and measured heating pattern as a function of stack angle.

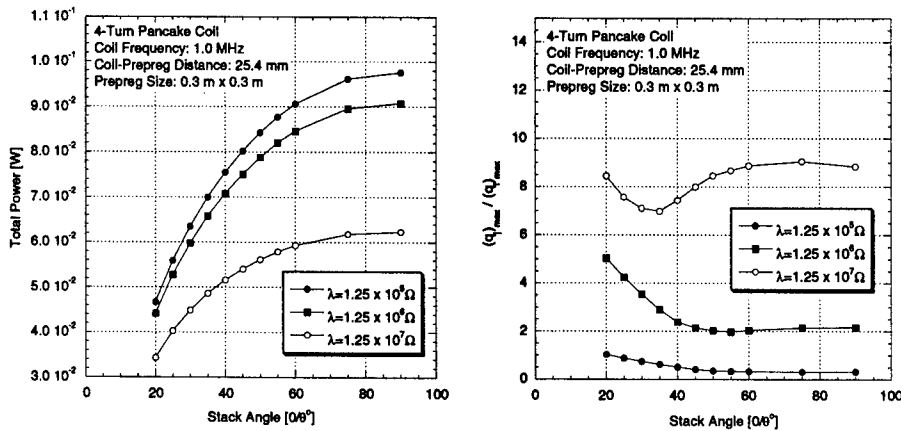


Figure 11. Heat generation as a function of stack angle.

**Prepreg Surface Quality.** Due to the junction dominated heating patterns in prepreg stacks, prepreg surface quality can significantly affect the heating pattern. Uniform contact between plies results in a more uniform contact resistance distribution over the area of the ply, and will result in more uniform heating patterns. This is clearly indicated in Figure 12, where heating patterns for two prepreg types AS4/PEEK and AS4/PEI are compared. The AS4/PEEK system had a “smoother” and more uniform surface quality, resulting a “cleaner” heating pattern. This can be critical for uniform heating during induction processing of carbon-based prepreg systems.

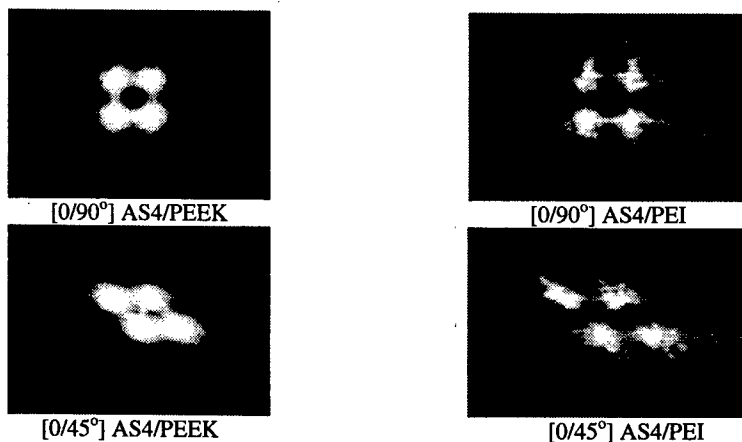


Figure 12. Heating patterns for two-ply prepreg stacks with differing surface quality

**CONCLUSIONS**

A numerical model was proposed to predict in-plane heat generation patterns during induction heating of carbon fiber reinforced thermoplastic prepregs. The predicted heating patterns

showed excellent agreement with the experimental data for 2-ply prepreg stacks ranging from cross-ply [0/90] to varying angles [0/30]. The heating pattern shifts from a square or rectangular case for cross-ply to parallelogram shape for angle-ply. Small angles tend to enhance edge heating effects and increase junction dominance due to increasing fiber lengths.

## REFERENCES

1. Zinn S, Semiatin SL, Elements of Induction Heating: Design, Control and Applications, Palo Alto, CA, Electric Power Research Institute, 1988
2. Xiao XR, Hoa SV, Street KN, "Repair of Thermoplastic Composite Structures by Fusion Bonding," 35th International SAMPE Symposium, April 2-5, 1990
3. Nagumo T, et al, "Evaluation of PEEK Matrix Composite," 32nd International SAMPE Symposium, April 6-9, 1987
4. Benatar A. and Gutowski, T. G., "Methods for Fusion Bonding Thermoplastic Composites," SAMPE Quarterly, Vol. 18, No. 1, October 1986
5. Benatar A, Gutowski TG, "A Review of Methods for Fusion Bonding Thermoplastic Composites," SAMPE Journal, January/February 1987
6. Cogswell FN, et al, "Thermoplastic Interlayer Bonding for Aromatic Polymer Composites," 34th International SAMPE Symposium, May 8-11, 1989
7. Border J, Salas R, "Induction Heated Joining of Thermoplastic Composites without Metal Susceptors," 34th International SAMPE Symposium, May 8-11, 1989
8. Miller AK, et al, "The Nature of Induction Heating in Graphite-Fiber, Polymer-Matrix Composite Materials," SAMPE Journal, Vol. 26, No. 4, July/August 1990
9. Lin W, Buneman O, Miller AK, "Induction Heating Model for Graphite Fiber/Thermoplastic Matrix Composites," SAMPE Journal, Vol. 27, No. 6, 1991
10. Lin W, Miller AK, Buneman O, "Predictive Capabilities of an Induction Heating Model for Complex-Shape Graphite Fiber/Polymer Matrix Composites," 24th International SAMPE Technical Conference, Vol. 24, 1992
11. Fink BK, McCullough RL, Gillespie JW, "A Local Theory of Heating in Cross-ply Carbon Fiber Thermoplastic Composites by Magnetic Induction," Polymer Engineering and Science, Vol. 32, No. 5, 1992
12. Fink BK, McCullough RL, Gillespie JW, "A Model to Predict the Planar Electrical Potential Distribution in Cross-ply Carbon-fiber Composites subjected to Alternating Magnetic Fields," Composite Science and Technology, Vol. 49, 1993
13. Fink BK, Gillespie JW, and McCullough RL, "Experimental Verification of Models for Induction Heating of Continuous-Carbon-Fiber Composites," Polymer Composites, Vol. 17, 1996
14. Fink BK, McCullough RL, Gillespie JW, "A Model to Predict Through-Thickness Distribution of Heat Generation in Cross-ply Carbon-fiber Composites Subjected to Alternating Magnetic Fields," Composite Science and Technology, Vol. 55, 1995
15. Yarlagadda S, et al, "Rapid Automated Induction Lamination (RAIL) for High Volume Production of Carbon Thermoplastic Laminates," Proceedings of SAMPE-ACCE-DOE-SPE Midwest Conference, September 12-14, Dearborn, MI, 2000, p. 393-402
16. Yarlagadda S, et al, "Heating Mechanisms in Induction Processing of Carbon Fiber Reinforced Thermoplastic Prepreg," Proceedings of the 45<sup>th</sup> International SAMPE Symposium, Long Beach, CA, May 2000
17. Kim HJ, et al, "A Study on the Induction Heating of Carbon Fiber Reinforced Thermoplastic Composites," 9<sup>th</sup> US-Japan Conference on Composite Materials, Japan, July, 2000
18. Yarlagadda S., et al., "A Study on the Induction Heating of Conductive Fiber Reinforced Composites," submitted to the Journal of Composite Materials, March 2001

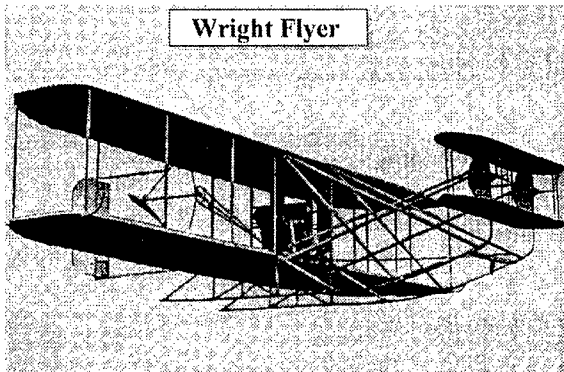
**SESSION 7:  
INDUSTRIAL APPLICATIONS  
& CASE STUDIES**

**AEROSPACE COMPOSITES COMMERCIAL POTENTIAL – A REAL OPTION**

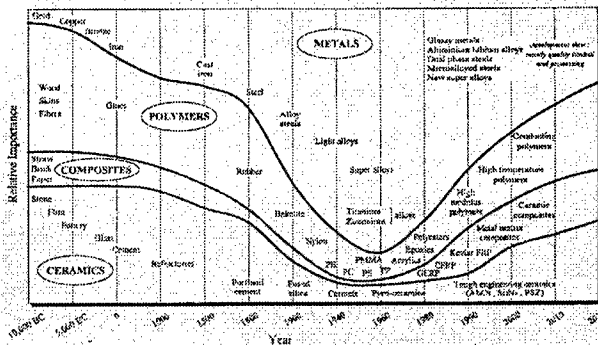
George Cather / Sam Wilson\*

**History of Composites**

As can be seen from the aircraft below (1909) Composites are not new to Aerospace.



**Evolution of Engineering Materials**



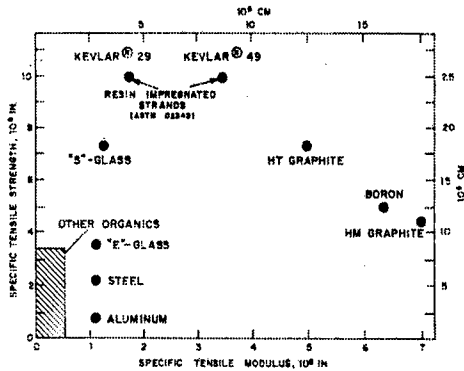
Glass fibres the fore runner to today's composites have been recorded as being used in the Egyptian (VXIII) dynasty which was around 1500BC although real commercial use was not until the 1930's. As we can see later, despite their low modulus/strength and relatively high weight, glass fibres in-conjunction with aluminium alloy still has potential for today's Aerostructures.

\* Bombardier Aerospace Shorts

**Introduction to Advanced Composites**

The first of the 'Advanced Composites' (High modulus, high strength continuous fibres) began with Boron / Epoxy in the early 1960's. However although used in some military applications this material had major drawbacks preventing its wide spread commercial use i.e. excessive fibre production costs, bend radii no less than 25mm and diamond coated tools were needed for machining drilling and trimming.

The availability of commercial Carbon fibre in 1967 is the real starting point of today's composite technology. The first recorded use of graphite fibre was in 1879 when Thomas Eddison used them in his electric light, however it was not until 1963 in the UK when graphitising Polyacrylonitrile (PAN) was developed

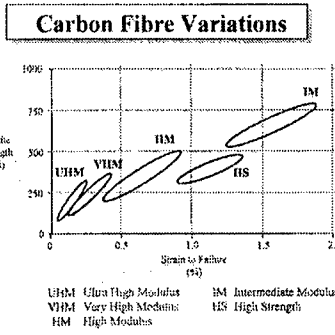
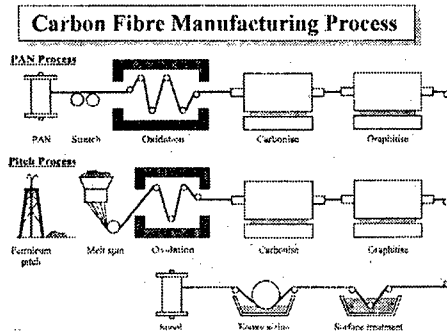


The latest of the advanced fibres Kevlar® (an aramid) was developed in 1965 by Du point and commercially available around 1970. Despite its relative low cost, excellent tensile properties and low density aramid is not favoured for today's structural components because of its low compression properties, difficulties in machining and it is hydroscopic with a very high differential between its in-plane and out-of-plane thermal expansion. As a consequence it has been reduced to niche applications such as fairings or for impact resistance.

	GLASS	CARBON	ARAMID
Tensile Strength	X	✓	✓
Tensile Modulus	X	✓	-
Compressive Strength	-	✓	X
Compression Modulus	X	✓	-
Impact Strength	-	-	✓
Interlaminar Strength	✓	✓	-
Tensile Fatigue	X	✓	-
Density	X	-	✓

**Carbon fibre**

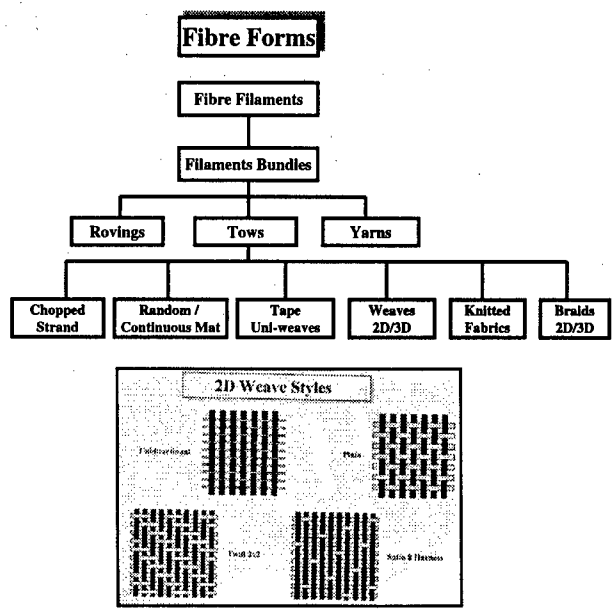
Carbon fibre can be manufactured from a pitch or polyacrylonitrile (PAN) precursor. PAN based carbon gives properties, which are ideally suited for commercial aerospace use and depending on the temperature at which it is graphitised, fibres with a range of properties can be produced.



**The Manufacture of Structural Laminates**

**Fabrics**

In order to change carbon fibre into structural laminates the fibres have to be available in various forms. Examples of these are shown below

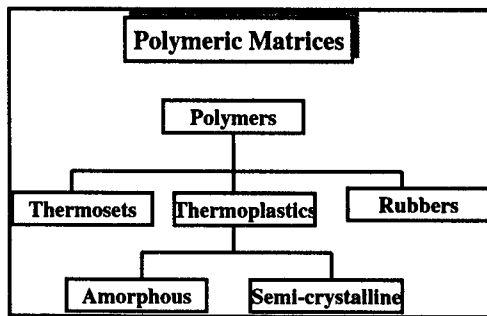


### Matrix

The next stage in the manufacturing process is to choose a suitable matrix. There are many available from which to select that appropriate to the application.

E.g. thermosets include

- Polyester
- Vinyl ester
- Epoxy
- Bismaleimide
- Cyanate ester
- Polyimide

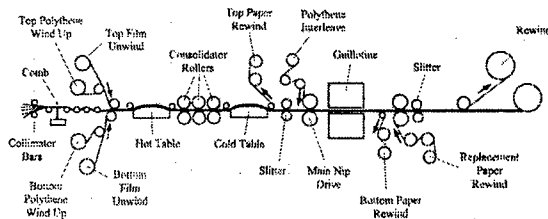


Within aerospace the overwhelming favourite is epoxy because of its generous processing window and good mechanical / physical properties. As a consequence many epoxy formulations have been developed and combined with the different fibre variations to optimise both compression after impact and hot/wet strength (discussed later)

### Prepreg Manufacture

Before manufacture of the composite the carbon fabric or aligned tows have to be pre-impregnated with a tacky semi-cured resin. There are two methods of achieving this 'Solution Treatment' (being phased out due to high use of solvents) and 'Hot Melt' shown below. The pre-impregnated fabric (Prepreg) is coated on both sides with plastic film, rolled up, sealed in a bag and stored in a freezer at -18C to prevent advancement of the cure.

#### Hot Melt Coating Impregnation



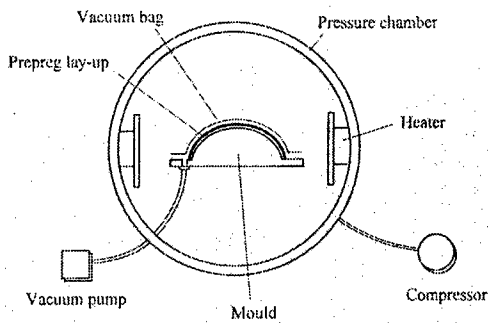
### Trim Lay-up and Bagging

The prepreg rolls are removed from the freezer, thawed, cut to size and carefully tacked together (often manually) on the mould form in a special dust free, humidity controlled room. The plies are vacuum-sealed to the mould form (Tool) using 'Expendable materials' i.e. release films, breather fabrics covered by a plastic film that is temporarily sealed to the tool periphery 'Bagging'.

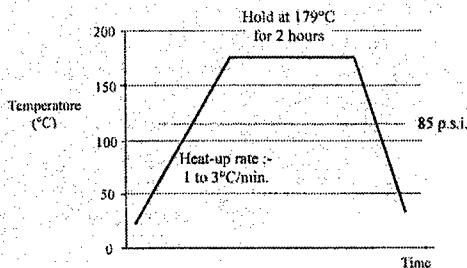
### Autoclave cure and Tool strip down

Within aerospace autoclave processing (see below) is the predominant manufacturing procedure used to produce carbon / epoxy components. This involves heating the tools/ plies in a pressure vessel (Autoclave) and using pneumatic pressure (in a nitrogen atmosphere to reduce fire risk) consolidating the composite plies against a single sided tool until the resin is cured. Typical temperatures and pressures of 6 Bar and 177 C are used (see below). The parts are then removed from the autoclave, the expendable materials removed, discarded and the parts carefully removed from the tool.

### Autoclave Moulding



### Typical Epoxy Laminate Cure Cycle



**Why Composites**

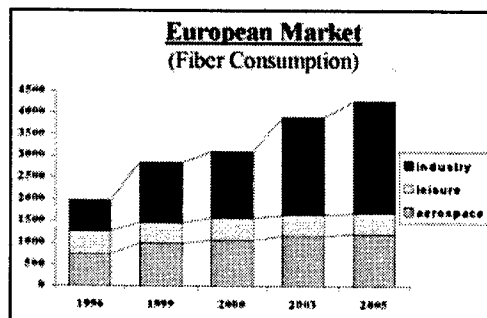
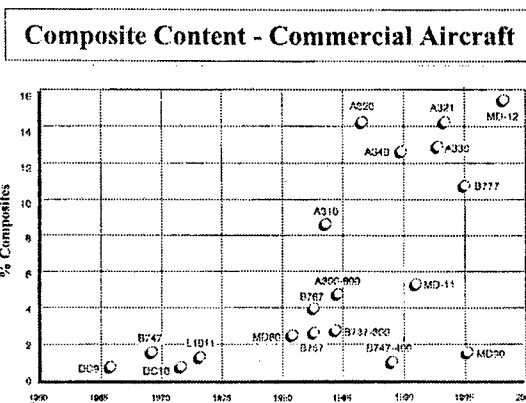
Advanced composites are used in high performance vehicles and sports goods so it is little wonder that they are used in Aerospace applications

The reasons for use are relatively straightforward, one or a combination of the following

1. To avoid the high tooling costs that would be incurred in producing metallic components with complex three dimensional curvature
2. To reduce weight from between 15-25% (due to their improved properties such as strength, stiffness)
3. Corrosion resistance
4. Fatigue resistance
5. Obtain smooth aerodynamic profile

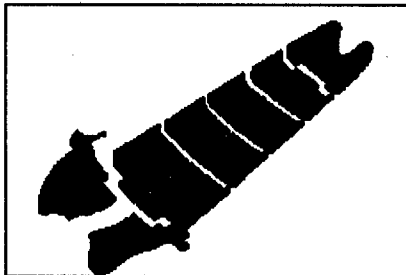
Within Aerospace composite applications have been increasing with time, however unless their cost can be reduced their usage is not predicted to increase significantly (unlike the Industrial & Leisure sectors).

Indeed the drive on first cost in aerospace has been so great there have been more recent examples where current composite structures have been redesigned and certified in lower cost metal (accepting the weigh penalty).



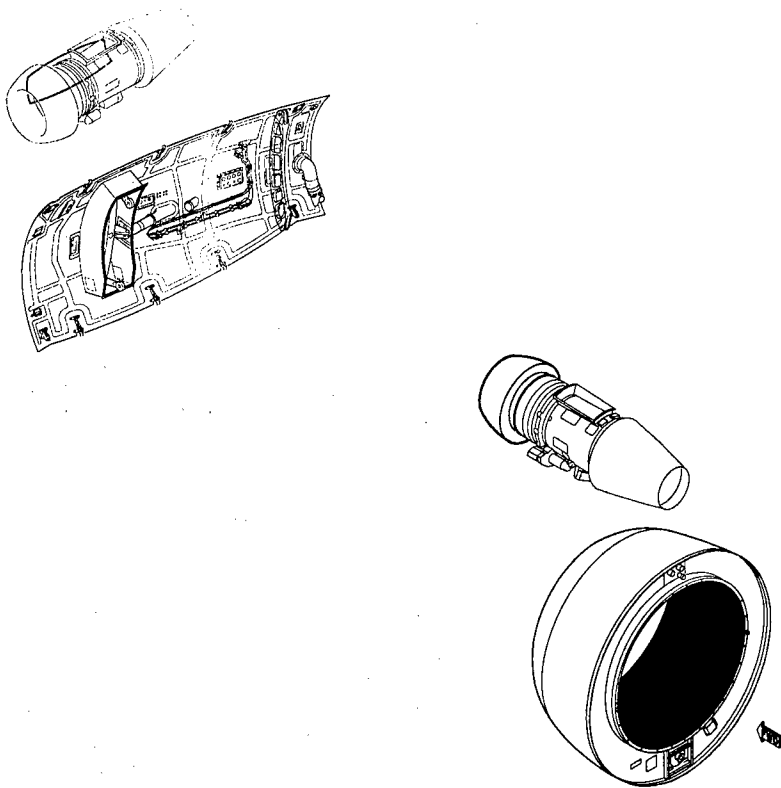
**Typical applications are shown below**

1) 'Wing to Fuselage Fairing' (and other smaller fairings, strakes etc) are a few of the current applications where potentially both cost (because of their complex 3D profile) and weight benefits can be obtained



Example  
Global Express wing  
to fuselage Fairing

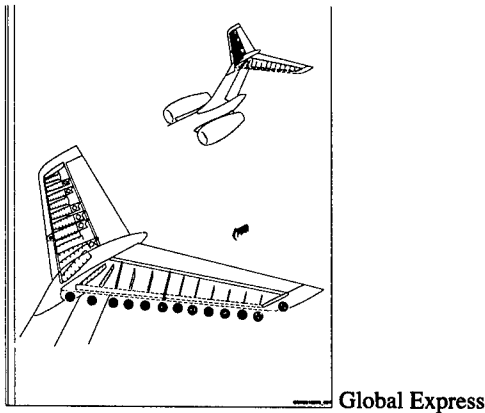
Another ideal application is Nacelle Structures where lightweight, stiff, aerodynamically smooth structures are produced in composite



**Primary structures**

Primary structures are another good example where composites can offer weight saving and fatigue resistance benefits. However because of the high cost of these applications they are only considered where the weight saving will offer the most benefit for example in the tail section of Aircraft (especially on longer-range aircraft).

The example shown is the Bombardier Global Express Horizontal stabiliser manufactured in Intermediate modulus carbon toughened materials



Other traditional composite applications include

Applications	Principal Composite benefits	Aircraft Manufacturers
Under floor beams	Weight, stiffness, corrosion	Boeing
Flaps	Weight, stiffness, fatigue, smoothness	Boeing Airbus, Bombardier
Ailerons	Weight, stiffness, smoothness	Boeing, Airbus, Bombardier
Elevator	Weight, stiffness, smoothness	Boeing, Airbus, Bombardier
Raydomes	Special Radar properties	Boeing, Airbus, Bombardier
Rudder	Weight, stiffness, smoothness	Boeing, Airbus, Bombardier
Wing Tip fairings	Weight, stiffness, smoothness	Boeing, Airbus, Bombardier
Interior panels	Weight, good fire properties	Boeing, Airbus, Bombardier

**Drawbacks - Manufacturing Costs**

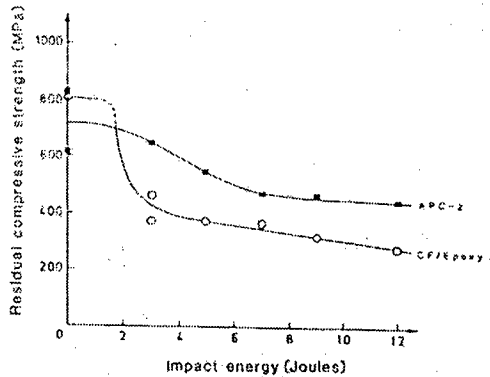
There are three principal reasons preventing the wide spread introduction of 'Composites' within commercial aerospace (of which the first is the most important)

1. Very high Cost
2. Poor damage tolerance
3. Low through thickness strength

Material suppliers attempted to address the damage tolerance and through thickness strength aspects by offering new high performance thermoplastic matrices such as Polyetheretherketone (PEEK) with the additional promise of rapid processing speeds and the ability to rework. Unfortunately this also had the effect of substantially increasing the raw

ICMAC - International Conference for Manufacturing of Advanced Composites

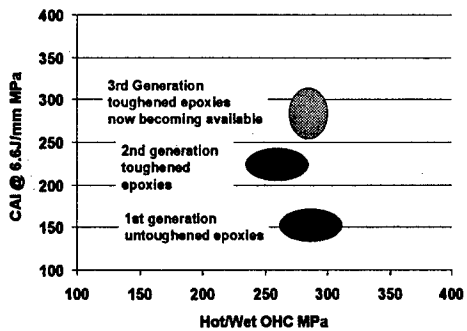
material cost making matters even worse. Also although the inter ply strength increased by an order of magnitude this only translated into a slight improvement in damage tolerance. For these reasons, and the requirement to re-order plant and equipment to process these materials the wide spread introduction of these materials never materialised.



Residual compressive strengths after impact of CF/epoxy and CF/PEEK

The suppliers again responded by toughening the thermoset matrices (with thermoplastics) in combination with improved fibres, which gave important improvements in damage tolerance, plus the existing autoclave processing infrastructure could be used. However this did not address the major cost hurdle because the raw material cost typically increased by a factor of 2. As a consequence other ways of addressing this had to be considered.

Carbon Epoxy Relative Performance



Manufacturing costs.

When composites were first introduced they were in average 2.5 times the cost of metals and while this situation has improved throughout the years because of the introduction of mechanised processes (examples below) the cost is still to high.

---

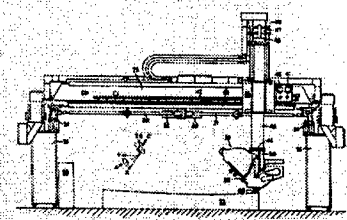
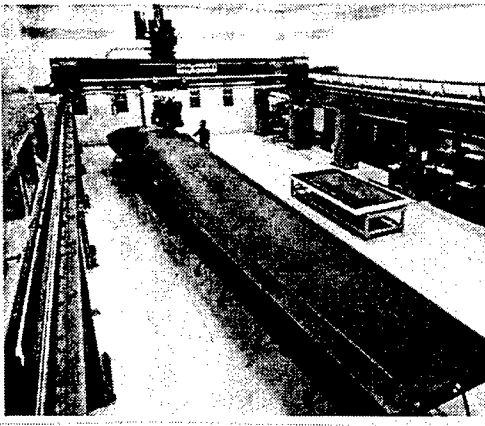
ICMAC - International Conference for Manufacturing of Advanced Composites

Improved processes: -

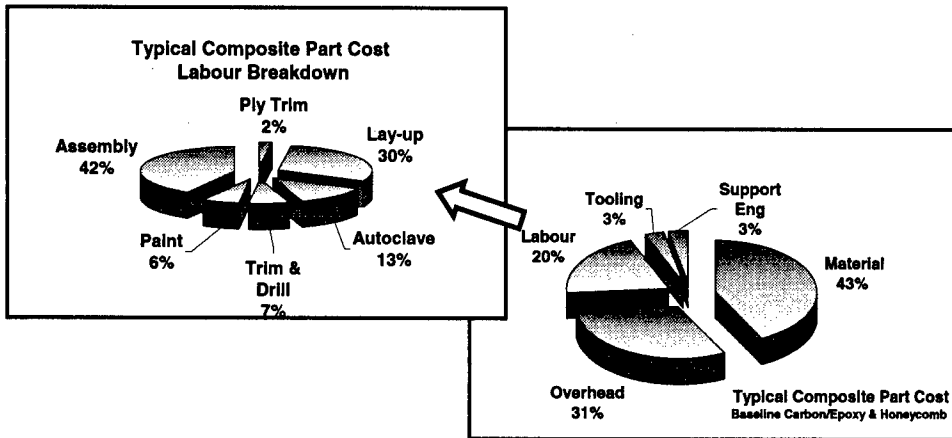
- Computerised planning & ordering
- Automated ply trim and nest
- Automated Contour Tape Laying
- Automatic diaphragm ply forming (Hot ply Debulking )
- Laser assisted ply positioning
- Multi-axis post cure trim and universal fixtures
- Water-jet trimming
- Automated Ultra-sonic Non-Destructive-Testing (NDT)
- Reusable polymeric bagging

Ply placement into the mould is highly labour intensive and in the 1980's the USA Government funded several major initiatives such as automated 'Pick &Place', 'Tape Laying', 'Dedicated Plants' with the specific aim to overcome this problem. These were largely unsuccessful i.e. except for contour tape laying which encountered many problems but after approximately 22 years the technology can now be regarded as mature. As a consequence all the major composite manufactures have purchased equipment.

**Tape Laying**



Cincinnati Milacron, Ingersoll, and more recently Torres offer tape-laying systems at a cost of between \$ 2-4 million. Lay-down speeds 10-15 m/min and up to 12 controllable axes. The average rate for the best of these machines is between 4 to 15Kg /hr (with a scrap rate between 5% to 20%) depending on the size and complexity of the structure.



**Material costs**

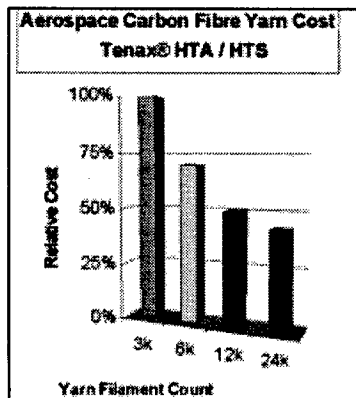
As a consequence the Industry had to review more fundamental processes, which addressed the whole manufacturing cycle, and focused on the more significant aspects such as 'Raw Material'.

The objectives were to utilise processes which could:

1. Eliminate the Pre-impregnation stage, which does not add value and is wasteful in terms of expendable materials and freezer costs
2. Utilise baseline materials and possibly impart toughness in other ways
3. Employ processes, which can use lower cost carbon.

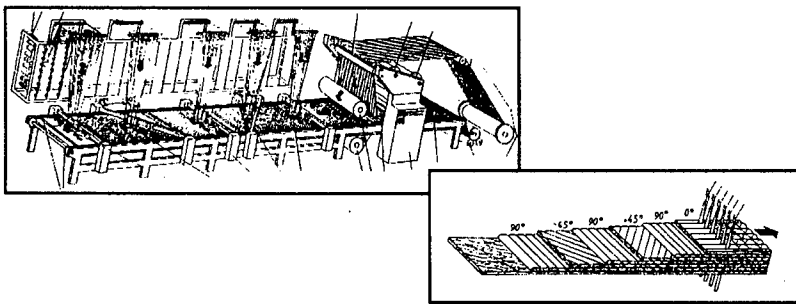
**Carbon cost**

Processes that could use larger size Tows were an obvious target because the industry standard 3K was the most costly in relative terms compared with larger tows see below.



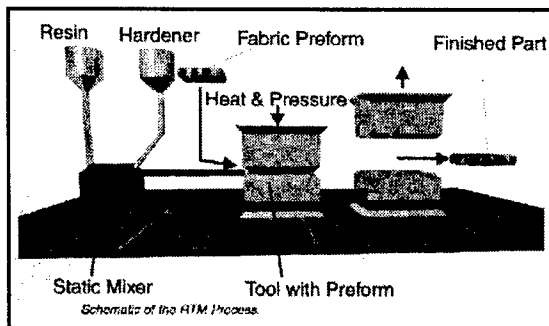
**Processes with low cost raw material potential**

1. Weaving; '2D' and uniweave fabrics of acceptable weights have been produced using 6K and 12K tows although there is small "handleability" penalty.
2. Warp Knit Non-Crimp-Fabrics: fabrics have been produced which utilise 12K and 24K tows. Also because layers with multiple orientations can be "stitched" together significant savings can be made in Lay-Up and ply trim.
3. Tow Placement; process (discussed later) has long term potential to use large prepreg tows.



**New cost effective Laminating Technologies**

**Resin Transfer Moulding**



Resin Transfer Moulding involves placing dry fibres in a closed mould at appropriate structural orientations, injecting the partially filled cavity with resin, applying heat to cure the assembly resulting in a near net finished component.

The process has been around for thirty years but it is only recently that resins have become available with good structural properties and sufficiently low viscosity/processing windows to enable the production of low void laminates with the high aerospace standard fibre volumes.

This technology combined with improved design offers significant opportunities to cut recurring cost in the following areas

ICMAC - International Conference for Manufacturing of Advanced Composites

1. Raw material costs

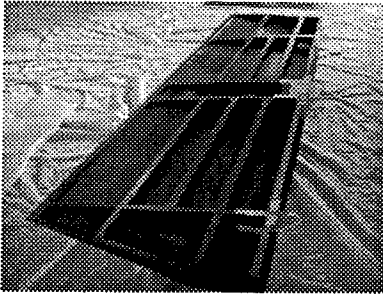
- NO prepregging stage
- NO roll refrigeration or the cost of plastic films etc.
- Fabrics with larger tows
- Removal of Honeycomb core cost (Honeycomb gives operators problems in terms of repair)

2. Simple Monolithic design of discrete elements (also offers more damage tolerance)

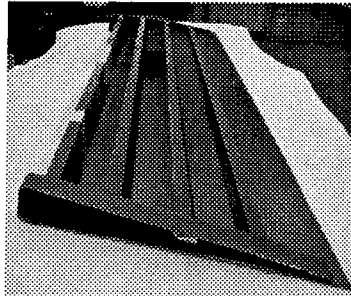
- Reduced preforming / lay-up time. Multiple layers diaphragm formed.
- Substantially reduced assembly time because the components are injected together, very accurately and net shape (no machining). Assembly tooling costs also significantly reduced.
- Reduction in mechanical fastening by integrating/bonding parts during injection
- No out life concerns

Note: The process has higher tooling costs so the larger the number of parts the more these can be amortised. Design for manufacture and Assembly can result in a compromise in weight. Design modifications can be costly. The larger the structure the greater the Non-Recurring-Cost and the higher the process risk.

RTM is ideal for control surfaces ribs, and small spars.

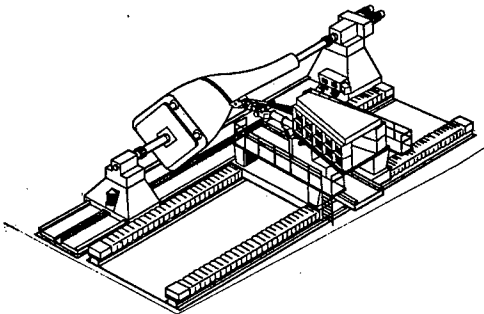


RTM Aileron optimum weight



RTM Aileron Design for  
Manufacture and Assembly

Tow Placement



#### ICMAC - International Conference for Manufacturing of Advanced Composites

Tow placement involves placement of multiple prepreg tows onto a mandrel, which can be revolved on an axis ie a cross between a tape layer and filament-winding machine.

Cincinnati Milacron (and Hercules / Alliant Techsystems) offer tow placement systems at a cost of between \$ 3-5 million offering lay-down speeds typically 6 m/min.

The technology is very impressive however also very complicated Each machine is in effect up to 32 mini tape layers cutting and placing tows beside each other, all with individual feed control.

As a consequence the "tape" does not have to follow geodesic or "natural" paths, which give the user a wide amount of design flexibility. This together with the revolving axis allows lay-up on more complex shapes such as; space structures, 'wing to fuselage fairings', nacelle structures, pressure bulkheads, empennage skins / tailcones.

The average rate for the best of these machines is between 2Kg/hr (for those which stop the head when cutting) and up to 10Kg /hr (when cutting on the fly) with an impressive scrap rate less than 5%. These rates could be much less depending on the size and complexity of the structure.

With regard to the manufacture of relatively flat " wing skin" structures tow placement has limitations in terms of working envelope, minimum course length and production rate when compared to tape layers.

Many of the existing systems have been purchased through military, space and off-load programmes obvious exception being the manufacture of the Raytheon Premier 1 Fuselage manufacture.

This is an interesting concept but it focuses in an area where there are highly competitive metallic technologies both conventional and emerging and where a new metallic composite has become available see below.

In addition the technology has been abandoned for the production of GE 90 fan blades.

Because it took Tape laying several decades to mature and coupled with the limited amount of towpreps available (with the suitable handling characteristics) it is reasonable to assume that some form of manual intervention will be required with this process for the foreseeable future. None-the-less it does appear to have recurring cost cutting potential in the areas mentioned above.

Also in the future this technology has the potential to use prepreg tows but until these can be produced from the raw fibre (with sufficient width and thickness control) unidirectional tape has to be slit which will incur a cost penalty typically in excess of 25%.

Another problem is that the technology is only aimed at automating the skin lay-up and complex integral stiffeners often have to be manually laid-up and of course lay-up is typically only 6 % of the total part cost.

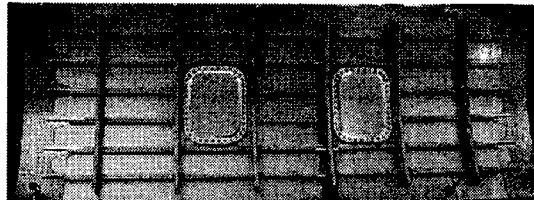
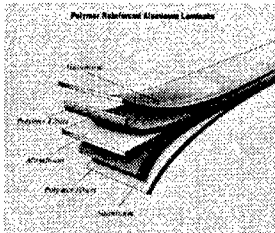
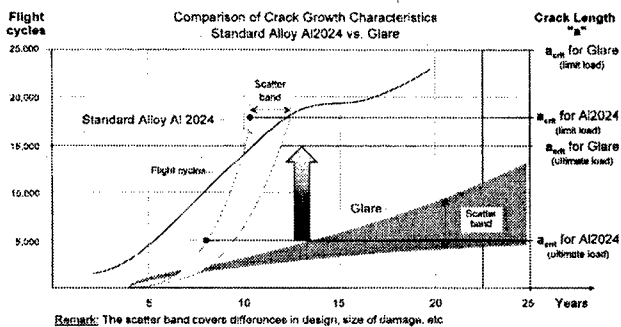
#### **Glare**

Glare<sup>®</sup> is the most important member of the family of Fibre Metal Laminates structural aerospace materials. The laminate material consists of alternating layers of thin, high strength aluminium alloy sheets and fibre impregnated adhesives.

Developed in the early 1990's, Glare<sup>®</sup> offers weight savings for a variety of aircraft applications, as well as potential cost savings in aircraft manufacturing and operation and improved safety characteristics.

## ICMAC - International Conference for Manufacturing of Advanced Composites

Testing and evaluation has increased steadily over the last 10 years to the point where AIRBUS have selected Glare as the preferred fuselage crown panel material on sections of the recently launched A380 aircraft. In future years, as further variants of the A380 enter service the volume of Glare® usage on each aircraft type will increase.



## Thermoplastics

A relatively new thermoplastic Polyphenylenesulphide (PPS) offering a substantial raw material cost reduction compared to PEEK. PPS/ carbon material in the form of flat laminated panels can be processed in a manner similar to punching and forming Alloy sheet.

Processing can very rapid, eg. Consisting of

1. Water jet cutting of the sheet to produce a blank (Shapes cut out of an optimised nest)
2. High speed infra-red heating
3. Rapid transfer to a press
4. Press formed (typically net size) in seconds

Fokker, Dornier Fairchild, Bae, Aerospatiale, Daimler Chrysler, have successfully used this process to produce simple Ribs and Boeing have used it to produce simple angles and 'S' shaped brackets.

The advantages are rapid processing and weight saving.

The main disadvantage being because the laminate is a constant thickness the applications are limited (unless combined with welding or autoclave curing)

With regard to cost the process can be competitive with thermosets but more expensive than punched / formed metallic ribs.

Welding – Component Integration

## ICMAC - International Conference for Manufacturing of Advanced Composites

Thermoplastic components can be welded together, eliminating the cost and weight of rivets which are typically \$ 0.5 / rivet. As a consequence the greater the number of rivets eliminated the greater the cost saving.

Many different types of welding are possible including Ultrasonic, Induction, Friction (vibration/spin), Thermal and Resistance (possibly the most mature, some IPR held by Fokker SP).

Welding of thermoplastic components offers the potential for cost reduction for structures, which are more complex than simple constant thickness ribs.

Airbus has applied this technology on the A340 500/600 Multi-Rib Thermoplastic J Nose leading edge but they not claimed any specific cost reduction using PPS and fibreglass reinforcement.

### Advantages Claimed by AIRBUS:

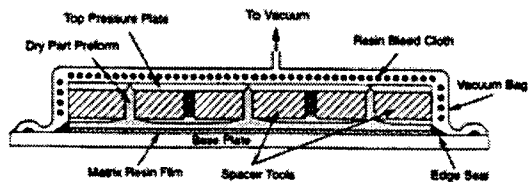
- Weight Saving (J Nose provides greater than 20% over the existing structure)
- Ease of Manufacture
- Improved damage tolerance.
- Improved Inspection
- Reduced number of parts

Note Thermoplastics have excellent Fire Smoke and Toxicity properties making them attractive for interior structures.

## Nearly Mature Emerging Technologies

### Infusion processes

The forerunner of these technologies was Resin Film Infusion (RFI) in which Boeing have patents. It involves the placement of resin in the form of a film or cast block either above and / or below a dry preform prior to the application of (1) Vacuum; (2) Heat and (3) Pressure. See figure. However, the increased 'bulk' volume at the start of the process leads to tooling complexities. In addition estimation of the quantity of resin required could present problems in terms of either producing dry patches or low fabric volumes (resin rich).



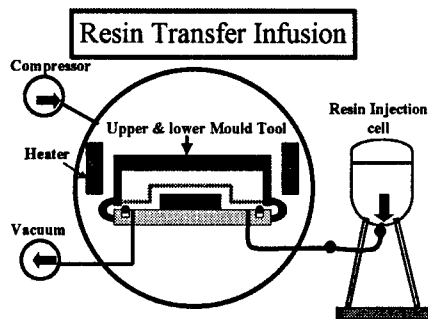
Airbus (UK) has developed a derivative called Semi-preg in which resin film is tacked to one side of the dry fabric. In addition to the bulk problems this technology also has resin application (prepregging) stage and handling / lay-up complexities.

### Liquid Infusion processes

There are many variants of this technology (RTM, RIFT, VARI<sup>®</sup>, SCRIMP<sup>®</sup>, VARTM<sup>®</sup>) all of which involve the application of liquid resin into the component or over its surface.

Daimler / Chrysler and Dornier Fairchild are currently trying to implement a variant of the liquid infusion technology called 'Single Line Injection (SLI<sup>®</sup>)' into production. Typical examples include Pylon Fairings (5-600 parts produced, 98 A/C sets, cost saving over hand lay-up 40% and 6% over RTM), Large beaded ribs on the Airbus 340 500-600 and Wing Skins on the CEC funded TANGO Programme. It involves the injection of liquid resin, through the autoclave shell and over the surface of a 'bagged' dry preform, which is infused to form a laminate (absorbed normal to surface) and cured in the autoclave. Subsequently any surface excess resin is removed through the removal of peel ply.

Bombardier have patented their own version of the technology: Resin Transfer Infusion (RTI) which involves injecting resin over the surface of the preform using Low pressure RTM equipment which is facilitated through the use of one-sided semi-flexible tool. Autoclave pressure is used to quicken the 'wet-out cycle', remove excess resin prior to cure and minimize voids during the cure cycle etc. See sketch



The process has been demonstrated by producing a Complex Wing Skin Section, with integral co-injected/cured stiffeners (3M X2M, 159 Kg) and an integrally stiffened C Spar (3M x 0.4M)

RTI process benefits include:

- Reduced weight due to the use of Advanced Composite Materials.
- Low Cost Materials (use of dry fabrics with multiple layers of unidirectional fibres "stitched" together (Non-crimp-fabrics NCF) which utilise heavy weight tows)
- Preform Lay-up advantages (multiple layers of fabric can be placed in one operation reducing lay-up time)
- No Prepreg out-life concerns (Large prepreg structures typically have to be laid up and cured in 10 days dictating the Autoclave cure schedule)
- No prepregging Costs (the processing, storage and expendable material cost of prepreps can be high)
- Potentially better thickness tolerances over prepreg
- Utilises existing Autoclave Composite manufacturing Infrastructure.

---

#### ICMAC - International Conference for Manufacturing of Advanced Composites

The RTI process is ideally suited to integrally stiffened wing skins, spars, under-floor beams and pressure bulkheads.

#### Benefits of use of Autoclave in conjunction with Resin Transfer Moulding

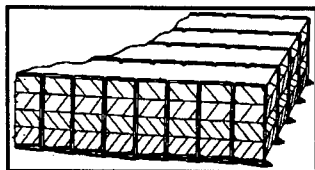
- Flexible for use over a range of component sizes (and multiples off) and for other processes and cure regimes)
- Efficient, controlled Heat-up & Cool Down (No Part Contamination)
- Simplified Tooling (No Bending Moments, No Press requirements) No Internal Stress Problems, Tool stripping Simple i.e. the autoclave pressure consolidates the laminate and holds the tool closed.
- No Health & Safety Concerns
- Tooling Costs Minimised, simpler because one side semi-flexible (Approx. 5% > Autoclave co-cure Tools)
- Flexible for design changes compared to RTM

#### Future Technologies options

##### Stitching

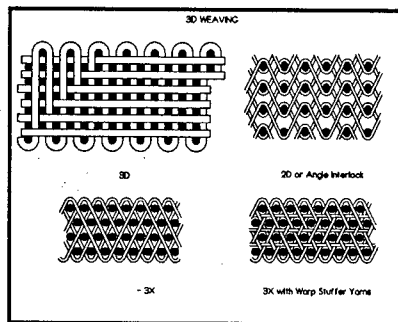
Preform stitching is under consideration for use in conjunction with Liquid infusion technologies in order to impart improved through thickness properties, which can be used to effectively contain damage and eliminate the need for mechanical fastening. The most famous example of the technology was developed by Boeing to produce wing skins as part of the NASA ACT programme.

Several companies now offer automated (double and single side) stitching equipment. The process will incur a cost penalty which has to be offset against a reduction in fastener costs and the improved properties which should eventually result in weight saving.



##### “3D” Weaving

“3D”weaving is a reliable textile technology, which can produce ‘near net’ integrally stiffened performs manufactured using high tow count carbon fibres. The technology could be used in conjunction with the Liquid Infusion technologies (or other automated non-aerospace) technologies to produce low cost laminates which have high through thickness strength / toughness. Currently these laminates incur a major weight penalty because the technology does not have the fundamental ability to weave at +/- 45 degrees however several companies / academic establishments are investigating ways to overcome this.



### Conclusion

Utilisation of composites within aerospace is largely governed by their cost, which in turn is set by the market, and unless the technology can compete directly with metals their use will be confined to largely their current applications.

New emerging technologies such as RTM, Tow placement and thermoplastics have the potential to achieve cost reduction provided the correct application is selected (chosen both in terms of technology and component size)

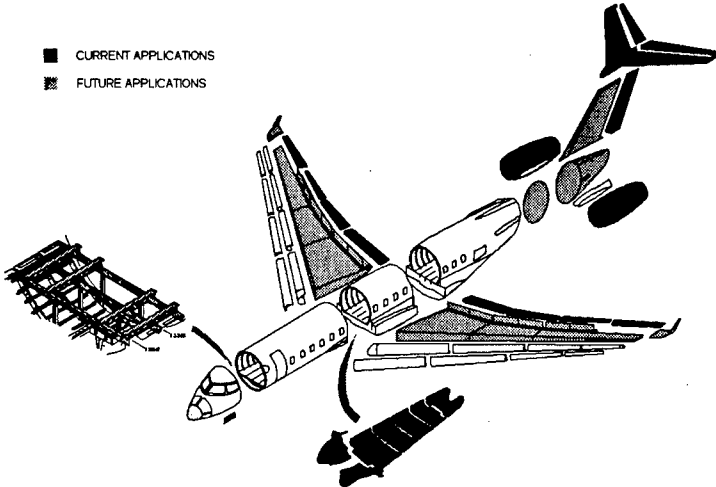
We have demonstrated by using Resin Transfer Moulding and Design for Manufacture and Assembly to produce flight control surfaces that we save up to 20% against the equivalent metallic components.

In addition new Resin Infusion technologies such as RTI have the potential to translate these saving into much larger structures.

As a consequence new structures can be considered for as “real commercial alternatives to metallics”.

Due to their enhanced properties new metallic composite materials such as Glare<sup>®</sup> also show new market potential

ICMAC - International Conference for Manufacturing of Advanced Composites



Other options include Glare for upper fuselage panels.  
Carbon Keel Beams & Thermoplastic / glass Leading edges.

**MANUFACTURE AND FUTURE DEVELOPMENT OF ADVANCED COMPOSITE  
ENGINE NACELLE ACOUSTIC LINER COMPONENTS**

**Richard Parkes \***

**INTRODUCTION**

The design and manufacture of engine nacelles for civil turbofan installations represents a major part of "Bombardier Aerospace, Shorts" business activities. Environmental issues have raised the status of engine noise to a level where the provision of effective acoustic treatment within the nacelle represents a major technological differentiator in new products. Generally, the internal inlet and fan exhaust air wetted surfaces of an engine nacelle incorporate a specially designed structure, consisting of a porous facing skin, honeycomb core and a solid closing skin, that attenuates the noise through the range of operating conditions of the engine.

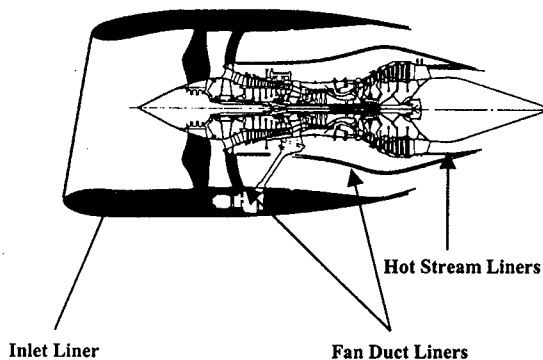


**Figure I : Areas of Acoustic Treatment In a Nacelle**

"Bombardier Aerospace, Shorts" core competencies in the provision of nacelle acoustic treatments were developed initially with metallic structures and then in the innovative application of advanced composite technologies. The company has further developed a "total" nacelle capability, including the design and manufacture of thrust reversers and currently supplies a range of nacelle components for engines produced by the world's leading engine manufacturers. "Bombardier Aerospace, Shorts" must strive to continue to develop its technology base in order to consolidate its market position in the supply of lightweight composite nacelles.

Key to maintaining a technological edge in this highly competitive field, is the ongoing development of the composite acoustic liner.

\*Bombardier Aerospace, Shorts

This paper describes how the current, patented composite liner was developed and details the ongoing research and development into new innovative designs, materials and manufacturing techniques. These include the development of advanced composite perforated facing skins, a double layer liner with inserted septum and the development of components to meet more stringent acoustic performance criteria and customer requirements. It is critical that these are developed to meet both future acoustic legislation and customers ever reducing cost and weight targets.

### ACOUSTIC LINER CONFIGURATIONS

#### (i) "Simple Perforate" Acoustic Liner Structures

The first effective sound suppression structures consisted of a honeycomb core sandwich structure, bonded to a perforated aluminium facing sheet on the air wetted surface and a solid aluminium closing skin. The acoustic response of this type of structure is controlled by the percentage open area (POA) of the perforated skin, the skin thickness and the honeycomb core depth [1].

However, this type of liner is generally only satisfactory for attenuating sound at one specific engine operating condition and will be considerably less effective at off design conditions. This is termed "nonlinear" behaviour. As the noise characteristics (frequency content and sound pressure levels) of a jet engine are constantly shifting as the operating conditions vary, this "nonlinear" behaviour degrades the overall acoustic performance of the liner.

#### (ii) "Linear" Acoustic Liner Structures

A development of this original concept, was the manufacture of a sound suppression structure, which was more effective in terms of broad band frequency absorption [2]. This was achieved by reducing the size and spacing of the holes in the facing sheet while still maintaining the POA. In short, a more linear response is provided by the incorporation of a very large number of very tiny holes. As there were many costly processing problems associated with producing the quantities of very tiny holes required the most expedient and cost-effective method was to use a woven wire cloth or mesh. The porosity of the mesh (and subsequently the acoustic response) can be adjusted by selection of wire diameters, spacing and weave style to produce the desired properties.

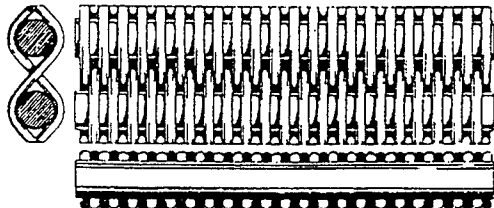


Figure II : Typical Woven Wire Mesh Geometry

The woven wire mesh material, when it is adhesively bonded to a large POA (> 30%) perforated aluminium skin for structural support, provides the desired linear response and is the basis for a series of sound suppression structure concepts within the aerospace industry. The generic term used to describe this type of structure is, single layer, linear acoustic liner.

(iii) "Double Layer Linear" Acoustic Liners

Producing a double layer, linear acoustic liner, can further increase the range of attenuated frequencies [2]. In this case a wire mesh layer (septum) is bonded between two honeycomb cores, as shown in Figure II. The two honeycomb layers have different depths so to maximise attenuation at two different frequencies and thereby increase the overall range of attenuation. The disadvantage of the double layer structure is that it is heavier and more costly to manufacture than the single layer system.

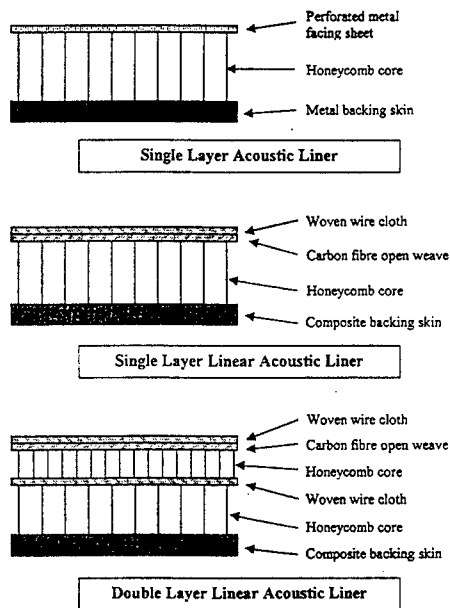


Figure III : Alternative Acoustic Liner Configurations

Other types of acoustic panels have been developed, such as Extended Reaction Liners (or Bulk Absorbers) which are characterised by the core being resistive (porous) as well as reactive. In this case the sound waves can travel along the liner inside the bulk absorber material, as well as inside the compartmented honeycomb cells. This type of liner construction is not commonly used due to its tendency to absorb fluids.

A more recent theory in terms of perforated liners has been the concept of an "enhanced perforate". This consists of a perforated facing sheet with smaller (approximately .005 - .010") closely pitched holes. The acoustic performance of this structure would rate somewhere between a simple perforate and a linear liner. Difficulties in developing a method

of producing the required number of tiny holes have led to limited development of this concept.

In the main the acoustic liner configurations detailed in Figure III represent the current industry standard.

In order to ensure that "Bombardier Aerospace, Shorts" (who were the first to manufacture the patented composite single and double layer linear liners) can maintain a technological edge in this highly competitive field, a development programme has been undertaken. One of the main objectives of this Nacelle Inlet Acoustic Liner programme was the provision of innovative manufacturing processes which will enable manufacture of "Bombardier Aerospace, Shorts" next generation acoustic treatments.

This programme has been part funded by the Industrial Research and Technology Unit (IRTU).

Prior to detailing the ongoing research activities the development of the current nacelle acoustic liner is described.

#### **DEVELOPMENT OF THE CURRENT COMPOSITE NACELLE ACOUSTIC LINER**

In 1979 - 1984 Shorts completed a development programme to design and manufacture composite demonstrator nose cowl components and fan cowl doors as alternatives to the then current aluminium alloy structures used in typical nacelles [3]. The objectives of the development programme were as follows:

- To design/develop flight worthy components, including the capability of resisting lightning attachments and meeting induced voltage requirements, of withstanding a bird strike and the ability to resist fan blade off effects (during simulated operational conditions).
- Gain weight savings at an economic cost when compared to existing metal structures.
- Complete static and fatigue tests for structural compliance and establish allowable material properties for each composite material used.

Key to the development of the composite acoustic liner was the production of a porous carbon fibre facing skin to act as a support sheet for the wire mesh, to replace the industry standard, aluminium component. A number of techniques were investigated unsuccessfully, eg drilling, punching (prepreg and laminate). It is obviously possible to mechanically drill holes in laminates, but the large numbers of small holes required for the support sheet type components (eg 90,000 in a typical segment) resulted in an extremely slow, cost prohibitive and high scrap rate process. There were also issues with the loss of strength of the laminate with so much material removed during the drilling process.

The solution was found in the use of a carbon fibre open weave fabric [3]. This consists of a carbon fibre plain weave, woven to a POA of greater than 30% (as shown in Figure IV) impregnated with a controlled flow, high temperature curing, epoxy resin.

This carbon fibre open weave material provided Shorts with a cost effective method of producing a lightweight, linear acoustic facing sheet. From an acoustics standpoint the open weave material served principally to support the micro-porous wire mesh.

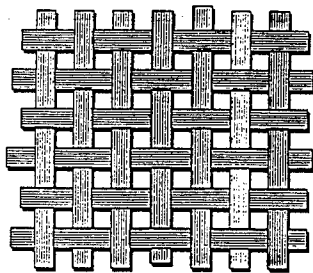


**Figure IV Carbon Fibre Open Weave Fabric**

Lightweight "Nomex\*" honeycomb was incorporated to replace the traditionally used aluminium core and a solid carbon fibre epoxy laminate skin was incorporated to replace the aluminium backing sheet to complete the composite linear acoustic liner design.

It is important to note that in the manufacture of acoustic liners to stringent acoustic performance criteria, the bonding and adhesive application processes must be strictly controlled. Any variation in the adhesive blockage of the wire mesh (either face sheet or septum) can degrade the acoustic performance characteristics, compromise mechanical integrity, or affect the cosmetic quality of the acoustic panels. The following methods of adhesive application were developed to ensure that the acoustic performance criteria would be met.

\*Du Pont trade name

**(i) Robotic Application of Spray adhesive**

A process of robotically spraying a liquid epoxy adhesive to the inner surface of the cured carbon fibre open weave was developed, to facilitate the bonding of the wire mesh. This allowed the strict control and uniformity of application to ensure consistent levels of adhesive blockage of the mesh could be achieved.

**(ii) Automated Reticulation**

To apply film adhesive to honeycomb core panels used in current design acoustic liner structures a process called automated reticulation was developed. Basically this process is performed on dedicated equipment as follows. The unsupported film adhesive is positioned on top of the honeycomb core, a preheat lamp positioned on a moving gantry, passes over the assembly to tack the adhesive to the cell edges. An air knife also attached to the gantry, blows hot air up through the core and the adhesive bubbles up to a point of low integrity, bursts, and forms back onto the top of the cell edges. This allows bonding to perforated substrates while still maintaining a high degree of porosity. Reticulation is utilised in the bonding of core to facing skin and also in the bonding of a septum between two honeycomb cores.

In the case of the facing sheet, given that the adhesive bead is concentrated around the top of the honeycomb cell edges, there is always the possibility that, during curing, the adhesive may flow down through the open weave support sheet and into the wire mesh causing staining. This is minimised by strict control of materials and tailoring of the processes to meet specific customer needs.

Using a generic design based on the methodology outlined above, "Bombardier Aerospace, Shorts", build both single and double layer, composite linear acoustic liner components for the following aircraft: single layer liners - Boeing 757/767; MD90; Global Express GX/GV; Airbus A330: double layer liners - Airbus A320; A321; A319. The components have proved to be lightweight, strong, durable and damage tolerant.

### ONGOING RESEARCH AND DEVELOPMENT ACTIVITIES

Use of the carbon fibre open weave has provided "Bombardier Aerospace, Shorts" with a cost effective method of producing a lightweight, linear acoustic facing sheet. While the design is relatively simple and effective, the fact that customer specifications will become increasingly more stringent in the near future means that further R&D is essential in order for Shorts to consolidate its market position.

Research is going on into various permeable materials as possible alternative facing sheets but the most viable possibility for significant improvement in composite acoustic liner performance would be the ability to manufacture a range of perforated, composite skins. This is equally true for either the linear type liners where the perforated skin would be a direct replacement for the open weave material, or for the "simple" or "enhanced" perforate type of liners.

Research is also going on into a more effective method of producing double layer liners and also a more effective method of controlling adhesive flow, which can currently be detrimental to the cosmetic surface finish of acoustic panels.

### Development of a Perforated Composite Support/Facing Sheet

The objectives here are to evaluate alternatives to existing perforate technologies in three categories:

1. "Simple" perforate (open area 5-12%)
2. "Enhanced" perforate (open area 4-10%)
3. "Support" perforate (open area 30-34%)

The technical viability of a number of composite perforation processes is currently being assessed.

#### (i) Laser Drilling

When considering laser drilling multiple holes in CFC's two key requirements were identified; the hole quality (heat affected zone) and the hole production rate.

There is no doubt that lasers can be used to drill excellent quality holes in many different types of material and it is reasonable to assume that this includes carbon fibre composites.

With certain laser types and techniques this can be done with little or no heating effect.

However, the hole production rate (time to process each panel) is an important consideration. Unless the holes can be drilled quickly, it could take many hours to produce each panel. Also, it should not be assumed that the laser that could produce the best quality holes would be the same as the one that could drill at the quickest rate. So, hole quality and process speed may be conflicting requirements and the choice of laser and drilling technique could be a compromise between the two.

In order to meet the requirements for hole quality and process speed, it is necessary to determine the optimum combination of laser wavelength, repetition rate, pulse length, energy and drilling technique. Tests have been carried out using several laser sources e.g. Nd: YAG, Excimer Xecl, Nd: YVO<sub>4</sub>, at different wavelengths. The differences between percussion and trepanned drilling have also been investigated.

Some preliminary mechanical testing has been performed and the results are encouraging.

Further tests are to be carried out to confirm the optimum laser and drilling technique. Test samples will be provided for mechanical (including hot/wet ) testing and acoustic fatigue testing.

Work is also being carried out to assess the feasibility of controlling the laser cutting depth. This would have the advantage of allowing the perforation of a finally bonded component, with or without an internal septum.

The innovative aspects of this work are being patented by "Bombardier Aerospace, Shorts".

#### (ii) Ultrasonic Z Pinning

This method (patented by Aztex Inc.) employs carbon or titanium "Z" pins which are inserted into a silicone rubber mat which is located on top of a prepreg lay-up. An ultrasonic anvil is then used to push the pins into the prepreg. The pins remain in place during cure and after cure the ultrasonic anvil is used to remove the pins thus producing a perforated laminate. The diameter of the pins has to be greater than 0.020" and the rubber mat can be reused up to 20 times.

Some A4 size test samples have been prepared but further optimisation of the process is required. Test samples are to be manufactured for mechanical tests and micro-examination to determine hole quality.

One of the main advantages of this method is that no reinforcement fibres are removed to form the holes, therefore a high degree of mechanical strength is retained.

This is a viable option for future production of "simple" perforates.

#### (iii) Perforation of Thermoplastic Materials

This aspect of development is aimed at assessing the viability of perforating flat sheets of reinforced, engineering thermoplastic material and subsequently thermoforming them to the final component shape. This would allow high speed, multi drill head perforation of flat sheets prior to the thermoforming process.

The material selected for the trials was polyetherkeytoneketone (PEKK) [4] reinforced with five plies of woven carbon fibre fabric (3K-70-PW) in a balanced lay up. The PEKK thermoplastic material, because of its semicrystalline nature demonstrates an excellent balance of physical properties: strength at elevated temperature, chemical resistance and hydrolytic and thermal stability. The reinforcement chosen was specified so as to allow a direct comparison with materials currently in production use i.e. carbon fibre reinforced (3K-70-PW) epoxy resin.

Significant mechanical and thermal analysis testing has been performed and in the main has shown equivalence between the PEKK and the commonly used epoxy composite materials. Some initial thermoforming work has been successfully performed on small scale panels. Successful thermoforming of production scale components will need to be demonstrated and further mechanical tests will be required to ultimately prove the viability of this concept.

### Development of Septum Layer Insertion Process

The concept of a double layer liner is based upon the principle of single honeycomb cells with a permeable membrane or septum layer dividing the core into two along its axis. Using the previously described technology this is achieved by sandwiching a sheet of porous media between two layers of honeycomb core. The inevitable misalignment of the honeycomb cells, due to cell size discrepancies and varying radial alignment compromises to a degree, the acoustic efficiency of this principle. However, if a method was available, alignment of the honeycomb cells could potentially increase the noise attenuation capability of the double layer liner by up to 3 – 4 Effective Perceived Noise Level, Decibels (EPNdB).

Any process concerned with slicing the honeycomb cell walls, inserting or bonding the septum such that the walls re-align is very difficult and expensive to achieve.

Boeing has developed a method of curing a layer of thermoset resin within the cells (using a eutactic mandrel technique) and subsequently laser drilling to create the perforations. They have subsequently patented this method of curing and laser drilling [5].

No other septum layer production techniques are known.

A new process concept is being developed by "Bombardier Aerospace, Shorts" in conjunction with the Warwick Manufacturing Group (WMG), which employs the principles of laser or UV light curing to produce a lateral, permeable membrane within a single sheet of honeycomb.

The basis of the process is that the honeycomb core is suspended in a bath of UV light curing resin, to a predetermined depth and the surface layer of resin is cured using various techniques including masking or selective laser curing, or a combination of both.

The objective of this work is to develop the process and materials into a viable industrial operation which is simpler, faster, more cost effective and acoustically more efficient than the Boeing technique, thus enabling the manufacture of a technically superior acoustic liner.

"Bombardier Aerospace, Shorts" hold the industrial property rights for this method of producing a generated septum layer.

The critical process development issues are as follows:

- Generation of Septum layer by Ultraviolet Light or Laser Curing
- Development of Hole Generation Technique
- Evaluation of Septum Layer/Hole Generation Viability
- Mechanical Evaluation of Septum Layer
- Acoustic Evaluation of Septum Layer
- Drapeability of Honeycomb With Septum Layer Inserted

#### Progress to Date

A number of resins have been evaluated against the agreed selection criteria with good results on small scale panels. Solid septums have been successfully produced within nomex honeycomb cores. The thickness of the layer can be varied by changing the exposure time.

#### ICMAC - International Conference for Manufacturing of Advanced Composites

The candidate resin systems have demonstrated good high temperature resistance and they are flexible enough to conform during a subsequent forming process while still rigid enough not to distort during the bonding cure cycle.

Good mechanical strength of the generated septum has been achieved and hole forming trials using optical masking of the UV light source and selective curing using a UV laser have also proved to be extremely promising.

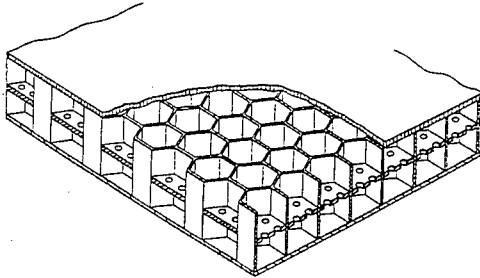


**Figure V: Sketch Showing An Inserted Septum Layer**

#### **Controlling Adhesive Flow in Acoustic Liner Structures**

Reticulation parameters vary in the production scenario between contracts and in an effort to control the adhesive flow (and potential staining of the face sheet) some of the equipment temperatures employed necessitate running the reticulation machine near maximum.

The potential adhesive staining is a predominantly cosmetic issue and is controllable on a contract specific basis i.e. tailoring the process parameters between different components. From the quality viewpoint and with the constant drive within industry towards more robust processes and lean manufacturing, the ideal scenario would be a standard reticulation cycle for all contracts, which employed the minimum temperatures and air pressures possible within the range of contracts considered.

#### **Use of Lightweight Random Mat (Scrim) at Bond Interface**

A current development to provide a solution to the above issues involves the incorporation of a light weight polyester or glass scrim at the bond interface (between honeycomb and open weave support sheet). It is projected that this will have a two-fold advantage:

1. The potential of providing a barrier to the adhesive bleed through thus eliminating any potential staining effect.
2. The barrier nature of the scrim means that a heavier bead of adhesive may be tolerated at the honeycomb interface. This in turn has the potential for :
  - The standardisation of the reticulation parameters ie no tailoring per contract to reduce the potential for adhesive staining of the face sheet
  - Maintaining the honeycomb/facing sheet bond strength

Progress to Date

A glass random mat scrim has been selected from a short list and a number of tests have been performed. In all cases the results have proven that the scrim has eliminated the potential for adhesive staining, with no detrimental effect on either acoustic performance or mechanical strength. By incorporating the scrim it has been proven that the above objectives can be met. The process has been patented by "Bombardier Aerospace, Shorts". Negotiations are ongoing with the relevant customers to agree the necessary qualification/certification test requirements etc prior to incorporation into the production process.

Conclusion

This paper has detailed some of the current and ongoing research and development activities with regard to the "Bombardier Aerospace, Shorts" composite acoustic liner design. Many other technologies have also been under investigation but the developments detailed are those which have shown most promise and are the most likely to help in further developing core competencies and maintaining a technological edge in this highly competitive field.

References

- [1] Guess, A W  
Calculation of Perforated Plate Liner Parameters From Specified Acoustic Resistance and Reactance.  
Journal of Sound and Vibration, 1975, 40 (1), 119-137.
- [2] Reil, F J and Rose, P M  
Adhesive Bonded Noise Suppression Structures for Commercial and Military Aircraft  
SAMPE Quarterly, October 1984, 45-49.
- [3] McGarel, Dr W  
Application of Composite Materials for Production Nacelle Structures.  
Proceedings of International Symposium on "Advanced Materials for Lightweight Structures", Noordwijk, The Netherlands, 25-27 March 1992.
- [4] Chang, I Y  
PEKK as a New Thermoplastic Matrix for High Performance Composites.  
Industrial Report, E.I. Du Pont de Nemours and Co. Inc. Fibres and Composites Development Centres, Wilmington, Delaware 19880-0702.
- [5] Diepenbrock, Jr., et al, The Boeing Company  
Method of Making a Cellular Core With Internal Septum.  
United States Patent No. 4,257,998 Mar. 24, 1981.

**RTM- A COST EFFECTIVE COMPOSITE MANUFACTURING PROCESS FOR CONTROL SURFACES**

**MARK BRANIFF (Bombardier Aerospace Shorts)**

**ABSTRACT**

A typical civil air transport wing consists of a main torsion box of ribs and spars with articulated control surfaces forming the trailing edge structure. This arrangement of control surfaces experiences considerable loads during certain critical flight phases. As a consequence these structures become complex in terms of stiffness / load introduction requirements and incur a higher assembly / parts cost count due to intricate design features. A cocured monolithic composite philosophy was identified as a potentially more efficient design if a suitable manufacturing technique were available. The resin transfer moulding (RTM) process offered the potential to inject low cost, complex one-piece components, if the various resin processing, tool manufacture, and preform generation issues could be resolved. This paper describes how Bombardier Aerospace (Shorts) developed the RTM process from simple flat laminate production into a multi-spar stiffened composite aileron destined for service on the RJ200/700/900 regional jet family. This exercise included all aspects of resin injection, tool development, net shape preform manufacture, press design, part design, and manufacture of sub-elements / full scale components. Cost savings and weight reductions are detailed against an existing metallic base line.

**INTRODUCTION**

The RTM process has matured over the last ten years with the introduction of number of components in to service by such companies as Airbus, Boeing, Raytheon, ASTA, etc. The common theme is cost saving through integration of parts and lower raw material costs. RTM is a stand alone, closed mould process, which removes the autoclave from the typical production scenario. Cured ply thickness is no longer controlled by autoclave pressure but instead relies on the accuracy of the machined mould. Tooling and facilitation costs are higher relative to autoclaving but the reduction in recurring costs can be considerable. Selection of the correct part geometry in conjunction with a medium/high build rate, are essential in order to justify the typical RTM set-up costs. A build rate of one a day usually maintains the manufacturing cell at an optimum state.

Because cured ply thickness is controlled by tool geometry there is an opportunity to design substantially unitised structures. This was the approach adopted for the re-engineered RJ 200 aileron. The exercise started as a DTI/MOD part funded CARAD programme entitled "IMPACT", co-ordinated through DERA with the participation of Hexcel composites, GKN Westlands Aerospace, Dowty propellers, DML, and Bombardier Aerospace.

## OBJECTIVES

In order to avoid over simplification the envelope and load case from an existing RJ 200 Aileron were employed. This is a typical metallic component, manufactured in house, with known recurring costs. The programme objectives were as follows-

- Design and manufacture of a production standard RJ composite Aileron.
- A 20% weight saving combined with significant recurring cost saving.
- Establish a mechanical and physiochemical database for RTM 6 resin and Hexcel G0926 6k bindered fabric.
- Finalise preform and injection processes.
- Perform a full-scale static test.

A risk assessment was performed and a number of technical issues identified-

- Repeatable injection of complex 3-D shapes.
- Manufacture of low cost tooling with sufficient geometric accuracy.
- Preform accuracy.
- Process/quality control and NDT considerations.
- Integration of metallic details.
- Part distortion.
- Certification implications.
- Assessment of recurring and non-recurring costs relative to metallic equivalents.

## METHODOLOGY

In order to address these issues the following methodology was adopted. A decision was made to reduce the risk by introducing a half-length sub-element torsion specimen, which deviated from the original programme submission. The following tasks were planned-

- Full-scale scheme to assess feasibility.
- Half scale sub-element test specimen to evaluate:
  - Design/stress assumptions
  - General component quality
  - Skin to rib interface
  - Installation of metal fittings
- Optimise RTM process through computer aided simulation and flexible porting package.
- Development of low cost tooling package employing simple electrical heating and pneumatic clamping.
- Implementation of accurate net size preforming techniques through ultra-sonic trimming, die stamping and flat packing fixtures.
- Manufacture of a demonstrator incorporating production features based on an existing load case whilst applying lessons learnt from the sub-element phase.
- Full-scale static test to validate design and structural integrity.
- Derive realistic costs for future introduction of RTM flight components.

## RTM AILERON DEVELOPMENT

Figure 1 illustrates the current metallic aileron design, which consists of approximately 115 parts, 1600 fasteners and weighs 34lbs. The objective was to reduce parts count by 75%, fastener count by 50% and weight/cost by 20%.

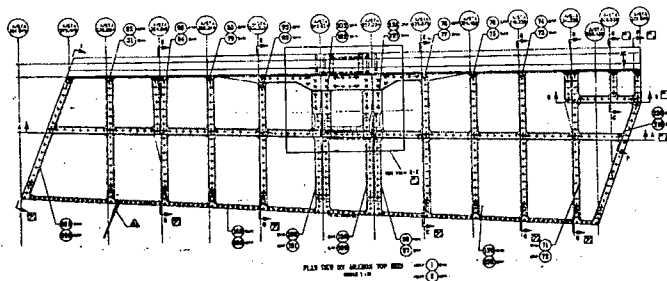


Figure 1 existing RJ 200 metallic aileron

### SUB-ELEMENT

The complex nature of the design with multiple ribs, auxiliary centre spar and machined titanium centre hinge fitting, indicated high-localised loads and significant air loading. A sub-element specimen was designed as per figure 2, which would address tool manufacture issues and general RTM process parameters.

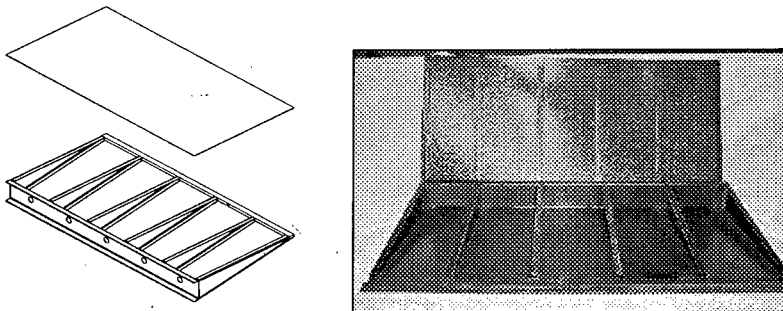


Figure 2- Sub-element design and injected part

**PREFORMING**

The sub-element was designed as a post-buckled, multi-rib, cocured box with mechanically fastened top skin. The bindered fabric and resin were supplied by Hexcel composites (G926 5-harness/RTM6 resin). The RTM process relies on the manufacture of accurate net size preforms. This was achieved by employing various ply cutting techniques such as traditional Gerber/ultra-sonic CNC methods and die stamping as seen in the textile industry. Cost savings can be achieved by pre stacking the desired orientations prior to cutting. The flat packs of plies are located in dedicated stacking tools, which allow accurate placement of part plies. The stack is in an over size condition and can be tacked around the periphery which allows transfer to the preform tool. Special location features ensure that the preform aligns precisely with the preform tool surface. Figure 3a-e illustrates the sequence.

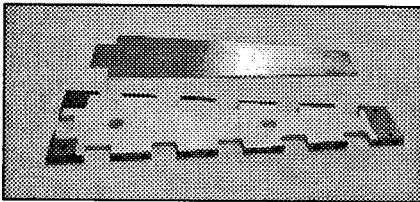


Fig 3a Rib stacking tool

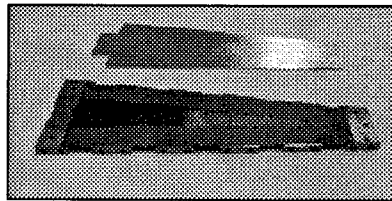


Fig 3b over size plies in position

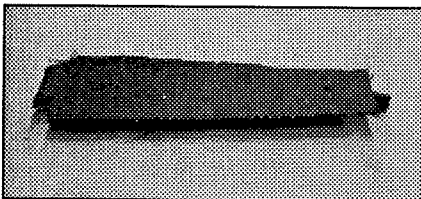


Fig 3c tacked plies located on preform tool

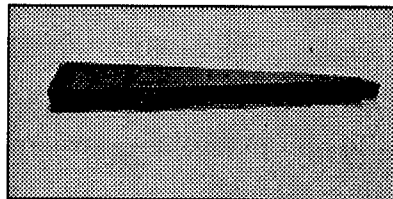


Fig 3d Rib after preform cycle

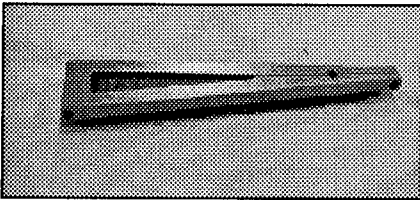


Fig 3e Dedicated trim media in position

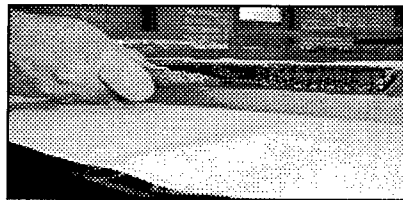


Fig 3f manual trimming of rib flange

The preform cycle which activates the binder is performed at 100-125°C ,at full vacuum, for twenty minutes. The key to successful preforming is to cool the material to 35-40°C before releasing the vacuum. Figure 4 shows typical infra-red, diaphragm

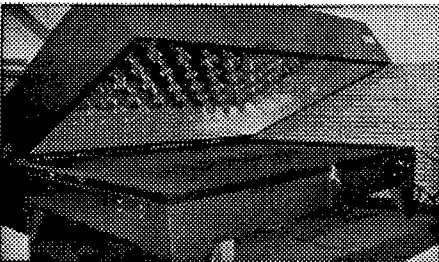


Figure 4 Typical infra-red perform equipment

forming equipment, which simplifies much of the traditional hand lay-up associated with prepregs.

### TRIMMING

Further cost can be removed from the process by employing semi-automated trimming techniques. Figure 5 shows a small ultra-sonic knife mounted on a power slide which trims spar and rib flanges in a single pass. In order to minimise equipment cost and complexity the part must be designed with the process in mind.

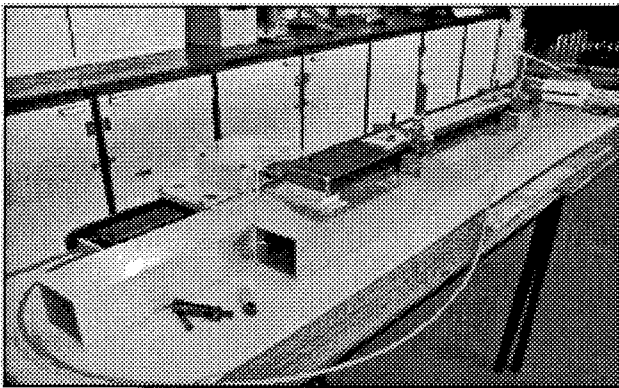


Figure 5 Ultra-sonic trimming cell

### INJECTION CELL AND TOOLING

RTM exerts considerable pressure within the tooling during the injection process. This can either be reacted by the inherent stiffness of the tool or through an external clamping arrangement. In order to minimise cycle time, a pneumatic press system is employed which allows through shuttling of tools and rapid tool break down. Figure 6 illustrates a schematic of the RTM injection cell designed for sub-element manufacture.

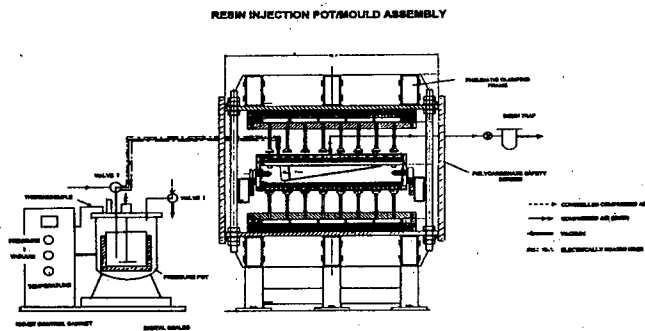


Figure 6 Sub-element tool injection cell

The injection tool was sized for thermal expansion and was manufactured from a steel billet with solid internal steel mandrels. Resin was injected through a single port and allowed to track around the periphery of the part along dedicated machined channels. Resin exit was through multiple ports on the part upper surface placed at the theoretical last point of fill. This venting approach can only be employed with the novel press design illustrated above. The press platens consist of a series of pressure pads, which permit access to the tool vent line pipe work. The heating system was built into the tool and consisted of low cost electrical cartridge elements embedded in alloy plates. Heating and temperature monitoring was controlled by a spec view data acquisition system. Figure 7 shows the injection tooling partially loaded and a schematic of the tool build.

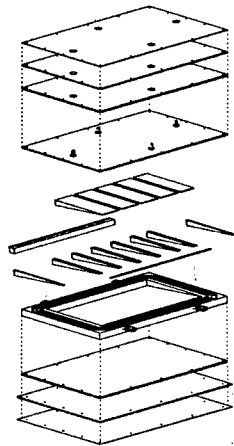
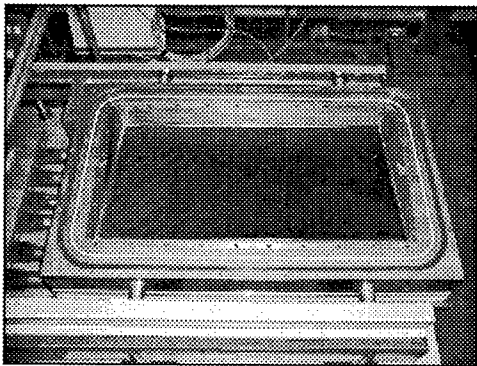


Figure 7 Sub-element tool and part loading

### SUB-ELEMENT TORSION TEST

The sub-element specimen was designed to be evaluated in a torsion loading mode as shown in figure 8. The results of this testing, with impact damage, fully validated the post buckled design assumptions.

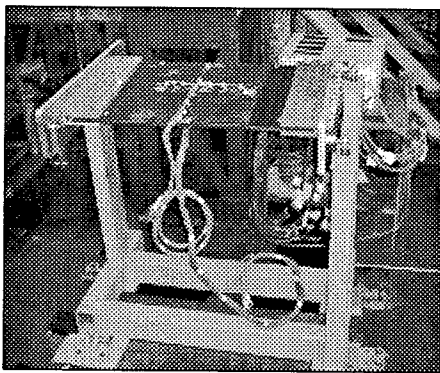
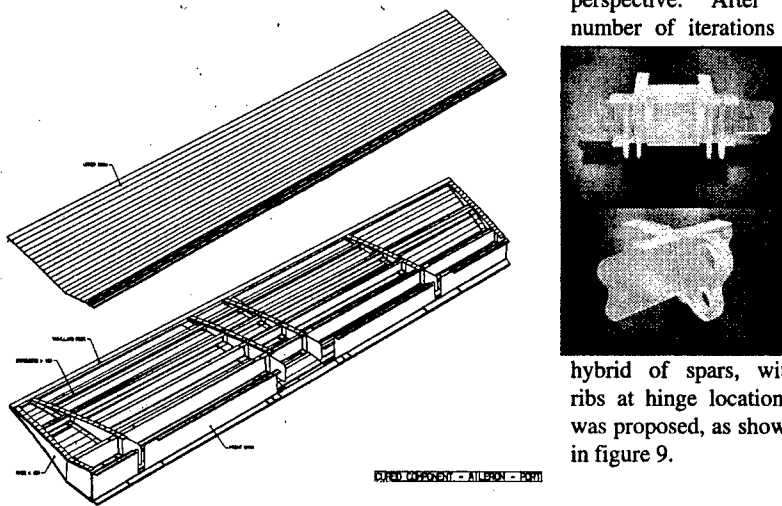


Figure 8 strain gauged test specimen

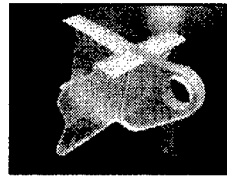
### FULL SIZE AILERON DEVELOPMENT

A preliminary RJ aileron design and stress analysis indicated that a multi-spar stiffened structure may be more efficient from a weight and general performance perspective. After a number of iterations a



hybrid of spars, with ribs at hinge locations, was proposed, as shown in figure 9.

Figure 9 Aileron schematic with rapid prototyped hinge brackets



This solution was weight optimised at the expense of DFMA (design for manufacture and assembly). There were approximately twenty two individual composite details which required kiting, preforming, trimming and loading. The internal mandrel tool count reached fifty-eight individual pieces in order to facilitate tool release. The objective of this part of the programme was to determine how complex a part could be successfully injected. Tool design and tolerancing techniques were optimised in conjunction with part release characteristics and general quality. Figure 10 shows the injection mould tools and internal mandrels.

A complete suite of preforms was manufactured on dedicated alloy tools. The perform process was that developed previously during sub-element manufacture. The alloy tools caused cycle problems due to the inherent high thermal mass of aluminium. Ply

trimming was accomplished with glass fibre overlays, which ensure accurate flange definition.

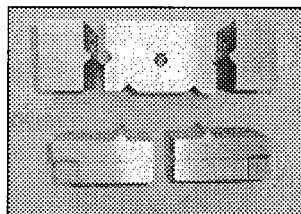
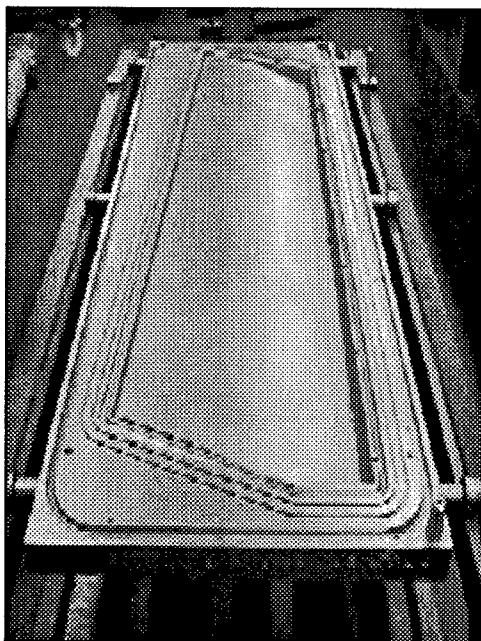
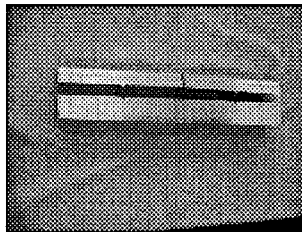


Figure 10 Aileron base injection tool and internal mandrels

The injected aileron was assembled and assessed for resistance to damage from lightning strike. Figure 11 shows a typical aileron box and upper skin prior to assembly.

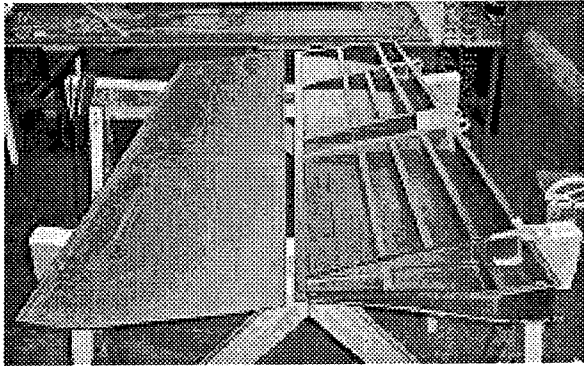


Figure 11 Injected aileron with rapid prototyped hinges. Note integral spar and ribs cocured to bottom skin.

#### **PRODUCTIONISATION (not funded by IMPACT)**

Based on the experience gained through out the course of the development programme and the indicated cost saving potential, the decision was taken to re-certify the existing metallic RJ200 aileron as an RTM alternative. The previous demonstrator design was extremely weight efficient (22%), but complex in terms of the number of internal mandrels required to generate the integral shapes. The design was refined by employing DFMA principles, into a predominately multi-spar geometry with only a residual centre rib feature necessitated by the high actuator in put loads. This reduces the internal mandrels from 58 to 18, which significantly improves tool loading and strip down cycle times. Figure12 shows a CAD model of the optimised design.

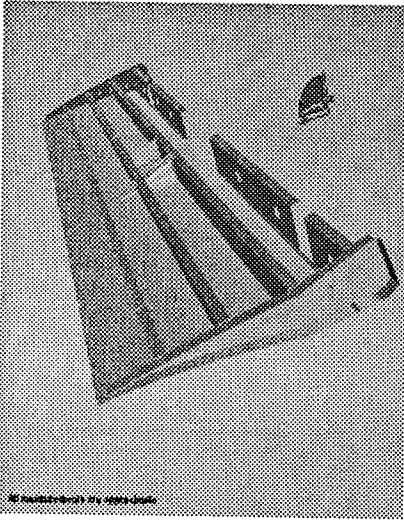


Figure 12 Production RJ 200 aileron model

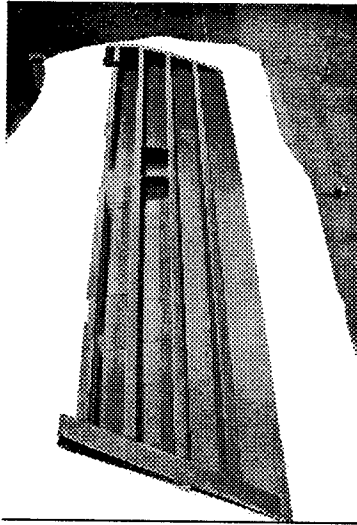


Figure 13 injected aileron prior to assembly

Figure 13 shows the injected aileron with simplified spars and ribs. The end ribs have been reversed to aid tool removal and the majority of the part periphery was manufactured net size. The trailing edge was changed to a glass fibre constant section pultrusion, which saved considerable cost in comparison with the traditional alloy or tufnol item. The aerodynamic profile was changed to accommodate this feature. The upper skin was injected insitu and incorporated an integral leading edge, which reduced the level of assembly and number of fasteners. The centre hinge was changed from titanium to aluminium, which again saved considerable cost but with a weight penalty, which was absorbed by the efficiency of the multi-spar composite box.

A typical certification programme is now under way with entry into production scheduled for early 2003. A build rate of one set per day is anticipated, which will require a degree of semi-automation in terms of performing, trimming, tool loading and tool cleaning/release application. All these activities have been demonstrated and facility installation is currently under way.

## ACHIEVEMENTS

Table I shows a comparison between the original metallic and RTM aileron cost savings

	Fabricated parts	Bought in parts	AGS	Cost
CRJ Family Metallic Aileron	113	1248	1572	Baseline
Equivalent RTM Aileron	28	91	750	20%

Table I

The programme objectives were exceeded in terms of cost reduction. However, weight saving was sacrificed in order to maximise cost saving. Damage tolerance has also been enhanced through the use of multiple spars, removal of honeycomb and the associated slightly thicker skin gauges.

## CONCLUSION

Traditional composite aero structures have offered weight savings but at the expense of recurring and non-recurring costs. This is the result of relatively high raw material costs, a labour intensive manufacturing process and protracted certification procedure. The RTM process in conjunction with DFMA principles offers, the potential to employ lower cost materials in the form of constituent components with improved utilisation ratios. The generation of shaped fabric preforms may be automated through multi-ply die cutting, diaphragm forming, and ultra-sonic trimming. The injection philosophy is a closed mould process producing net size parts requiring minimal finishing.

The expertise has now matured to a level, which can be offered on future airframes whether civil or military. The monolithic integrally stiffened structural concepts dictated by RTM avoid the in-service problems often associated with conventional honeycomb systems and allow simplified repair techniques.

The key to obtaining a cost competitive composite structure is multi-fold

- Select the right structural application
- Design the structure to be RTM process friendly
- Employ metallic features at high load concentrations (i.e. keep the composite details simple)
- Ensure a suitable build rate exists to allow tool/facility amortisation.
- Reduce mechanical assembly through structural integration.
- Provision for automated non destructive test (C-scan)

RTM is not the answer to all composite processing problems. The technology will continue to mature in terms of material advances and optimised processing. Bombardier Aerospace plans to exploit this technology on larger structures in the future by applying the manufacturing demonstrator building block approach used successfully on this programme.

## ABSORBING COMPOSITE STRUCTURES MADE BY RTM

**TA Turner, NA Warrior, F Robitaille, CD Rudd, EJ Cooper**  
**School of Mechanical, Materials, Manufacturing Engineering and Management,**  
**University of Nottingham, UK**

### ABSTRACT

Lightweight composite materials are being exploited in the automotive industry due to their high specific energy absorption allowing lighter and safer vehicles to be constructed. In spite of considerable amounts of research, the nature of the crush process is not fully understood due to the complex damage mechanism which involves a number of different failure modes. Previous studies document the effect of differing fibre volume fractions, fibre types, textile architecture, crush rate and sample geometry, but little is known about the effect of processing parameters and process-related defects encountered in industrial parts. This paper is focussed on the effect of processing parameters on the specific energy absorption (SEA) of the final part. The effects of process temperature, resin formulation and postcure time are investigated. Efforts have been made to establish the contribution of various in-plane properties to the final SEA value.

### INTRODUCTION

Vehicle safety is an increasingly important factor as lightweight materials are exploited in the automotive industry (1). The concept of crashworthiness of a vehicle is intimately related to the energy absorption of the structure. Kinetic energy dissipation by progressive crushing of composite structures can be twice as effective as steel on a specific energy absorption basis, Farley (2).

A major advantage of composite structures is that they exhibit an almost rectangular force-displacement curve, where the force quickly rises to a maximum value and remains essentially constant thereafter. This results in higher energy absorption for a given peak force, lower decelerations, and improved passenger protection.

While legislative pressures are forcing OEM's to develop lightweight body structures, the understanding of composites crash behaviour is still incomplete. A main difficulty in specifying an energy absorbing composite front end is the large number of variables upon which the failure mode and energy absorption depend. Previous studies document the roles of constituent materials and reinforcement architectures for laboratory quality laminates, Hull (3), but little is known about the effects of process-related defects encountered in industrial parts.

The global objectives of this EPSRC funded project are to investigate the effects of different fabrication parameters on impact energy absorption in thermoset composite

structures, to advance formal scientific understanding of the effects of practical industrial aspects of crash performance, and to provide design guidelines. Data will also be provided for concurrent finite element modelling of the crush.

The above objectives led to the definition of a moulding and testing programme based on tube crush and supported by the measurement of in-plane properties, fracture toughness, degree of conversion and void content. Two different resins were selected in collaboration with the industrial partners. SEA is only one factor to be considered in designing vehicle structures; high in-plane properties are also required. Blears et al. (5) have shown that although aligned fabrics can give higher volume fractions and in-plane properties, a similar improvement in SEA over random mat is not realised. In the overall project, both a 0/90° stitchmat fabric and a continuous filament random mat are to be studied. Toughening methods such as stitching, resin tougheners, and interleaves are also to be investigated.

In this paper, results are presented for polyester resin random mat tubes under quasi-static crushing, and for in-plane coupon testing.

## METHODOLOGY

The work presented involves a fixed preform lay-up of 5 layers of Vetrotex Unifilo U750-450 450 g/m<sup>2</sup> continuous filament random mat injected with Reichhold Norpol 631-610 polyester at variable cure temperatures and post-cure times. Flat plaques are moulded under the same conditions. Tube performs are made manually on a bespoke winder; plaque preforms are made in a standard heated press.

The lengths of the moulded tubes and crush samples are 500 mm and 100 mm respectively. Three tubes are produced for each moulding configuration (moulding temperature and post-cure time). Configurations are identified as R1, R2, R3 and R4, and tubes are labelled as m1, m2 and m3 in each case. An extensive list of secondary moulding parameters (temperature, humidity, mixing time, etc.) is compiled for each configuration. Four samples are cut from each moulded tube and crush tested, so that each moulding configuration effectively leads to 12 crush tests. The tubes are injected along their length from a peripheral end gate. Samples are identified as to their axial position in the mould; sample A is near the inlet, followed by B, C and D at the outlet.

The plaques from which the coupon tests are extracted measure 538 mm by 517 mm; the injection gate extends along one of the shorter edges. One flat plaque is produced for each moulding configuration. Three samples are cut for each coupon test in each of two orientations, parallel and perpendicular to the injection direction.

All samples are injected at 1.5 bar without vacuum assistance. Injection times vary from 1 to 2 minutes with gel occurring within around 3 minutes, depending on tool temperature. The cure time was set at 30 minutes for all mouldings. The post-cure temperature was set at 80°C. Closed-loop heated tooling is used to manufacture the specimens; the moulding process is closely controlled to ensure consistency.

The experimental plan presented here (cure temperature, post-cure time) represents part of the overall programme, which is a full factorial Taguchi matrix. The moulding configurations are shown in Table 1.

<i>Configuration</i>	<i>Cure temp. (°C)</i>	<i>Post-cure time (min)</i>
R1	50	0
R2	50	60
R3	70	0
R4	70	60

Table 1. Moulding configurations.

## TESTING

Crush testing is carried out on a 1000 kN Instron 8500 servo-hydraulic testing machine. The tubes are placed between two ground steel platens and loaded at 10 mm/min. The tube crushing technique employed in this project relies on a 45° crush trigger which acts as a stress concentration, limiting the initial load and preventing buckling, Thornton (4). The trigger allows a progressive crush to occur whereby the tube splits at mid-thickness around its periphery and fronds form inside and outside (Figure 1). Typically the tube will reach a steady state crush load within 10 mm of applied displacement.

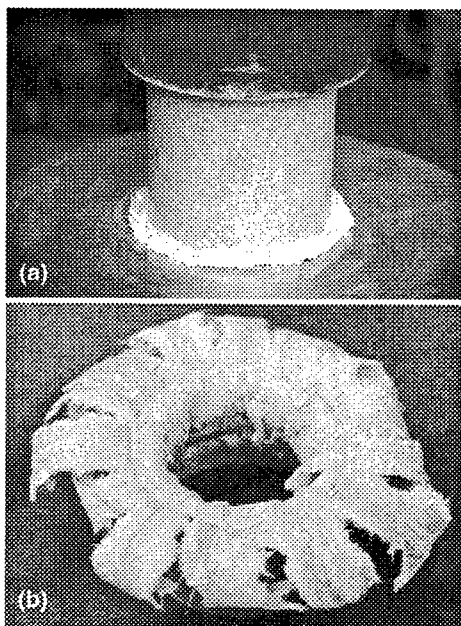


Figure 1. Tube undergoing crush test (a); inner and outer fronds (b)

In-plane tensile, compressive & shear coupon testing are carried out on a 100 kN Instron 1195 electro-mechanical testing machine, to ASTM standards, at 0.5mm/min. Tensile and compressive properties are reported in this paper. A Perkin-Elmer DSC1 differential scanning calorimeter (DSC) is used to ascertain the degree of conversion for the moulded tubes and plaques. All moulded parts are stored in a freezer to prevent further cure taking place before the DSC testing is completed.

## RESULTS

Figure 2 shows load-displacement curves for a typical set of four crushes from one moulding. The graph shows the chamfer being crushed for the first 5 mm. After the formation of a centre-wall crack and steady crush zone, the load increases gradually to the steady-state crush load. SEA values are obtained by taking the area under the load-displacement curve between 5 mm and 50 mm of crush. Knowledge of the mass per unit length allows the specific energy absorption to be calculated. The overall shape of the curve is close to the ideal force-displacement characteristic discussed in the Introduction.

The data presented in Table 2 shows the specific energy absorption (kJ/kg) and standard deviation for 4 samples (A, B, C & D) in each of the 3 mouldings (m1, m2 & m3) made for each configuration (R1, R2, R3 & R4). Averages appear in Figure 3.

The data shows that the 60 minutes post-cure has a significant effect in improving the crush performance. This difference is also seen in the in-plane coupon test data shown in Table 3. The standard deviations and results variability in crushing are higher than those of conventional tests.

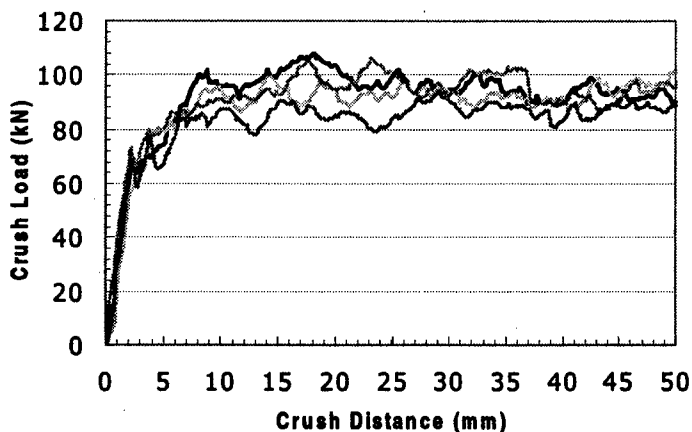


Figure 2. Load-displacement curves showing variation obtained from 4 crush samples extracted from one tube moulded with configuration R2.

<i>Tube</i>	<i>SEA Smpl A (kJ/kg)</i>	<i>SEA Smpl B (kJ/kg)</i>	<i>SEA Smpl C (kJ/kg)</i>	<i>SEA Smpl D (kJ/kg)</i>	<i>SEA Tube Average</i>	<i>Std Dev</i>	<i>SEA Config. Average</i>	<i>Std Dev</i>
R1-m1	21.91	18.71	29.41	31.47	<b>25.37</b>	6.1		
R1-m2	33.87	37.32	26.46	35.01	<b>33.17</b>	4.7		
R1-m3	36.52	30.98	37.55	42.76	<b>36.95</b>	4.8	<b>31.83</b>	5.9
R2-m1	63.40	61.17	56.78	62.69	<b>61.01</b>	3.0		
R2-m2	62.52	62.36	61.49	59.61	<b>61.50</b>	1.5		
R2-m3	51.98	46.64	51.90	56.28	<b>51.70</b>	3.9	<b>58.07</b>	5.5
R3-m1	38.01	21.40	15.83	25.79	<b>25.26</b>	9.4		
R3-m2	40.07	18.93	12.21	21.47	<b>23.17</b>	11.9		
R3-m3	34.24	22.79	21.01	23.25	<b>25.32</b>	6.0	<b>24.58</b>	1.2
R4-m1	54.93	47.67	33.64	55.41	<b>47.91</b>	10.2		
R4-m2	58.41	49.61	36.87	52.06	<b>49.24</b>	9.0		
R4-m3	57.62	28.06	11.90	26.23	<b>30.95</b>	19.2	<b>42.70</b>	10.2

Table 2. Specific energy absorption (kJ/kg) for samples, tubes and configurations. A, B, C & D represent 4 samples taken along the length of 1 tube; m1, m2 & m3 represent three tubes moulded in the same configuration.

The reduction in properties observed with a rise in temperature (configurations R1 and R3, Tables 2 and 3) results from the fact that the catalyst becomes unstable when used at higher temperatures. This was foreseeable as the catalyst used for these tests is known from manufacturer's data to be unstable at 70°C; however these mouldings are part of a larger experimental plan.

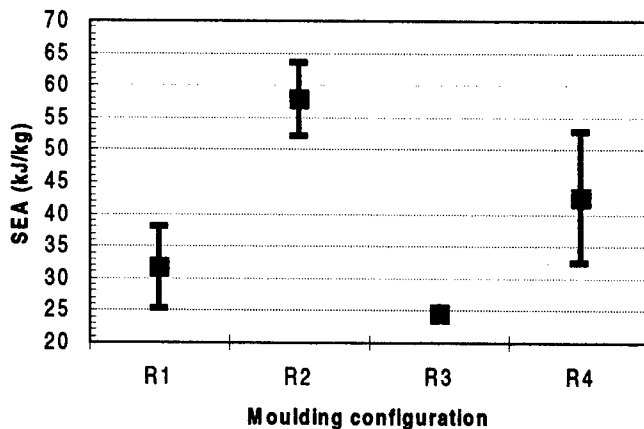


Figure 3. Specific energy absorption for samples moulded at configurations R1 to R4. (error bars represent  $\pm$  standard deviation)

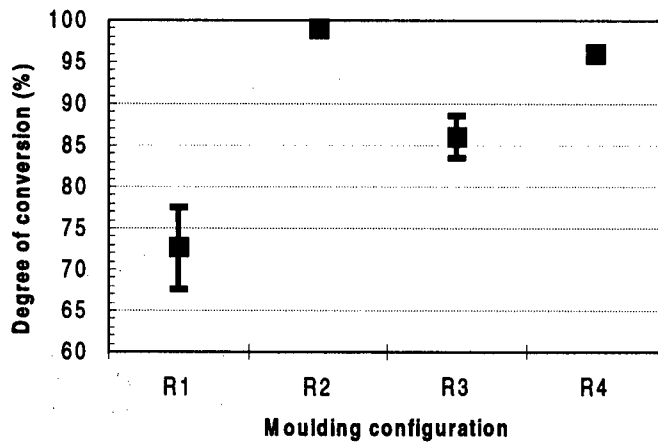


Figure 4. Degree of cure for all samples moulded at configurations R1 to R4.

The DSC results presented in Figure 4 show the average and distribution of the degree of conversion of the neat resin for all samples moulded in configurations R1 to R4. Neat resin samples were taken from the inlet and outlet ends of the mouldings; each point and distribution ranges shown in Figure 3 were generated for 3 mouldings and 3 samples at each end for a total of 18 DSC samples per configuration.

The DSC results show that the cure variability decreases for higher cure levels. They also show that configuration R4, where the moulding temperature is 70°C, actually shows a lower cure than configuration R2 with a moulding temperature of 50°C. Post-curing has a far more significant effect on overall cure levels than higher cure temperatures: mouldings at 50°C followed by a modest 60 minutes post-cure give conversion levels of 99.1%.

In-plane tests have been completed for tensile and compressive loading; results are presented in Figures 5 and 6, and Table 3. Plaques were moulded under the same processing conditions as the tubes and cut on a water-jet cutter. Six samples were taken from each plaque and for each test, three in each direction. There are differences between the two directions, due to the anisotropy of the quasi-random mat used. The 0° identifiers in Figure 5 and 6 and in Table 3 refer to samples of which the main direction is parallel to the resin flow.

The ultimate compressive stress properties presented in Table 3 and Figure 5 show similar trends to the SEA. The modulus data presented in Table 3 and Figure 6 also shows similar general trends to the SEA data. Standard deviations varied from 2% to 20%.

**Ultimate Stress Properties**

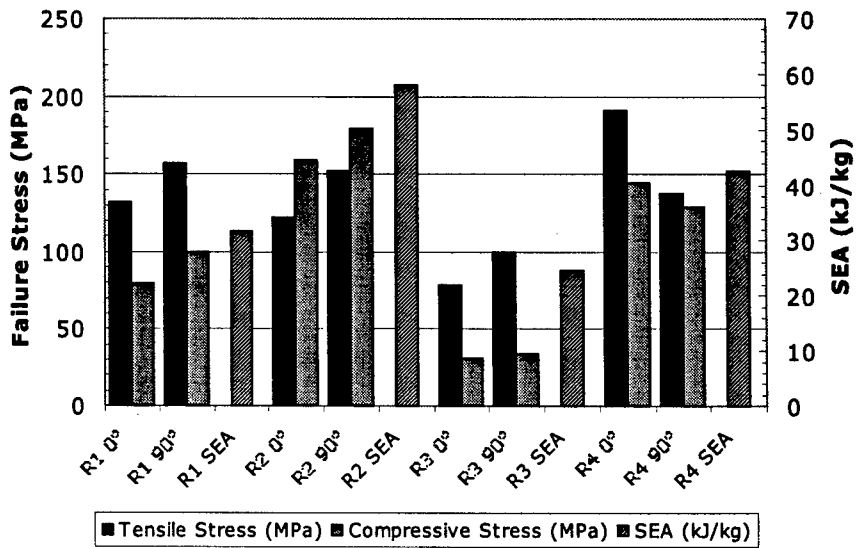


Figure 5. Ultimate stress properties of tensile and compressive plaque samples.

**Tensile & Compressive Moduli**

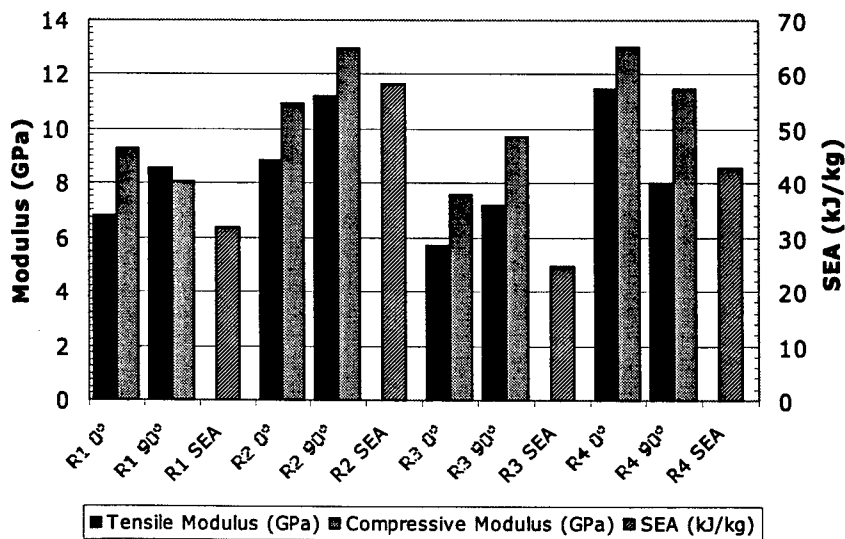


Figure 6. Tensile and compressive moduli for plaque samples.

	<b>SEA (kJ/kg)</b>	<b>Ultimate Stress, Tensile (MPa)</b>	<b>Ultimate Stress, Compressive (MPa)</b>	<b>Tensile Modulus (GPa)</b>	<b>Compressive Modulus (GPa)</b>
R1-0°	31.8	131.6	79.3	6.8	9.3
R1-90°	31.8	157.0	99.5	8.6	8.1
R2-0°	58.1	121.7	159.4	8.8	10.9
R2-90°	58.1	151.7	178.8	11.2	12.9
R3-0°	24.6	79.0	30.5	5.7	7.6
R3-90°	24.6	100.2	33.9	7.2	9.7
R4-0°	42.7	191.3	144.5	11.5	13.0
R4-90°	42.7	137.4	128.5	8.0	11.5

Table 3. Measured in-plane properties.

In order to better characterise the crush mechanism, correlations of various in plane properties to the SEA values were formally investigated. Regression analysis was used and a Student F-test applied. For a given data set, a value of  $f$  is calculated from the error and regression sums of squares. These sums correspond to the residuals and to the general variation present in the data; they are easily calculated, Devore (6). The calculated value of  $f$  is compared to tabulated values of  $F$ . The latter values represent the probability that a true hypothesis is rejected for a significance level  $\alpha$ . Generally speaking, higher  $F$  values correspond to better correlations; these values depend on the sample size and chosen confidence level  $\alpha$ . A smaller value of  $\alpha$  corresponds to a more stringent test and a better correlation.

The results of the correlation analysis appear in Table 4. The critical  $F$ -value for acceptance of the hypothesis for  $\alpha=0.05$  is  $F_{0.05,1,7} = 5.59$ . For  $\alpha=0.01$ , the critical value is  $F_{0.01,1,7} = 12.25$ . None of the hypotheses relating the SEA to the in-plane properties listed in Table 4 (tensile stress, compressive stress, tensile modulus, compressive modulus) can be accepted at a confidence level  $\alpha=0.01$ , although the ultimate compressive stress is close. The ultimate tensile stress shows the faintest correlation. Both moduli pass the test at a lower confidence level of  $\alpha=0.05$ . The data and regressions (dotted lines) appear in Figure 7.

	<b>Ultimate Stress, Tensile (MPa)</b>	<b>Ultimate Stress, Compressive (MPa)</b>	<b>Tensile Modulus (GPa)</b>	<b>Compressive Modulus (GPa)</b>
<b>f value</b>	0.84	12.16	7.55	8.29

Table 4. Correlation coefficients.

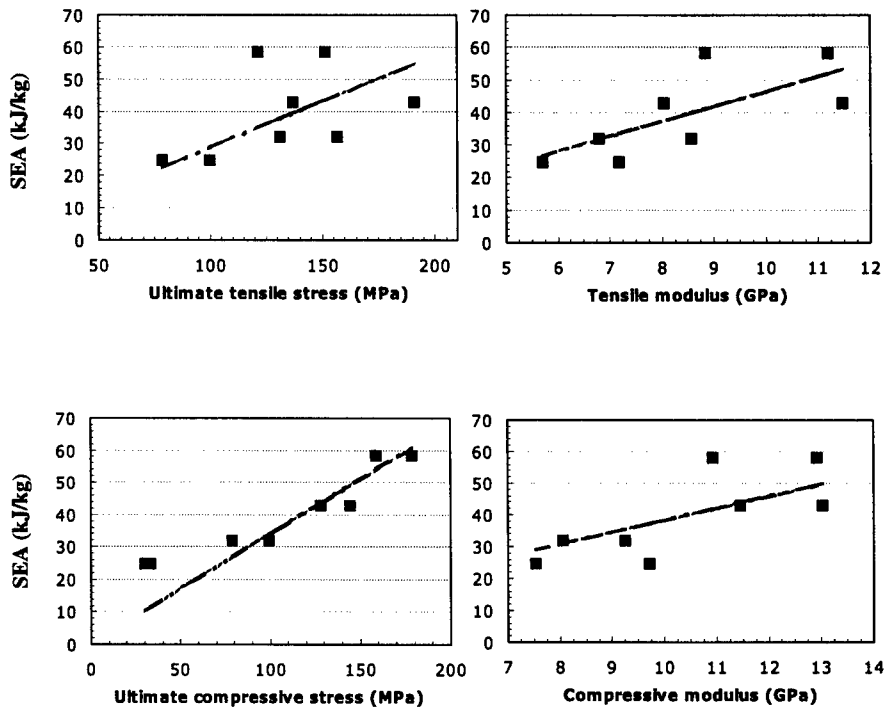


Figure 7. Correlations of the tensile and compressive ultimate stresses and moduli to the specific energy absorption.

## DISCUSSION AND CONCLUSION

Resin properties were seen to have a significant effect on crush performance, independent of other factors such as fibre type and volume fraction. The results demonstrate that very poor energy absorption can result from inappropriate processing strategies and that designed performance may not be realised in practice.

There is a high intrinsic variability in all crush results and to a lesser extent in the in-plane results, although this does improve at higher cure levels. Proper selection of the processing strategy can reduce the variability; hence the present work aims at improving both the performance and its predictability.

It has been established that short post-cures can give high levels of conversion, which has relevance to industrial targets for processing times. Postcure has been shown to be of greater benefit than higher cure temperatures although the extent of this fact will be better established with future results to be determined with the

vinylester resins. Within the limits of the current study compressive ultimate stress has been shown to give the best correlation with final crush properties.

### ACKNOWLEDGEMENTS

The authors gratefully acknowledge the support of the EPSRC MaPEA (Materials Processing for Engineering Applications) programme and the industrial partners: Ford UK, Lotus Cars and Reichhold UK.

### REFERENCES

- 1 Euro-NCAP World Wide Web homepage [www.euro-ncap.com](http://www.euro-ncap.com)
- 2 Farley G L, Journal of Composite Materials 17 (1983) 167
- 3 Hull D, Composites Science and Technology 40 (1991) 377
- 4 Thornton P H, Journal of Composite Materials 13 (1979) 247
- 5 Blears J et al. (Department of Metallurgy and Materials Science, University of Liverpool) 'EAC report. 10' University of Liverpool (1982)
- 6 Devore J L, Probability and Statistics for Engineers and the Sciences, Brooks/Cole (1987)

VACUUM INJECTION MOULDING  
FOR LARGE STRUCTURAL APPLICATIONS

W.D. Brouwer  
E.C.F.C. van Herpt  
M. Labordus  
Centre of Lightweight Structures  
Delft, the Netherlands

1. INTRODUCTION

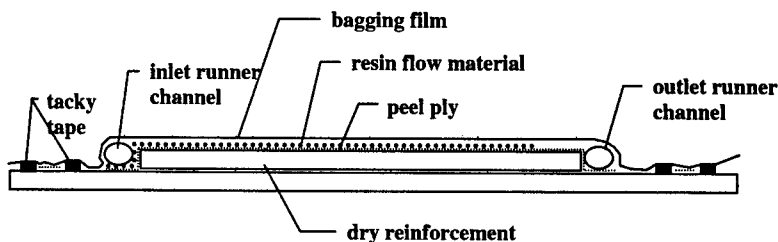
The resin infusion processes are a group of closed mould techniques that enable the manufacture of large structures with high mechanical properties. It is a closed mould technique in which fibrous material is impregnated by a resin flow. Whereas vacuum injection uses vacuum at the outlet side, resin transfer moulding (RTM) uses increased pressure at the inlet. Both techniques are often used for the following reasons;

- Decreasing cost, compared to the traditional handlay-up or autoclaving the labour cost is reduced considerably.
- Increased mechanical properties, high fibre volumes up to 60% are possible while the composite material can be made void free.
- Environment and health. The closed mould technique prevents hazardous styrene emission.

This paper describes the latest technological developments within vacuum injection moulding. First the basic technology is explained and methods are discussed that enable an improved injection in order to produce a void free composite. Then two examples of successful industrial applications are discussed. The first example is a 20 m long rotor blade, where a short cycle time was an important design criterion. Secondly the manufacturing strategy of a 16 m boat hull is explained and it is shown how computer simulations can help with the design.

2. THE RESIN INJECTION TECHNOLOGY

Resin transfer moulding (RTM), Vacuum Assisted Resin Injection (VARI), SCRIMP and resin infusion are various names that describe a process, which is basically very simple: Dry reinforcement is placed in a mould, the mould is closed and resin flows into the mould and impregnates the reinforcement. The driving force for the flow of the resin is a pressure difference.



To fully implement the resin injection technology one needs to understand the basic principle and the possible variations. When injecting a homogeneous material with a resin, the filling time of the injection of a rectangular strip can be calculated by using Darcy's Law (for simple line infusion):

$$\text{fill - time} = \frac{\varphi \cdot \eta \cdot l^2}{2\kappa \cdot \Delta P} \quad (1)$$

ICMAC - International Conference for Manufacturing of Advanced Composites

With	$\phi$	porosity of the reinforcement
	$\kappa$	permeability of the reinforcement
	$\eta$	viscosity of the resin
	$l$	flow distance (length of the strip)
	$\Delta P$	applied pressure difference (constant during the injection)

Eq. (1) clearly shows how different parameters influence the fill time and hence the cycle time of a product. The parameters can be split in:

**Material properties:**

- Resin viscosity.  
The viscosity of the resin is usually limited to 100 to 500 mPas. The filling time is directly related to the viscosity (see equation 1). Consequently there is not much to be gained in trying to optimise resin viscosity.
- Reinforcement porosity and permeability.  
The porosity of most reinforcements used is in between 0.5 and 0.85. The permeability of reinforcements however, can differ greatly. This can be used to optimise fill time (also by applying additional highly permeable feeder materials).

**Product properties:**

Size, volume and shape of the structure (influencing flow distance).

**Process properties:**

- Pressure difference.  
Large products can only be manufactured cost effectively using a vacuum injection technique, since the use of pressure would require very stiff and very costly moulds. This implies that a maximum pressure difference of approximately 1 bar can be achieved.
- Injection strategy (influencing flow distance).

### 3. TOWARDS VOID-FREE PROCESSING

The quality of fibre composites is to a large extent governed by the process parameters and materials used in the manufacturing. One of the more important quality aspects is the void content in the finished part. This is due to the detrimental effect which voids have on many properties, such as mechanical properties, dielectric properties, surface finish, etc. In other words, it is beneficial to keep the void content to a minimum.

Two aspects of voids in composites have attracted most attention, namely, void formation and influence of voids on mechanical properties. Concerning void formation, the main causes are generally due to variations in permeability on a filament and filament bundle scale, outgassing of dissolved gas in the resin, evaporation of volatile components in the resin, shrinkage of the resin and leakage in connections and mould.

One way of reducing the void content is to use degassed resin. There are basically two advantages of using degassed resin:

1. greatly reduced risk of outgassing from the resin
2. increased capability to dissolve bubbles in the resin that are formed during flow.

Ad 1. The gas concentration at equilibrium generally increases linearly with respect to the absolute pressure (Henry's law), where the gas concentration at absolute vacuum is zero.

Thus, for manufacturing methods where the mould is evacuated (vacuum injection, RTM, etc.), it is likely that the resin will become over-saturated with gas when exposed to a lower absolute pressure. For an epoxy resin, it can be measured that the equilibrium gas concentration of nitrogen at atmospheric pressure is approx. 1.7 % by volume. These 1.7 % of dissolved gas may not seem like a considerable amount of gas, but at a vacuum pressure of 20 mbar, which is commonly used in vacuum injection, this would expand 50 times if brought out of solution.

Ad 2. If bubbles are formed during flow due to ill impregnation, and the resin is not yet saturated, the gas from the bubble can dissolve in the resin. The amount of gas, that can dissolve, depends on the saturation level of the resin, the diffusion speed of the gas molecules in solution in relation to the gel-time of the resin, the absolute pressure and of the characteristics of the gas-resin system.

The standard procedure to degas resin is simply to expose the resin to partial vacuum. The idea is to make use of the fact that the gas solubility decreases as the pressure is reduced (Henry's law), where at absolute vacuum the gas solubility is zero. So, if the pressure is decreased, at a certain moment, the resin will become over-saturated and gas should come out of solution. But the dissolved gas is dispersed as molecules and not as bubbles. Therefore, gas will only come out of solution if bubbles or bubble nuclei are already present in the resin. What in fact will happen when the pressure is reduced, is that the bubbles, which have been whipped in during mixing of the resin, will increase in size (Gas Law). With increasing size, the rising speed of the bubbles also increases (Archimedes' Law). This will result in a foaming resin, suggesting that the resin is being degassed. In fact, the resin is mainly "de-bubbled"! Of course, some of the dissolved gas will indeed diffuse into these rising bubbles which resulted from mixing or pouring the resin in a different container thereby entrapping air in scratches or imperfections in the container. If no bubbles or bubble nucleation sites have been added, the standard degassing procedure will not cause any outgassing at all.

So, standard degassing is highly questionable if performed by simply reducing the pressure. If no bubble nucleation sites or bubbles are present there will not be any outgassing.

Two other methods for degassing the resin are more effective:

#### **adding nucleation material**

Vacuum injection experiments with different fibre reinforcement materials have shown quite a different void content and void distribution. The main cause of voids with these experiments was outgassing of the resin. Apparently, some reinforcement materials (like Unifilo™) exhibit better bubble nucleation properties than other materials, and therefore will result in laminates with a higher void content. This material contains bubble nuclei as entrapped air in cavities.

The difference in gas concentration between the entrapped air and the dissolved gas causes gas molecules to diffuse from the resin into the entrapped air.

So the trick is to bring the resin into contact with such a nucleation material at reduced pressure prior to the actual injection. This leads to a much more effective degassing procedure and a better laminate quality during and after injection.

Materials that have been proven to be very effective are Scotch Brite and Unifilo glass mat

#### **sparging**

A container is filled with resin. The pressure in this container is reduced to a pressure below the injection pressure to be used during the vacuum injection process. At the bottom, air is fed into this container. The air is forced through a very fine filter, thus creating many small bubbles. These bubbles rise through the resin. At the reduced pressure, the resin will be over-saturated with air (or components of air). The difference in gas concentration between the air bubble and the dissolved gas causes gas molecules to diffuse from the resin into the bubble. This process continues until a new equilibrium situation is reached, e.g. the resin is saturated (but no longer over-saturated) with air.

If degassed resin (either by adding a nucleation material during degassing or by sparging) is used during the vacuum injection process, and the injection pressure is higher than the degassing pressure, there is no risk of outgassing of the resin. There will even be the possibility of dissolving some bubbles, which have been formed during the flow of resin, entrapping air in fibre bundles.

#### 4. EXAMPLE 1. THE 20 METER ROTOR BLADE

The competition between composite rotor blade manufacturers force them to highly optimise engineering and production procedures. The time-to-market of new types of rotor blades is very short. Every year the blade's length is increased by several meters reacting on the market demands for higher energy output. Current LM Glassfibre Holland rotor blades are shown in fig. 1. The turbine has three rotor blades with a length of approximately 20 m. Fig. 2 shows a worker inspecting the joint of the root to the axle.

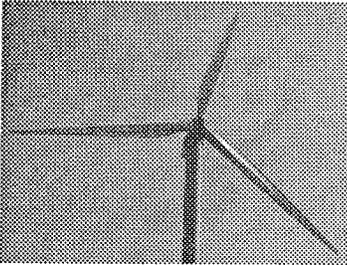


Fig. 1 A current LM wind turbine with rotor blades of approx. 20 m long

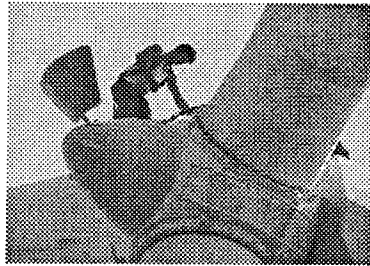


Fig. 2 A worker inspecting the root of the rotor blade

The rotor blades shown in fig. 1 and 2 are made of two shells consisting of 1200 kg vinyl-ester resin, 1300 kg of glass fibre reinforcement (approx. 75% unidirectional and 25%  $\pm 45^\circ$  fabrics) and PVC foam core. The shells are bonded together with adhesives.

Optimisation of the production processes is necessary due to required short cycle times and the protection of workshop personnel and the environment; the allowed emission of styrene from vinyl-ester resins (conventionally processed with open mould techniques) has recently been decreased in the Netherlands. So, sound and fast production is the driving force for innovative production methods like vacuum injection.

Two years ago LM and Centre of Lightweight Structures TUD-TNO co-operated in a project that aimed an industrial implementation of the vacuum injection technique into the workshops of the composites processing company. Key issue in this implementation was the choice of the right processing strategy in combination with the materials used. For a product of this size this determines whether a reliable and quick manufacture can be assured.

Fig. 3 shows the root of the rotor blade (the part nears to the axle) just before the vacuum injection process is started. The glass fibre reinforcement (the white material along the edges) lies in the mould; it is covered successively with a release fabric (not visible), a flow enhancing knitted fabric, a runner and a nylon film. The film is sealed on the mould flanges with tacky tape. A vacuum is applied between mould and film, so the complete lay-up is compressed in the mould.

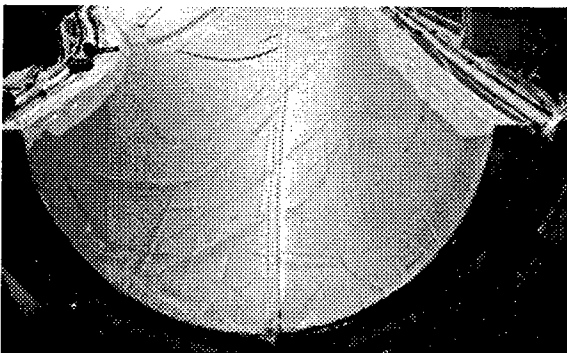


Fig. 3 The root of the rotor blade just before the vacuum injection process starts

ICMAC - International Conference for Manufacturing of Advanced Composites

A liquid vinyl-ester resin will be flowing from a resin container through the runner in the length of the mould. The resin then flows through the flow enhancing knitted fabric into the reinforcement while impregnating the fibre bundles completely. This process is shown in fig. 4 in which the two flow fronts are visible on both sides of the runner. In the left bottom corner the sealing is visible. The filling of the mould takes approximately 1 hour. After the cure of the resin the rotor blade half can be released from the mould.

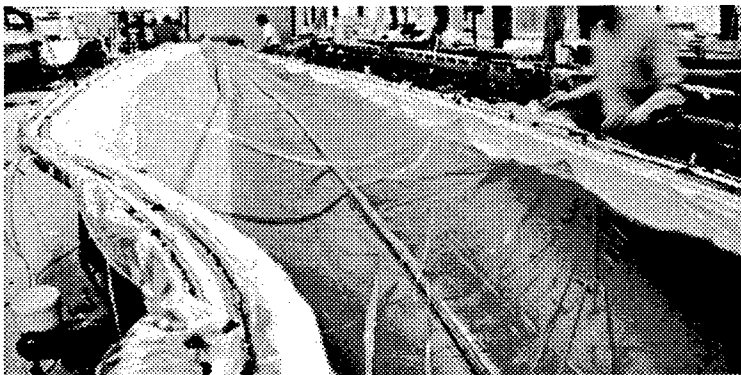
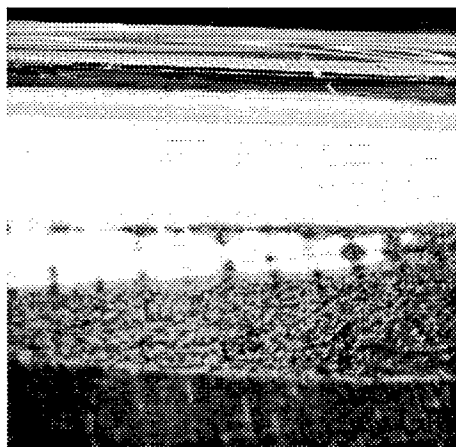


Fig. 4 One rotor blade half during vacuum injection.

Fig. 5 shows a detail of the sandwich part in the rotor blade. The sandwich structure is left in the rotor blade of fig. 4, between the flow front and the left mould edge. So, the resin is just entering the foam core. The core consists of small square blocks of PVC foam on a fabric back. Consequently, small channels are present between the blocks in which the resin can flow rapidly. These channels thus support fast mould filling.



- ← nylon film
- ← sealing between film and mould flange
- ← glass fibre reinforcement
- ← small channels in PVC foam core being filled with resin
- ← 'impregnated' foam core
- ← flow enhancing knitted fabric with resin

Fig. 5 Cross section of the wind turbine sandwich

## 5. EXAMPLE 2. INJECTION STRATEGIES FOR A BOAT STRUCTURE

Below a main part of a boat will be discussed in detail: the hull-shell.

The Contest 55 hull is both a long (16.4 m), wide (4.5 m) and high (2.5 m) product to inject in one shot. The height results in a hydrostatic pressure difference which results in a lower driving force for the injection. There are three basic variations possible on the edge injection strategy to distinguish:

1. Edge injection downward
2. Edge injection upward
3. Edge injection sideways

The injection downward is not preferred for two reasons. Firstly, bubbles in the resin and laminate will be entrapped more easily and secondly, there is higher risk on the occurrence of dry spots due to racetracking of the resin through highly permeable runner channels.

The injection upward can only be carried out with sequential injection channels (otherwise injection time will be too long). This however, would result in about 10 sequential injection channels each of which need to be controlled and opened at the right time.

Based on the requirement to have a simple process there was a clear preference for an injection with a grid of injection channels in which the majority of the channels would allow for a sideways injection. This would allow for one single resin inlet port (and consequently also one resin tank level to control). This grid would consist of a main injection channel running from the stern to the bow (via the keel) and branches of channels from the main channel in the keel to the flange (with the deck). The overall injection channel pattern is shown in Fig. 6 (from the Dutch mould filling simulation software RTM-worx).

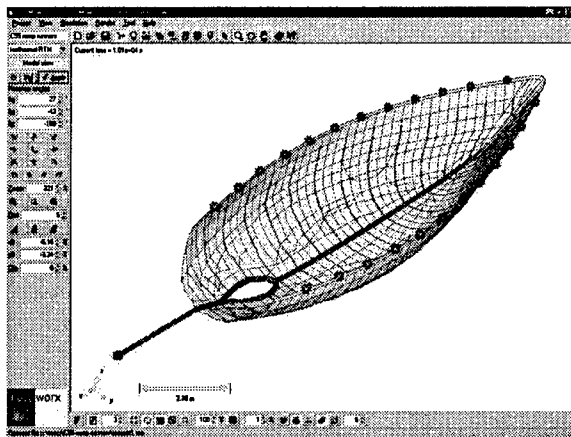
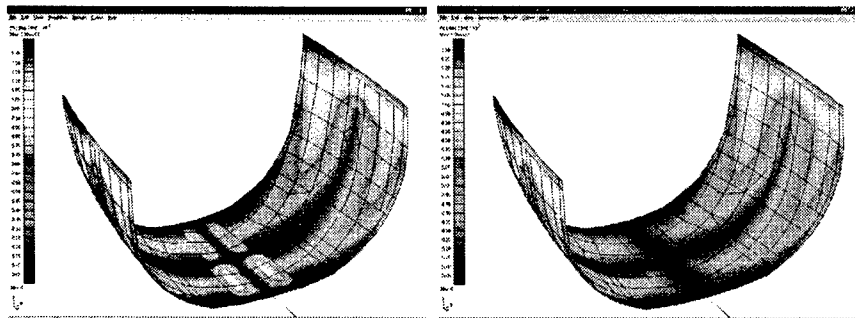


Fig. 6: The injection strategy and position of the injection channels.

Based on the overall chosen injection strategy we must verify that there are no local details, which can cause the formation of dry spots or else, disturb the injection. The Balsa core was sufficiently permeable. Therefore there was no additional feeder material required on all laminates containing Balsa. However, the laminate used in the keel would have a low overall permeability. In addition there is a substantial thickness change. This could cause dry spots on the keel, which were clearly shown using flow-front simulations. Figures 7 and 8 show the simulations done without (Fig. 7) and with (Fig. 8) additional feeder material on top of the reinforcement. A small scale experiment was carried out to validate this simulation result.



**Fig. 7:** Part of the hull with dry spot formation at the location of the keel.

**Fig. 8:** Part of the hull without dry spot formation.

A small part of the hull laminate was injected on a flat plate. This part consisted of the keel laminate (partly with and partly without additional feeder material) and the balsa sandwich laminate shown in Fig. 9. It was injected using a main injection channel at the edge of the keel laminate and an injection channel branch in the middle of the laminate. The carefully registered flow-front proved the occurrence of a dry spot on the part without the feeder material and the absence of a dry spot on the part with the additional feeder material.

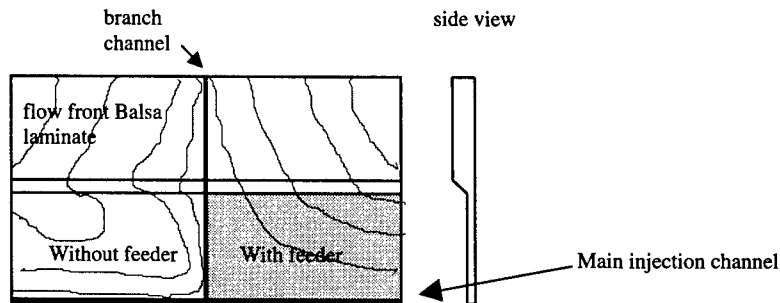


**Fig. 9:** Test injection set up and resulting flow front.

To determine the injection strategy of a part with many edges one must consider that every edge can lead to a highly permeable channel, causing resin racetracking. The least and most favourable situation will occur when the resin flow-front is progressing perpendicular and, respectively, parallel to the runner channel. This is shown in Fig. 10 and Fig. 11. When the resin flow-front is perpendicular with the runner channel the flow-front will be disturbed and the resin will flow much faster through the runner channel (shown in Fig. 10). In Fig. 11 it can be clearly seen that a runner channel, parallel to the flow-front will not cause disturbances of the resin flow front. When using simulation software to identify the filling pattern of a complex structure one must realise that runner channels can occur. This should be included in the simulation of the filling pattern.

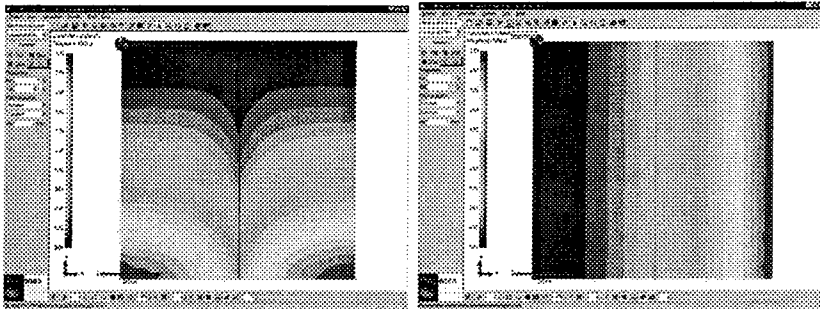


**Fig. 10:** Disturbance of resin flow-front due to a runner channel perpendicular to the flow-front.

**Fig. 11:** No disturbance of resin flow-front due to a runner channel parallel to the flow-front.

Concluding one can say that a successful injection of a large structural components is mainly determined by the following aspects:

- 1) the geometry of the product,
- 2) the materials used in the product,
- 3) the injection tooling and materials
- 4) the injection strategy

The first two often can't be changed because it is prescribed by the structural design. But with the right tooling and strategy it has been proven that very large and complex structures can be manufactured in a one shot vacuum infusion process.

Below the actual injection of the boat hull and the release from the mould are shown.



**Fig. 12:** Half way the injection process

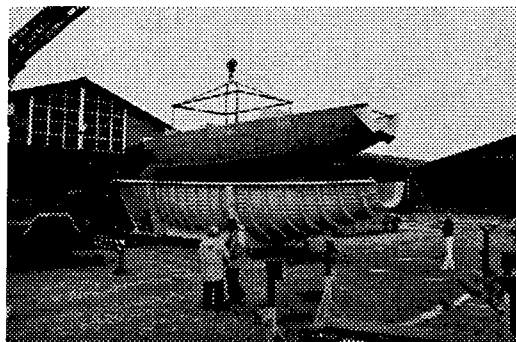


**Fig. 13:** Release from the mould

## **POSTERS**

**AUTOMATED PREFORM MANUFACTURE: ROBOTIC HANDLING, IN-SITU  
MEASUREMENT OF PROPERTIES AND LAY-UP SIMULATIONS**

**Prasad Potluri**

**Textile Composites Group, Department of Textiles  
UMIST, Manchester, UK**

**ABSTRACT**

The paper presents some important issues related to automated manufacture of low cost composites. The process of cutting fabric panels from broadcloth and assembling individual pieces had its origins in the clothing industry. The paper investigates the advances made, and the problems encountered in clothing automation projects during 1980s, with a view to adopt some of the relevant techniques to composites manufacture. Handling and subsequent processing of laminate materials is characterised by their non-linear limp behaviour. Process simulation has been identified as a key step towards full-scale automation. The paper describes some automated test methods for measuring the non-linear material properties, required as constitutive properties for simulations. A commercial robot conducts a series of tests on a dry laminate material. The tests include in plane shear, thickness compression, tensile, bending and friction. Process simulations such as laying-up, fabric folding and draping were conducted, based on the measured properties.

**INTRODUCTION**

While substantial progress has been made in automating the resin impregnation and moulding processes, preform assembly and subsequent handling is still performed manually. A number of research groups developed 3D textile preforms; these preforms are generally difficult to drape over surfaces with large curvature, have limited flexibility in changing local thickness and the fibre-orientations, and exhibit poor resin permeability. Composite preforms will continue to be manufactured by assembling individual plies, cut from broadcloth. In order to make substantial increase in the use of composites in cost-sensitive markets, such as the Automotive industry, composites manufacturing should be fully automated.

Mills (1) identified three important areas for developing affordable composites for aerospace applications; to replace prepreg with lower cost materials, to automate material deposition and to produce components moulded to net thickness. Clearly there is a trend towards using dry fabrics in place of prepregs. Complete automation of the preform manufacture will result in improved repeatability and reduced cycle times. However, very limited work has been reported in this area (2,3,4). Sarhadi (2) and his team developed automated handling techniques from their experience from clothing automation. In fact, extensive research work was conducted in 80's to automate the clothing industry; some relevant issues are presented in the next section. Rudd (3) reported a study on robotic tow placement to create near net preforms. This technique can also be used in conjunction with dry fabric plies to create local reinforcements.

## CLOTHING AUTOMATION

In the early 80s, major research programmes were initiated to automate the clothing industry, as a response to stiff competition from the low-wage countries. Significant national programmes included Japan's National Apparel Automation project (5), TC<sup>2</sup> project in USA (6). In Europe, a number of university-based research projects (7,8,9,10) were initiated. The issues addressed in these research projects have a direct relevance to composites manufacture.

Garment production typically involves four distinct steps; fabric cutting, de-stacking/ ply-separation, handling/ transportation of the fabric panels and sewing/ making-up. Automated fabric cutting systems are very well developed in the clothing industry. Recently, this technology is being used for cutting single layers of carbon fabrics, using mechanical or laser cutting devices, in the Aerospace Industry. In the clothing industry, many layers of fabric are cut as a single bundle; separating a single piece of fabric from the bundle is the most difficult task to automate. Ply separation devices were developed based on techniques like blowing a jet of air (11), electro-adhesion (12), chemical adhesion (13), piercing pins (14), and a human finger-like arrangement (15).

While these projects resulted in sophisticated robotic systems, full-scale automation in the clothing industry did not materialise due to an important technical limitation; de-stacking a single ply from a large bundle could not be achieved reliably, and cutting individual plies is not economical in apparel manufacture. However, in composites industry, mainly single plies are cut using either mechanical or laser cutters, and hence this process is amenable to full scale automation.

Following observations can be made from the clothing automation research:

- Ply cutting systems are very well established in clothing industry and, more recently composites industry (16). A variety of cutting technologies, including mechanical, laser and water jet, originally developed for the apparel market, are being employed to cut composite plies.
- In clothing industry, a large number of fabric layers are cut together. De-stacking or ply separation was the single most reason for the failure of clothing automation. However, it is economical to cut single plies in the composites industry, and hence ply separation is not an issue.
- Fabrics are flexible limp materials and readily buckle with small compressive loads (due to gravity). Prior knowledge of the mechanical properties of the fabrics is important for the successful implementation of automated handling (17).
- A number of devices were developed to transport a fabric panel to a joining station. Vacuum grippers (18), friction plates (19) and electro-static (2) grippers hold the entire fabric surface and hence suitable for relatively small pieces. These grippers are bulky for relatively large fabric panels. These panels may be clamping at an edge and dropped gradually on to a horizontal surface (20).

## PROCESS SIMULATIONS

Traditionally, laminate plies are laid by hand either on a flat surface or directly on a mould surface. A number of plies are laid one on top of the other in the required orientations to assemble a stack. Fabrics exhibit highly non-linear behaviour and readily bend and buckle under their own weight. Relatively large fabric plies should be lifted from a cutting table without excessive distortions. Similarly, fabric plies should be positioned on an existing stack without distorting the underlying layers. The laying process requires skill and dexterity and hence cannot be easily replicated by a robotic device.

In the present work, a large deformation modelling technique (21) was employed to simulate lifting and laying fabric panels (figure 1 and figure 2). The modelling technique takes into consideration the weight per unit area and the non-linear bending moment versus curvature relationship of the fabric panels. Figure 1 shows the lifting sequence (1,2 ...14). Similar sequence, in the reverse order, can be used for placing a fabric on a table/ mould surface. A robot, equipped with a gripping device, should be programmed to follow the sequence. At each position, robot gripper should be positioned and oriented to align with the fabric tip to ensure distortion-free handling.

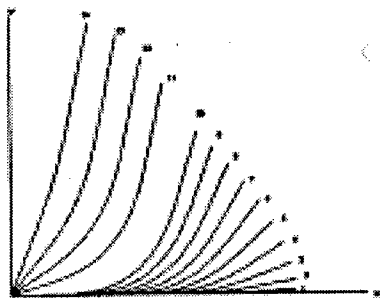


**Fig 1: Simulation of fabric lifting or placement sequence.**

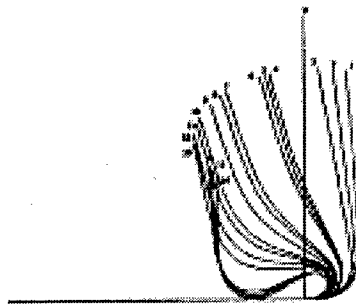


**Fig 2: Simulation of folding sequence**

Multi-layered preforms may also be produced by folding a fabric panel (22); the preform width for each layer can be changed to achieve 3D variation in the thickness direction. Fold simulations are shown in fig 2 and fig. 3. The fold geometry depends on the fabric bending stiffness, which in turn can affect the final width, after compaction. Again, robot trajectory can be programmed, using the above simulations, to achieve a distortion free folding.

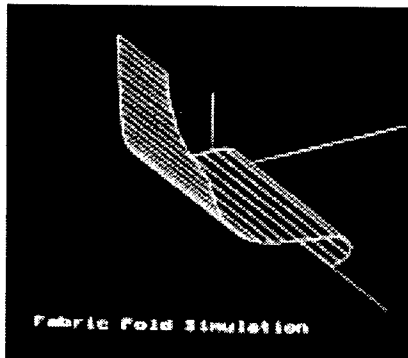


Fig 3: Fabric fold simulation

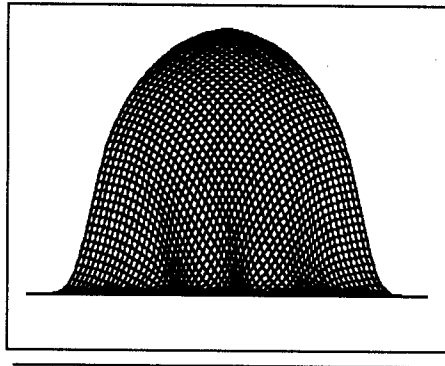


Fig 4: Drape simulation

Fabric panels are draped onto double curvature mould surfaces, before injecting the resin or thermoforming. Forming simulation is performed using kinematic drape algorithms (23), ignoring the forces involved during the forming process. Explicit FEM codes such as PAM-FORM may be used for simulating thermoforming process (24), taking into consideration the non-linear tensile, bending, shear and frictional behaviour of the ply material. The key to such simulations is the accurate measurement of mechanical properties. The next section presents an automated approach for measuring the mechanical properties required for simulation.

#### AUTOMATED TESTING

The quality of process simulations, described in the previous section, depend on the accurate measurement of non-linear material properties. While majority of the traditional tests are conducted until failure, simulations require the properties in the low stress regions. These tests can be potentially conducted during the material handling process, thus enabling rapid acquisition of data. Automated in-process measurement is particularly suitable because of the number of geometrical and material variables involved in the simulations; any change in the specifications would need a fresh run of the simulations. Cartwright (24) proposed some experimental tests for evaluating the ply properties, in order to accurately simulate the manufacturing processes, such as thermo-forming. They identified inter-ply shearing, intra-ply shearing and out-of plane bending as the three important properties that should be measured accurately.

In the present work, a commercial robot arm is employed for conducting various mechanical tests. The manipulator (fig 5) is equipped with a 3-axis load cell and a pneumatic gripping device. With the aid of a fixed clamp and a fabric manipulation attachment, the robot applies a series of load cycles on a ply material. This is a flexible system and hence can potentially conduct a variety of tests, under any specified test conditions. The force data in three directions is acquired through a data acquisition system, and the strain data is computed from the manipulator displacements in Cartesian space (19).

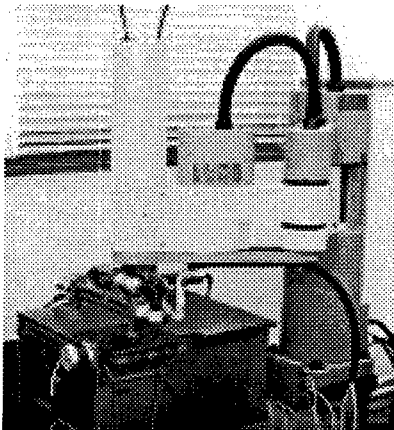


Fig 5: Robotic tester

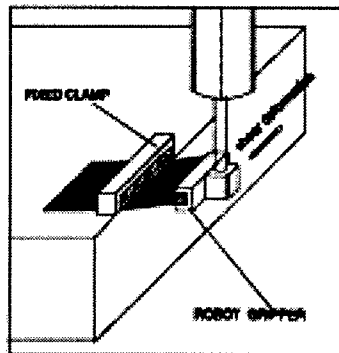


Fig 6: Shear and Tensile Tests

Following tests have been identified:

1. Shear test: measures the intra-ply shear stiffness and shear limit. This data is important for conducting drape simulations.
2. Bending test: measures a non-linear bending moment versus curvature relation. Bending stiffness is important for the simulation of moulding or thermoforming processes (24)
3. Friction test: measures inter-ply shear forces or frictional force between a ply and the tool surface (24)
4. Compression test measures the ply thickness under a specified pressure. This data is important for producing components moulded to net thickness (1)
5. Tensile test measures the ply extensibility under a specified load. This information is important for highly mouldable materials such as knitted preforms.

Figure 6 shows the test scheme for conducting a shear test. A fabric panel is positioned inside a fixed pneumatic clamp, using a manipulation device attached to the robot arm. The fabric is then clamped between the fixed clamp and the robot gripper. For conducting a shear test, the robot gripper is moved sideways along a circular trajectory, while maintaining a small tension to avoid fabric buckling. The resulting shear force versus shear strain relationship is recorded as shown in figure 7. The shear test can be conducted until the shear lock limit. A similar arrangement can be used for measuring the tensile force versus strain data, by moving the gripper away from the fixed clamp at a pre-determined strain rate. The test parameters such as the effective sample length and the strain rate can be readily hanged to suit a variety of ply materials.

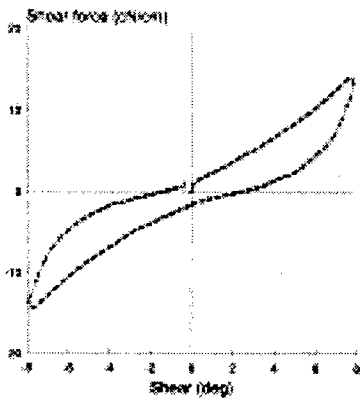


Fig 7: Shear force vs shear strain

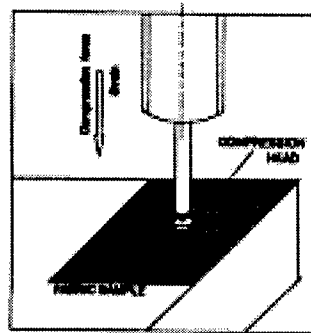


Fig. 8: Compression test

The compression test, as shown in figure 8, is a relatively simple test to conduct. A circular compression head, attached to the end of the robot arm, gradually applies pressure on a single ply or on a final assembly, and the resulting thickness is recorded. Figure 9 shows the pressure versus thickness graph. Because of the nesting phenomena, thickness of the final assembly cannot be accurately predicted from the individual plies. For accurate control of the final thickness and fibre volume fractions, thickness should be measured on the final assembly, at a number of locations.

Figure 10 shows the arrangement for conducting cantilever-bending tests on fabrics. A manipulation device, attached to the robot, pushes the fabric ply over an edge resulting in the formation of a cantilever, with a large deformation. A retro-reflective sensor, attached to a stepper motor, tracks the fabric edge to measure the bending angle for each cantilever position. As a result, a series of bending lengths and bending angles are measured during a test. Figure 11 shows the simulation of fabric cantilevers, for each bending angle and bending length. Using this data and the fabric weight per unit area, the non-linear moment-curvature relation, as shown in figure 12, can be computed using a numerical technique developed by the author (25). Moulding or thermoforming simulations performed using a non-linear bending model would be more accurate in comparison to the assumption of a linear model. The bending test can also be conducted on fabric panels with any arbitrary geometry, and hence ideally suited for in-situ measurement.

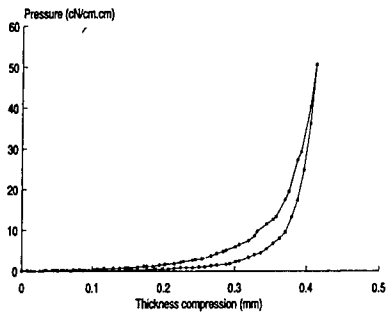


Fig 9: Pressure vs thickness graph

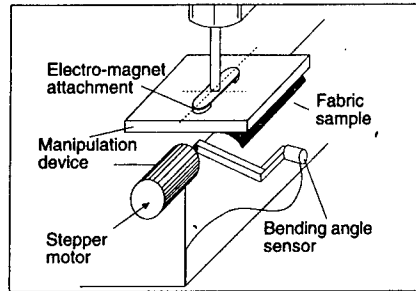


Fig 10: Non-linear bending test

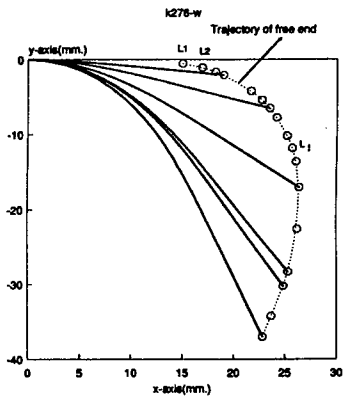


Fig 11: simulation of cantilever bending

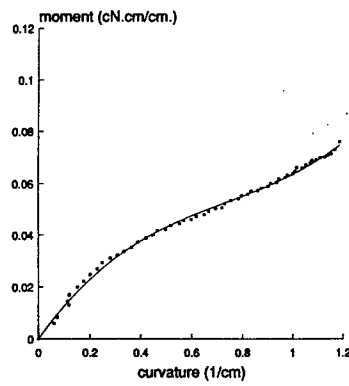


Fig 12: Non-linear moment curvature relation

A friction test is conducted, as shown in figure 13, for assessing the shear force between the mould surface and a fabric ply. A metallic contactor, attached to the robot arm, is dragged on the fabric surface and the resulting frictional force is measured using the three-axis load cell. Inter-ply shear force can also be measured using this equipment. This test can be conducted by placing a dead weight on two fabric layers and pulling the top layer with respect to the bottom layer.

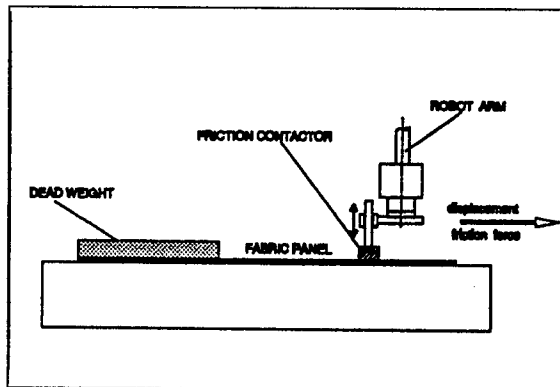


Fig 13: Friction test

## CONCLUSIONS

Further growth in composites will depend on the reduction of manufacturing costs. This can be achieved by automating the preform assembly process to complement the advances made in automating the moulding/resin impregnation processes. The paper investigates the possibility of adopting some of the gripping and handling techniques developed in the clothing industry. While these techniques were not highly satisfactory in handling relatively flimsy (eg single jersey) textile materials at commercial manufacturing speeds, composites industry offers a better chance for the following reasons:

- Composite plies are cut in single layers and hence ply separation is not issue.
- Prepregs and dry fabric laminates are relatively stable and hence easy to handle.
- Manufacturing cycle times are much higher in composites industry and hence further improvements are possible, where as it was difficult to reduce the cycle times in the clothing industry.

Process simulation is the key to the successful implementation of automation. Simulation of Robot trajectory, with the help of a large deformation modelling technique, helps to minimise the ply distortions during lay-up. The paper presents an automated approach to measuring the constitutive material properties required for simulations.

REFERENCES

1. Mills A, Composites: Part A 32(2001) 955
2. Zang Z, Sarhadi M, Journal of Material Processing Technology, 61 (1996) 104
3. Rudd C D, Turner M R, Long AC, Middleton V, Composites A: 30 (1999) 1105
4. Stuart M J, Johnson N J, Dexter H B, Marchello J M, Grenoble R W, 'Automated fabrication technologies for high performance polymer composites', AGARD Spring 98 Workshop on Intelligent processing of high performance materials, Brussels, May 11, 1998.
5. Ogawa SD, Japan's Automated Sewing System: A National research and design project, Bobbin, 25 (1984) 82
6. Abernathy, F H, Pippins D, (TC)<sup>2</sup> Apparel, Textile and Education at its best, Bobbin, 28 (1986) 162
7. Greshon D and Porat I, Robotic sewing using multi sensory feedback, 16<sup>th</sup> International Symposium on Intelligent Robotics, Brussels, (1986) 338
8. Edberg B and Nilsson N, Computerised Clothing Manufacturing: A means for survival, Proc. Annual World Conf., The Textile Institute, May 1985
9. Lower J M, Bobbin, 26 (1985) 78
10. Kemp D R, Taylor G E, Taylor P M, Pugh A, Robot Grippers (ed. Pham D T and Heginbotham W), IFS publishing, 1986
11. Kemp D R., Taylor G E., Taylor P M. and Pugh A., 'A sensory gripper for handling textiles' in Robot Grippers (Ed by Pham D T. and Heginbotham W B.), IFS (1986)
12. Monkman G J, Taylor P M, Farnworth G J, International Journal of Clothing Science and Technology, 1 (1989) 14.
13. Monkman G J, Shimmin C, International Journal of Clothing Science and Technology, 3 (1991) 6.
14. Sarhadi M, Nicholson PR, Simmons JE, Advances in gripper technology for apparel manufacturing, Proceedings of the Institution of Mechanical Engineers: UK Research in Advanced Manufacture, paper C372/86, London, Dec 1986, pp 47-53.
15. Ono E and Aisaka N, International J of Clothing Science & Technology, 4 (1992)16
16. Gerber Technology: [www.gerbertechnology.com](http://www.gerbertechnology.com)
17. Brown P R, Buchanan, Clapp T G, Journal of the Textile Institute, 81 (1990) 1.
18. Nicholson PR, Sarhadi M, 'Flexible porous materials handling in a CIM environment', in Production Research: Approaching the 21<sup>st</sup> Century (ed. Pridham M and O'Brien C) Taylor & Francis Ltd, 1991.
19. Potluri P, Atkinson J, Porat I, Mechatronics, 5 (1995) 245.
20. Gunner M B and Taylor P M, Placing fabrics on to moving surfaces, 1<sup>st</sup> Int. Clothing Conference, Bradford, UK, 1990.
21. Potluri P, Porat I and Atkinson J, Journal of the Textile Institute, 87 (1996)
22. Tewfic T, Sarhadi M, Novel folding device for manufacturing aerospace composite structures, Proceedings of SPIE-The International Society for Optical Engineering, 4192 (2000), 212.
23. Ramgulam R, PhD thesis, UMIST (1999).
24. Cartwright BK, de Luca P, Wang J, Stellbrink K and Paton R, Some proposed experimental tests for use in finite element simulation of composite forming, ICCM 12, Paris 1999.
25. Potluri P, Robotic testing of low-stress mechanical properties of fabrics, PhD Thesis, UMIST (1995)

**BIAS EXTENSION MEASUREMENTS ON DRY AND PREIMPREGNATED NON-CRIMP FABRIC CARBON FIBRE REINFORCEMENT**

**Kevin Potter.**

**Aerospace Engineering Department. University of Bristol.**

**ABSTRACT**

The behaviour of woven reinforcements has been extensively studied under conditions of bias extension in the dry state, and to a lesser extent in the preimpregnated condition. The work reported here covers the measurement of the deformation characteristics of a non-crimped carbon fibre reinforcement fabric under various conditions of impregnation. The results show that for the sample sizes tested the behaviour of the NCF material exhibits major deviations from the predictions of the pin-jointed-net model developed for woven cloth.

**INTRODUCTION**

Woven reinforcement has proven to be very important in the manufacture of composite components and can be used as part of a cost control strategy. The reasons for this are tied up with both the level of, and uniformity of, the mechanical properties that can be achieved, and with the ease with which the material can be handled and applied to the mould. Unidirectional prepreg requires great care in hand lay-up to ensure that it conforms to the tool surface without wrinkling or bridging being generated. Equally, if an error is made in lay-up, the prepreg will have to be discarded as the deformations in unidirectional prepreg are irreversible, ref 1. These factors increase the costs of high quality manufacture using this material. Woven material is much easier to handle and apply to a tool surface than unidirectional prepreg and if any errors are made the reversibility of the deformation in this material means that the errors are correctable without discarding the material, ref 1. These advantages of woven cloth have led to the widespread use of this material and a substantial effort has gone in to understanding and modelling the behaviour of woven cloth as it is deformed over a given mould surface or other geometry. The centrepiece of this understanding is the pin-jointed net model and all analytical approaches incorporate this model into their calculations, in some cases with additional effects such as tow slippage, refs 2/3/4. With the increasing emphasis on cost reduction there has been a drive towards the mechanical forming of stacks of reinforcement rather than hand lay-up, using several different approaches, e.g. ref 5. In this case the reversibility of the deformation of woven cloth is no longer relevant and the very sharp increase in the forming loads as the warp and weft begin to interact strongly can be a positive disadvantage. Materials which lack the fixed kinematic link between warp and weft might have some advantages in this case, as additional deformation could be available compared to that possible with woven cloth. It has been demonstrated that the global behaviour of cross-plyed stacks of UD prepreg also obeys the pin-jointed-net model, although the details of the deformation processes are different and no true kinematic link exists between the layers of prepreg, ref 6. Another reinforcement form that has been identified as having potential for cost saving is non-crimp fabrics (NCF). These are made by incorporating rows of (generally knitted) stitches to hold together multiple layers of reinforcement. These reinforcements may be much heavier than conventional cloths or UD prepreg, the reduced ply count arising from this being another source of potential cost saving. The work reported here discusses the performance of one type of NCF under conditions of bias extension and compares this performance to the predictions of the pin-jointed-net model.

Measurements have been carried out in three different conditions, which might relate to three different fabrication routes.

## MATERIALS

Saertex: +/-45 carbon fibre, 4 layer NCF, 586gsm with 6gsm PES chain stitching at 45° to the fibre directions. The geometry of the cloth was as shown in fig 1.

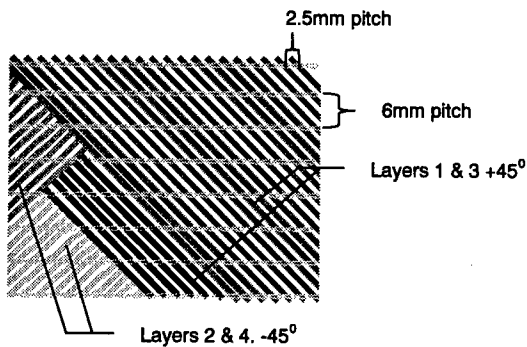


Fig 1. Structure of NCF cloth tested

This material was tested both along the PES knit direction and perpendicular to this direction.

The tests were carried out as received; impregnated with Hexcel 913 resin film; and as semi-preg. The material might be used in the as-received state (with the addition of a small amount of powder binder) in the production of press-moulded preforms for RTM; in the semi-pregged state (i.e. with resin films bonded to the surface) in the RFI process; and in the fully impregnated state for hand lay-up or diaphragm forming.

Hexcel 913 film was used for full and partial impregnations. The film was of 42 gsm and 4 films were applied to each side of the fabric. Total weight of 913 resin was 336gsm giving a prepreg of 36% by weight resin.

Full impregnation was carried out for 30 minutes at 60C under full vacuum.

Semi-preg (partial impregnation) was made by applying films as before, but only applying vacuum for 10 minutes at room temperature.

### Sample types.

Stitched direction dry, stitched direction impregnated, stitched direction semi-impregnated, perpendicular to stitches dry, perpendicular to stitches impregnated, perpendicular to stitches semi-impregnated (six sample types in all).

The NCF material was extremely hard to handle and prepare specimens from. The fibre tows were very easily distorted and only the slightest loads were required to deform the cloth in the

dry state. Equally, cutting the material was very difficult to achieve without distorting the cloth. Even with a fresh scalpel blade the cutting forces could drag tows through the PES knit fibres.

### TEST METHODOLOGY

There are two main methodologies that have been reported for investigating the deformation properties of woven and similar reinforcements. These are the picture frame test (ref 7) and a simple tensile test of a sample of material cut at  $45^\circ$  to the test axis. One aim of this work was to investigate to what extent this material followed the predictions of the pin-jointed-net model. As the picture frame test imposes this behaviour on the sample it was felt to be inappropriate and tensile testing was used. This test is well reported elsewhere and will not be described here in detail, ref 8. The test piece is shown in fig 2.

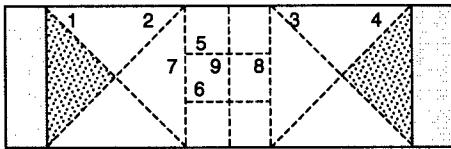


Fig. 2. Specimen marking-up requirements for bias extension tests

Lines 1 & 2 and 3 & 4 (lines following fibre directions at  $90^\circ$  to each other) were used to give a quick visual inspection of the shear angle and to visualise fibre slippage in the area where the maximum slip might be expected (crossover points between lines 1 & 2 and between lines 3 & 4). Lines 5 & 6 and 7 & 8 give the transverse and longitudinal strains respectively and line 9 is drawn across the centre of the gauge length to help to identify the point during the test at which any buckling starts.

Initial measurements were taken as follows.

Distance 7-8. Distance 5-6. Specimen width. Distance edge to 5. Distance edge to 6

In principle (according to the pin-jointed-net model) the two hatched areas in fig 2 should remain undistorted giving a deformed shape as shown in figure 3.

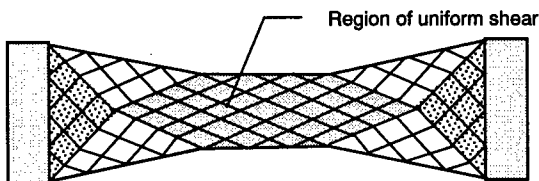


Fig 3. Idealised post-test geometry assuming that pin-jointed-net model is followed exactly.

In practice, deviations from the ideal behaviour are to be expected, and the set of lines marked on the surface permitted these deviations to be examined.

Specimen dimensions were as follows:

Width: 9cm Total length: 32cm Ungripped length: 26cm

Length of uniform shear region: maximum 17cm, minimum 8cm.

Samples were tested over a range of speeds from 10 to 100mm/min, and were tested at 20C

To obtain strain data a series of video images were captured during the test and longitudinal and transverse strains were extracted from these. These values were compared with the predictions of the Pin-jointed-net assumption to determine to what extent the various samples obeyed this assumption. The onset of any buckling was also ascertained to give a value for the limiting deformation under unsupported conditions.

## RESULTS

### 1. Load/extension behaviour

As noted earlier the NCF material proved to be very difficult to handle, especially in the dry state. The majority of samples were found not to be at exactly  $\pm 45^\circ$  when the video images were examined. The analysis of the results took the initial angle into account, by setting this angle as the basis for the pin-jointed-net calculations. Table 2 shows the load versus longitudinal strain results for the bias extension tests.

Sample	Rate mm/min	Load (N) at noted longitudinal strain					
		5%	10%	15%	20%	25%	30%
NCF dry	10	0.8	1.4	3	8	25	28
NCF dry	30	0.6	1.3	2.3	5.8	14	30
NCF dry	100	0.9	1.5	3.3	8	18	34
NCF dry ⊥	10	0.34	0.46	0.55	0.8	1.1	1.7
NCF dry ⊥	30	0.38	0.49	0.63	0.8	1.3	2.1
NCF dry ⊥	100	0.5	0.67	0.92	1.2	2	3.1
NCF dry ⊥	100	0.5	0.67	0.83	1.1	1.8	4.2
NCF Semi	10	2.7	3.8	5.6	14.5	33	
NCF Semi	100	7.3	9.6	13.7	22.7		
NCF Semi ⊥	10	3.0	3.4	3.8	4.7	8	
NCF Semi ⊥	100	7.1	8.2	8.7	9.9	12.6	22
NCF Prepreg	10	11.4	14	18	26	38	70
NCF Prepreg	10	11.4	14.5	17	24	38	70
NCF Prepreg	100	27.7	34	40	54	72	115
NCF Prepreg	100	27.5	34	41	53	74	120
NCF Prepreg ⊥	10	11.5	14.3	17.1	21.7	32.5	65
NCF Prepreg ⊥	10	12	15.3	19.5	27.5	42	85
NCF Prepreg ⊥	100	25	30	36	48	68	120
NCF Prepreg ⊥	100	27	34.5	43	57	92	170

Table 2. Load extension data

Figs 4, 5 & 6. show some of this data in graphical form. In each graph the vertical axis is Load in N, and the horizontal axis is longitudinal strain %.

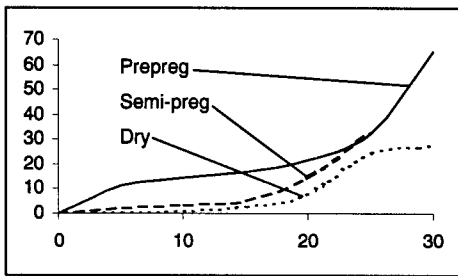


Fig 4. Load-extension results for samples tested at 10mm/min parallel to stitches

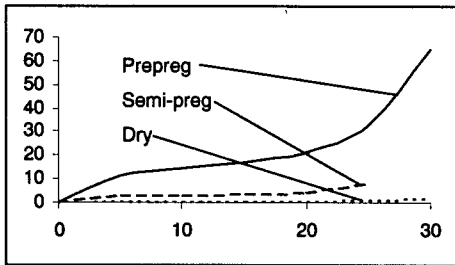


Fig 4. Load-extension results for samples tested at 10mm/min across stitches

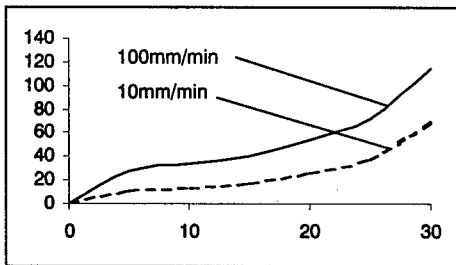


Fig 5. Load-extension results for prepreg samples tested parallel to stitches at different strain rates.

In the dry state there appears to be little or no effect of strain rate on the load at any given longitudinal strain for the samples tested along the stitch direction. The samples tested across the stitch direction seem to show some small rate sensitivity, perhaps 50% higher loads for a tenfold increase in rate. However the absolute values of load are very low and this appearance of a rate effect could well be illusory. The loads for the samples tested along the stitches are much higher than for those tested across the stitches. This disparity increases from a factor of

about 2 at 5% strain to about 10 at 30% strain. To check whether this difference in stiffness would lead to problems in forming, a sample of the dry NCF was formed over a hemispherical plug. The NCF was laid loosely over the hemisphere and forced into shape using a tube of slightly greater internal diameter than the diameter of the hemisphere. The formed shape appeared to be essentially uniform and showed no evidence of any major distortion due to the differences in stiffness along and across the stitch fibres.

In the semipregged state the load to give a specific deformation is increased and there is a clearer rate effect, as would be expected. The difference in loads between the two test directions is substantially reduced by the semipregging, but is not completely removed at higher strains.

In the fully prepregged state there is a further increase in the load to give a specific deformation, and a clear rate effect in both test directions, with the loads being approximately twice as high for the samples tested at the ten times higher rate. The difference in loads between the two test directions is essentially removed in the fully prepregged state.

## **2. Gross buckling behaviour**

When either dry or prepregged woven cloth is tested under conditions of bias extension, out of plane buckling occurs during the test, ref 9. This can be at the onset of major warp/weft interactions for dry cloth or can occur at an earlier stage for prepregged cloth. Stacks of crossplied unidirectional prepreg may buckle during test or may remain unbuckled, largely depending on test conditions, ref 6. Narrow samples and slow test rates produce much less buckling than wide samples or rapid testing. A freedom from buckling is associated with the ability to slip within and between layers in the prepreg stack. None of the samples reported on in this work displayed buckling behaviour, even when fully impregnated. This would indicate a greater tendency to slippage for the NCF materials than for stacks of unidirectional prepreg. It would be expected that any increased tendency to slippage would be accompanied by deviations from pin-jointed net behaviour.

## **3. Local tow wrinkling**

Tow wrinkling has been reported in the testing of stacks of crossplied unidirectional prepreg subjected to bias extension testing, ref 6. This tow wrinkling is thought to be caused by the presence of a small number of misaligned tows, which can control the overall deformation such that some tows experience a reduction in length and hence buckle and become wrinkled. The edges of such samples are free of wrinkled fibres over some distance, which is a measure of how easily slip occurs between the tows.

No tow level wrinkling or differences between edges and centre of the sample was seen in the tests on dry NCF. No tow level wrinkling or differences between edges and centre of the sample was seen in the tests on semipregged NCF tested in the stitch direction. Slight tow level wrinkling was seen in the test on semipregged NCF tested across the stitch direction at 100mm/min, but not at 10mm/min. All fully prepregged NCF samples tested showed some tow level wrinkling, see fig 6. The level of wrinkling was highest for samples tested across the stitches at a fast rate and lowest for samples tested along the stitches at a slow rate. The overall levels of tow wrinkling appeared to be lower than when testing cross-ply stacks of UD prepreg. As reported for cross-ply stacks of UD prepreg some tows remain straight, even though tows in close proximity to them become severely wrinkled. It was more difficult

to detect a clear edge effect with NCF than with cross-plyed stacks of UD prepreg. However, the best estimate is that a wrinkle free edge of about 1cm is present in the worst case and for the samples showing only slight wrinkling no clear edge effect could be detected, that is say there was no clear line at which wrinkling ceased, but rather a gradual reduction in wrinkling towards the sample edges.

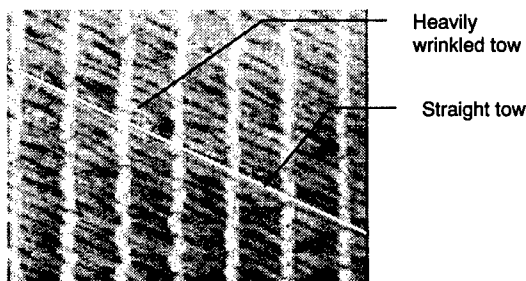


Fig 6. Tow level wrinkling can be seen in tested samples of NCF. This sample was tested at 100mm/min across the stitches. (Approx 30% elongation)

#### 4. Comparison with the predictions of the pin-jointed-net model.

To permit comparisons between the test samples and the pin-jointed-net model the measured tow angle can be compared to the tow angle calculated from the measured extension using the pin-jointed net model as a basis for calculation, ref 6. Fig 7 shows typical results for an impregnated sample.

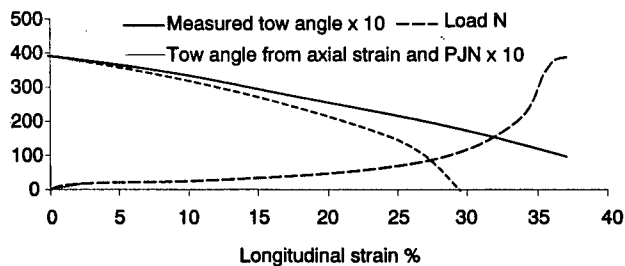


Fig 7. Longitudinal strain vs. load and measured and calculated tow angle for a prepregged specimen tested across the stitches at 100mm/min.

An alternative approach is to plot the measured lateral strain and calculated lateral strain against the longitudinal strain. This is shown in fig 8 for a dry NCF sample tested across the stitches. This sample was subjected to an axial extension far greater than the maximum that would be predicted to be possible on the basis of the pin-jointed-net model and the initial tow angle. The pin-jointed-net model would predict that the width would fall to zero (100% lateral strain) at a longitudinal extension of less than 30% (due to the starting angle being less than 45°). Of course, this cannot happen in practice and the tows in a woven cloth would lock at a much lower angle leading to a very sudden increase in load and buckling out of plane. For the

dry NCF, tow rotation is always at a lower level than would be predicted by the pin-jointed-net model and ceases completely at a tow angle of about  $10^{\circ}$ . Extension beyond this point takes place at an essentially constant tow angle. Rather than the load picking up rapidly when the fibre rotation ceases it tends towards a plateau value.

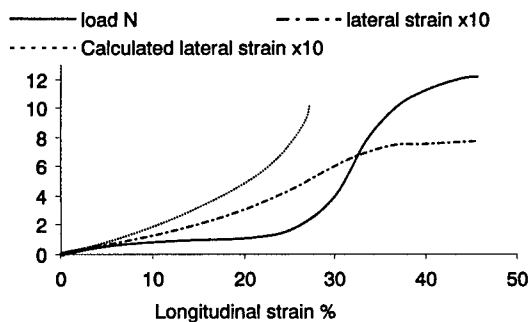


Fig 8. Longitudinal strain vs. load and measured and calculated lateral strain for a dry specimen tested across the stitches at 100mm/min.

All samples tested, irrespective of rate, direction of testing and degree of impregnation showed major deviations from the predictions of the pin-jointed-net model.

## DISCUSSION

The NCF material is quite different from conventionally woven materials. Tows can slip past one another in this material with relatively little resistance, so that this deformation mode dominates the overall deformation at high strains and has a major influence on the forming at any strains; at least for the scale of testpiece considered here. In addition, buckling could not be initiated in the tests reported here. The concept of a 'locking angle' is essentially meaningless for the NCF as a limitation to deformation. Although there does appear to be an angle at which tow rotation ceases this does not lead to buckling of the sample, rather the deformation mode switches to one based purely on the drawing of tows through the knit stitches.

It might be expected that for very large samples of cloth the NCF material behaviour would tend towards being more closely modelled by the Pin-Jointed-Net model. However, close to the edges of even large sheets of NCF a great deal of tow slippage would be expected. Based on the observations made in this work, tow slippage could be expected to be possible for 1cm or perhaps more in the fully prepregged state (depending on deformation rate), for a few cm in the semi-impregnated state, and probably for 10s of cm in the dry state.

This NCF material would appear to be an excellent candidate material wherever a very conformable reinforcement is required. The ability to slip tows past one another as well as scissoring in the Pin-Jointed-Net fashion should assist in the forming of complex shapes where the deformability of cloth or cross-ply UD stacks is marginal or insufficient. This will be particularly true for dry and semipregged NCF, for fully prepregged NCF only rather local slip is likely to be possible.

However, it cannot be assumed that any drape prediction software based on the pin-jointed-net assumption will give an adequately accurate simulation of the draping of the NCF over any given shape. Indeed, unless the sheet of NCF being formed is very large it is likely that the output from prediction software will be in error as to final fibre angles. Even for very large sheets of NCF the predictions of software based on the pin-jointed-net model are likely to be in error within a few cm of the edge of the sheet. Whether these theoretical shortcomings are relevant in real simulations and forming can only be examined experimentally. For geometries in which only a limited level of deformation is required the predictions of drape prediction software should be adequate, so long as they are used with care.

Lastly, it must be emphasised that the results reported here are for a specific variant of non-crimped-fabric. The options available in the production of NCFs are very wide and it is by no means axiomatic that the results reported here can be read across to other systems.

## CONCLUSIONS

The NCF material in dry, semipregged and prepregged forms is extraordinarily deformable, by a combination of tow rotation (scissoring) and slippage of tows through the knit stitches. This material could not be made to buckle in any of the tests performed, even at extreme strains.

The NCF material is not well simulated by the Pin-Jointed-Net model, at least for the samples size used here. The deviations from the pin-jointed-net model would not be detected in the picture frame shear test, fully justifying the use of a bias tensile test to measure the deformation behaviour.

The draping performance of this material will not in general be accurately predicted by drape software based on the pin-jointed-net model.

Despite the potential problems with predictions of the forming behaviour the extreme formability of the NCF material makes it well worth while to study this material further.

## REFERENCES.

1. Potter KD. The influence of accurate stretch data for reinforcements on the production of complex structural mouldings. Parts 1 & 2. Composites. July 1979. Pp 161- 173
2. Billoet JL, Cherouat A. Meso-structural behaviour of composite fabric for the simulation of manufacturing of thin composite by shaping process. Proc ICCM 12 Paris. 1999.
3. Long AC, Rudd CD. A simulation of reinforcement deformation during the production of preforms for liquid moulding processes. Proc Inst mech Engrs. Vol 208. 269-277. 1994
4. Lai C-L, Young W-B. Modelling the fiber slippage during preforming of woven fabrics. Proc ICCM12 Paris. 1999
5. Potter KD. Chapter 3. Resin Transfer Moulding. Chapman and Hall. 1997.
6. Potter KD. Bias extension measurements on cross-plyed unidirectional prepreg. Composites Part A – in press

ICMAC - International Conference for Manufacturing of Advanced Composites

7. McGuinness GB, OBraidaigh CM. Development of rheological models for forming flows and picture-frame shear testing of fabric reinforced thermoplastic sheets. *J Non-Newtonian Fluid Mechanics* 73, 1-2, pp 1-28. 1997
8. Wang J, Page JR, Paton R. Experimental investigations of the draping properties of reinforcement fabrics. *Composite Science and Technology*. 58. Pp229-237. 1998
9. Prodromu AG, Chen J. On the relationship between shear angle and wrinkling of textile composite preforms. *Composites Part A*, 28, 5, pp 491-503. 1997

**ACKNOWLEDGEMENT**

This work was kindly supported by GKN Westland Helicopters Ltd.

---

ICMAC - International Conference for Manufacturing of Advanced Composites

**APPLICATION OF FIBRE METAL LAMINATES ON  
A FUTURE REGIONAL JET AIRCRAFT**

K Poston (Bombardier Aerospace - Short Brothers plc, Northern Ireland)

Within the aerospace industry there are currently a number of advanced technologies which could be employed in the design and manufacture of fuselage structures to improve performance and reliability and achieve both cost and weight reductions. From the Bombardier Aerospace group perspective Fibre Metal Laminates such as GLARE are the most readily exploitable and closest to market.

The primary advantages of GLARE include high specific strength and stiffness, excellent fatigue and crack growth properties, superior impact and damage tolerance characteristics and high residual strength. The excellent fatigue and residual strength properties can be utilised through new design concepts to reduce structural weight. In service, these properties can be translated into increased inspection intervals, resulting in a reduction of maintenance, and the total life cycle, costs of an aircraft.

Although GLARE can be fabricated and assembled using conventional aluminium alloy sheet metal processes, the material offers a number of manufacturing opportunities that can be exploited to reduce fabrication and assembly costs.

Initial work within the Bombardier Aerospace group was focused on the evaluation of a Flap Demonstrator and assessing the damage tolerance capabilities of both ARALL and GLARE. GLARE was also selected as the material of choice for the Learjet 45 Radome front bulkhead on the basis of superior bird impact resistance. A recent Design Study to investigate the weight saving potential of using GLARE as a fuselage skin material on the Learjet 45 business jet predicted potential weight savings of 21% and 13% for the upper and lower fuselage respectively.

The Bombardier Aerospace group is currently involved in a GLARE Technology Demonstration programme focused on the design, manufacture and assembly of four full scale GLARE fuselage panels representative of the Dash 8 - 400 aircraft which will be subjected to static, fatigue and damage tolerance testing.

**INVESTIGATION INTO THE EFFECTS OF DRY MEDIA PAINT REMOVAL ON  
COMPOSITE AIRCRAFT STRUCTURES**

FRED ANDREWS  
BOMBARDIER AEROSPACE SHORTS  
BELFAST

The paper will summarise research carried out on the removal of paint from carbon fibre based epoxy composites. The project was sponsored and co-ordinated by Bombardier Aerospace – Shorts in collaboration with Materials Ireland and the Composite Research Group at The University of Limerick.

Solid media was used for paint removal in this project because of the known detrimental effects of traditional chemical paint strippers on epoxy resins. As well as this the legislative prohibition of methylene chloride and the phenol derivatives of these chemicals make their use undesirable even on metallic materials.

Although research and testing has been carried out by various organisations on the effects of solid media on metallic surfaces less has been published with regard to the effects of solid media on composite materials. Some Aerospace companies give limited clearance for the use of wheat starch, but not for plastic media (MIL-P-85891) on composite structures.

This paper details the laboratory test work undertaken to determine the effects of both Type V acrylic and wheat starch on carbon fibre composite epoxy panels which simulate actual aircraft components.

The test analysis includes the evaluation of the effects of dry media on surface morphology, various mechanical properties (static and dynamic), interfacial adhesive bonds and panel distortion.

Although it has been known for some time that paint removal by hand abrasion is detrimental to the integrity of the surface structure of composite materials, this work confirms that properly controlled dry media stripping is less damaging and more cost effective. One of the objectives of this work was to provide guidelines for process parameters.

**TOWARDS THE DESIGN OF SANDWICH PANEL COMPOSITES WITH  
ENHANCED THERMAL AND MECHANICAL PROPERTIES BY VIRTUE OF  
POSSESSING AN AUXETIC CORE**

J P M Whitty, A Alderson, P Myler and B Kandola.  
Bolton Institute, Faculty of Technology, Deane Road, Bolton BL3 5AB, UK

**ABSTRACT**

The finite element (FE) method has been used to study the mechanical and thermal properties of both conventional and auxetic (i.e. negative Poisson's ratio) honeycombs, which may be used as the cores of sandwich panel composites. In order to examine the thermal stress values in the honeycombs the edges were constrained to remain rigidly fixed, which also represents a first approximation to the real situation of the cores in sandwich panels. Using a maximum stress failure criterion, failure of the internal honeycomb structures was simulated using a crack propagation method developed in-house. Results are presented showing that the cell-wall stress build up in the auxetic honeycomb was significantly reduced relative to the conventional honeycomb under thermal loading. The data imply that for identical temperature gradients, the auxetic core will undergo significantly less internal damage and de-bonding than the conventional core in sandwich panel applications. Conversely, the conventional honeycomb performs better (i.e. has lower cell wall stress build up) than the auxetic honeycomb under hydrostatic loading conditions. The crack propagation routine shows that the size and pathway of the crack formed during the simulation is dependent on the size of the failure stress distribution used in the routine, and indicates that full failure of the honeycomb (defined by full propagation of a crack from one edge to another) occurs for a much reduced rib defect density (~5%) than predicted in previous simulations (~35%) which employed a random defect generation routine.

**INTRODUCTION**

Sandwich panel composites are widely used in the automotive and aerospace industries and typically consist of a foam or honeycomb material sandwiched between two outer laminate skins (Fig. 1). The result is a high strength to weight material, ideal for aircraft wings or car doors. The strength and stiffness of these composites is in part dependent on the foam or honeycomb structure employed. Similarly, the ability to tailor the curvature of a sandwich panel composite used in, for example, curved body parts for cars and aircraft, is related to the panel mechanical properties and therefore the geometry of the structure of the cellular core material (1). For example, Fig. 2(a) shows a conventional honeycomb deforming by hinging of the honeycomb cell walls (ribs), leading to the cells elongating along the tensile loading direction but contracting laterally. Hence this honeycomb network has a positive Poisson's ratio and it has been shown (1) that a sandwich panel composite containing a positive Poisson's ratio honeycomb core adopts a saddle shape (anticlastic curvature) upon out-of-plane bending (Fig. 3(a)). However, if the honeycomb geometry is modified so that the cells adopt the 're-entrant' geometry shown in Fig. 2(b), then the cells elongate both along and transverse to the tensile loading direction, giving rise to a negative Poisson's ratio, known as *auxetic* behaviour (2). An auxetic panel subject to an out-of-plane bending moment has been shown (1) to naturally adopt a doubly-curved or dome shape (synclastic curvature - Fig. 3(b)) by virtue of possessing a negative in-plane Poisson's ratio. The potential of auxetic sandwich panels in curved body parts for cars and aircraft is clearly evident.

Given the applications for sandwich panels, the way in which the core material reacts under mechanical and thermal loading conditions is clearly of importance from a design viewpoint. A number of analytical and numerical (e.g. finite element - FE) models for prediction of the mechanical properties of honeycombs are present in the literature. Gibson and Ashby (3) developed an analytical model based on flexure of the ribs, formulating expressions for the in-plane mechanical properties (i.e. Poisson's ratios, and Young's and shear moduli). This work was expanded by Evans and co-workers (4,5) who developed models that incorporated rib hinging (change of rib angle) and rib stretching (change in rib length). The models allow these deformation mechanisms to occur concurrently with rib flexure. Overaker et al (6,7) developed an elastic compliance matrix for honeycomb deformation and investigated the effect of relative density changes due to rib thickness variations on the in-plane mechanical properties. Scarpa et al (8) have also used the FE method and the analytical flexural model to investigate such changes. Each of these models predicts that reduction in the relative density significantly reduces the strength and stiffness of the honeycomb. The analytical approaches are very successful at predicting the mechanical properties of pristine (defect free) honeycombs.

However, to accurately predict the properties of these materials subject to damage-inducing processes either in production or in service, models are required to predict the material properties in the presence of broken ribs (i.e. when defects are present in the core material). A number of attempts have been made to model the mechanical properties of honeycombs with broken ribs which usually employ the use of numerical techniques. Silva and Gibson (9) used the FE method to investigate the strength and stiffness of regular and irregular conventional honeycombs. This was achieved by randomly deleting ribs from the finite element mesh. They reported that the regularity of the honeycomb increases strength, while deletion of the ribs reduces both strength and stiffness. Additionally, they found these properties decreased to zero when ~35% of the ribs were removed at random, consistent with the formation of a continuous path predicted from percolation theory. We have recently (10,11) used the FE method to investigate the effects on the mechanical properties of conventional and re-entrant honeycombs of three rib deletion scenarios: deletion of 'diagonal', 'vertical' and vertical-plus-diagonal ribs - see Fig. 2). This work showed that deletion of only vertical ribs actually leads to slight enhancement of the honeycomb stiffness in the direction perpendicular to the vertical ribs (Fig. 4(a)). Additionally, the magnitude of the Poisson's ratio was also shown to increase for this loading and defect combination, implying that the corresponding Poisson's ratio of an auxetic honeycomb becomes *more* negative (Fig. 4(b)).

In this paper we report results from a comparative modelling study of the mechanical and thermal properties of honeycomb core materials possessing negative and positive Poisson's ratios. A crack propagation method is also presented to enable a more realistic simulation of defect generation to be considered. In the thermal models, a thermal gradient is applied from one edge to the opposite edge of the honeycomb to simulate the effects of heat on the surface of the sandwich panel. In this scenario the 2D honeycomb structure is an approximation to a 3D foam core material. In the mechanical models, a bi-axial stress is applied in the plane of the honeycomb to simulate in-plane stresses that may occur within the sandwich panel during service. In this latter scenario the honeycomb may represent the actual core material, or can again be considered as an approximation to a 3D foam core.

## MODELS AND METHODS

The conventional and re-entrant geometrical parameters are shown in Fig. 2. The honeycombs consist of vertical ribs of length  $h$  and diagonal ribs of length  $l$  at an angle  $\theta$  to the horizontal. Identical rib dimensions, based on one of the Alderson et al (12) honeycomb geometries, were used for both the conventional and re-entrant honeycombs modelled:  $h = 0.78\text{mm}$ ,  $l = 0.54\text{mm}$ , rib thickness  $t = 0.086\text{mm}$  and rib depth  $b = 0.128\text{mm}$ . In the case of the re-entrant honeycomb  $\theta = -23^\circ$ , whereas  $\theta = +23^\circ$  for the conventional honeycomb. The intrinsic material properties were taken from (12): rib Young's modulus  $E_{rib} = 4.4\text{ GPa}$  and rib Poisson's ratio  $\nu_{rib} = 0.56$ .

### Finite Element Models

Two proprietary F.E. packages were used to perform the calculations: ANSYS (13) and SDRC I-DEAS (14). The second package was employed mainly for verification purposes. Each rib was modelled using one (diagonal rib) or two (vertical rib) idealised beam elements. Arrays of  $21 \times 21$  unit cells were modelled, although as the crack propagation routine was rather computationally expensive models were limited to  $11 \times 11$  unit cells in this case.

### Thermal Loading

The nodes on each edge of the honeycomb were clamped from movement in any direction and from rotation in the  $(x,y)$  plane. A thermal gradient was applied by holding the nodes of one edge at temperature  $T_0$  and the nodes of the opposing edge at  $T_1$ . A Newton-Raphson optimisation routine was employed to ensure convergence. For the initial load step a convergence load was approximated thus:

$$F = A\epsilon E_{ga} \quad (1)$$

where  $F$  is the total reaction force at the constrained edge to which the thermal load  $T_1$  is applied,  $A$  is the cross sectional area of the edge and  $\epsilon$  is the applied thermal strain (i.e.  $\epsilon = \alpha\Delta T$  where  $\alpha$  is the average coefficient of linear expansion of the honeycomb and  $\Delta T$  the absolute temperature change ( $= T_1 - T_0$ )).  $E_{ga}$  is the appropriate Young's modulus of the honeycomb calculated from the analytical flexure model (3). For subsequent load steps the total reaction force at the constrained edges was used as the convergence force for the next load step.

### Bi-Axial Loading

Forces (to induce  $\sim 0.1\%$  strain) were applied to the nodes of two orthogonal edges of the honeycomb model. At the edges opposite to the edges to which force was applied, the nodes were constrained from movement in the direction perpendicular to the edge and from rotation in the  $x,y$  plane. However, the restrained nodes were free to move parallel to the edge direction. In this paper we consider only the case of hydrostatic loading, which was achieved by ensuring that the total nodal reaction force divided by the area of the edge ( $=$  the applied stress) was equal for both orthogonal edges to which displacement was applied.

### Crack Propagation

In order to simulate realistic defect generation in the honeycomb core a crack propagation routine has been developed. The routine assigns each honeycomb rib with a failure stress taken from a normal distribution. The Von Mises stress induced in each rib due to the particular loading condition being investigated is then calculated and the rib with the maximum ratio of the Von Mises stress to failure stress identified. This rib is the first rib which will fail when the applied load is such that the stress in the rib exceeds the assigned failure stress of the rib by an infinitesimal amount. The rib is thus deactivated from the model. The model is then resolved and the next rib with the maximum ratio of the Von Mises stress to failure stress is identified as the next rib to fail in the crack propagation routine. The process is repeated until a continuous crack is formed from one edge to another. This routine has the advantage that local stress concentration effects are taken into account, thus giving a more realistic defect generation scenario than the random rib deletion scenarios studied to date.

For the mechanical properties calculations, stresses and strains and the derived honeycomb mechanical properties (Poisson's ratios and Young's moduli) were calculated as described in (11).

## RESULTS & DISCUSSION

### Thermal Modelling

Preliminary FE calculations showed that the rib stresses were all negative (i.e. compressive) if a positive temperature gradient (heating) was applied; for negative temperature gradients (cooling) the converse was observed. Upon heating the internal structure tends to expand but is constrained from movement by the fixed boundary conditions applied in these simulations. Thus, the ribs expand against one another with the result that compressive rib stresses are expected. Opposite effects are expected for cooling. Thus, it can be concluded that the FE model reacts in a physically sensible manner.

Figure 5 shows the comparison between the calculated maximum stress values in the equivalent ribs of the conventional and auxetic honeycombs subject to an identical temperature gradient in the x direction. Almost all the rib stresses lie below the equality line indicating that more stress build up is observed in the conventional honeycomb. This can be understood qualitatively by considering the schematic inserts in Fig. 5 which show the expected thermal stress build up at the rib junctions in the two types of honeycomb. For the conventional honeycomb thermal expansion of the ribs causes a build up of stress at the junction as a consequence of the fact that the ribs are expanding against each other, leading to eventual failure at the junction. For the auxetic (re-entrant) honeycomb, on the other hand, the ribs are able to expand into free space at the junction, i.e. they are not acting against each other to the same extent, leading to reduced thermal stress build up and therefore the junction will be expected to remain intact to greater thermal loads.

Hence the FE models indicate that auxetic honeycombs will have enhanced thermal properties such as thermal shock resistance. From standard expressions (15) the thermal shock resistance,  $\Delta T_c$ , of an isotropic material is related to the Poisson's ratio,  $\nu$ , by

$$\Delta T_c \propto (1-\nu) \quad (2)$$

Equation (2) illustrates that the thermal shock resistance of a material is predicted to be enhanced when  $\nu$  is negative (i.e. an auxetic material) compared to positive (a non-auxetic material), consistent with the FE model calculations for the honeycombs presented in this paper.

#### Hydrostatic Loading

Figure 6 shows a plot of the maximum stress in each of the re-entrant honeycomb ribs against the maximum stress in the equivalent ribs in the conventional honeycomb. The data all lie above the equality line in Fig. 6, indicating that the rib stress build up due to hydrostatic loading is higher for the re-entrant (auxetic) geometry. Additionally, there are two distinct regions of data: a low stress region corresponding to the vertical ribs and a high stress region corresponding to the diagonal ribs.

The increased stress build-up for the auxetic membrane when subject to hydrostatic loading can be explained by considering the schematics in the inserts of Fig. 6, which show the components of each applied stress causing flexure of the diagonal ribs (known to be the dominant deformation mechanism in the honeycombs investigated here (12)). In the case of the conventional honeycomb the components of the vertical and horizontal applied stresses causing flexure of the diagonal ribs are acting in opposite directions on the rib and thus tend to cancel each other out, leading to only a small flexure stress acting on the ribs. For the auxetic honeycomb, on the other hand, the components of the vertical and horizontal applied stresses causing flexure of the diagonal ribs act in the same direction and so are additive, leading to a large flexure stress acting on the ribs, consistent with the FE model calculations.

#### Crack Propagation

The size and pathway of the major crack formed in the crack propagation routine was found to be related to the distribution of failure stresses. The wide failure stress distribution typically produced a longer crack which penetrated a greater depth from the loading edge than for the narrow failure distribution (Fig. 7). It would appear that for the wide failure stress distribution crack propagation is governed by the generation of defects over the entire area of honeycomb before crack formation occurs through connection of a number of these sites. For the narrow failure stress distribution the crack forms very close to the edge to which load is applied (where the stress in the ribs is largest) and crack propagation is now dictated by local stress concentration at the crack tip, leading to the major crack forming approximately parallel and near to the loading edge.

It is interesting to note that, even for the widest distribution used in this work, on average only ~ 5% of the cell walls are removed before full failure of the honeycombs occurs. This is well below the 35% observed by Silva and Gibson (9) for random deletion of ribs. Hence, the crack propagation routine predicts failure in real honeycombs will occur far earlier than predicted by the random rib deletion studies.

Figure 8 shows the effect on the honeycomb Young's moduli due to failure of a conventional honeycomb through crack propagation for loads applied in the horizontal ( $x$ , Fig. 8(a)) and vertical ( $y$ , Fig. 8(b)) directions. Both  $E_x$  and  $E_y$  decrease as the crack propagates. The size of the failure stress distribution is found to effect the variation in these mechanical properties, the narrower the distribution the greater the reduction in the elastic modulus.

Work is progressing on integrating the crack propagation routine into the thermal and bi-axial loading scenarios. This will ultimately enable a predictive tool to be developed to aid in the optimal design of honeycomb core materials to be used, for example, for inclusion in sandwich panel composites applications subject to a range of different loading conditions during service.

#### SUMMARY AND CONCLUSIONS

Finite element approaches have been employed to investigate stress build-up in the honeycomb cores of sandwich panel composites, due to hydrostatic and thermal loading conditions. A crack propagation routine has also been developed for the FE method to approximate in-service failure of the honeycomb core. The calculations predict that the thermally-induced stress build-up in the honeycomb ribs can be minimised by transforming the geometry from a conventional honeycomb to a re-entrant (auxetic) honeycomb. However, this same conversion actually leads to detrimental performance of the honeycomb when subject to hydrostatic loading, i.e. stress build-up in the honeycomb ribs is increased in the re-entrant honeycomb compared to the conventional honeycomb. The crack propagation routine provides a more realistic simulation of internal failure processes than the random deletion of ribs studied previously, indicating that a significantly reduced number of ribs are required to fail for full failure of the honeycomb than predicted from random defect generation. A reduction in the elastic moduli of the honeycomb is predicted as crack propagation proceeds.

#### ACKNOWLEDGEMENT

The authors gratefully acknowledge the financial support of the EPSRC (JPMW - Doctoral Studentship).

#### SYMBOLS

$h$  = vertical rib length (m)

$l$  = diagonal rib length (m)

$\theta$  = honeycomb angle (radians)

$t$  = rib thickness (m)

$b$  = rib depth (m)

$E_i$  = Young's modulus in  $i$  direction ( $N/m^2$ )

$E_{ga}$  = flexure model Young's modulus ( $N/m^2$ )

$E_{rib}$  = rib Young's modulus ( $N/m^2$ )

$\nu_{rib}$  = rib Poisson's ratio

$\nu_{ij}$  = Poisson's ratio due to load in  $i$  direction

$T_0$  = low absolute temperature (K)

$T_1$  = high absolute temperature (K)

$\Delta T$  = absolute temperature difference (K)

$F$  = total reaction force (N)

$A$  = cross sectional area of edge ( $m^2$ )

$\alpha$  = average coefficient of linear expansion ( $K^{-1}$ )

$\Delta T_c$  = thermal shock resistance (K)

$\nu$  = Poisson's ratio of isotropic material

$\epsilon$  = applied strain (m/m)

#### REFERENCES

1. Evans KE, *Compos Struct* 17 (1991) 95
2. Evans KE, Nkansah MA, Hutchinson IJ, Rogers SC, *Nature* 353 (1991) 124
3. Gibson LJ, Ashby MF, 'Cellular Solids: Structure and Properties', Pergamon Press (Oxford), 1988
4. Evans KE, Alderson A, Christian FR, *J Chem Soc Faraday Trans* 91 (1995) 2671
5. Masters IG, Evans KE, *Compos Struct* 35 (1997) 403
6. Overaker DW, Cuitino AM, Langrana NA, *Mechanics of Materials* 29 (1998) 43
7. Overaker DW, Cuitino AM, Langrana NA, *J Appl Mech* 65 (1998) 748
8. Scarpa F, Panayiotou P, Tomlinson G, *J. Strain Analysis* 35 (2000) 383
9. Silva MJ, Gibson LJ, *Int J Mech Sci* 39 (1997) 549
10. Alderson A, James BW, Nazare F, Whitty JPM, Wolfenden AG, Proceedings of the 11th International Conference on Deformation, Yield and Fracture of Polymers, Cambridge, UK, (2000) 343
11. Alderson A, James BW, Nazare F, Whitty JPM, Wolfenden AG, Proceedings of the 9th European Conference on Composite Materials - ECCM9, Brighton, UK, (2000). CD-ROM
12. Alderson A, Rasburn J, Ameer-Beg S, Mullarkey PG, Perrie W, Evans KE, *Ind Eng Chem Res* 39 (2000) 654
13. ANSYS 5.5.1, University edition, UP19981001, ANSYS Inc, 1994
14. US Department of Defence (DOD). Structural Dynamics and Research Group, I-DEAS masters series 6, 1996
15. Anderson JC, Leaver KD, Rawlings RD, Alexander JM, 'Materials Science', 4th ed., Chapman and Hall (London), 1990

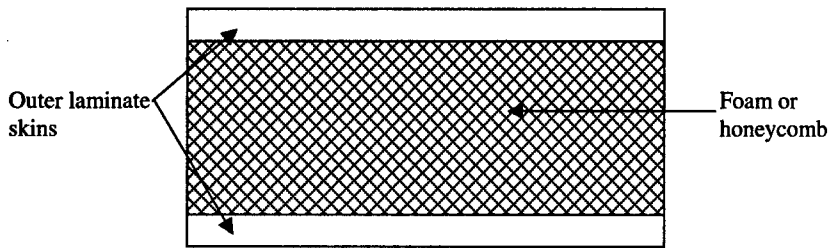


**Fig. 1.** Schematic sandwich panel composite consisting of an inner cellular core material sandwiched between two outer laminate skins.

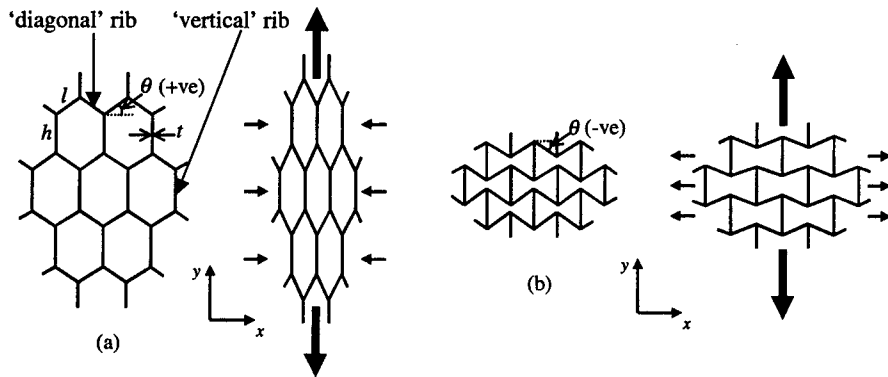


**Fig. 2.** (a) Conventional honeycomb deforming by hinging of the ribs leading to a positive Poisson's ratio. 'Vertical' and 'diagonal' ribs are also indicated. (b) Re-entrant honeycomb deforming in the same manner leading to a negative Poisson's ratio.

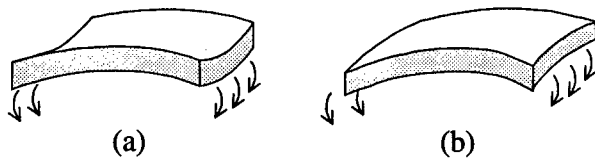


**Fig. 3.** Curvature of (a) positive and (b) negative in-plane Poisson's ratio panels.

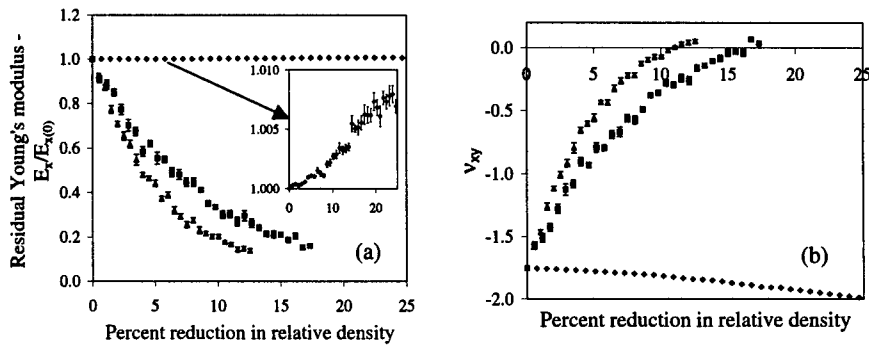


Fig. 4. (a) Young's modulus ( $E_x$ ) and (b) Poisson's ratio ( $v_{xy}$ ) for the re-entrant honeycomb vs % reduction in relative density due to random deletion of diagonal-plus-vertical ribs (squares), vertical ribs (diamonds) and diagonal ribs (triangles). Taken from (11).

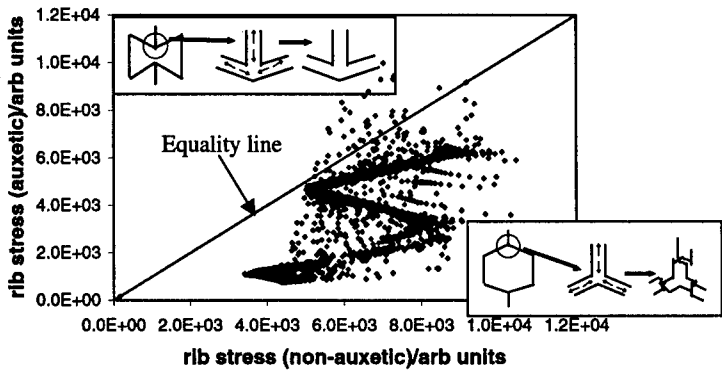


Fig. 5. Comparative thermally-induced maximum rib stress plot for auxetic and non-auxetic honeycombs subject to an identical horizontal thermal gradient. Inserts show thermal expansion of ribs at junction.

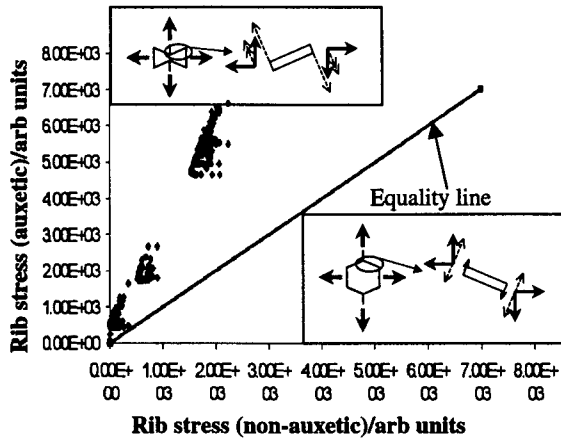


Fig. 6. Comparative maximum rib stress plot for auxetic and non-auxetic honeycombs subject to hydrostatic loading. Inserts show components of applied vertical and horizontal stresses causing flexure of diagonal rib.

ICMAC - International Conference for Manufacturing of Advanced Composites

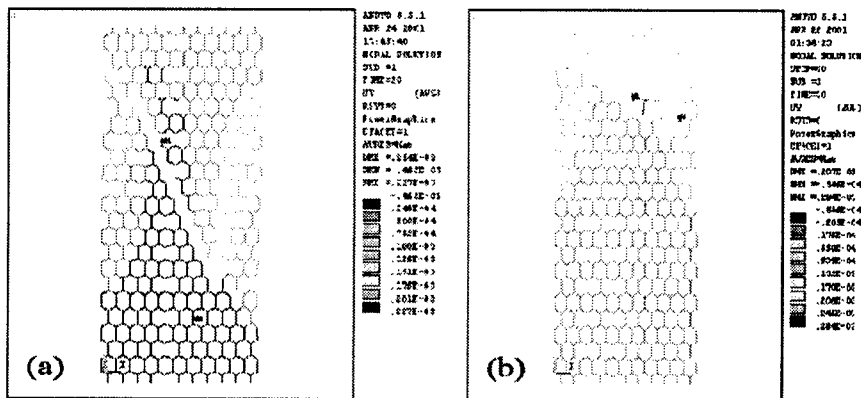


Fig. 7. Typical cracks simulated using the crack propagation routine for (a) wide and (b) narrow failure stress distributions. Cracks are formed for a load applied to the top edge in the vertical direction.

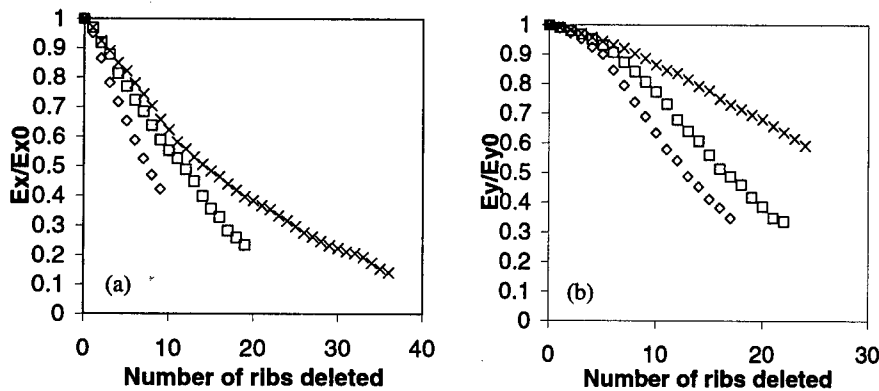


Fig. 8. Conventional honeycomb Young's modulus vs number of ribs deleted for cracks propagating due to a load applied in the (a) horizontal and (b) vertical directions. Crosses are for a wide failure stress distribution, squares an intermediate distribution and diamonds a narrow distribution.

## **THE APPLICATION OF A GENERAL FIBRE ARCHITECTURE MODEL FOR COMPOSITE MECHANICAL PROPERTY PREDICTION**

J.J. Crookston, B.J. Souter, A.C. Long and I.A. Jones

*School of Mechanical, Materials, Manufacturing Engineering and Management,  
University of Nottingham, University Park, Nottingham, NG7 2RD, UK*

### **ABSTRACT**

An approach to modelling composite component mechanical behaviour is described. Drape modelling is used to determine shear deformation of the reinforcement due to preform manufacture and subsequent material orientations. Alternatively, this information may be obtained using a photogrammetric technique, which is also outlined. Mechanical property prediction is carried out on an element-wise basis for use in prediction of macroscopic (component) mechanical performance by finite element (FE) analysis. Results of such analyses are included showing the change in mechanical response over the geometry of a component. A modular method is employed such that various mechanical property models can be incorporated as appropriate, and an important section of the work is the development of a three-dimensional description of a textile unit-cell to enable FE analysis to be used to determine properties by mesomechanical methods. This textile description is general, enabling accurate modelling of both woven and warp-knitted (non-crimp) reinforcements.

### **INTRODUCTION**

For liquid composite moulding (LCM) processes such as resin transfer moulding (RTM), reinforcement materials need to be deformed to conform to the component shape, altering both the fibre orientation and the angle between warp and weft fibres. Many studies have been conducted in the field of drape analysis of textile composite preforms [1-4] and in some cases this work has been performed to facilitate permeability or mould filling simulations [5]. Considerably less work has been published relating to the mechanical properties of the resultant composite structure after draping.

It is generally considered that the only significant mode of deformation during draping is fabric shear [1]. It is clear that when a fabric is sheared the mechanical characteristics of the material will be changed, as the reinforcement orientation has a significant effect on laminate stiffness and strength; if the reinforcement is sheared by up to 40°, so the principal directions of stiffness and strength will also change.

The nature of the work in hand is to interface a drape model developed previously [6] with macroscopic FE analysis techniques. This involves determination of component mechanical performance based on properties obtained by mesomechanics, determined at element level according to reinforcement shear during draping. This is implemented in a modular fashion such that properties predicted by any model can be incorporated easily enabling rapid evaluation of models using simple or complex components. Results from the drape model for a conical component for two fabrics, a plain-weave and a warp-knitted textile, are shown in

Figure 1. These results will be used to demonstrate the effect of reinforcement deformation on mechanical performance.

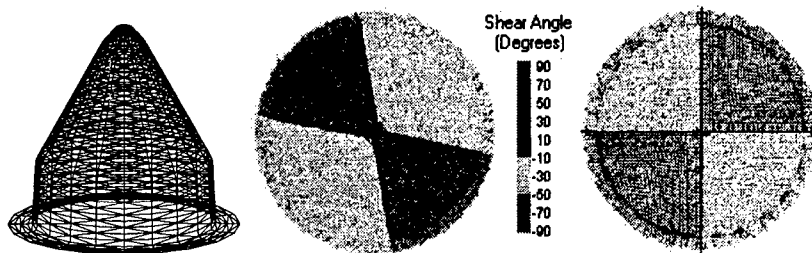


Figure 1. Conical component mesh (left); Drape simulation output (plan view) for warp-knitted (non-crimp) material (middle) and plain-weave material (right).

### PREDICTION OF MECHANICAL PROPERTIES

When conducting structural analyses of composite components, it is important to consider the effects of reorientation of reinforcement to maximise the advantages obtainable from such materials. Many approaches exist to predict mechanical properties of composite materials with respect to their orientation and, in some cases, with respect to shear deformation, e.g. due to preform manufacture or draping. Basic analytical methods begin with the rule of mixtures (ROM). Rudd et al [7] tested samples manufactured by RTM with sheared fabric reinforcement preforms and compared the tensile moduli with those found using the Krenchel-modified ROM. Agreement was noted, with predictions suggesting higher moduli than those determined experimentally. Smith et al [8] also conducted experimental tests using flat plaque samples manufactured from sheared fabrics with a range of ply angles. Comparisons were made with predictions from classical laminate theory (CLT) which appeared to give good agreement. CLT has been adopted by the authors as an acceptable first approximation, particularly when used to simulate stitched (non-crimp) fabrics, since the approach neglects the effects of crimp, or waviness, present in woven reinforcement materials.

The issue of crimp is addressed by Hofstee and van Keulen [9], who propose a method incorporating a repeating element for woven fabrics in which reinforcement tows are assumed to follow curved paths. This method also allows for nesting of multi-layered reinforcements by incorporating a geometric shift such that the warp/weft crossover of one layer lies above the gap between tows of the layer below; this improves fibre volume fraction predictions for laminates. Subsequently isostress or isostrain assumptions are made, i.e. constant stress or strain respectively are assumed throughout the tow volume, and CLT is applied using these properties. The latter two methods calculate laminate properties assuming two layers of fibre and a thin layer of (isotropic) material to represent the matrix properties. Hofstee and van Keulen consider this to be a major cause of the considerably lower predicted stiffness compared with that determined experimentally in bias tensile tests, for angles included between warp and weft fibres of less than  $90^\circ$ . Conversely it was noted that excellent agreement was observed for angles between fibres greater than  $90^\circ$ . To overcome the limitations of such simplified approaches, the three dimensional unit cell model has been proposed by a number of authors, notably Lomov et al [10] and Tan et al [11]. A similar method was also suggested by Bigaud and Hamelin [12], whose predicted results

appear to show excellent correlation to experimental data for plain- and satin-weave fabrics. The fundamental shortcomings of the approaches detailed in the literature are the inability to describe a combination of: (i) general fabric architecture, (ii) effects of shear deformation on mechanical properties due to reorientation and subsequent change in fibre volume fraction, and (iii) failure envelopes for composite materials.

The approach taken by the present authors is to use a general geometric description of a fabric such that any reinforcement can be easily modelled once certain simple geometric parameters are known. The foundations of this model were developed by Robitaille et al [13,14] and the purpose of the work in hand is to extend the description to enable the solid modelling of a unit cell of material, taking into consideration shear deformation due to preform manufacture. This will be further extended to incorporate the generation of a three dimensional mesh with each element characterised and assigned appropriate properties, such that FE simulations can be carried out on the micromechanical model to obtain mesomechanical (unit-cell) properties. A schematic illustration of the modelling process under development is shown in Figure 2.

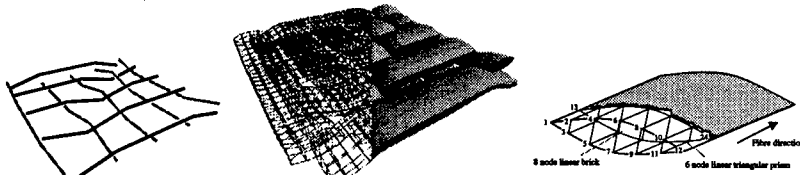


Figure 2. Graphical representations of the fabric geometric model - satin weave vector description (left) and corresponding tow mesh (right).

The basis of the model is a general description of reinforcement tow paths in vector form. Each path is constructed from a series of vectors, the start and end points of which define where possible interactions may occur with crossing tows (or threads in stitched materials).

To obtain a geometric description of the tows, the cross-section shape and the volume occupied by each tow must be defined along its length. Many descriptions impose a uniform shape to define the tow cross-sections within a unit cell [15-17], but these models were created to analyse specific weave styles. In the general case under consideration, the assumption is used that the tow perimeter in contact with a crossing tow is dictated by the crossing tow's path, enabling full three-dimensional descriptions for all weave styles to be defined, where the cross-section shape is able to change along the tow length. Since the model is designed to enable the description of sheared fabrics, the tow width is modified according to the angle through which the material has been sheared, by a method similar to that proposed by McBride [17]; this also affects the calculated tow height. The tow width variation model used was compared with experimental measurements obtained using a video camera during shearing experiments [6] and an excellent correlation was observed.

The final step in generating the solid model is to produce a mathematical description of the tow surfaces. This is implemented using Ferguson (bicubic polynomial) patches, which are defined using 16 points on the surface. These are used to allow continuity of curvature between areas on the tow surface. This is required as contacting tow surfaces, i.e. the area between crossing tows, are defined using the same surface description, hence the various adjacent surfaces must have very different, but continuous, curvature.

In order to generate a mesh for the unit cell of composite, the rhombohedral volume containing the repeat unit must be determined, and within this the tow boundary points must be identified to give mesh co-ordinates for each axis. These are points coincident with the edges of tows, found by scanning along each axis and finding the points where tows cross one another. This procedure is repeated for each axis, and forms a basis for dividing the volume into prismatic elements.

Once a mesh is generated for the rhombohedral cell volume, a test must be performed to determine whether each element lies within the matrix or the reinforcement to enable determination of the material type. For the elements in the reinforcement, their proximity to the matrix/tow interface must be established as infiltration of resin into the fibre bundle may change with distance from the tow surface. For these elements, the tow direction must also be specified as the principal material direction for the element. Appropriate mechanical properties must be assigned to each element type.

On completing this procedure for a number of unit cells with different shear angles, each one is to be analysed using appropriate boundary conditions and load cases to enable the determination of the elastic constants for the bulk material in each case. Similarly, by the application of appropriate failure criteria within the analysis, the failure envelope may be determined. Results from these analyses can then be used within the procedure described in the following section as a model for mechanical properties to be incorporated in the analysis of components on an element-wise basis.

### PREDICTION OF COMPONENT PERFORMANCE

Work has been carried out to interface the University of Nottingham Drape Model with the Abaqus<sup>TM</sup> Standard FE package. The methodology used to produce input files for Abaqus, using the draped output, is described below.

The basis for this analysis is an iterative model for draping of bi-directional textiles, which is able to predict the variation in fibre orientations and volume fraction ( $V_f$ ) over a three dimensional component. This is described in detail elsewhere [6]. A geometric mesh is loaded into the modelling application, and a draping simulation is performed. At this stage, material shear data are incorporated to give an accurate representation of fabric behaviour during draping. The modelling application is used to provide node co-ordinates, element definitions (node numbers used as vertices) and material directions (consisting of direction vectors for the warp and weft fibres).

A photogrammetric strain analysis system, CamSys<sup>TM</sup>, is also available. This enables a three dimensional model to be developed from two photographs taken from different directions, in addition to analysing shear strain in the fabric. It is envisaged that this will offer an alternative means of specifying geometry and material orientation to that offered by the drape model. A rectangular grid is marked onto a flat, undeformed piece of reinforcement fabric, the lines being marked in the warp and weft fibre directions. This fabric is subsequently draped to form the required geometry, whereupon a deformed grid is clearly visible. An accurately machined cubic target block is mounted on the preform and two photographs are taken of a section of the grid from different angles, and including the target block in the images, as shown in Figure 3. These images are loaded into the CamSys<sup>TM</sup> software, which is able to recognise automatically the orientation of the target cube, hence calculating the

relative positions of the camera in each photo. The software also recognises the points where gridlines intersect and hence, using trigonometry together with its knowledge of the original grid spacing and camera positions, a three dimensional map of these nodes is generated. These data may subsequently be imported into the modelling application to enable experimentally obtained fibre directions to be incorporated into analysis. This also has the potential to allow analysis of a component for which no electronic geometry is available. Results of shear strain analysis of the conical component under consideration obtained using this system are illustrated in Figure 4.

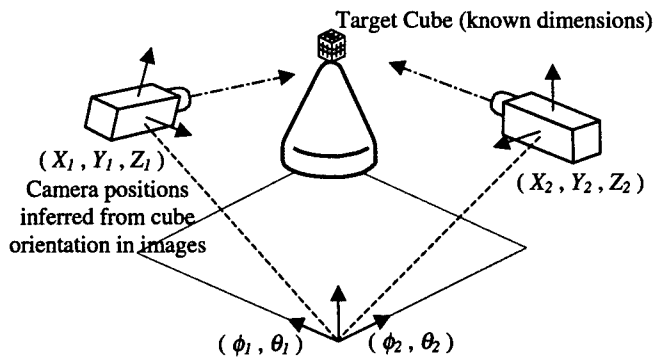


Figure 3. Schematic arrangement of photogrammetry system.

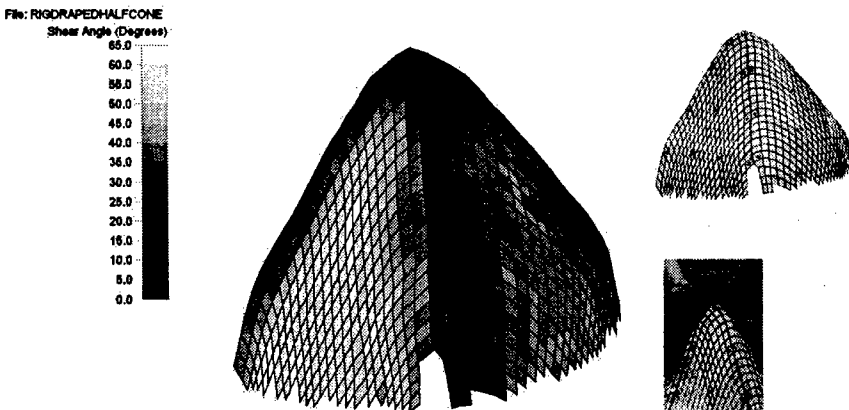


Figure 4. Results of experimental shear angle analysis from photogrammetry system (insets, lower: single photograph used in generating data, upper: photographic representation of 3D component after photogrammetric combination of images).

The orientation and shear data, obtained by either method described above, are then used by the property prediction module of the modelling application. This module is designed to be easily modified, and as a first approach calculates mechanical properties using the ROM (Equations 1a and 1b) for properties in the fibre direction:

$$E_1 = V_f E_f + (1 - V_f) E_m \quad (1a)$$

$$\nu_{12} = V_f \nu_f + (1 - V_f) \nu_m \quad (1b)$$

where subscripts *f* and *m* represent fibre and matrix properties respectively. The Halpin-Tsai relationships (Equations 2a and 2b) are used for transverse and shear properties:

$$E_2 = \frac{E_m (1 + \xi \eta V_f)}{1 - \eta V_f} \quad \text{where } \eta = \frac{E_f - E_m}{E_f + \xi E_m} \quad (2a)$$

$$G_{12} = \frac{G_m (1 + \xi \eta V_f)}{1 - \eta V_f} \quad \text{where } \eta = \frac{G_f - G_m}{G_f + \xi G_m} \quad (2b)$$

where  $\xi=2$  for  $E_2$  and  $\xi=1$  for  $G_{12}$ . [18].

This provides data for Abaqus to calculate laminate material properties for each element. CLT calculations will be incorporated into the module in due course, producing a complete stiffness modelling module, which will be suitable for incorporating new stiffness models as well as including failure criteria. As results become available from the unit-cell FE analyses described above, these may also be utilised using suitable semi-empirical property models. The approach adopted is described schematically in Figure 5, while the current implementation of the elastic property model is shown in Figure 6.

The results presented in Figure 7 show the effect of draping on displacement under a fixed load in two simulations of a conical component subjected to a radial pinch loading. Material data used are given in Table 1. Multiple load cases are used, each applying the pinch load at a different position around the draped component geometry. The trend is toward quarter-cone symmetry for plain-weave reinforced component, while the peak present at 90° for this simulation is observed to shift in correlation with the shift of the 0° shear path for the warp-knitted fabric, illustrated in Figure 1. Correlation with the output from the drape model is evident, the results highlighting the importance of the incorporation of drape data into structural analyses.

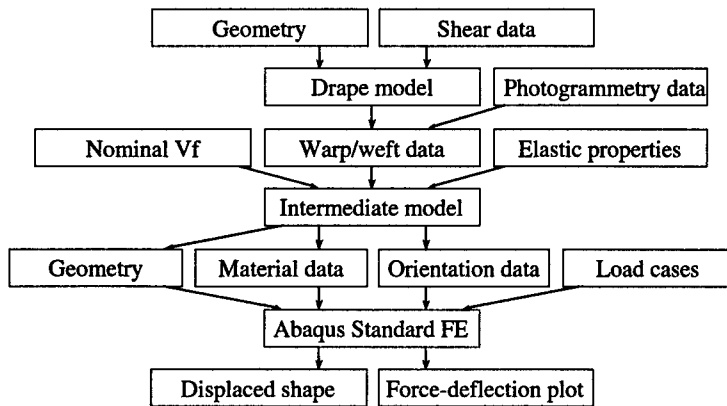


Figure 5. Overall approach to component mechanical performance modelling.

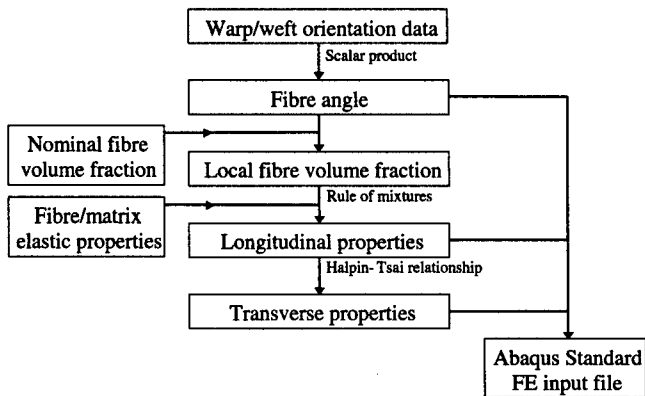


Figure 6. Current implementation of intermediate stiffness model, incorporating internal routines within Abaqus Standard to calculate laminate properties.

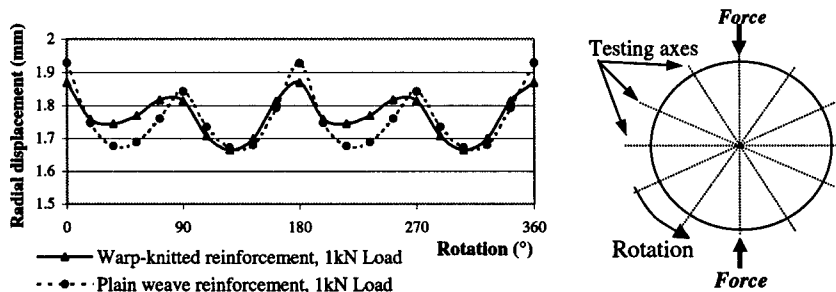


Figure 7. Results of FE analysis of the conical composite part, illustrated in Figure 1, using two reinforcement types (left); outline of testing procedure (right).

Table I. Material properties used to obtain analysis results in Figure 7.

Fibre modulus	70 GPa
Fibre poisson's ratio	0.3
Matrix modulus	1.5 GPa
Matrix poisson's ratio	0.3
Nominal fibre volume fraction	0.5

## DISCUSSION

The results shown using the initial implementation of the described methodology illustrate the potential application for such a technique in composite component design and analysis. The importance of more accurate descriptions of material behaviour is demonstrated, particularly for highly draped components.

The intention of the authors is to develop a generic approach to mechanical analysis of components via a mesoscopic model for mechanical properties at element level. Ultimately the intermediate stiffness model will be provided by FE analysis of solid models for a general textile composite unit cell, incorporating changes in properties due to shear deformation during preform manufacture.

Models will be validated using mechanical test data for a range of engineering components in addition to simple test specimens. Failure criteria will also be incorporated to enable complete component performance modelling with a modular approach, allowing the incorporation of new models as they become available.

#### ACKNOWLEDGEMENTS

The work is funded by the EPSRC, and the authors wish to express their gratitude to The Ford Motor Company, Dowty Aerospace Propellers, ESI and Formax UK for their support. The authors also wish to thank Tim Baillie for his contribution to the implementation of the stiffness model.

#### REFERENCES

1. Mohammed, U., Lekakou, C. and Bader, M.G., "Experimental Studies and Analysis of the Draping of Woven Fabrics", *Composites: Part A*, 2000, Vol. 31, pp. 1409-1420.
2. Gutowski, T., Hoult, D., Dillon, G. and Gonzalez-Zugasti, J., "Differential Geometry and the Forming of Aligned Fibre Composites", *Composites Manufacturing*, 1991, Vol. 2, pp. 147-152.
3. Rozant, O., Bourban, P.-E. and Manson, J.-A.E., "Drapability of Dry Textile Fabrics for Stampable Thermoplastic Preforms", *Composites: Part A*, 2000, Vol. 31, pp. 1167-1177.
4. Daniel, J.L., Gasser, A., Hivet, G., Soulat, D. and Boisse, P., "Effects of Fabric Mechanical Behaviour on Finite Element Simulations of Preform Manufacture", *Proceedings of the 5<sup>th</sup> Conference on Textile Composites*, 2000, Leuven, Belgium.
5. Hammami, A., Trochu, F., Gauvin, R. and Wirth, S., "Directional Permeability Measurement of Deformed Reinforcement", *Journal of Reinforced Plastics and Composites*, 1996, Vol. 15, pp. 552-560.
6. Souter, B.J., Long, A.C., Robitaille, F. and Rudd, C.D., "Modelling the Influence of Reinforcement Architecture on Formability", *Proceedings of the 9<sup>th</sup> European Conference on Composites Materials*, 2000, Brighton, England.
7. Rudd, C.D., Long, A.C., McGeekin, P., Cucinella, F. and Bulmer, L.J., "Processing and Mechanical Properties of Bi-directional Preforms for Liquid Composite Moulding", *Composites Manufacturing*, 1995, Vol. 6, pp. 211-219.
8. Smith, P., Rudd, C.D. and Long, A.C., "The Effect of Shear Deformation of the Processing and Mechanical Properties of Aligned Reinforcements", *Composites Science and Technology*, 1997, Vol. 57, pp. 327-344.
9. Hofstee, J. and van Keulen, F., "Stiffness Models as an Interface Between Drape Simulation and Structural Analysis: An Overview", *Proceedings of the 5<sup>th</sup> Conference on Textile Composites*, 2000, Leuven, Belgium.
10. Lomov, S.V., Gusakov, A.V., Huysmans, G., Prodromou, A. and Verpoest, I., "Textile Geometry Preprocessor for Meso-mechanical Models of Woven Composites", *Composites Science and Technology*, 2000, Vol. 60, pp. 2083-2095.

---

ICMAC - International Conference for Manufacturing of Advanced Composites

11. Tan, P., Tong, L. and Steven, G.P., "Micromechanics Models for the Elastic Constants and Failure Strengths of Plain-Weave Composites", *Composite Structures*, 1999, Vol. 47, pp. 797-804.
12. Bigaud, D. and Hamelin, P., "Mechanical Properties Prediction of Textile Reinforced Composite Materials Using a Multiscale Energetic Approach", *Composite Structures*, 1997, Vol. 38, pp. 361-371.
13. Robitaille, F., Clayton, B.R., Long, A.C., Souter, B.J. and Rudd, C.D., "Geometric Modelling of Industrial Preforms: Woven and Braided Textiles", *Proceedings of the Institute of Mechanical Engineers*, 1999, Vol. 213, Part L, pp. 69-84.
14. Robitaille, F., Clayton, B.R., Long, A.C., Souter, B.J. and Rudd, C.D., "Geometric Modelling of Industrial Preforms: Warp-knitted Textiles", *Proceedings of the Institute of Mechanical Engineers*, 2000, Vol. 214, Part L, pp. 71-90.
15. Peirce, F. T., "The Geometry of Cloth Structure", *Journal of the Textile Institute*, 1937, Vol. 28, Issue 3, pp. T45-T96.
16. Kemp, A., "An Extension to Peirce's Cloth Geometry to the Treatment of Non-Circular Threads", *Journal of the Textile Institute*, 1958, pp. T44-T48.
17. McBride, T.M. and Chen, J., "Unit-Cell Geometry in Plain-Weave Fabrics During Shear Deformations", *Composites Science and Technology*, 1997, Vol. 57, pp. 345-351.
18. Daniel, I.M. and Ishai, O., "Engineering Mechanics of Composite Materials", *Oxford University Press*, 1994, pp. 73-76.

### Ultrasonic Cure Monitoring of RTM6 Epoxy Resin

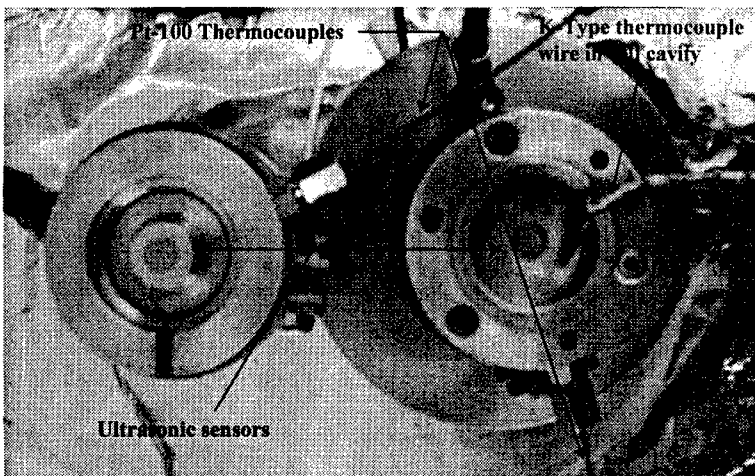
*J McHugh, J Döring, W Stark, Federal Institute for Materials Research and Testing, Berlin, Germany*

*I K Partridge, Advanced Materials Department, Cranfield University, Bedford, UK*

This poster presents a non-destructive ultrasonic method suitable for the cure monitoring of thermosetting resins. The propagation of ultrasonic waves corresponds to a dynamic mechanical deformation at high frequencies being imposed on the curing polymer. The elastic properties of the material through which the wave passes will influence the speed of its propagation and amplitude. By measuring the ultrasonic sound transmission parameters, namely the velocity and the attenuation, it is possible to monitor the curing process.

The ultrasonic method employs two longitudinal ultrasonic transducers, which operate in through transmission. The sensors plus equipment and software (US-Plus) were developed for the process monitoring of thermosetting moulding compounds and are capable of withstanding high temperatures and pressures. (Rath, 1999<sup>1</sup>, Döring 2000<sup>2</sup>)

RTM6 is the trade name for a resin transfer moulding epoxy amine resin system. Ultrasonic measurements were performed throughout the curing process on RTM6 resin. A specially constructed measuring cell, containing two ultrasonic sensors mounted on opposite sides of the cell cavity, was employed and is shown below. The objective of this study is to provide a correlation between the evolution of cure and the ultrasonic parameters. To aid in interpretation Differential Scanning Calorimetry and Rheometric techniques are used and the results reported.



<sup>1</sup> Rath, M., Döring, J., Stark, W., Hinrichsen, G., "Process Monitoring of Moulding Compounds by Ultrasonic Measurements in a Compression Mould" NDT&E International, 33, 123, (2000).

<sup>2</sup> Döring, J., Bartusch, J., McHugh, J., Stark, W. Contribution to Ultrasound Cure Control for Composite Manufacturing" 15<sup>th</sup> World Conf. on NDT, Rome, (2000)

**HYBRID PROCESSING OF COMPOSITE/METAL LAMINATES FOR  
LIGHTWEIGHT AUTOMOTIVE BODY STRUCTURES**

B M Weager, C D Rudd

*School of Mechanical, Materials, Manufacturing Engineering and Management  
University of Nottingham, University Park, Nottingham NG7 2RD, UK*

**ABSTRACT**

**1.1.1**

Hybrid thermoplastic composite/metal laminates have been prepared by non-isothermal compression moulding of Twintex<sup>®</sup> or GMT and steel or aluminium. Composite/metal adhesion is dominated by mechanical phenomena such as keying or interlocking. Bonding has been achieved by surface pre-treatment of the metal, to increase the number of mechanical keying sites, or by incorporation of a modified polymer at the composite/metal interface, to improve flow into the keying sites. Enhanced bonding has been observed when using a combination of surface treatment and polymer interlayer. The composite/metal interfacial bond has been tested using short beam shear and single cantilever beam testing. Surface treatments and fracture surfaces have been evaluated using optical and electron microscopy.

**INTRODUCTION**

Thermoplastic matrix composites are thought to have many potential applications in the automotive industry, specifically to reduce vehicle weight and manufacturing cost. To minimise capital investment, it is preferable to select materials that can be joined conveniently into parent metal structures (e.g. pressing, folding, spot welding, painting etc.), thereby reducing expenditure on new tooling and machinery. It is thought that hybrid fibre/metal laminates, consisting of alternate plies of sheet metal and thermoplastic composite, could yield significant weight reductions while avoiding major investment in new equipment.

Fibre/metal laminates (FML) such as GLARE<sup>®</sup> and ARALL<sup>®</sup>, which are based on thermosetting matrices and aluminium, have been under development for the aerospace industry since the early 1980s [1]. These materials have been found to exhibit excellent fatigue resistance, impact resistance and damage tolerance [2], and are being considered for commercial aircraft such as the Boeing A380. To date, thermoplastic-based hybrid laminates have received little attention in this aerospace driven sector. However, they are thought to have potential applications in the automotive industry, due to faster production times and higher recyclability than thermosets. Hylite<sup>®</sup> is an aluminium/polypropylene/aluminium sandwich sheet developed by Corus for use in automotive bonnets. A weight saving of 65% has been reported [3] for a Hylite<sup>®</sup> part over a steel part of equal stiffness, but the cost is currently prohibitively high. Reyes and

Cantwell [4] have produced laminates of unidirectional glass-fibre reinforced polypropylene and aluminium, using amorphous chromate treated aluminium and a polypropylene maleic anhydride interlayer to improve bonding. They have found high interfacial fracture toughness values ( $G_I=2400\text{J/m}^2$ ) and excellent impact properties.

The aim of this work is to identify suitable surface treatment systems for bonding two glass-fibre/polypropylene composites (Twintex<sup>®</sup> and GMT) to aluminium and steel.

## EXPERIMENTAL

The materials under investigation are Twintex<sup>®</sup> (Vetrotex), a commingled woven composite consisting of glass fibre tows and polypropylene strands, and GMT (Symalit), a random glass/polypropylene composite. Hybrid laminates have been produced by non-isothermal compression moulding of pre-heated sheet metal and composite stacks. The metals were given various surface treatments prior to heating and moulding. Steel surface treatments included grit-blasting, zinc galvanising and phosphating. Aluminium surface treatments included grit-blasting, sulphuric acid anodising (SAA), and PT2, a hydrolysing treatment developed by Alcan (subject to patent EP0796300B1) to improve adhesion of paints and adhesives to aluminium. Scanning Electron Microscopy (SEM) was used to evaluate the topography of the treated surfaces. Where appropriate, a polymer interlayer was incorporated at the metal/composite interfaces. The interlayer materials included two polypropylene-graft-maleic anhydride (PP-g-MAH) copolymers, Fusabond<sup>®</sup> M613-05 (DuPont) and No. 426512 (Sigma-Aldrich), and a polypropylene adhesive film XAF 23.101 (Sarna-Xiro/Cornelius UK).

Interfacial bonding has been evaluated using Short Beam Shear (SBS) and Single Cantilever Beam (SCB) mechanical tests. Specimens were cut using both abrasive water jet cutting and bandsaw/milling techniques. Fracture surfaces have been examined using optical and electron microscopy.

## RESULTS & DISCUSSION

Table I summarises the qualitative bonding behaviour of the material and surface treatment combinations attempted. Surface treatment of the metal, or the incorporation of a polymer interlayer, was found to be essential in obtaining adhesion between the composite and metal. Figure 1 contains SEM micrographs of selected surface treated metals. Composite/metal bonding was found in general to depend on the availability of mechanical keying sites on the metal surface. For example, adhesion was observed when employing grit-blasting and anodising treatments, which exhibit the greatest surface roughness and greatest number of pores. Bonding was achieved when using all three types of polymer interlayer. This is thought to be a result of improved flow and intimate contact between the polymer and the metal surface, arising from the lower molecular

ICMAC - International Conference for Manufacturing of Advanced Composites

weight and hence lower viscosity of the modified polymers. Some polar bonding may result from the presence of maleic anhydride reactive groups near the metal surface.

Surface Treatment	GMT		Twintex®	
	Steel	Alu	Steel	Alu
Untreated (cleaned)	×	×	×	×
Emery Abrasion	×	×	×	×
Grit Blasting	✓	✓	✓	✓
Zinc Electrocoat	×			
Zinc Galvanealed	×			
Phosphating	×			
Anodising (SAA)		(✓)		
PT2				×
PP-g-MAH interlayer (Aldrich)	✓	✓	✓	✓
Fusabond® PP-g-MAH (DuPont)	✓	✓	✓	✓
PP adhesive film	✓	✓	✓	✓

Table I - Summary of hybrid laminate moulding, ✓ - bonding, (✓) - partial bonding, × - no bonding.

Improved bonding was achieved by using combinations of surface treatment and polymer interlayer. For example, without a polymer interlayer bonding was not achieved for phosphated steel or PT2 treated aluminium. But the addition of a polymer interlayer resulted in good bonding. It is suggested that the polymer interlayers make greater use of mechanical keying sites and therefore improve mechanical adhesion (interlocking).

Photographs of selected short beam shear (SBS) test specimens are shown in Figure 2. Multiple shearing can be seen in all specimens, suggesting that the test is measuring the shear strength of the composite along with that of the composite/metal interface. This is due to the point of maximum shear not corresponding to the composite/metal interface.

Figure 3 contains two SEM micrographs of SBS test specimen fracture surfaces; PP-g-MAH residue is widespread and there are isolated residual composite. This suggests that the fracture grows mainly at the PP-g-MAH/metal interface and often into the relatively brittle PP-g-MAH interlayer. Only occasionally does the crack grow into the tougher composite. Early indications are that single cantilever beam (SCB) testing is more successful in evaluating the properties of the composite/metal interfacial bond. However, this work is still in its early stages.

## CONCLUSIONS

- Adhesion enhancing surface treatments are required to bond polypropylene-based composites to steel and aluminium.

#### ICMAC - International Conference for Manufacturing of Advanced Composites

- For these materials, bonding is predominantly a mechanical process of keying and interlocking and therefore depends (1) the surface topography of the metal and (2) the viscosity of the polymer at the metal surface.
- Bonding is improved by using a combination of a metal surface treatment and modified polymer interlayer.
- Polypropylene-graft-maleic anhydride (PP-g-MAH) improves bonding but is relatively brittle and provides an easy crack propagation path.
- A polypropylene adhesive film enhances bonding and is comparatively tough.
- Suitable treatments for aluminium are grit-blasting, sulphuric acid anodising (SAA) and PT2, a hydrolysing treatment developed by Alcan (patent EP0796300B1).
- Suitable treatments for steel are grit-blasting and phosphating.
- Short beam shear (SBS) testing is inappropriate for evaluating the interfacial bonds as the position of maximum shear is not at the composite/metal interface.

#### FUTURE WORK

The next stage of this work is to use the single cantilever beam (SBS) test to make quantitative comparisons of the interfacial fracture toughness of composite/metal bonds with the various surface treatments and polymer interlayers. Drop weight impact (DWI) testing will also be carried out and delamination measured using a thermal imaging camera. Other surface treatments to investigate include amorphous chromating, phosphoric acid anodising (PAA), silanes and primers.

#### ACKNOWLEDGEMENTS

The authors acknowledge the continued support of Ford Motor Company and the technical assistance of Alcan International Limited.

#### REFERENCES

1. Gunnink, J.W., M.L.C.E. Verbruggen, and L.B. Voegesang, *ARALL, a light weight structural material for impact and fatigue sensitive structures*. Vertica, 1986. **10**(2): p. 241-254.
2. Voegesang, L.B. and A. Vlot, *Development of fibre metal laminates for advanced aerospace structures*. Journal of Materials Processing Technology, 2000. **103**: p. 1-5.
3. Veenstra, E.W., *Aluminium-plastic-aluminium sandwich for maximum weight reduction in body panels*, . 1993, SAE.
4. Reyes, G. and W.J. Cantwell, *The mechanical properties of fibre-metal laminates based on glass fibre reinforced polypropylene*. Composites Science and Technology, 2000. **60**: p. 1085-1094.

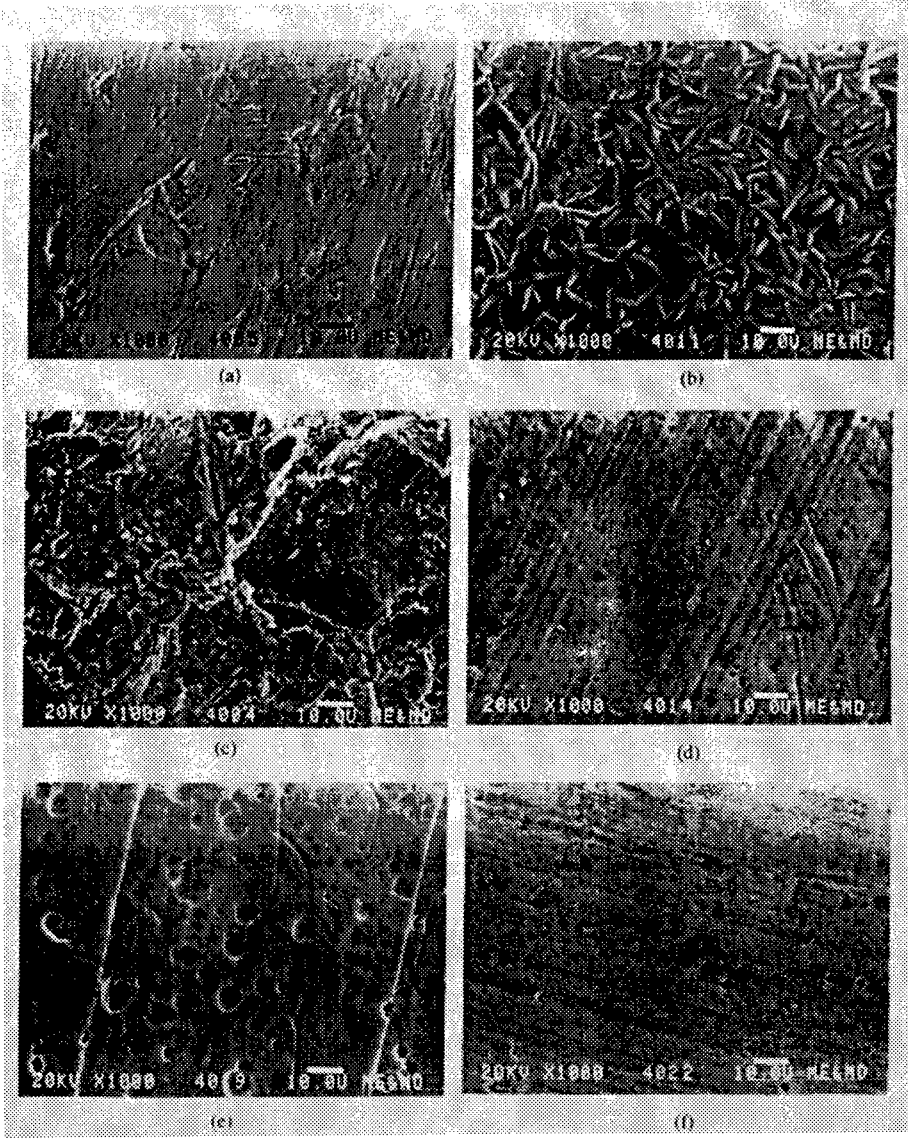
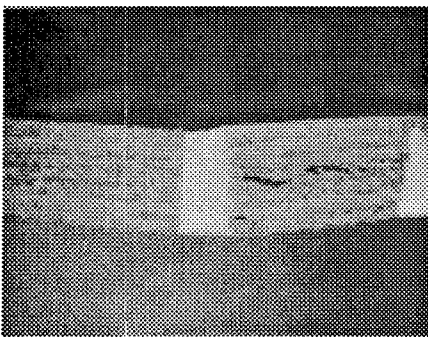
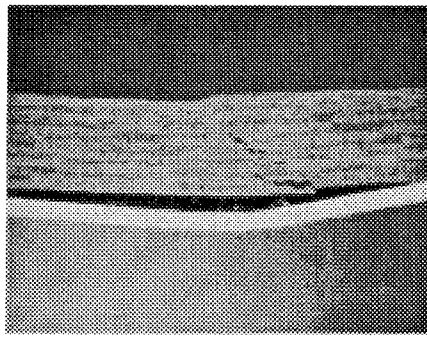


Figure 1 – SEM micrographs of metal surfaces, (a) untreated steel, (b) phosphated steel, (c) grit blasted steel, (d) untreated aluminium, (e) SAA anodised aluminium, (f) PT2 aluminium.

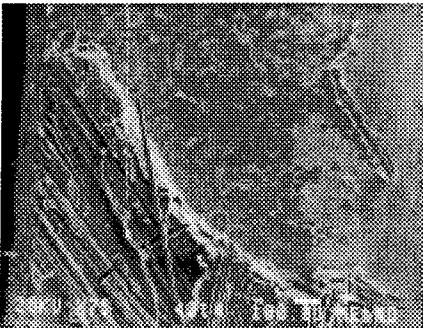


(a)

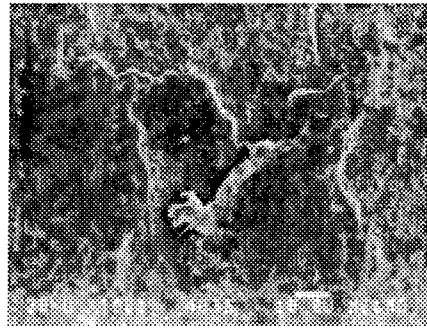


(b)

Figure 2 – Photographs of Short Beam Shear test specimens, (a) Twintex®, (b) Twintex®/PP-g-MAH/steel.



(a)



(b)

Figure 3 – SEM micrographs of short beam shear test specimen fracture surfaces, (a) GMT/PP-g-MAH/aluminium, (b) Twintex®/PP-g-MAH/steel.

**A Modified System for Design and Analysis of 3-D Woven Preforms**

J. Quinn, R. McIlhagger, A.T. McIlhagger P.P.J. Rogers.

Engineering Composites Research Centre (ECRE),  
Department of Electrical and Mechanical Engineering,  
University of Ulster at Jordanstown, Shore Road, Newtownabbey,  
Co. Antrim, BT37 0QB, Northern Ireland, UK.

**Abstract**

This paper describes a system to predict the properties, in particular, the areal density and z-axis fibre content of a 3-D-woven preform. Previously the model used had incorporated an idealised yarn path to describe the placement of a warp yarn within the fabric. The idealised yarn path was found to provide some correlation between predicted and actual values particularly for integrated structures. It was felt however that the idealised yarn model did not truly reflect the actual yarn path for an interlinked structure and a lenticular model was put forward as a replacement. Following the same procedure as in previous work fabrics were produced and tested. Prediction made using the lenticular model was found have a reasonable correlation in terms of both areal density and % z-axis fibre prediction than the idealised model.

**Introduction**

Traditionally composite components are manufactured using the lay-up technique. Fibre reinforced laminates have been used for many years in the boat building industry[1], aerospace and automotive industry[2],[3],[4]. The use of laminates has been limited by a number of factors including, manufacturing problems and some inferior mechanical properties when compared to some of the more mainstream materials such as aluminium. In the lay-up process, layers of reinforcement (dry reinforcement or prepreg) are stacked on top of one another to form a laminate and then processed by various different methods depending in the application of the final component. This is a long and arduous process and does not lend itself readily to the cost conscious and lean production schedules of today. Added to this, laminates have, in the case of prepreg, a high-added cost derived from the manner in which they must be handled and stored. With rising interest in the use of composite materials for applications not related to the high tech aerospace and high-end car markets, there is a need for the development and understanding of other methods of preform manufacture that will be more attractive to these sectors.

One possible solution to the problems associated with production of composite component using laminates that has come under considerable review over the last number of years is the use of 3-D woven preforms. Techniques involved in the manufacture of these textiles allow the production of near net shaped preforms, thereby reducing a portion of the cost of component manufacture. 3-D woven preforms can also provide improvements in mechanical properties of composite components, one area highlighted by literature is that of interlaminar shear strength

[5], however there are also reported improvements in damage tolerance and impact resistance [6].

3-D woven composite structures have a number of distinct advantages over 2-D counterparts and these are outlined in below:

- 3-D weaving can produce near net shaped preforms
- 3-D woven composites with complex geometry's can be less expensive to produce
- 3-D weaving allows the tailoring of properties for specific applications
- Better r delamination resistance and damage tolerance

3-D weaving takes a number of different forms, orthogonal, layer interlock and, multi-axis woven textiles. Weaving of these technical textiles can be achieved quite easily with the modification of the standard weaving machinery used to manufacture cloth for textile applications. The 3-D weaving process involves the integration of Z-axis or through the thickness yarns within the structure of a multi-layer dry reinforcement. The nature of the design process for these structures allows the designer/engineer to weave properties into different areas of the reinforcement, hence facilitating the tailoring of the mechanical properties of the composite for different situations. Research has been completed on design and optimisation of 3-D woven carbon reinforcements for use in lower leg prosthesis. The lower leg prosthesis [7] was designed on the basis of energy conservation and the versatility of the 3-D weaving process allowed the designer to allocate different stiffness properties along the length of a limb shaped component. This work concluded that 3-D woven reinforcements offered significant potential for stiffness tailoring with controlled fibre placement in three mutually perpendicular directions. Added to this, recommendations were made for work to be completed on strength analysis and stiffness optimisation of 3-D woven composites based on the fibre architecture.

In 3-D weaving, the warp (or  $0^\circ$  direction) yarns provide through-the-thickness (TTT) reinforcement to consolidate the preform. The TTT yarns are arranged in different areas and levels of the reinforcement according to the net shape and mechanical properties required. These TTT yarns have been shown to provide increases in interlaminar shear strength of composite components. The XS design system and manufacturing facilities within the University of Ulster have been discussed previously [8], and they provide an in house source of fabric design data. A model has been presented by the author to describe the architecture and division of yarn within the fabric as well as prediction of thickness and fibre volume fraction ( $v_f$ ).

Prediction of the properties of these weave structures can play a large part in the understanding of the fabric structures involved with 3-D woven textile usage. Prediction of the fabric properties can be of use in areas including the modelling of textile structures for finite element analysis. Previously [8] a model was presented using an idealised yarn path model shown in Figure 1.

3D Woven fabric sample

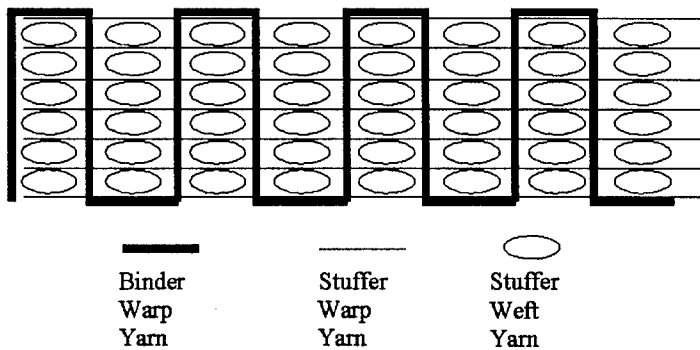


Figure 1 Idealised yarn path through an interlinked 3-Dwoven-fabric structure.

The idealised yarn path provided the basis of a model for predicting the percentage fibre in each direction and areal density. However it was noted in the paper that the idealised yarn path was not a true reflection of the yarn path and that a model close to the actual yarn path must be used. It is proposed to use a lenticular-based model to describe this. Figure 2 shows an illustration of the lenticular style yarn path.

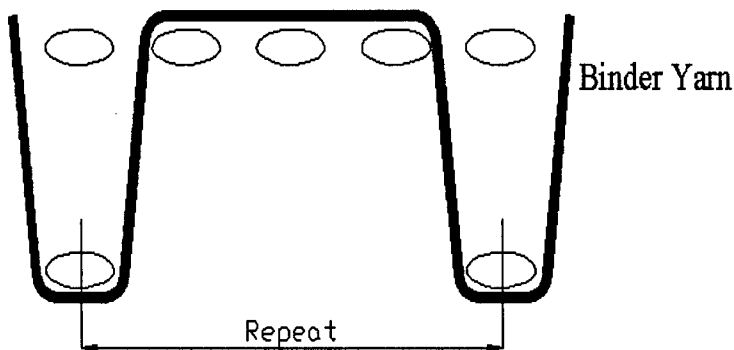


Figure 2 Lenticular yarn path representation ( equivalent to a 4 harness satin)

**Theoretical Approach**

The approach adopted is to sum the volumes of all yarns in each of the mutually perpendicular directions to determine the total volume of yarn in the fabric structure and hence using the densities of the constituent parts the weight per unit area can be determined.

**Methodology**

A family of three interlinked samples were selected, an interlinked structure being defined as a multi-layer structure with warp binder yarns only linking the top and

bottom layers of weft yarns, the binders passing through the complete thickness of the structure. In between these layers a number of stuffer warp yarns are inserted, in these samples the number was four. Three interlinked structures were equivalent to a 4, 6 and 8 harness satin arrangement for the binder yarns.

These three fabrics were designed using the XS program and as indicated above the lifting plan was generated in preparation for fabric production. Representative one-metre lengths of each of these fabrics were produced using an electronic Jacquard controlled DATAWEAVE loom with a rapier for weft insertion. The fabrics were produced from a 12k 800 tex carbon fibre warp (Toray T300) using a weft insertion rate of 60 picks/min again with 12k (800 tex T300) carbon fibre weft.

The resulting fabrics were analysed as follows. The areal density and fabric thickness were measured using standard methods[9],[10]. The fabric structures were inspected carefully to ensure that the relative positions of the warp and weft yarns were in keeping with the original designs. The structures (10 cm by 10 cm) were analysed and the lengths of the stuffer warp yarns, the binder yarns and the weft yarns were measured in the fabric, and individually after being gently straightened under minimum tension. The weights of all the warp stuffers, the weft yarns and the binder yarns were also measured. All of these results were recorded on a spreadsheet for further analysis.

In parallel, knowing the warp and weft densities, the interlink density and the fabric thickness the reinforcement properties were determined. It is expected that similar data on a range of integrated fabric structures will also be presented in further validation of the system.

**Results**

The XS design system parameters for the weave structure are shown in Table I

Fabric Code	Warp Stuffer Density (ends/cm)	Weft Density (picks/cm)	Interlink Density (links/6 picks)	Yarn Count (tex)
A	3	2	1.5	800
B	3	2	1.0	800
C	3	2	0.75	800

Table I. Fabric design specification.

Visual analysis of the fabric allowed the information in Table II to be collected. It is clear from Tables I and II there is some good correlation between the design parameters and the actual properties achieved by the loom.

Fabric Code	Warp Stuffer Density (ends/cm)	Weft Density (picks/cm)	Interlink Density (links/6 picks)	Areal Density (g/m <sup>2</sup> )	Fabric thick. (mm)
A	2.4	1.9	1.7	2301	4.4
B	2.3	1.9	1.1	2296	4.0
C	2.3	2.0	0.75	2187	3.8

Table II. Fabric analysis

Dismantling the fabric structures yielded the following data. Since the yarn count for all yarns was the same the values of X, Y and Z represent the fibre volume fractions in the three mutually perpendicular directions.

Fabric Code	Warp Stuffer Length (cm)	Weft Yarn Length (cm)	Warp Binder Yarn Length (cm)	X (%)	Y (%)	Z' (%)
A	10.02	10.12	10.98	58.4	40.0	1.6
B	10.17	10.22	10.92	57.7	41.1	1.2
C	10.04	10.32	10.38	56.3	43.2	0.6

Table III. Fabric analysis by length measurements.

The difference between the yarn length measurements in the fabric and when flattened gives a measure of the degree of crimp, particularly in the warp stuffer and the weft directions. Table IV shows the predicted properties for the fabrics used generated by the revised lenticular model.

Fabric Code	Mean Warp Stuffer Length (cm)	Mean Weft Yarn Length (cm)	Mean Warp Binder Yarn Length (cm)	X (%)	Y (%)	Z' (%)
A	589	400	20.0	58.4	39.6	2.0
B	1326	939	21.9	58.0	41.1	1.0
C	2240	1670	26.7	56.9	42.4	0.7

Table IV. Fabric property prediction by Lenticular Model.

A comparison of the design, predicted ideal, predicted lenticular and actual fabric properties are shown in Table V.

Fabric A	Thickness	Areal Density (g/m <sup>2</sup> )	X (%)	Y (%)	Z' (%)	Fibre Volume Fraction
Measured	4.4	2301	58.4	40.0	1.6	29.4
Idealised	3.6	2385	58.6	36.3	5.2	37.7
Lenticular	4.0	2302	58.4	39.6	2.0	32.5
Design	4.0	2708	62.0	35.5	2.5	38.2
Fabric B	Thickness	Areal Density (g/m <sup>2</sup> )	X (%)	Y (%)	Z' (%)	Fibre Volume Fraction
Measured	4.0	2296	57.7	41.1	1.2	32.2
Idealised	3.6	2335	56.8	39.6	3.6	36.9
Lenticular	4.0	2221	58.0	41.1	1.0	31.4
Design	4.0	2674	62.8	35.9	1.3	37.8
Fabric C	Thickness	Areal Density (g/m <sup>2</sup> )	X (%)	Y (%)	Z' (%)	Fibre Volume Fraction
Measured	3.8	2187	56.3	43.2	0.6	32.3
Idealised	3.6	2313	56.9	40.4	2.8	36.5
Lenticular	4.0	2263	56.9	42.4	0.7	32.0
Design	4.0	2660	63.2	36.1	0.8	37.8

Table V Comparison of Idealised and Lenticular yarn path representations

It can be seen from Table V the lenticular model used to represent the yarn path is much more accurate when predicting the % z axis fibre. Note this is when the %z axis fibre is assumed to be the difference in mean binder length and mean warp stuffer length, the difference being the interlink fibre length. In terms of both z' axis fibre prediction and areal density the correlation between the actual fabric properties and the predicted properties using the lenticular model is very good.

### Conclusions

Previously in the prediction of the fabric properties an idealised model was used to describe the yarn path through a 3-D-woven preform, it was found that although there was some correlation between the actual and predicted values it was not a very strong relationship. Revision of the model has led to the use of a lenticular model describing the yarn path. It has shown a good correlation between the actual and predicted values. Z-axis fibre content prediction in particular has been improved to a large extent. Further work in this area has now to include prediction of fully integrated fabric structure properties.

**References**

- [1]Smith CS. Design of marine structure in composite Materials London Elsevier Applied Science 1990
- [2]Haresceugh RI Aircraft and Aerospace applications of Composites In: Kelly A editor; Concise encyclopaedia of composite materials Oxford: Pergamon Press 1989. Pp 1-7
- [3]Niu MCY. Composite Airframe Structures, Hong Kong: Conmilin Press 1992
- [4]Beardman P. Automotive Components : fabrication. Kelly A editor; Concise encyclopaedia of composite materials Oxford: Pergamon Press 1989. Pp 24-31
- [5] S.T. Matthews, B.J. Hill, A.T. McIlhagger and R. McIlhagger Proc. The Sixth International Conference on Automated Composites Sept. 99 Bristol, pp 195-201
- [6] M.H. Mohamed et al 3TEX Inc. Sampe Journal May/June 2001
- [7] Limmer, L.; Weissenbach, G.; Brown, D.; McIlhagger, R.; Wallace, E. Composites - Part A: Applied Science and Manufacturing, v 27, 4, (1996), p 271-277
- [8]J.P. Quinn, B.J. Hill, R.McIlhagger Composites A 32 (2001) 911-914
- [9]Standard test method for fabric areal density. ASTM Standard D 3776.
- [10] Standard test method for fabric thickness. ISO Standard 4603 Textile Glass – Woven Fabrics Determination of Thickness.

**The Automatic Generation of a Solid Model of a Plain Weave Structure.**

Desmond Brown and Margaret Morgan  
University of Ulster Jordanstown

**Abstract**

Visualisation of complex 3-D textile structures used to reinforce advanced composite materials can be extremely difficult. 3-D models to assist in visualisation are recognised as very helpful. In addition they can be used as the basis for parametric studies and Finite Element analysis, although the latter downstream use puts considerable demands upon the solid model.

This paper describes a technique to automatically generate a parametric solid model of a woven textile reinforced composite material. The solid model is generated using a program file written in I-deas© Open Language. The input data describes the cross-sectional shape of yarns. The system uses this data to automatically generate a set of basic yarn "parts". It then proceeds to put these together in an assembly with appropriate constraints maintaining the correct relative positions of the yarns. This assembly constitutes the RVE of the fabric structure. To demonstrate the principle, the approach is applied to the modelling of a 2-D plain weave structure.

**Introduction**

In order that the potential of 3-D woven textile reinforced composite materials can be fully realised, it is essential that mechanical characterisation data of the composite structure is either readily available or able to be accurately predicted. It is well documented that the mechanical behaviour of a woven reinforced composite structure is heavily influenced by the shape and material type of the reinforcement [1-5] Whilst the construction of a materials characterisation database is ongoing [6] it is unlikely, given the number of reinforcement variations that are available, that a comprehensive database covering all design situations, will be developed. As the manufacturing technology associated with the production of 3-D woven structures becomes more sophisticated the types of 3-D structures that can be produced will be greater.

The need therefore exists for the capability to accurately predict the mechanical performance of a reinforced composite material. This capability relies, in part, on the textile technologist's ability to accurately model the reinforced composite structure.

**2 Dimensional and 3 Dimensional Weaving**

The weaving process can produce both 2D and 3D structures. Traditionally 2D weave patterns were produced consisting of interlaced yarn fibres in the X and Y directions - commonly known as the warp and weft respectively. The composite structure is manufactured by 'laying-up' multiple 2D patterns in specific fibre orientations -  $0/90^\circ$  and  $\pm 45^\circ$ . These  $\pm 45^\circ$  fibre orientations significantly increase the resistance to in-plane shear. Typical 2D laminae forms include uni-directional tape, plain weaves and 5 harness satins. The lay-up process is very labour intensive, process repeatability is difficult and consequently inspection time is great. Manufacturing costs are significantly greater than for traditional metallic components typically five times greater than for aluminium[7].

In 3-D weaving the textile reinforcement has fibre in all three axes -

X direction - traditional warp yarn,  
Y direction - traditional weft yarn and  
Z direction - the through-the-thickness yarn which, in principle, can be either from the warp or the weft, although in practice it is generally from the warp.  
The weaving process is a highly developed cost effective manufacturing procedure which has the potential to significantly reduce the manufacturing lead times for composite reinforcements. Conventional looms with minimal modification can be used - thus large capital investment in highly specialised machinery is not required.

### 2-D and 3-D Woven Reinforcements

It is important to distinguish between 2-D and 3-D reinforcements. Cox [8] defines the dimensionality of a structure as its ability to carry an 'important' load in two or three linearly independent directions. Examples of 2-D woven reinforcements include orthogonal plain, twill and satin weaves are shown in Figure 1.

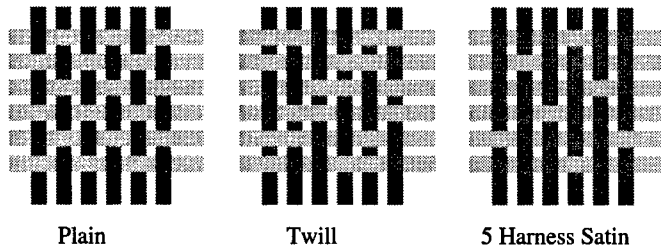


Figure 1

Composites reinforced with these types of structures have the ability to transmit an important load along the two perpendicular axes, the X and Y axes, or the warp and weft respectively in weaving terminology.

Using the classification developed by Cox, the main types of 3-D woven reinforcement are angle interlock and orthogonal interlock weave patterns. These 3-D structures can carry 'important' loads in the X, Y and Z directions. An orthogonal interlock weave system is essentially a special case of an angle interlock weave system where the interlinking yarns in the Z axis are perpendicular to the warp yarns. Examples of these structures are shown in Figure 2.

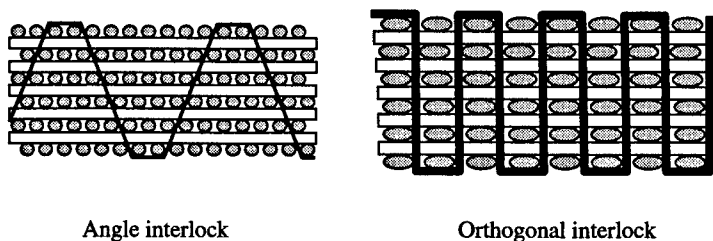


Figure 2

### **Advantages of 3-D Textile Reinforcements**

3-D textile reinforcements have a number of advantages when compared to 2-D reinforcing systems. Whilst composite materials reinforced with 2-D systems exhibit high in-plane stiffness, their inter-laminar strength is very low. When an out-of-plane load is applied delamination of the composite layers can occur and this leads to damage or failure. Ko [9] demonstrated that only a small amount of through-the-thickness reinforcement was required to significantly increase the damage tolerance of the composite structure. This was achieved at the expense of a small decrease in the level of in-plane stiffness.

Another significant advantage 3-D reinforcements have when compared to 2-D systems is their ease of use or handleability. One of the manufacturing costs associated with the production of reinforced composite materials is the labour intensive lay-up process. 3-D fabric reinforced structures are much easier to manipulate during the manufacturing process and since the 3-D reinforcement integrates or combines a number of layers, much less handling is required.

### **Manufacture of Angle Interlock Reinforcing Structures**

3-D structures can be produced on a modified Jacquard loom. On the loom the warp yarns enter more than one layer of weft yarns. Today most Jacquard looms are electronically controlled and programmed. The flexibility offered in terms of available weave patterns and number of layers entered, means that a wide variety of weave structures can be produced. The process allows an almost infinite number of different fibre architectures to be produced. The textile reinforcement can be matched to stiffness requirements and complex structures can be woven with very little direct labour input. The integrated preform thus produced is very appropriate for modern impregnation methods such as Resin Transfer Moulding (RTM). There is no requirement for labour intensive lay-up and costly inspection with this automated process and consequently manufacturing costs are greatly reduced. This cost reduction is described in previous work by Hill et al [10]. This reduction in manufacturing costs offers great potential for increased usage of textile composites in products where weight saving is advantageous – car manufacture, sports equipment, leisure products etc.

### **The Need for a Solid Model**

The development of highly automated, programmable weaving technology means that a wide variety of 3-D angle interlock reinforcing structures can be produced. Many geometric variations of the reinforcing structure are possible. Thus the composite design team must take decisions regarding the optimum shape and type of woven reinforcement for a given application. Tools are needed to aid this decision-making process. One such tool is the use of a solid model of the proposed weave structure. For design purposes it is considered that the most useful model satisfies two essential criteria:

1. automatic generation of the model
2. the ability to extract geometric data from the model.

This paper describes a method for automatically generating a solid model. A prototype system for the extraction of geometric data has been described elsewhere [11]. The geometric data is required for input to analysis systems such as that

developed by Limmer and Brown [12] which predicts the mechanical performance for a given reinforcement.

#### **Region to be Modelled**

The unit cell approach is the basis for the development of the solid model. The micromechanical concept [13] of the Representative Volume Element (RVE), the smallest possible repeating volume element, can be used to predict the properties of the whole composite. The RVE for a given weave architecture is the region to be modelled. The ability to sub-divide the RVE to examine the sub-volumes is essential, as previously described in work by Weissenbach et al [14], particularly since the RVEs for many 3D woven reinforcements tend to be relatively large. It is not uncommon for the RVE to span the thickness of the whole fabric and typical in-plane dimensions are 20 x 12 mm[15].

#### **Predictive Capability**

The predictive capability based upon a solid model of the reinforcement is potentially a very valuable design tool. Firstly, unsuitable fibre architectures can be eliminated early in the design process. Secondly, it allows optimum textile reinforcement patterns to be identified and therefore development time for particular applications is greatly reduced. The predictive capability means that the need for mechanical testing and the amount of mechanical testing required, is also reduced and confined to the chosen composite. This is advantageous to the design and manufacturing process as mechanical testing can significantly add to the cost of manufacture both in terms of increased labour cost and increased manufacturing lead times for components. To provide predictive capability, it is considered essential that the solid model be generated automatically once the user has input the key parameters describing the weave architecture. This immediately raises the issue of how best to facilitate this basic data input.

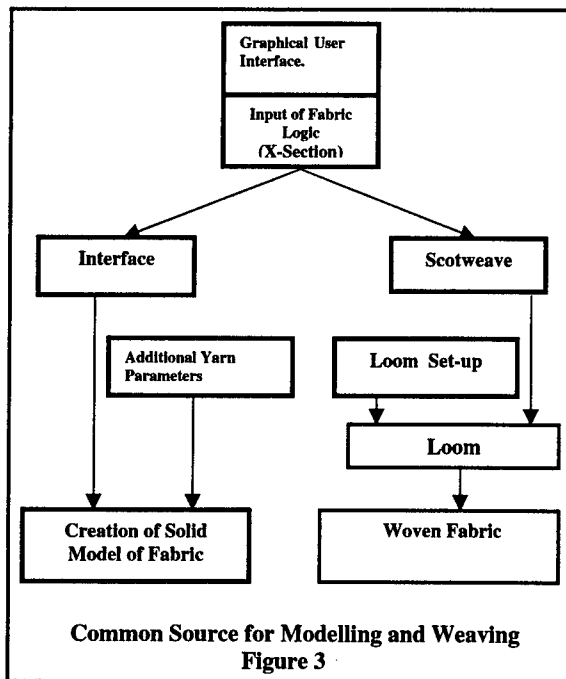
#### **Data Integrity Issues**

An existing piece of specially commissioned software, called X-SECTION [16] is used in the procedure to automatically generate the solid model. This has been developed as a front end for the commercial SCOTWEAVE [17] package specifically for the design of 3-D fabric structures. X-SECTION incorporates a purpose designed graphical user interface to facilitate the design of such woven structures. Essentially the X-SECTION program captures what the authors have called the "fabric logic" i.e. the relative positions of the warp and weft yarns within the fabric but excluding those aspects of the weaving which depend upon the loom set-up e.g. the amount of weft beat-up. X-SECTION is closely coupled with the SCOTWEAVE package and thus allows the loom control data, via the appropriate post-processor, to be generated and written to a floppy disc for transfer to the loom Jacquard controller.

The "fabric logic" from the X-SECTION program will provide the basic data for the generation of the solid model. It is not considered appropriate to develop a new user interface within the solid modelling software for this purpose. Also from a data integrity perspective it is considered important that the data used in the loom control has the same common source as that used to create the model. In a data validation scenario the value of a common source for the weave structure is self-evident. In the

specification of the X-SECTION program the need for an interface to solid modelling was identified and has been provided.

The utilisation of the single starting point for these two branches is shown schematically in Figure 3. Just as the "fabric logic" has to be supplemented with loom set-up data before fabric can be woven, so a number of additional parameters have to be furnished to enable the creation of the solid model of the fabric. It is conceivable that using a given "fabric logic", different solid models could be produced, each representing a different degree of idealisation or a different loom set-up. This approach allows for commencement with a relatively simple model and development of more complex models as may prove necessary for better correlation with experimental results.



#### Input Parameters

Textile technologists and engineers must take fundamental design decisions regarding key yarn parameters. For woven textile reinforcements two key parameters are data relating to yarn cross sectional shape and yarn path.

There are a number of different shape functions that are normally used to describe the cross sectional shape of a yarn. In this paper, a lenticular shape has been chosen to represent the cross sectional area. The modelling work was carried out using Ideas 7 [18]. It was decided that the lenticular section could best be constructed using a rectangle whose length and height was equal to the length and height of the lenticular section. A three point arc could then be used to create the wireframe of the lenticular shape. Dimensional and positional constraints were applied so that the model generated could be easily changed to represent different yarn aspect ratios. Since the model is of a balanced weave i.e. the warp and weft yarns have identical shape functions, it was decided that the yarn paths of the warp and weft should be based on the same geometry.

#### Creation of the Solid Yarn using Sweep Option

There are a number of options available in Ideas that can be used to create a solid model of a woven yarn. After much experimentation it was decided that the best way to create the solid is to use the sweep command. Two data sets are required to enable a sweep to take place, the sweep path and the cross section to be swept. The sweep path is used to orient the cross sections in space. With reference to Figure 4, one arc from the lens is used as the sweep path, and the wireframe of the second copy is used as the cross sectional shape to be swept. For demonstration purposes, an aspect ratio of 5 has been chosen with the height and length of the lenticular section equal to 25 mm and 125mm respectively.

Since associativity between the two copies was maintained the x and y model dimensions may be changed by altering the aspect ratio of the yarn cross section.

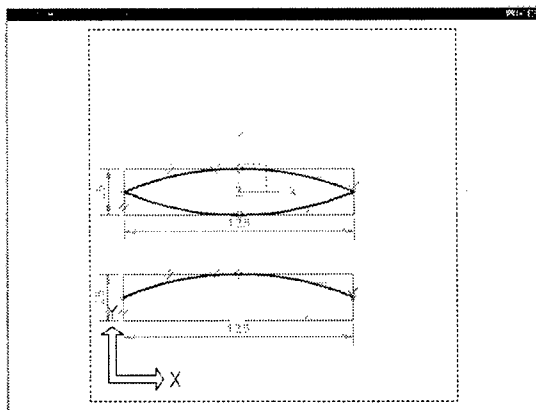


Figure 4

Reference planes are used as shown in Figure 5a to facilitate the later arrangement of assembly instances in the weave assembly. The swept solid is thus created (Figure 5b).

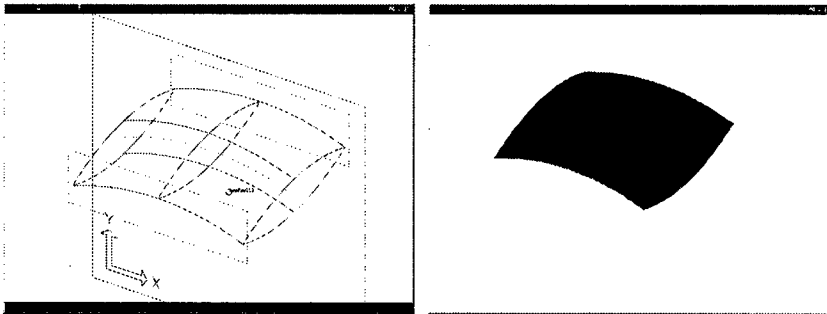


Figure 5a and 5b

#### Assembling the RVE

Individual instances of the yarn element are then placed into an assembly hierarchy. The instances were rotated and moved until the correct orientation and positions were obtained.

This method is a computationally efficient way of creating a solid model of a plain weave fabric. Instances of the part can be moved, rotated and positioned in a manner consistent with the applied assembly constraints. Figure 6 shows the assembled RVE of a balanced plain weave structure. Interference checking reveals that all surfaces are 'just touching' i.e. there is no overlapping or gaps in the model. It can be shown that there is face to face contact over adjoining surfaces of adjacent yarns

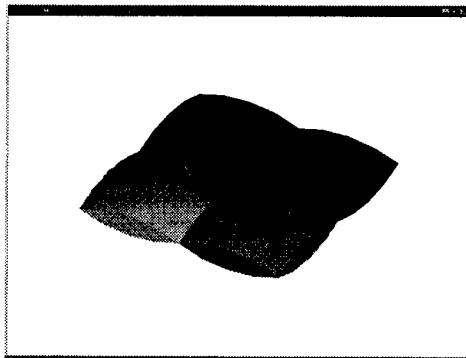


Figure 6

#### Automation of the Modelling Process

Program file creation is termed Open Language programming. A program file is an "external file of I-deas commands that can be developed from within the I-deas software package and then edited with the host editor" [18]. Open Language programming is essentially macro based programming where the output is a text file

consisting of command mnemonics and screen pick locations which can be used to run an I-deas session.

The modelling procedure as previously described has been successfully automated using Program files. Whilst these files require further refinement they produce good results very quickly. The user inputs a required yarn height and width and the model is produced. The user can also quickly modify the aspect ratio and the model will be automatically updated. Figure 7 shows the model for aspect ratios of 10 and 3 respectively. For the purpose of clarity, only the weft yarns are displayed.

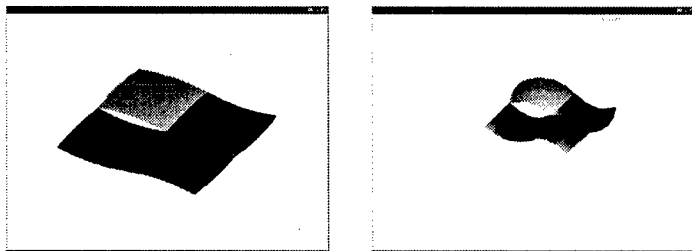


Figure 7a and 7b

### Conclusions

A system to automatically generate a solid model of a 2-D plain weave structure has been demonstrated. The methodology can be applied to 3-D weave structures. Such a solid model is a useful communication tool for multi-disciplinary design work. The model created has all of its contact surfaces just 'touching' and there are no gaps in the structure. Whilst this represents a degree of idealisation, it is essential for downstream Finite Element analysis of the composite for stiffness prediction.

### References

1. Dickinson, L., Mohamed, M. and Bogdanovich, A. '3-D Weaving: What, How and Where' 44<sup>th</sup> International SAMPE Symposium 1999
2. Ganesh, V. K., Ramakrishna, S., Teoh, S. H. and Naik, N. K. 'Microstructural Design of Textile Composites' Materials and Design Vol 18, No 3 1997
3. Bannister, M. K. and Hertzberg I., 'Mechanical Performance and Modelling of 3D Woven Composites'. Proceedings of 4<sup>th</sup> International Conference on Automated Composites, ICAC 1995 pp109-116.
4. Dreschler, K. and Brand, J., 'The Potential of Advanced Textile Structural Composites for Automotive and Aerospace Applications' 4<sup>th</sup> International SAMPE Conference Tokyo 1996
5. Vandeurzen, P., Ivens, J. and Verpost, I. Mechanical Modelling of Solid Woven Fabric Composites Ed Miravete Woodhead Publishing Ltd 1999

ICMAC - International Conference for Manufacturing of Advanced Composites

6. Soden, J., Hill, B., McIlhagger, R. and Miller, L. 'An Integrated Computer System for the Design and Analysis of 3-D Woven Engineering Composites' ICAC Egypt 1998
7. Brand, J. and Dreschler, K., 'Applications of composites in transportation industry', 3rd International Tex Comp Symposium, Aachen 1996.
8. Cox, B.M. and Flanagan, G., Handbook of Analytical Methods for Textile Composites, Rockwell Science Center, Thousand Oaks, CA, 1996
9. Ko, F.K. 'Textile Structural Composites' (Eds T.W. Chou and F.K. Ko), Elsevier, New York, 1989, pp129-171
10. Hill B.J., McIlhagger, R. and McLaughlin, P. 'Weaving Multilayer Fabrics for Reinforcement of Engineering Composites' Composites Manufacturing Vol 4 No 4 1993
11. Brown, D. and Morgan, M., 'Solid Modelling of a Woven Textile Reinforcement: A Prototype System for the Automatic Extraction of Geometric Data', Polymers and Polymer Composites, 1999.
12. Limmer, L. and Brown, D. 'Estimation of the Elastic Stiffness for 3-D Textile Reinforced Composite Materials' International Conference on Composites Materials 1994
13. Pandey, R. and Hahn, H.T. 'Visualization of Representative Volume Elements for Three-Dimensional Four-Step Braided Composites' Composites Science and Technology 1996
14. Weissenbach, G., Limmer, L. and Brown D., 'Representation of Local Stiffness Variation in Textile Composites' Polymers and Polymer Composites Vol 5 1997
15. Limmer, L. and Brown, D. 'Comparative Determination of the In-Plane Shear Modulus of Textile Composites by the Two-Point Plate Twist and V-Notched Beam Shear Tests' 4<sup>th</sup> European Conference on Composites: Testing and Standardisation 1998.
16. Hewitt, J.A., Brown, D. and Clarke, R.B. 'A System for Modelling and Manufacture of Woven Composite Materials' International Conference on Automated Composites 1995
17. SCOT Innovation and Development Ltd, The Scottish College of Textiles, Netherdale, Galashiels, TD1 3EY, Scotland.
18. Structural Dynamics Research Corporation Milford, Ohio 45150

---

ICMAC - International Conference for Manufacturing of Advanced Composites

**MAINTAINING THE STABILITY OF A THREE-DIMENSIONAL WOVEN  
PREFORM BY INCORPORATING A THERMOPLASTIC YARN WITHIN THE  
WEAVE STRUCTURE**

P.P.J. Rogers, A.T. McIlhagger, J. Quinn, R. McIlhagger

Engineering Composites Research Centre (ECRE)  
University of Ulster at Jordanstown, Shore Rd., Newtownabbey,  
Co Antrim, N. Ireland, BT37 0QB.

**SUMMARY**

Work has been carried out to stabilise the structure of three-dimensional woven carbon fibre preforms. A readily available polyethylene yarn has been incorporated within the weave structure and by the application of temperature and pressure it has been used to consolidate the shape of a carbon fibre preform. Upon testing the plastic was found to have had a positive effect on maintaining the stability of the preform. Impregnation of a modified preform was then carried out by Resin Transfer Moulding. The mechanical properties of a composite made from the modified preform were comparable with those of a conventional composite.

**INTRODUCTION**

Carbon, glass and aramid fibre reinforced composite articles provide high strength at low part weight, making these materials ideal for use in areas such as the aerospace industry. The use of liquid injection techniques such as Resin Transfer Moulding (RTM) is becoming increasingly popular due to the intensive labour and high costs associated with autoclave processing.<sup>1, 2</sup> For these techniques the reinforcement material is assembled initially producing what is known as a preform. Preforms handle as a single body and can be easily and accurately placed into high precision RTM tooling rather than having to build up the reinforcement layer by layer by hand. A variety of methods exist for the production of preforms and the mechanical properties of the finished composite will be largely determined preform type used.<sup>3</sup>

In recent years, textile methods have found increasing importance in preform production. Work carried out at the Engineering Composites Research Centre (ECRE) has demonstrated that using a specially developed software design package (XS)<sup>4</sup>, three-dimensional preforms can be woven on a conventional Jacquard loom to a near-net-shape. A variety of net shapes e.g. T-skins and I-beams have been produced and it has also been shown that preform properties, such as the amount of through-the-thickness fibre in the structure, can be predicted and controlled.<sup>5, 6, 7</sup> There are still some problems associated with the use of three-dimensional woven preforms such as maintaining the stability of the preform structure and for producing near-net-shape. Without stabilisation, the preform is readily distorted upon handling, particularly at the edge where fibre loss may also occur. Fibre loss and preform distortion may lead to the production of composites with compromised mechanical properties.

Binders commonly used in the production of preforms include pastes, sprays and powders. For example, Faiz et al <sup>8</sup> describe a method for the production of a preform. The method involves building up a stack of fibre sheets with binder applied to each layer and cutting the sheets to the desired shape by laser. The binder was applied throughout the preform but the binder only fused the layers at the points where the laser cut. It was also proposed that as the laser cuts, the cut ends of the fibre sheets fuse with the binder rather than with each other, thus maintaining resin permeability at the edges of the finished preform. This would also provide additional structural integrity and prevent fraying or unraveling of the fibres.

Reavely et al <sup>9</sup> demonstrated a method for producing stabilised preforms by dispersing a polymeric binder between adjacent layers of fibre and after compressing the preform binding it by using hot air. The temperature of the hot air was a function of the type of binder used, the speed with which the polymer was to be melted and the thickness of the preform. The authors recognised that a balance must be struck between adding sufficient thermoplastic to give the required stability and affecting the properties of the finished composite.

Methods such as these would be impractical for use with the production of three-dimensional woven preforms where it would not be possible to ensure that the binder material was evenly spread onto a preform that was still attached to the loom. Including the binder as a thermoplastic yarn woven into the preform structure was therefore considered as an alternative.

This paper describes work carried out on three-dimensional woven preforms constructed for use in RTM. Using a conventional loom, preforms were produced that incorporated a thermoplastic yarn within the architecture of the preform. A readily available Polyethylene monofilament yarn was used as the thermoplastic.

## **EXPERIMENTAL**

### **Stabilising the preform structure**

In the first part of the research, stabilisation of preform structures was carried out by the inclusion and consolidation of a thermoplastic yarn. Testing was then carried out to ascertain the effectiveness of the stabilisation process. Three-Dimensional carbon fibre preforms were produced on a standard Jacquard loom. A high-density Polyethylene yarn, obtained from Industrial Net and Twine (Hillsborough), was included by weaving it in parallel with warp yarns. The thermoplastic yarn was made to act as an adhesive by the application of heat and pressure. For this phase of the work three configurations were tested, these were;

1. A structure containing two thermoplastic yarns that follow the pathways of two of the integrating carbon fibres. (PEZL)
2. A structure containing six thermoplastic yarns that follow the pathways of six of the stuffer carbon fibres in layers 1-6 of a 6-layer preform. (PEXS)
3. A control sample of preform that does not contain any of the thermoplastic yarn. (NONE)

Apparatus was designed and constructed in order to measure the force of the bond produced by the thermoplastic and compare these results with those given for a preform containing no thermoplastic. This testing was carried out using samples with dimensions of 100mm x 100mm. The consolidated thermoplastic yarn was included as part of the weave structure at a position approximately 25mm from the edge of the sample. The samples were placed in a computer-controlled Floor Model Instron 6025 Tensile Testing machine and tested. The preform sample was held in place at the top by placing a series of metal pins through the thickness of the preform a set distance below the thermoplastic yarn and at the bottom by a fabric grip. The apparatus used is represented by Figure I below. The crossheads of the machine were moved apart at a constant rate of 10 mm/min.

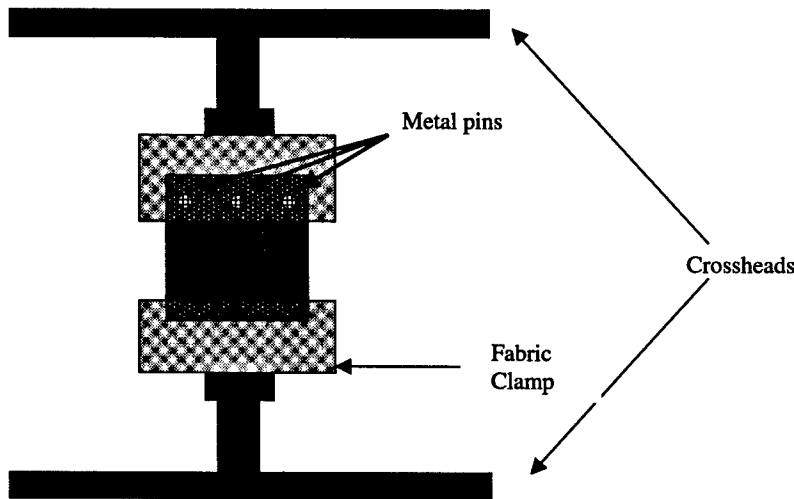


Figure I : Showing the apparatus used for the testing of preforms

#### Production and testing of composite samples containing the thermoplastic

In the second part of the work, preform samples containing various amounts of the consolidated thermoplastic were used to produce composite samples. These were to be mechanically tested to gauge what effect if any the presence of the thermoplastic had on the properties of the composite. In order to allow for a direct comparison between preforms containing thermoplastic yarns as stuffers and as integrating yarns, an additional group of samples were included for testing. These samples contained two thermoplastic yarns woven in parallel with carbon fibre stuffer yarns at layers 2 and 5 (PAXS).

ICMAC - International Conference for Manufacturing of Advanced Composites

The matrix system used for the RTM processing of the preforms was an epoxy resin supplied by Ciba Polymers. This was a two-part system of LY-564 resin and HY-2954 hardener suitable for RTM. The mix ratio used was as stipulated by the manufacturers, 100 parts weight resin and 35 parts weight hardener. The fabric preform dimensions used for the RTM process were 250mm in the weft direction by 310mm in the warp direction; the thermoplastic was included at a distance of approximately 25 mm from either side of the structure. The vacuum impregnation resin injection technique consisted of first mixing the resin and then degassing it for 1 hour at 30°C to remove voids suspended in the liquid. It was then injected into the tool at 75°C at 750 millibar absolute. After injection, the temperature was increased to 100°C and the composite cured at this temperature for 1 hour. The tool consisted of an aluminium base and caul plates with thermocouples attached for data recording and oven temperature control. The tool was sealed using a rubber gasket and nylon bag arrangement to which a vacuum was applied.

Composite samples were cut using a diamond cutter and then polished to the required dimensions using 320 grit wet and dry paper. A grid containing blocks measuring 10mm x 10mm was drawn on the composite to allow for thickness measurement to be carried out. The thickness was measured at the line intersections using a micrometer with barrels 6.8mm in diameter and the results were recorded and analysed using Microsoft Excel. Testing was carried out to determine what effect if any the presence of the thermoplastic yarn had on the mechanical properties of the composite. The test methods selected were Interlaminar Shear Strength testing (ILSS) and Flexural testing. The Composite Research Advisory Group (CRAG) standard methods for Flexural and Interlaminar Shear Strength testing (methods 200 and 100 respectively) were used.<sup>10</sup>

## RESULTS

### Testing bond strength in preforms obtained using thermoplastic yarn

Table I below shows the results that were obtained when the yarn pull out testing was carried out on each of the preform types.

<u>SAMPLE TYPE</u>	<u>AVERAGE FORCE VALUE (NEWTONS)</u>	<u>COEFFICIENT OF VARIATION (CV) (%)</u>
<u>NONE</u>	35.69	8.05
<u>PEZL</u>	85.72	18.7
<u>PEXS</u>	146.40	15.36

Table I: Results obtained from fibre pull-out testing

From the table above it can be seen that both samples containing consolidated thermoplastic yarns had an average pull-out force significantly higher than the control sample. The pull-out force required for the PEXS sample containing the six thermoplastic yarns as warp stuffer yarns was greater than that of the PEZL sample containing only two thermoplastic yarns. This difference is explained by the amount of thermoplastic present in the samples, there is approximately three times as much thermoplastic present in the PEXS samples than there is in the PEZL samples.

These results suggest that the presence of a consolidated thermoplastic yarn, woven into the preform structure would have a significant effect on the stability of a preform. The presence of such a consolidated thermoplastic yarn at the edge of preform would mean that a significant force would be required in order for fibre loss or preform distortion to occur. Hence it is anticipated that such preforms could be handled without any risk of fraying or damage.

**Measurement of presence of the thermoplastic yarns on the properties of the composite**

The effect of the presence of the consolidated thermoplastic yarn was determined by mechanical testing of composite samples. Flexural testing was carried out on samples and the results of these tests are shown in the table below. Flexural Strength and modulus are fibre dominant properties, for this reason it was necessary to normalise the results obtained in terms of fibre volume fraction so that comparisons can be drawn.

The results of the flexural testing of the composite sample in Table II below show that the lowest values both of flexural strength and modulus are obtained for the samples that contain the largest amount of thermoplastic (PEXS).

<u>SAMPLE TYPE</u>	<u>FLEXURAL STRENGTH (MPa)</u>	<u>CV (%)</u>	<u>FLEXURAL MODULUS (GPa)</u>	<u>CV (%)</u>
<u>NONE</u>	13.30	10.15	27.57	4.46
<u>PEZL</u>	14.45	16.67	26.37	16.57
<u>PEXS</u>	11.99	19.68	21.92	19.72
<u>PAXS</u>	16.55	18.25	34.52	23.37

Table II: Normalised Flexural properties of all test samples

This may suggest that the use of this amount of thermoplastic will have a detrimental effect on the flexural properties of the composite. However comparison of the composite samples containing only two of the thermoplastic yarns PAXS (two thermoplastic yarns included as stuffer yarns) and PEZL (two thermoplastic yarns included as integrating yarns) gave results that were comparable to, and in some cases higher than, the values obtained for the control samples. Indeed the flexural properties of the composite would appear to be improved by the presence of two of the thermoplastic yarns, especially when included as a stuffer yarn.

<u>SAMPLE TYPE</u>	<u>INTERLAMINAR SHEAR STRENGTH (MPa)</u>	<u>CV (%)</u>
<u>NONE</u>	36.15	6.30
<u>PEZL</u>	38.04	7.04
<u>PEXS</u>	34.37	8.55
<u>PAXS</u>	32.44	9.24

Table III: Results of Interlaminar shear strength testing on all samples

The results of the Interlaminar Shear Strength testing (ILSS) carried out on samples are shown in Table III above. The results of the ILSS testing show no significant differences in the properties of samples that do or do not contain the thermoplastic yarn, the average value obtained for the control samples was higher than that for the samples containing the most thermoplastic yarn (PEXS) and also one of those that contained two thermoplastic yarns (PAXS).

However the result obtained for the samples that included the thermoplastic woven in parallel with through-the-thickness carbon fibres (PEZL) are higher than that obtained for any of the other samples. It may be the case that the inclusion of the thermoplastic yarns through-the-thickness acts to improve the ILSS of the finished composite.

### CONCLUSIONS

A polyethylene yarn has been incorporated within the structure of a three-dimensional woven carbon fibre preform. Testing showed that a significantly greater force was required to pull out a carbon fibre yarn from the preform in samples that contained the consolidated thermoplastic. This is an indication that fused thermoplastic yarns would significantly improve the stability of the preform. Impregnation of a modified preform was then carried out by RTM and samples were produced for mechanical testing. The results of this mechanical

---

ICMAC - International Conference for Manufacturing of Advanced Composites

testing showed that the properties of the composite produced from the modified preform were comparable with those of a conventional composite. In some cases the presence of the thermoplastic may even have a beneficial effect on the properties of the composite. Hence it is concluded that preforms with fused thermoplastic monofilaments can be used to improve the handilability of preformns without significantly affecting the composite performance.

#### ACKNOWLEDGEMENTS

The authors wish to thank Roy Brelsford and Roy Carton for their assistance and advice in weaving the preform samples and in the processing and testing of composite samples. Financial support from Bombardier Aerospace Short Brothers plc. through a CAST award is also gratefully acknowledged.

#### REFERENCES

- 1 Abraham D and McIlhagger R 4th International Conference on Automated Composites 6-7th September 1995 p299-306
- 2 Mouritz AP, Bannister MK, Falzon PJ and Leong KH Composites: Part A, No. 30 (1999) p1445-1461
- 3 Ko FK Proceedings 1<sup>st</sup> Japanese International Sampe Symposium 1989, p1482-1487
- 4 Matthews ST, McIlhagger AT and McIlhagger R The Sixth International Conference on Automated Composites 1999 p195-201
- 5 Soden JA, Weissenbach G and Hill BJ Composites: Part A No. 30 1999 p213-220
- 6 Harper CM, Hill BJ and McIlhagger R Proceedings of the 9th Conference of the Irish Manufacturing Committee - Technology in Manufacturing for Europe 1992 p488-501
- 7 Hill BJ, McIlhagger R, Harper CM and Wenger W Composites Manufacturing 5 No 1 1994 p25-30
- 8 Faiz RL, Diaz NJ and Reinfelder WC U.S. Patent 4,908,494
- 9 Reavely RT and Kim W U.S. Patent 4,988,469
- 10 'Test methods for the measurement of the engineering properties of fibre reinforced plastics', Composites Research Advisory Group (CRAG), Edited by PT Curtis, Technical report No. 88012, February 1988.

**ROLL-FORMED COMPOSITE BLADE STIFFENERS**

J.A. Lee

Airbus UK, Composite Research, Building 07C, Filton, BRISTOL BS99 7AR UK

**SUMMARY**

As a result of an AMCAPS II (Affordable Manufacture of Composite Aircraft Primary Structure) project led by Airbus UK in conjunction with Cranfield University, a technique has been developed for manufacturing aerospace quality blade stiffeners, or stringers, from carbon fibre-reinforced epoxy-matrix composites. The process involves pulling a flat laminate of material through a series of rollers that progressively form the desired cross-section. To date a number of stiffeners of up to 2.5m in length have been produced successfully. Both constant and jogged cross-section components have been manufactured. The results of dimensional and microscopical analyses suggest that components can be roll-formed with acceptable values of uniformity, void content and fibre volume fraction. Consequently, the process appears to be robust enough for developing into a production standard.

**INTRODUCTION**

The AMCAPS II programme was aimed at developing composite technology for the cost-effective manufacture of large aircraft structures. One process that was investigated within this programme was roll forming of blade stiffeners, or stringers. The remit of AMCAPS II was to develop technologies to a proof of concept stage. This paper describes the work undertaken within Airbus UK to take the basic roll-forming process and enhance it to a level where roll-formed products could be incorporated into test components.

The current method of manufacturing T-section blade stiffeners, or stringers, is to produce two L-sections and cure them back-to-back (Figure 1). The L-sections are manufactured by laying up flat laminates and forming them over blocks by using a hot diaphragm process. This approach is time consuming and will be increasingly difficult to employ as stringers of increasing length, in excess of four metres, are required. As a result an alternative technique is required. One potential cost-effective option is a process called roll-forming where a flat laminate of material is pulled through a series of rollers that progressively form the desired cross-section (Figures 2 & 3). There are several common operations between the two Ls manufacturing route and roll-forming which reduces the risk of the new process. However, a reduced number of activities, including no final machining of the stiffener blade, and a faster forming time means that there is around an hour saving per metre of component for a roll-formed component when compared with the present approach. Moreover, the continuous roll-forming manufacturing technique allows increased stringer lengths to be produced more easily through the use of automation and reduced handling. With continuous fibres in the blade top, the roll-formed stringer may be more efficient structurally. In order to achieve the same level performance for a given application, stiffeners with thinner flanges could be used leading to a weight saving.

## APPROACH

The first stage of the roll-forming process was to produce a flat laminate from the selected composite material. Three composite systems were investigated, AS4/8552 and UTS/M36, both supplied by Hexcel Composites, and HTS/977-2 from Cytec Fiberite. These materials were used as the potential customer projects for roll-formed stringers were also considering these composite systems. The blank was hand laid-up in a clean room environment in the same manner as any standard flat composite laminate. The pre-preg materials were laid onto a prepared flat surface and room temperature vacuum (-0.9bar) de-bulked every four plies for fifteen minutes. The nominal cured ply thickness was 0.25mm resulting in twenty plies being laminated to provide the required stiffener dimensions. The ply orientations were 0° (along the stringer), 90° (across the stringer) and  $\pm 45^\circ$ . The respective percentages of each fibre direction were 60/10/30. One difference from the normal procedure was the inclusion of four off nylon peel ply layers interleaved into the first 220mm of the blank as shown in figure 4. These leaders are used to attach the feed material to the pulling mechanism, which will be described later.

The roll-forming machine comprised of three main elements (Figure 5): a feed tray, a roller-box and a pull track. The feed tray was made from a sheet metal section that was enclosed to allow the blank to be held at the correct temperature prior to forming. The metal tray was shaped to the width of the blank. This provided support to the laminate on three faces and maximised the potential for correct alignment of the feed with the roller box. The roller box was positioned immediately adjacent to the feed tray. In this way any heat loss was prevented and the laminate was kept at a constant temperature. The roller box housed four sets of rollers that progressively transformed the flat laminate into the desired profile. Figure 6 describes how the profile was initiated; the feet and blade were established; then the blade height was defined; before the stringer was fully consolidated. Two 4.2kW fan heaters mounted vertically below the roller box were used to heat the rollers and the feed tray. The final component of the roll-forming machine was the pull track. Once the blank was transported to the feed tray, the peel ply leader was fed through the rollers and into pinch jaws on the pull track. The system was allowed to reach temperature before the blank was pulled through the rollers. A set of pinch jaws was used to grasp the peel ply leader and pull the blank through the rollers and out through the cooling chamber. As the stringer left the heated roller box, room temperature compressed air was impinged onto the component to "lock-in" the formed shape. Pull rates from 1m/min to 4m/min were evaluated.

After the blade stiffener was formed it had to be fully cured. The peel ply leader was cut from the stringer and the formed component transferred from the roll-form machine into an aluminium tool. The mould consisted of two tool halves, two end stops, a fillet section and a caul-plate (Figure 7). Aluminium tooling was selected as the optimum compromise between cost, thermal mass, co-efficient of thermal expansion and weight. A removable fillet section was used as this permitted different stringer geometry to be produced with the same tooling. By replacing only the fillet section, stringers could be cured with different blade heights or joggles. In order to aid assembly, the stringer was cured upside-down. The uncured stringer was placed in the tooling and trimmed to size. The stringer was completed with a noodle and a capping strip. An epoxy based structural void filler was used to manufacture pre-cured lengths of noodle. In order to achieve the correct profile the filler was cured between two bars of the desired diameter and then cut to length. After the noodle was located at the base of the stringer blade, the capping strip was laid on top. The capping strip was made from two plies

of the same pre-preg material as used in the rest of the stringer and trimmed to the width of the stringer foot. To maximise the potential for producing a flat stringer base a caul-plate was placed on top of the uncured assembly. The completed tooling was then enveloped bagged with breather material and a polyimide vacuum bag, and cured under heat and pressure in an autoclave according to the cure schedule recommended by the material supplier and adapted by Composite Research, Airbus UK. When the cured component was de-moulded it was de-flashed, cleaned and part marked.

## RESULTS

Stringers with various cross-section dimensions and up to 2.5m in length were manufactured successfully from three composite systems, AS4/8552, UTS/M36 and HTS/977-2. The limiting factor on the stringer cross-section was the width of the flat laminate, or the developed stringer shape. At present this is set at 190mm. Therefore, stringers with the required geometry could be made with an overall height of 90mm and foot width of 29mm ranging through to an overall height of 49.75mm and foot width of 110mm. Typical cross-sections were 60mm high by 65mm wide. Both constant and jogged stringers were produced. Different stiffener blade heights were achieved by altering the setting of the z-height forming wheel (Figure 5). The minimum blade height was defined mainly by the position of the rollers in station 2 (Figure 5). To date the feed laminates were constant width and thickness. Joggles of 1:10 have been manufactured successfully. The current tooling does not allow different foot widths therefore all the stringers produced have had parallel natural feet.

The process achieved the required manufacturing tolerances for the appropriate features, leading to process capabilities of at least 1.8.

The results of dimensional and microscopical analyses suggested that components could be roll-formed with acceptable values of uniformity, void content and fibre volume fraction. Sections taken from cured roll-formed stringers indicated that fibre volume fractions of between 58 and 61% and, void contents of between 0.4 and 0.7% were achieved consistently.

## THE WAY FORWARD

The next phase of the project is to advance the process to a technology readiness level where roll-formed components can be incorporated into demonstrator aerospace projects. In order to determine fully the capabilities of the roll-forming process, components with representative geometry are to be produced, evaluated and tested. This investigation will examine different material types, component geometry and configuration. In particular, stringers with grow-outs are to be produced. When the stiffener blade height is varied this automatically produces a different foot width. This relationship can be exploited in this application as the stringer design tends to require a drop-off in blade height with a corresponding foot grow out. These areas of extra foot width are required at the end of stringers and in the region where the stiffeners interface with ribs in order to allow fasteners to be inserted through the stringer feet and into the under-laying skin.

The roll-forming process will be developed to minimise part-to-part variability and maximise manufacturing efficiency, thereby producing cost-effective components of acceptable quality

#### ICMAC - International Conference for Manufacturing of Advanced Composites

consistently. To assist the optimisation of the process a PAM-FORM simulation is being generated. Modelling the process should increase understanding of the material movement during roll-forming leading to enhanced machine design and processing parameter definition.

Longer term it is planned to develop the current roll-forming machine to ensure that it has the necessary flexibility, robustness and cost effective operation for working in a production environment. These enhancements may include increased use of automation. At present the flat blanks used to feed the machine are hand laid. In order to increase efficiency the laminates could be automatically tape laid. Similarly, the capping strips are laid-up and trimmed by hand. A continuous length of capping strip could be fed directly onto the stringer section from reels situated above the roll-forming machine. The noodle could also be generated continuously by extruding the desired section of uncured structural filler into the formed stringer.

#### CONCLUSIONS

The results of dimensional, microscopical and non-destructive analyses suggest that components can be roll-formed with acceptable values of uniformity, void content and fibre volume fraction. Consequently, the process appears to be robust enough for developing into a production standard.

The successful manufacture of proof-of-concept articles has generated interest within other parts of Airbus, leading to roll-form technology being considered for future aircraft projects.

**FIGURES**

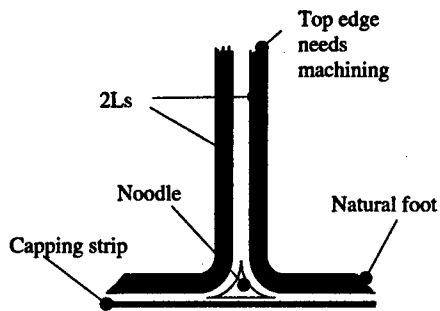


**Figure 1: Existing blade stiffener components**

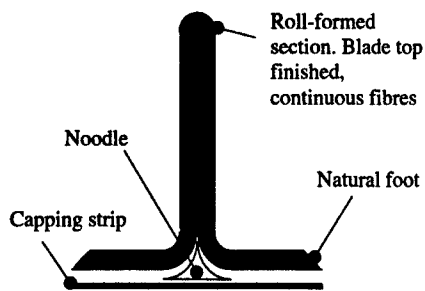


**Figure 2: Roll-formed stringer components**

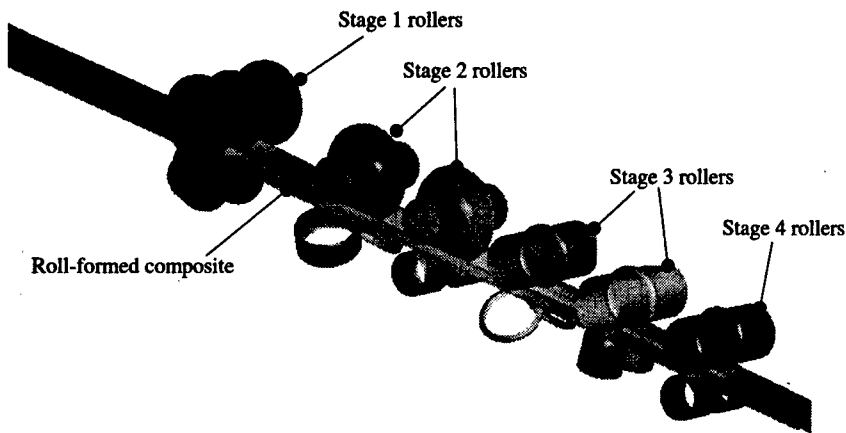


**Figure 3: Image from simulation of roll-forming process**

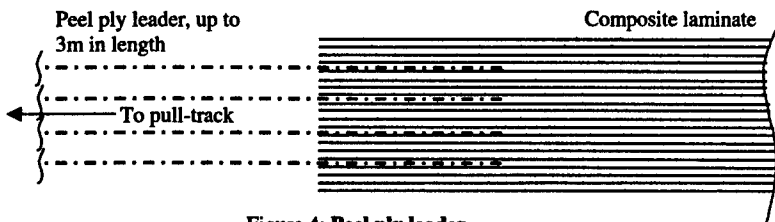


**Figure 4: Peel ply leader**

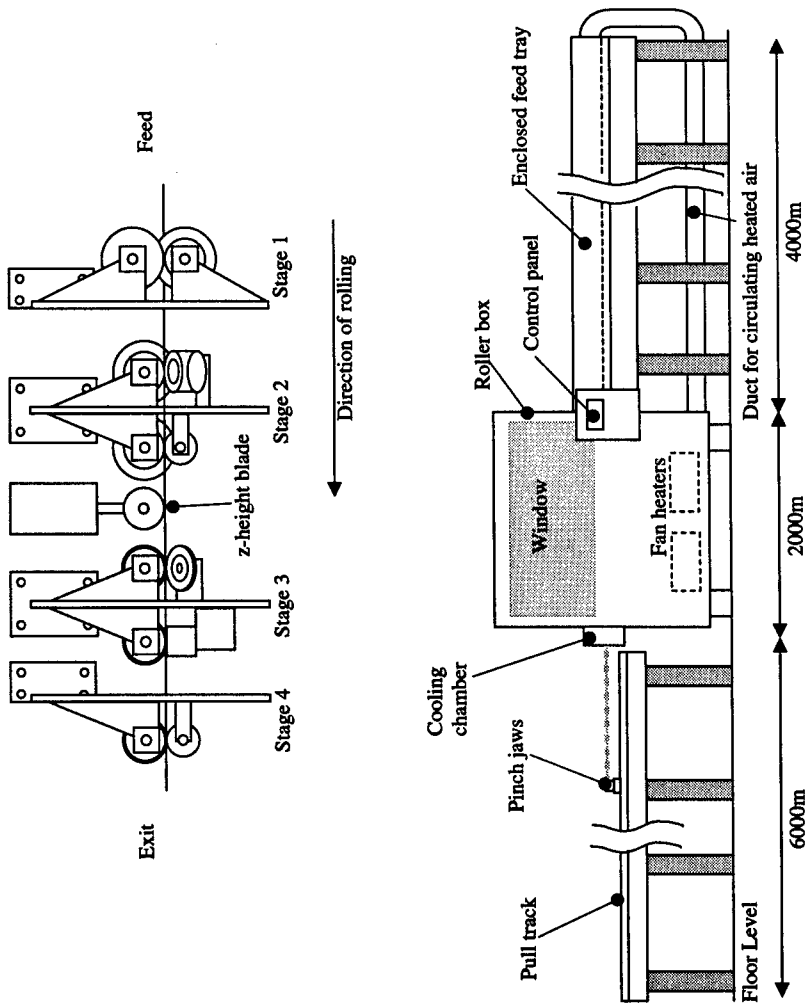


Figure 5: Schematic of roll-forming machine

© Airbus UK Ltd 2001

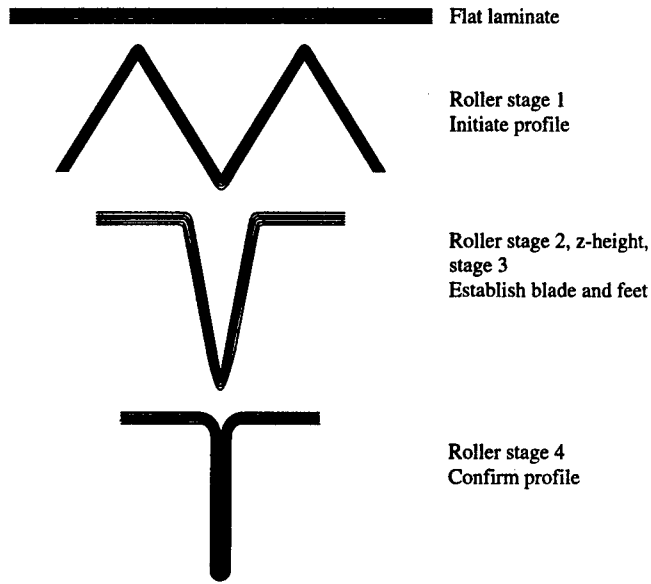


Figure 6: Roll-form stages

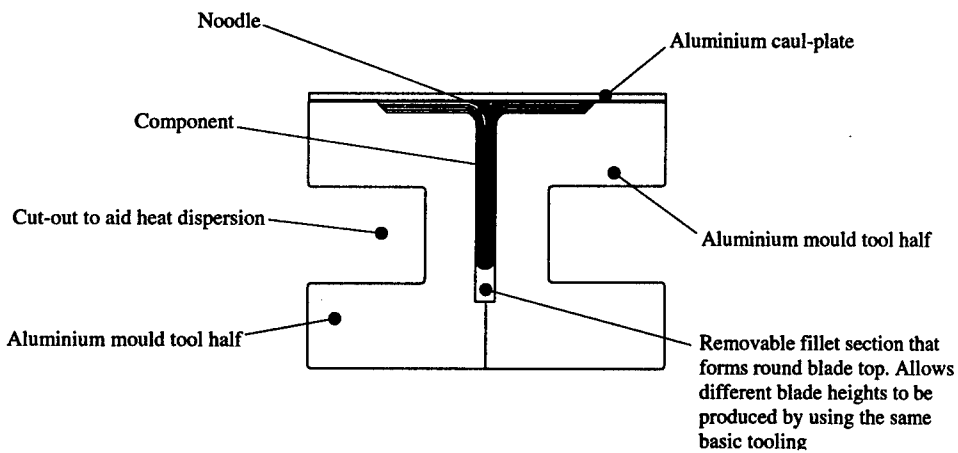


Figure 7: Mould tool cross-section

## ASSESSING QUALITY IN COMPOSITES MANUFACTURE

Graham D Sims, David Mulligan, Sam Gnaniah and Bill Broughton  
NPL Materials Centre, National Physical Laboratory

### 1. INTRODUCTION

Many composite materials are only manufactured at the same time as the product itself, either by bringing the major components (fibre, resin) together for the first time (eg filament winding) or through the final consolidation and cure (eg sheet moulding compounds, SMC). Due to the intimate linkage between the end performance and the quality of the processed material, improvements are required in the manufacturing quality as well as production rate.

A frequently given reason for the lower than expected application of composites is the unacceptable speed, quality and consistency of production. Often these criticisms relate to chopped strand mat reinforced material. However, they are not relevant to other materials, such as fabric based systems, where the consistency is inherently higher due to the better controlled fibre format. A glass-fibre fabric/epoxy used in several NPL programmes for test method development had a coefficient of variation of less than 3% for the ultimate tensile strength.

Nevertheless, there are several areas of composite processing where the availability of test methods could improve both the quality and consistency of manufacture. In this paper a cross-section of relevant activities are presented, including:

- process related standards and product specifications
- preparation of standard test panels for manufacture of test specimens
- measurement of glass transition temperature ( $T_g$ ) and degree of cure
- ultrasonic c-scan inspection

This summary is not comprehensive and other processing measurements areas exist requiring test methods and their subsequent standardisation.

In Section 2, national and international standards related to composites processing are reviewed. Consideration is mainly given to European (CEN) or international (ISO<sup>1</sup>) standards. A major EN ISO standard being published in ten parts covering different process routes for test panel manufacture is discussed in Section 3. Section 4 reviews the use of thermal methods (e.g. differential scanning calorimetry, dynamic mechanical analysis) for  $T_g$  and cure measurement. The standardisation of the use of the ultrasonic c-scan technique for test panel and product assessment is discussed in Section 5.

<sup>1</sup> ISO standards quoted that are in development include in national list additional prefixes indicating the state of development (i.e. ISO/CD = committee draft, ISO/DIS = draft international standard, ISO/FDIS = final formal vote). Technical comments should be made at CD stage.

## 2. STANDARDS RELATED TO PROCESSING

Initially, to obtain increased consistency and higher quality production, consideration of the incoming materials must be addressed. The matrices can be controlled in the main by the existing resin standards for unreinforced materials. Several standards relate to the fibres that influence their processability. These include, for glass-fibres, sizing solubility of rovings (ISO 13059), bulk density of chopped strands (ISO 15001) and mat thickness under load and recovery (ISO 3616).

Several standards are now being produced to measure the processability of composites in a similar manner to the basic rheological data that has been traditionally produced on unreinforced thermoplastics. Currently, a flow standard is being produced for SMC (EN ISO 12115), together with other standards for SMCs concerned with the degree of wet-out of fibres (EN 12575), curing behaviour (EN 12114) and linear shrinkage (EN 1842). A flow standard has also been drafted for thermoplastic mat composites (or GMTs). These flow standards use a common mould tool as both materials are processed in a similar manner. The tool is 200 mm x 400 mm, allowing a long flow path. In addition, several intermediate product specifications, above the base fibre or resin level, are under development that are likely to include reference to these test methods. Some of these specifications are listed in Table 1.

**Table 1** Intermediate product specification standards (pr = draft standard in CEN series)

SPECIFICATION	STANDARD
Textile glass - mats	not available
Textile glass - rovings	not available
Textile glass -woven fabrics	prEN 13417 Parts 1-3
Multi-axial multi-ply fabrics (NCF)	prEN 13473 Parts 1-3
Reinforced thermoset moulding compounds (SMC, BMC)	not available
Reinforced thermoplastic moulding compound	prEN 13677 Parts 1-3

For aerospace quality prepregates, recent standards cover resin flow (ISO 15034) and gel time (ISO 15040). In addition, within the EN Aerospace series product specification standards covering both glass and carbon-fibre based prepreps are being developed.

## 3. TEST PANEL MANUFACTURE STANDARD

The need to obtain correct manufacture of products is mirrored in the preparation of test plates prior to their cutting into test coupon specimen. An existing standard, ISO 1268, has been revised to cover the preparation of test panels by all currently available process routes for long-fibre composites (see Table 2). As new processes are developed, depending on their uniqueness, other parts or modification to existing parts can be expected. Several existing ISO standards (i.e. ISO 293-295) cover short fibre composites. ISO 1268 will dual numbered as the EN standard for test panel manufacture.

A procedure used in prEN 3074 for designation of the ply orientations will be offered as an annex to Part 1 of ISO 1268, so that all designations of lay-up of individual layers are based on the same

standardised format. The information on ply designation in the ASTM standard has also been included in the development process. Again, the use of standard procedures for ply definition and technical drawing needs to be applied to manufacturing.

**Table 2. ISO 1268 for test panel manufacture.**

Part 1	General principles
Part 2	Contact and spray-up moulding
Part 3	Wet compression moulding
Part 4	Moulding of preimpregnates
Part 5	Filament moulding
Part 6	Pultrusion moulding
Part 7	Resin transfer moulding
Part 8	Moulding of SMC/BMC
Part 9	Moulding of GMT/STC
Part 10	Injection moulding of BMC/DMC

The standard includes recommended quality checks. These requirements vary with the Part of the standard, but include assessment of visual defects (e.g. surface finish); C-scan ultrasonic inspection (see Section 5), measurement of the volume fractions of fibre, resin and voids; and measurement of the thickness consistency.

Part 4 of the revised standard for manufacture of test plates from prepregs was drawn from existing ISO standards, which it replaces (eg ISO1268, ISO 9353), EN Aerospace standards (eg EN 2743, prEN 2565) and an ASTM standard (ASTM D 5687). A round-robin validation of Part 4 was undertaken by NPL using a single stock of prepreg distributed directly from the supplier to eight sites for manufacture into standard 300 mm x 300 mm panels at three thickness commonly used for test coupons (i.e. 1, 2 and 5 mm). The results of the mechanical and physical tests, aimed at a quality assessment level showed a good level of consistency between sites [1].

#### 4. MEASUREMENT OF $T_g$ AND DEGREE OF CURE

There are a number of techniques that are routinely used to measure the  $T_g$  of composite materials after processing. The two most commonly used techniques are differential scanning calorimetry (DSC) and dynamic mechanical analysis (DMA). These two techniques are covered by ISO 11357 and ISO 6721 respectively. DSC uses small samples, typically 10 mg, and detects the  $T_g$  by a step change in the specific heat capacity. DMA uses larger samples, typically 40 mm by 10 mm by 2 mm and detects the  $T_g$  by changes in the viscoelastic properties of the material. Although these two techniques measure the  $T_g$  using different responses of the material, the values are often considered to give equivalent values, although this is generally not the case.. The measurement of  $T_g$  is of particular interest for composites and adhesives since it increases with the degree-of-cure of the material. So,  $T_g$  measurements are often used to confirm that materials are sufficiently cured. Recent work [2] has reported inter-laboratory testing on a set of four materials, consisting of:

- polyester resin
- carbon fibre-epoxy resin
- glass fibre-polyester resin
- epoxy resin adhesive

ICMAC - International Conference for Manufacturing of Advanced Composites

A sample of each of the four materials was supplied to each site. For each material, the glass transition temperature was determined by DSC and DMA. The  $T_g$  by DSC was taken as the point of inflection of the step-change in heat flow. For DMA the  $T_g$  was taken as the point of inflection of the decrease in storage modulus. (The procedures used for testing are presented in [2].) Three runs were requested for each material using fresh specimens.

The associated repeatability and reproducibility limits were determined for each of the materials and the values are shown in Tables 3 and 4; the two terms are defined below:

- Repeatability at the 95 % confidence limit - The difference between two single results found on identical material by one operator using the same apparatus within a short time interval will exceed the repeatability value on average not more than once in twenty cases in the normal and correct operation of the method.
- Reproducibility at the 95 % confidence limit - Single results on identical test material reported by two laboratories will differ by more than the reproducibility value on average not more than once in twenty cases in the normal and correct operation of the method.

Table 3. Precision data for DSC [1].

	Number of sites	Overall Mean (°C)	Repeatability Limit (°C)	Reproducibility Limit (°C)
Unreinforced polyester	8	92.55	3.88	6.13
Glass fibre-polyester	7	92.79	3.69	11.03
Carbon fibre-epoxy	8	137.75	5.23	15.62
Epoxy adhesive	5	55.64	2.89	12.86

Table 4. Precision data for DMA [1].

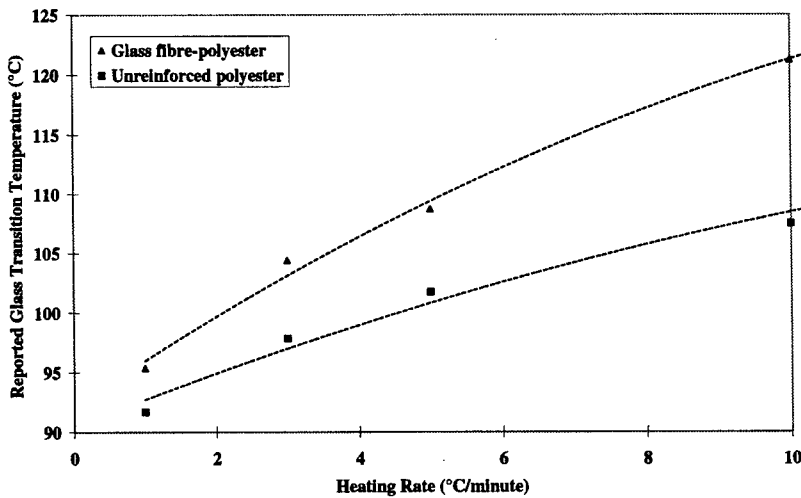
	Number of sites	Overall Mean (°C)	Repeatability Limit (°C)	Reproducibility Limit (°C)
Unreinforced polyester	7	93.35	2.92	25.69
Glass fibre-polyester	7	98.62	5.94	24.52
Carbon fibre-epoxy	6	157.95	4.93	15.85
Epoxy adhesive	5	70.38	5.08	17.61

For the polyester resin, the repeatability values for both techniques are good. However, for the reproducibility limits, the value from DSC is reasonable, but the value from DMA is much higher and would probably invalidate a comparison between sites for most applications. For the glass fibre-polyester material, the variation between sites for the DSC results is greater, but is still less than the variation between sites for the DMA results for either material.

It is useful to compare the average values of  $T_g$  by the two different techniques. It can be seen that the average  $T_g$  from DSC and DMA for the resin is similar. However, for the glass fibre-polyester the average  $T_g$  from each technique is different. The  $T_g$  from DMA is higher than that from DSC for the composite material. These results are consistent with Figure 1, which shows the effect of heating rate on the reported  $T_g$  of the resin and composite. It shows that due to

heating rate effects the composite material will show a higher  $T_g$  by DMA than the unreinforced resin. The extrapolated value for both materials at  $0\text{ }^\circ\text{C}/\text{min}$  agreed with each other and with DSC data. Further work is required before this agreement can be assumed more generally.

Figure 1. DMA results for  $T_g$  with the same resin, with and without reinforcement.



The results for the carbon fibre-epoxy composite show that the difference between the average of the two techniques is even larger for this material. The results are different to the polyester materials as there is very little difference between the two techniques in terms of the variation either within or between sites. The results for the epoxy adhesive show some difference between the two techniques, but the variation within the two techniques is similar. The epoxy adhesive material presents an additional problem because the material was not fully cured. This results in a large exotherm in the DSC trace, which in some cases overlaps the glass transition, so it cannot be analysed. Consequently, two sites were not able to report results.

These results show that the measurement of  $T_g$  for composites and adhesives presents additional challenges. These materials were selected as being representative of the materials routinely tested in commercial organisations. In fact, all these materials exhibited residual cure and this may be one of the factors that has an adverse effect on the agreement between laboratories.

## 5. ULTRASONIC C-SCAN INSPECTION

As noted in Section 3, manufacture of components for critical load-bearing applications requires confirmation of the required quality to satisfy safety and quality assurance requirements. Of the number of non-destructive test methods developed, ultrasonic C-scan inspection techniques are the most widely used to detect, measure and characterise manufacturing and in-service defects in composite materials. The techniques are routinely used in the aerospace industry.

#### ICMAC - International Conference for Manufacturing of Advanced Composites

A common concern among manufacturers was the lack of national or international standards, or universally accepted procedures that meet the requirements of all customers and users. As a result of this absence, the reliability and traceability of the techniques has been limited. Current standards are directed towards the inspection of metals. A number of companies within the aerospace industry are currently using either procedures recommended by major aerospace companies or in-house routines. The resultant time loss in changing from one system to another adds to manufacturing costs and increases the risk of human error.

A research programme was undertaken in 1994-1997 to establish a firm basis for a new set of procedures offered as the basis of future standards [3]. Several benefits were expected from the availability of standard procedures, including:

- Improved safety and quality assurance
- Reduced production and maintenance costs
- Reduced risk of human error
- Optimisation of manufacturing and processing methods
- Improved confidence in long-term performance

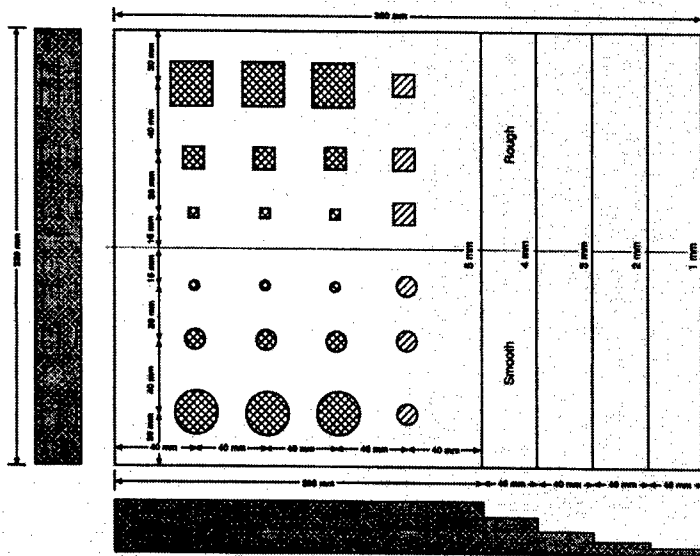
The United Kingdom (UK) Department of Trade and Industry (DTI) sponsored the programme under the Commercial Aircraft Research and Development (CARAD) programme. The work was led by the National Physical Laboratory (NPL Materials Centre) in conjunction with the Defence Evaluation and Research Agency (DERA) at Farnborough. Three procedures were developed and evaluated covering:

- Operational procedures for ultrasonic C-scan equipment (Part 1)
- Ultrasonic transducer calibration procedure (Part 2)
- Procedure for the preparation of reference panels with simulated defects (Part 3)

The operational procedure specifies methods for pulse-echo (both immersion and contact), single through-transmission (both immersion and contact) and double through-transmission inspection of flat or slightly curved composite panels.

Round-robin (R-R) validation exercises [4, 5] have been undertaken in conjunction with industry at both national and international levels in order to generate precision data and to identify any necessary adjustments to the operational procedure. The participants were ultrasonic test equipment manufacturers, material suppliers and end-users.

Figure 2 Stepped laminate panel with circular and square inserts



The participants in these RR exercises were required to inspect a stepped reference panel (see Figure 2) manufactured from carbon fibre-reinforced epoxy containing circular and square defects of known size (i.e. 6.35, 12.7 and 25.0 mm) and location using the operational procedure. The panel contained five discrete steps each 1 mm (16 plies) in depth for attenuation measurements. A quasi-isotropic laminate configuration was used. The stacking sequence per step was  $[45^{\circ}/0^{\circ}/-45^{\circ}/90^{\circ}/90^{\circ}/-45^{\circ}/0^{\circ}/45^{\circ}]_s$ . Artificial defects (representing delaminations) were fabricated using two layers of 50  $\mu\text{m}$  thick poly-tetrafluoroethylene (PTFE), sealed around the edges with heat-resistant tape to ensure an air gap. The artificial defects were placed between the 2nd and 3rd plies, at the mid-plane and between the 38th and 39th in the 5 mm thick section of the panel. The frequent accidental inclusion of single ply release film in laminates warranted the presence of single layers of square and circular shaped PTFE film positioned within the reference material at three different depths. The inserts, 12.7 mm in size, were located as shown in Figure 2 (right hand column). The panel had a smooth back surface with the front surface partitioned equally into smooth and rough finishes in order to assess the effect, if any, of surface finish on attenuation measurements.

Participants were requested to carry out absolute attenuation measurements on the stepped reference panel and to size the defects according to the -6 dB defect sizing method, where possible. UK participants included Aerostructures Hamble Ltd, British Aerospace Airbus Ltd, BNR Europe Ltd, BAE SYSTEMS (Military Aircraft), British Airways, Buehler Krautkramer, DERA, GEC Alstom, GKN Westlands (IoW), Hexcel Composites, Hurel Du Bois, Meccasonics

ICMAC - International Conference for Manufacturing of Advanced Composites

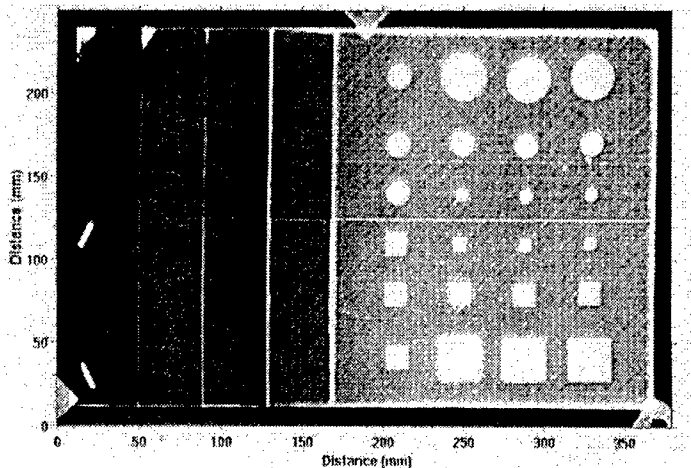
Ltd, Rolls Royce and Associates, St Bernards Composites Ltd, Shorts Bros Plc and Ultrasonics Sciences Ltd. USA participants in the international phase were Boeing Phantom Works (Long Beach, California), Sandia National Laboratories and Boeing/McDonnell Douglas (Puget Sound, Seattle).

The following observations were made from the reference panel R-R results:

- All participants detected the single- and double-layered PTFE inserts with the position of the defects being almost identical
- Differences in apparent defect size were dependent on the inspection technique and inspection parameters. It was not possible to reliably quantify those differences from visual inspection of the C-scan images
- Uncertainty in defect size increased with decreasing defect size
- Absolute attenuation measurements varied from 1.0 to 2.0 dBmm<sup>-1</sup> depending on the inspection technique and frequency response of the inspection transducer
- Differences in top surface finish have minimal effect on the relative attenuation measurements
- For glass-fibre based systems, the higher attenuation results in the use of lower frequency transducers, and lower sensitivity

Although surface roughness can contribute significantly to relative attenuation measurements, in this case, the difference in surface roughness of the two halves on the top surface of the laminate was insufficient to produce a noticeable difference. A typical C-scan image of the reference panel is presented in Figure 3.

Figure 3 C-scan image of stepped reference panel with defects.



---

#### ICMAC - International Conference for Manufacturing of Advanced Composites

The reference panel shown in Figure 3 can be used to establish, prior to inspection, that the ultrasonic C-scan equipment/instrumentation is functioning correctly and that the sensitivity and resolution is appropriately adjusted. Through further partnerships with industry, procedures have now been developed to simulate a wide range of commonly encountered defects (e.g. inclusions, delaminations, heat damage, chemical contamination and resin rich regions). Calibration or reference panels suitable for inspection of autoclave produced carbon and glass fibre-reinforced prepreg laminates up to 50 mm thick can now be produced.

Current work concerns the wider adoption of the C-scan procedures by industry through the development of the procedures as national and international (ISO) standards. Draft procedures have been submitted to the technical committee BSI ACE 56 (NDT) for consideration as a new work item for EN Aerospace standardisation. It is intended to broaden the scope of the procedures to include curved structures, sandwich constructions (e.g. foam and honeycomb core), and other processing routes (e.g. RFI - resin film infusion) and fibre formats (e.g. NCF - non crimped fabrics). Future work would involve procedures for simulating other production and in-service defects.

## 6. CONCLUSIONS

Several examples have been given of the development of test methods and product specifications related to the processing of composite materials. These inputs range from intermediate product specifications (eg moulding compounds), test methods for assessing correct processing (e.g. cure time, flow) of intermediates and improved assessment of processed material (e.g.  $T_g$ , c-scan inspection). The availability and traceability of these inputs contribute to increased quality and to increased confidence by designers, end-users and regulators.

## REFERENCES

1. Sims G D, "Validation results from VAMAS and ISO round-robin exercises", ICCM 10, Paper IV-195, Whistler, Canada, 1995
2. Mulligan D R, Gnaniyah S J P and Sims G D, "Thermal Analysis Techniques for Composites and Adhesives", NPL Measurement Good Practice Guide No. 32, 2000
3. Broughton W R, Sims G D, and Lodeiro M J, "Overview of DTI - Funded programme on Standardised procedures for ultrasonic inspection of polymer matrix composites" *Insight*, 40, 1, 1998
4. Broughton W R, Lodeiro M J and Sims G D, "Validation of procedures for ultrasonic C-scan inspection of PMC's: UK round-robin". NPL Report CMMT (A) 179, 1999
5. Broughton W R, Lodeiro M J and Sims G D, "Validation of procedures for ultrasonic C-scan inspection of PMC's: International round-robin". NPL Report MATC (A) 2, 2001

**Effect of lay-up and fiber angle on drilling behaviour of GFRP laminates**

J.Ramkumar, S.K.Malhotra and R.Krishnamurthy,  
Dept of Mechanical engineering,  
Indian Institute of Technology Madras  
India

Drilling status on GFRP laminates having following lay-ups was carried out:

- [i] [0]n
- [ii] [0/+45] ns
- [iii] [0/90] ns
- [iv] [0/+45/90] ns

Materials used for laminates were E-glass fiber unidirectional mat and hot cure epoxy 9LY 556 + HT 972 - Hindustan ciba -geigly) . Laminates of about 4 mm thickness were made by hand lay-up method. Drilling was carried out using high speed drilling machine and HSS normal drill. Speed and feed were varied and thrust and torque measured using tubular dynamometer. Optimum speed and feed combination (for which thrust and torque are minimum) was found to be different for different lay ups. Also, the magnitude of thrust and torque were found to be very much dependent on lay up of the laminates. It was observed that thrust and torque are maximum for [0/90] ns lay up and minimum for [0/+45/90] ns .

This can be explained as follows:-

1. In [0/90] ns laminates, there is an abrupt change in fibre angle as drill moves from one layer to another, which results in higher thrust and torque with rise in tool wear
2. In [0/+45/90] ns laminates, the change in fiber angle from layer to layer is gradual. This results in lowest thrust, torque and tool wear compared to other lay-ups.

---

ICMAC - International Conference for Manufacturing of Advanced Composites

**MULTI-SCALE MODELLING OF RESIN TRANSFER MOULDING**

S.C. McCallum<sup>1,3</sup>, P.D. Lee<sup>1</sup>, C.J. Lawrence<sup>2</sup>,  
T. Selerland<sup>3</sup>, P.D.M. Spelt<sup>3</sup>, and F.L. Matthews<sup>3</sup>

Imperial College of Science Technology and Medicine, London, England

1: Department of Materials, 2: Department of Chemical Engineering, 3: Centre for Composite Materials

Resin Transfer Molding (RTM) is a materials process used within the automotive, naval and aerospace industry to manufacture polymer composite structures. To manufacture a component using RTM the primary reinforcing constituent (pre-form) of the composite structure is placed into a closed mould tool. Polymer resin is injected under pressure into the mould impregnating the porous pre-form. The mould temperature is then raised to assist resin polymerization, after the final component has cured sufficiently it can be removed from the mould. Unsuccessful impregnation can lead to the formation of porosity, incomplete fibre 'wet-out' and fibre 'wash', features that can significantly affect the quality of the finished product. Since performing experimental studies is often expensive and time consuming, research is concentrating on developing computer simulations of the RTM process to improve product quality and reducing high process development costs associated with 'trial and error' manufacture.

Darcy's Law is currently used in RTM simulation packages to model mould infiltration at a macroscopic scale. However, some of the fundamental assumptions of Darcy's Law (e.g. 2-D Newtonian, Stokes flow without fingering) are not satisfied during the manufacture of thick composite structures. A multi-scale modelling approach that overcomes some of the limitations of Darcy's Law is achieved by coupling a micro-model solving for the flow on the length scale of the fibre bundles into a commercial computational fluid dynamics package such as CFX4 (AEA Technology). The coupling is achieved by simplifying general phase averaged flow equations so that the fiber-resin interaction and resin cure appear as source terms in the momentum and energy equations. The equations are then mathematically closed for a number of parameters including the drag force, which is imposed on a fiber bundle by the injected resin.

In earlier work, the drag force for a range of cylinder area fractions (0.1-0.6) was calculated from micro-scale simulations using CFX4. For the case of a square periodic array of impermeable cylinders (idealised fibre bundles) the results showed excellent agreement to the analytical solutions of Hasimoto (1959), Keller (1964) and numerical studies performed by Sangani and Acrivos (1982). In more recent work a micro-model of drag force has been incorporated into CFX4 to predict resin race-tracking on a macro-scale (on the length scale of the component). In addition, the cure stage of RTM has been simulated using a model developed within the Chemical Engineering Department - Imperial College, which predicts the change in resin viscosity as a function of time. The multi-scale model will be validated using experimental equipment designed within the Chemical Engineering Department - Imperial College and future work will involve full-scale validations with industrial collaboration.

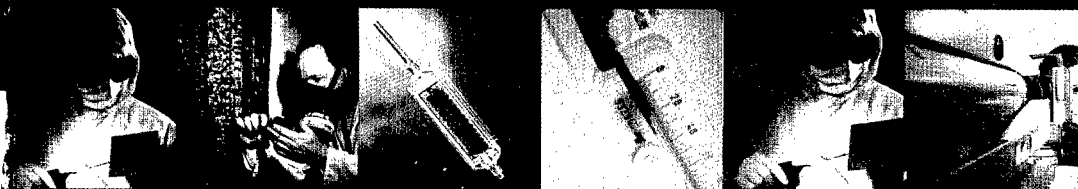
The final aim of the research is to develop a computational model of the infiltration and cure process of RTM for thin and thick polymer composite structures.

[stuart.mccallum@ic.ac.uk](mailto:stuart.mccallum@ic.ac.uk)

# Together we can make things better

Now, more than ever in Northern Ireland, technology is crucial to our economic well being. And innovation is the key to our success. The Industrial Research and Technology Unit can help with financial assistance, information and advice for encouraging research, technological development and technology transfer.

## B&D PROGRAMMES



## SCIENTIFIC SERVICES



## PROMOTING INNOVATION

Call IRTU today and together we can help you do whatever you do, better.

CALL US ON **028 9262 3000**

**irtu**

INDUSTRIAL RESEARCH & TECHNOLOGY UNIT

EMAIL: [info@irtu.detini.gov.uk](mailto:info@irtu.detini.gov.uk)

WEB: [www.irtu-ni.gov.uk](http://www.irtu-ni.gov.uk)

**IOM Communications Ltd**  
**1 Carlton House Terrace, London SW1Y 5DB, UNITED KINGDOM**  
**Tel: +44 (0)20 7451 7300 Fax: +44 (0)20 7839 2289**  
**Internet: <http://www.materials.org.uk>**

*IOM Communications Ltd is a wholly owned subsidiary of The Institute of Materials*  
*Registered with Charity Number 1059475 Printed September 2001*

*Copyright The Institute of Materials*